Reconfigurable Polymers *via* Supramolecular Self-Sorting

Eleanor May Hilton

Submitted in accordance with the requirements for the degree of Doctor of Philosophy

The University of Leeds

Faculty of Engineering and Physical Sciences

September 2023

Acknowledgements

Firstly, I would like to thank my PhD supervisors Prof Andrew Wilson and Dr Nicholas Warren their support, guidance, and encouragement throughout my PhD. Their belief in the project and my abilities has been a constant source of motivation. I would also like to extend a special thank you to Dr Yasmeen Jhons; I feel incredibly fortunate to have been able to work alongside you on this project. I couldn't have asked for a better colleague and feel lucky to now count you as a friend. In addition, I would like the academic and support staff at Leeds; in particular, Dr Mark J. Howard (NMR) and Dr Jeanine Williams (HPLC/MS). A massive thank you goes to all the members of the Warren and Wilson groups. It's been a privilege to have been part of such talented and knowledgeable research groups. Thanks in particular to Dr Michael Jinks and Dr Martin Walko for their excellent scientific guidance both in and out of the laboratory. Special thanks to Clarissa and Jonny for always being up for a coffee and chat or pint and a laugh. Many thanks go to all my family and friends who have supported me throughout my PhD. Thank you most of all to Tyron Hart for listening to all of my presentations that meant nothing to you and never failing to believe in my ability to complete this PhD.

Abstract

Certain small molecules with hydrogen bonding motifs (HBMs) are able to exhibit variable molecular recognition behaviour allowing them to spontaneously reconfigure facilitating self-sorting cascades and networks. Incorporation of HBMs into polymers has produced a new generation of supramolecular “smart” materials, however, there remains a need to develop multistate systems that are responsive to external stimuli. In this thesis the syntheses of visible-light responsive hydrogen-bonded supramolecular polymers are explored. Chapter 1 introduces the topics explored in this project through a review of relevant literature. The current understandings of hydrogen-bonding motifs, supramolecular self-sorting, polymeric materials and photoresponsive molecules are discussed. Chapter 2 details the synthesis and characterisation of photoresponsive hydrogen-bonding foldamers. Four foldamer designs are discussed and three are successfully synthesised and characterised. Chapter 3 examines the formation of photo-switchable supramolecular multistate systems using the foldamers described in chapter 2. Chapter 4 details efforts made towards the design and synthesis of reconfigurable hydrogen-bonding covalent polymers. Overall, this thesis covers progress made towards the goal of using supramolecular self-sorting to achieve reconfigurable polymers. Supramolecular polymers which can reconfigure in response to light stimuli have been developed, laying the foundations for future polymeric systems that can reconfigure using self-sorting.

Table of Contents

List of Abbreviations, Symbols and Formulae

A	Acceptor
A·T	Adenine-thymine base pair
AB	Azobenzene (NMR)
ACNH	1,1′-Azobis(cyclohexanecarbonitrile)
AIC	Amidoisocytosine
Ar	Aryl (NMR)
ATRP	Atom transfer radical polymerisation
AUPy	Dialkylaminoureidopyrimidinone
BA	Butyl acrylate
BB1	Benzoisoquinolino-napthypyridine
br	Broad (NMR)
C·G	Guanine-cytosine base pair
grad	Gradient
CB[7]	Cucurbit[7] uril
CB[8]	Cucurbit[8] uril
$CDCl_3$	Deuterated chloroform
cm^{-1}	Wavenumbers
CPD	2-Cyanopropan-2-yl benzodithioate
CTA	Chain transfer agent
D	Donor
d	Doublet (NMR)
Đ	Dispersity
DAD	Diaminopyridine acrylamide
DAN	Diamidonaphthyridine
DNA	Deoxyribonucleic acid
DOSY	Diffusion ordered spectroscopy
DP	Degree of polymerisation
eq	Equivalent
ESI	Ectrospray ionisation
EtBu	Ethyl butyl (NMR)
FRP	Free radical polymerisation
g	Gram(s)
GPC	Gel permeation chromatography
h	Hour(s)

HBM(s)	Hydrogen bonding motif(s)
HPLC	High-performance liquid chromatography
HRMS	High-resolution mass spectrometry
IR	Infra-red
ITC	Isothermal titration calorimetry
J	Coupling constant in Hz
K_a	Association constant
K_{dim}	Dimerisation constant
LC-MS	Liquid chromatography-mass spectrometry
LED	Light-emitting diode
M	Molar concentration
m	Multiplet (NMR)
m/z	Mass to charge ratio
MA	Methyl acrylate
mg	Milligram(s)
MHz	Megahertz
min	Minute(s)
mL	Millilitres(s)
mM	Millimolar
MMA	Methyl methacrylate
mmol	Millimole(s)
M_n	Number average molecular weight
M_w	Weight average molecular weight
NAP	Amidonaphthyridine
Nap	Naphthyridine (NMR)
NAPyO	Amidonapthyridone
NIR	Near-infrared
NMP	Nitroxide-mediated polymerisation
NMR	Nuclear magnetic resonance
o-chloroazobenzene	*ortho*-chlorinated azobenzene
o-fluoroazobenzene	*ortho*-fluorinated azobenzene
P	Poly
PSSs	Photostationary states
Pyr	Pyridylurea
RAFT	Reversible addition-fragmentation chain transfer
RDRP	Reversible-deactivation radical polymerisation

RTA-ATRC	Radical trap-assisted atom transfer radical coupling
s	Singlet (NMR)
SEI(s)	Secondary electrostatic interaction(s)
SP(s)	Supramolecular polymer(s)
t	Triplet (NMR)
^{t}Bu	Tertiary butyl
td	Triplet of doublets (NMR)
UIM	Ureidoimidazole
UPy	Ureidopyrimidinone
UV	Ultraviolet
UV-Vis	UV-visible absorption spectroscopy
δ	Chemical shift
λ	Wavelength
ν_{max}	Absorption maxima

List of Figures

List of Schemes

List of Tables

1. Introduction

Non-covalent interactions within and between macromolecules are responsible for some of the most complex and crucial biological processes seen in nature.[1] Biological life relies on non-covalent interactions such as the hydrophobic effect, *π–π* interactions, and hydrogen bonding to maintain the structure and properties of its macromolecules,[2, 3] as well as for carrying out precisely controlled processes such as cellular signaling cascades.[4]

Biomimetic molecular recognition motifs are of particular interest for the development of a new class of synthetic advanced materials.[5, 6] Being significantly weaker than covalent bonds,[2] non-covalent interactions allow molecules to interact in a reversible manner.[7] With different recognition motifs having variable affinities for association/disassociation this presents an opportunity for a system to sequentially and simultaneously alter its binding partners in response to the introduction of a new molecule or extremal stimuli,[8] and, ultimately the elaboration of reconfigurable materials i.e. materials that can change configuration and properties.

1.1 Hydrogen bonding

A non-covalent interaction prevalent throughout biology is hydrogen bonding. Hydrogen bonding occurs when an electronegative acceptor atom (usually nitrogen or oxygen), and electropositive donor atom (hydrogen attached to an electronegative atom) form an attractive interaction.[9] Whilst the affinity of a hydrogen bond is dominated by this electrostatic contribution, the acceptor (*A*) - donor (*D*) interaction also exhibits directionality.[10] A hydrogen bond arises from the interaction of the positive and negative dipoles along the direction of the electron lone pair leading to a linear interaction.

Not only do hydrogen bonds play important roles in biological systems, but they also represent a powerful tool for the assembly of reconfigurable supramolecular architectures.[11, 12] The directionality and selectivity exhibited by hydrogen-bonding makes this non-covalent interaction particularly interesting for use in synthetic systems.[12] Although the strength of a single hydrogen bond is relatively weak, this can be increased significantly by using multiple hydrogen bonds as part of a multivalent array.[13] The versatility of the strength of hydrogen bonding within such arrays presents an opportunity to tune specific hydrogen bonding motifs (HBMs) to have greater affinity for another particular motif.[8]

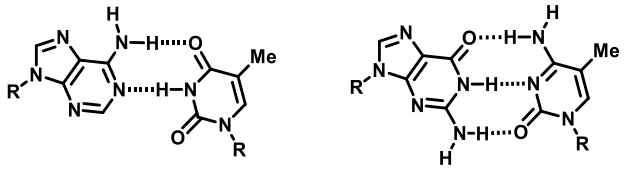

1·2 A·T
$K_a = 10^2\ M^{-1}$

3·4 G·C
$K_a = 10^4\text{-}10^5 M^{-1}$

Figure 1. Left- DNA base pair adenine and thymine (A·T) showing two hydrogen bonds between bases; Right- base pair guanine and cytosine (G·C) showing triple hydrogen bonding between bases.

An example of the aforementioned property can be observed by studying the binding of deoxyribonucleic acid (DNA) base pairs (Figure 1). The interaction between cytosine **3** and guanine **4** (C·G) has increased stability compared with the interaction between adenine **1** and thymine **2** (A·T). This change in stability can be attributed to additional hydrogen bond between the bases C·G compared with the two between A·T.[14] This theory is supported by measurements of the association constants (K_a) of derivatives of the nucleobases in chloroform. Experimentally determined K_a values for the G·C interaction (10^4-10^5 M^{-1}) have been found to be more than two orders of magnitude greater than those determined for the A·T interaction (10^2 M^{-1}).[15, 16]

1.1.1 Secondary electrostatic interactions

In addition to the number of donor and acceptor groups in an array, the order of the adjacent groups also has a significant impact on the association constants observed between hydrogen bonding dimers. For example, for a triple HBM with three donor groups (*DDD*) and its complementary motif with three acceptors (*AAA*), the binding affinity is usually higher than for a *DDA·AAD* dimer (Figure 2a).[17] This observation has been attributed to secondary electrostatic interactions (SEIs) that occur between adjacent donors and acceptors. The SEI model was established by Jorgensen and Pranata in 1990.[18] This model defined SEIs as the diagonal interactions between adjacent hydrogen bonds, which can be attractive or repulsive. For example, a *DDD·AAA* interaction contains four attractive SEIs whereas, *DDA·AAD* only contains two, and a *DAD·ADA* interaction contains four repulsive SEIs (Figure 2b). This theory views the interactions as single point charges and it is well supported by experimental data.[17, 19-21]

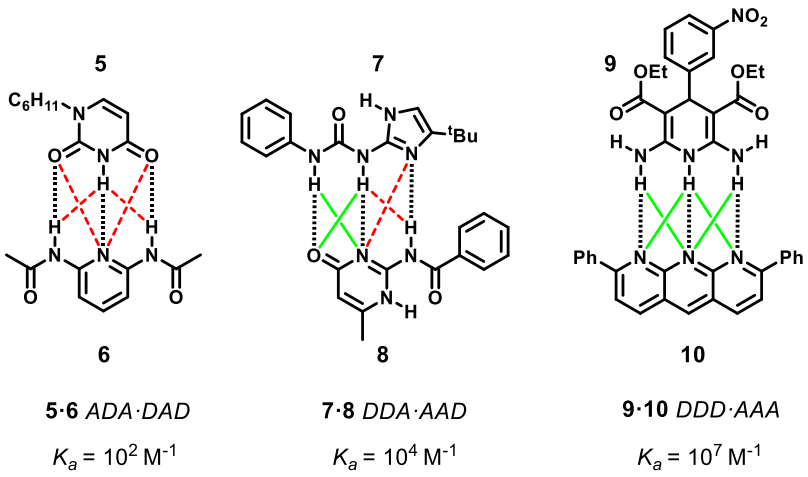

Figure 2. Examples of triply hydrogen bonded motifs with differing, experimentally determined, association constants (all K_a values determined by ^{1}H NMR in $CDCl_3$).[18] Black hashed lines represent hydrogen bonds, green lines show attractive SEIs and red dashed lines show repulsive SEIs.

Alternative explanations for this behaviour have been explored, with one study that investigated the interactions of DNA base pairs suggesting that the SEI theory ignores significant long-range interactions such as atom-atom pairwise interactions.[22] The importance of considering additional atom-atom pairwise interactions has since been confirmed by other groups.[23-25] The SEI model has also, more recently, been identified as an oversimplification in work by van der Lubbe *et al*.[19] Here, it was suggested that the interactions should be considered as a larger accumulation of charge around the frontier atoms rather than a single point charge. This theory arose from a computational study which found that charge accumulation on hydrogen bonded fragments is the result of both electrostatic interactions and σ-orbital interactions.

Although there is valid evidence that the SEI model oversimplifies the interactions by describing them as single point charges, it can still be said that the SEI model is predictive. The model provides a measure for charge accumulation between hydrogen bonding partners and is often in line with experimental association constant values. This means it can still be considered a reasonable basis for predicting and explaining differences in experimental binding strengths and remains a useful principle for designing hydrogen bonding arrays.

1.1.2 Intramolecular interactions

Another factor to consider when designing HBMs is the presence of intramolecular hydrogen bonding. Intramolecular hydrogen bonds can be responsible for either promoting or hindering the complexation of two HBMs. In the right configuration an intramolecular hydrogen bond will

effectively pre-organise the molecule for binding, however an intramolecular hydrogen bond that leads to a conformation in competition with the desired intermolecular interaction, can make binding less favourable. This is in agreement with Etter's rules, which state that intramolecularly bound six membered hydrogen bonded rings are favoured over intermolecular bonds.[26] This rule is attributed to the entropic penalty associated with binding two separate molecules over the binding within just one molecule.

A study performed by Zimmerman and co-workers demonstrated the impact intramolecular hydrogen bonding can have on association constant.[27] It had previously been reported that in an uncomplexed form, pyridylureas contain an intramolecular hydrogen bond (Figure 3a).[28] In this study it was determined that upon complexation with a naphthyridine (Figure 3b) the association constant was fairly low at 30 M^{-1}. This was attributed to the energetic penalty incurred by the necessary breaking of the intramolecular bond.

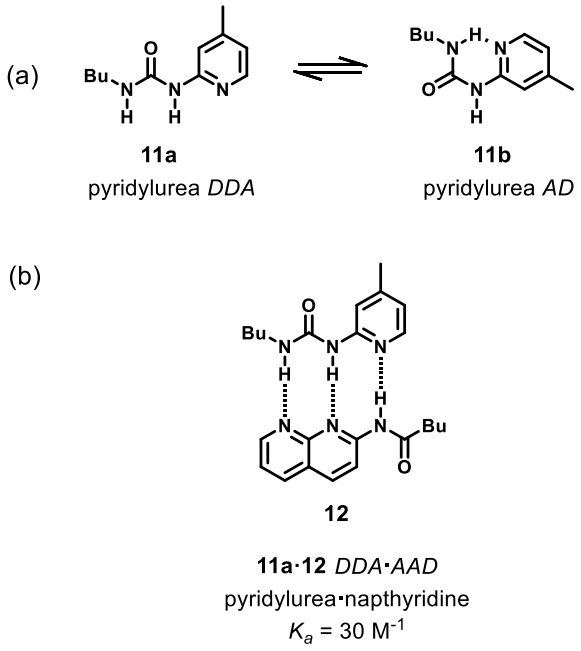

Figure 3. (a) Pyridylurea switches between conformations depending on the presence or absence of an intramolecular hydrogen bond; (b) Pyridylurea-naphthyridine complex formed upon breakage of the pyridylurea intramolecular hydrogen bond, K_a value determined by ^{1}H NMR titration in $CDCl_3$.[27]

In a study from Beijer and co-workers, complexes of diaminopyrimidines were examined.[29] Here, the *ADAD* dimer assembled from compound **13** with an amide lacking an intramolecular bond had a dimerisation constant K_{dim}= 170 M^{-1}, whilst exchange of the amide for a urea in compound **14** resulted in preorganisation and increased strength of self-association (K_{dim}= 2 x10^5 M^{-1}) (Figure 4). This work demonstrates the significant impact an intramolecular hydrogen bond can have on complexation.

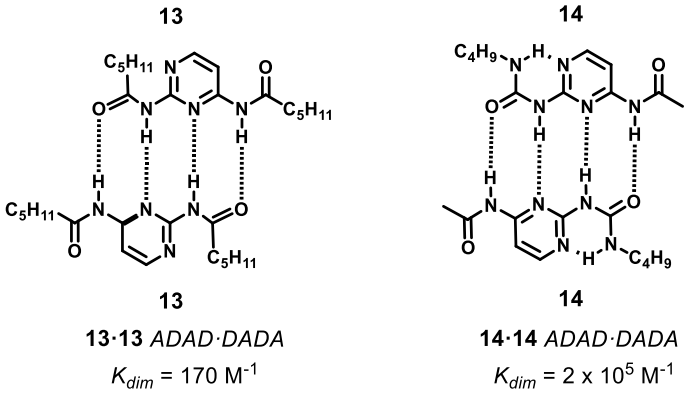

Figure 4. Complexation of diaminopyrimidines with and without intramolecular bonds. K_{dim} values determined by ^{1}H NMR titration in $CDCl_3$.[32]

Intramolecular interactions can also be used to explain changes in association constant observed when altering substituents on HBMs. Chien and co-workers synthesised a series of substituted pyrid-2-yl ureas to investigate the impact on the intramolecular hydrogen bonds.[30] Association constants for the interactions between pyrid-2-yl ureas **15** and **16** with cytosine **4** were determined. The K_a for **15·4** was found to be approximately half the magnitude of that for **16·4** (Figure 5). This observation was attributed to presence of an electron withdrawing group on pyrid-2-yl urea **16** and lack of such a group on pyrid-2-yl urea **15**. It was concluded that the addition of an electron deficient substituent resulted in preferential formation of intermolecular hydrogen bonds rather than intramolecular bonds, resulting in a higher K_a between **16** and **4**. These findings present an option to mitigate the impact of intramolecular bonding if seeking to design a HBM which is capable of forming undesirable intramolecular interactions.

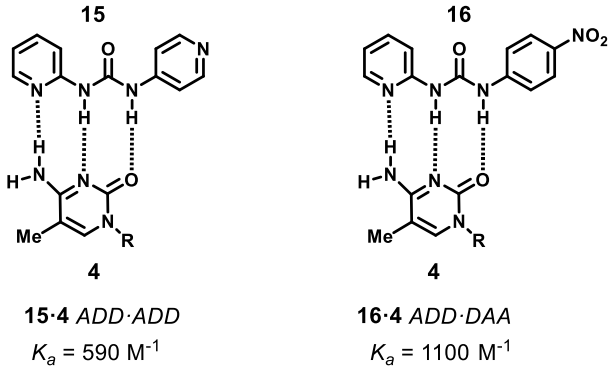

Figure 5. Complexation of pyrid-2-yl ureas **15** and **16** with cytosine **4**. K_a values determined by ^{1}H NMR titration in $CDCl_3$.[30]

1.1.3 Tautomerisation

When designing HBMs, it is also important to consider tautomerisation of the motif. Another factor to consider when designing HBMs is the ability of the motif to tautomerise. Often HBMs are heteroaromatic, meaning different tautomeric states can be formed; these tautomers may not display the desired array of donors and acceptors for an intermolecular interaction. Tautomeric effects are observed most commonly in quadruple HBMs as they usually possess a higher number of heteroatoms and each hydrogen bonding heteroatom added to the molecule increases the number of potentially accessible tautomeric states.[31]

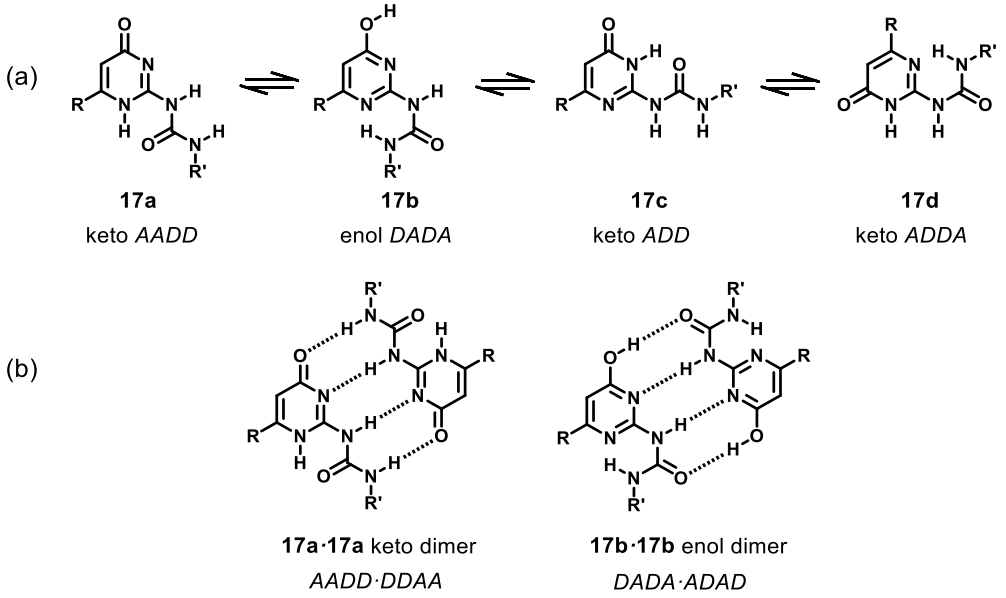

Figure 6. (a) Four tautomers formed by UPy, the keto form **17a** is the most prevalent in $CDCl_3$, the ADAD enol form **17b** is also present in $CDCl_3$, the ADD keto form **17c** is observed in dimethylsulfoxide but no dimerisation is evident, **17d** can be observed in the presence of a complementary molecule with a DAAD HBM. (b) The two homodimers formed by the UPy tautomers.[32]

One example of such tautomerism is seen in ureidopyrimidinone (UPy), a self-complementary, quadruple HBM (Figure 6). The expected array is the *AADD* keto form **17a**, however UPy is also able to adopt at least three other tautomeric states (**17b-d,** Figure 6a). Meijer and co-workers found the **17a** *AADD* array tends to be the most prevalent, but the motif was also able to form the **17b** enol equivalent with a *ADAD* array.[32] Within this work it was discovered that the array could be manipulated by changing the substituents at the 6-postion on the pyrimidone ring. Electron withdrawing substituents favoured the *DADA* tautomer whereas, election donting substituents favoured the *AADD* tautomer. This was attributed to the likely reduced stability of the enone structure in the pyrimidinone form when the substituent is electron withdrawing.

The existence of the different tautomeric states can be a problematic when attempting to design hydrogen bonded supramolecular structures, undesirable tautomers can lead to a decrease in association constants or prevention of the formation of a complex altogether. Whilst this effect may be looked upon unfavourably in some circumstances, it can be useful in more complex self-sorting systems as the ability to form multiple arrays presents an opportunity for a motif to bind to multiple components in one system. [33]

1.2 Supramolecular self-sorting systems

The term self-sorting refers to the high-fidelity recognition observed between individual components within complex mixtures. This recognition gives rise to specific complexes within the mixture rather than a library of all possible non-covalent configurations.[34, 35]. Self-sorting is ubiquitous in nature; biological systems have the ability to control self-assembly and aggregation in solution with high levels of precision. Such natural systems use non-covalent interactions to form multiple functional assemblies from numerous building blocks, simultaneously and in the presence of each other.[35] This has inspired great interest among chemists in the field of supramolecular self-sorting and to synthetically replicate the complex self-sorting seen in biological systems would be a significant achievement.

In order to attain the kind of supramolecular self-sorting seen in biology it is necessary to consider the behaviour of recognition motifs within complex systems, not just isolated systems.[36] The kind of self-sorting observed in such systems can be put into categories depending on the affinity of the components or depending on the final arrangements of the systems (Figure 7) We can consider the components as social (self-loathing) if they preferentially interact with components in the system other than themselves or, narcissistic (self-loving) if they prefer to interact with themselves.[37] When considering the final product of the system, we see integrative systems with just one final complex, and non-integrative systems with more than one final complex.[38, 39]

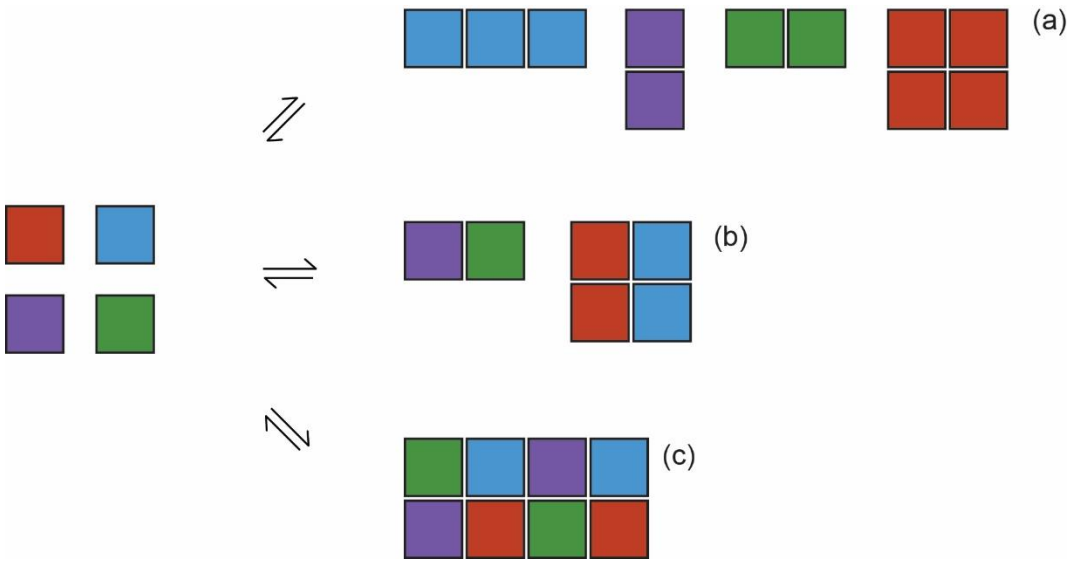

Figure 7. Different types of supramolecular self-sorting; (a) Shows non-integrative narcissistic self-sorting; (b) non-integrative social self-sorting and; (c) integrative social self-sorting.

A recent example of a self-sorting system was reported by Remón and co-workers, it demonstrated a chemical signalling cascade utilising cucurbituril host-guest interactions to generate a system reminiscent of cell signalling pathways (Figure 8).[40] This work shows multistep, competitive displacements in a four-component system. The system consists of two guests (a thioflavin mediator **18**, and dopamine **19** which is the released guest) and two cucurbituril homologues (CB[8] and CB[7]). By making use of the differing association constants of the host-guest complexes,[41] the system could be manipulated to release a neurotransmitter cargo upon introduction of a memantine external trigger **20** (Figure 8b).

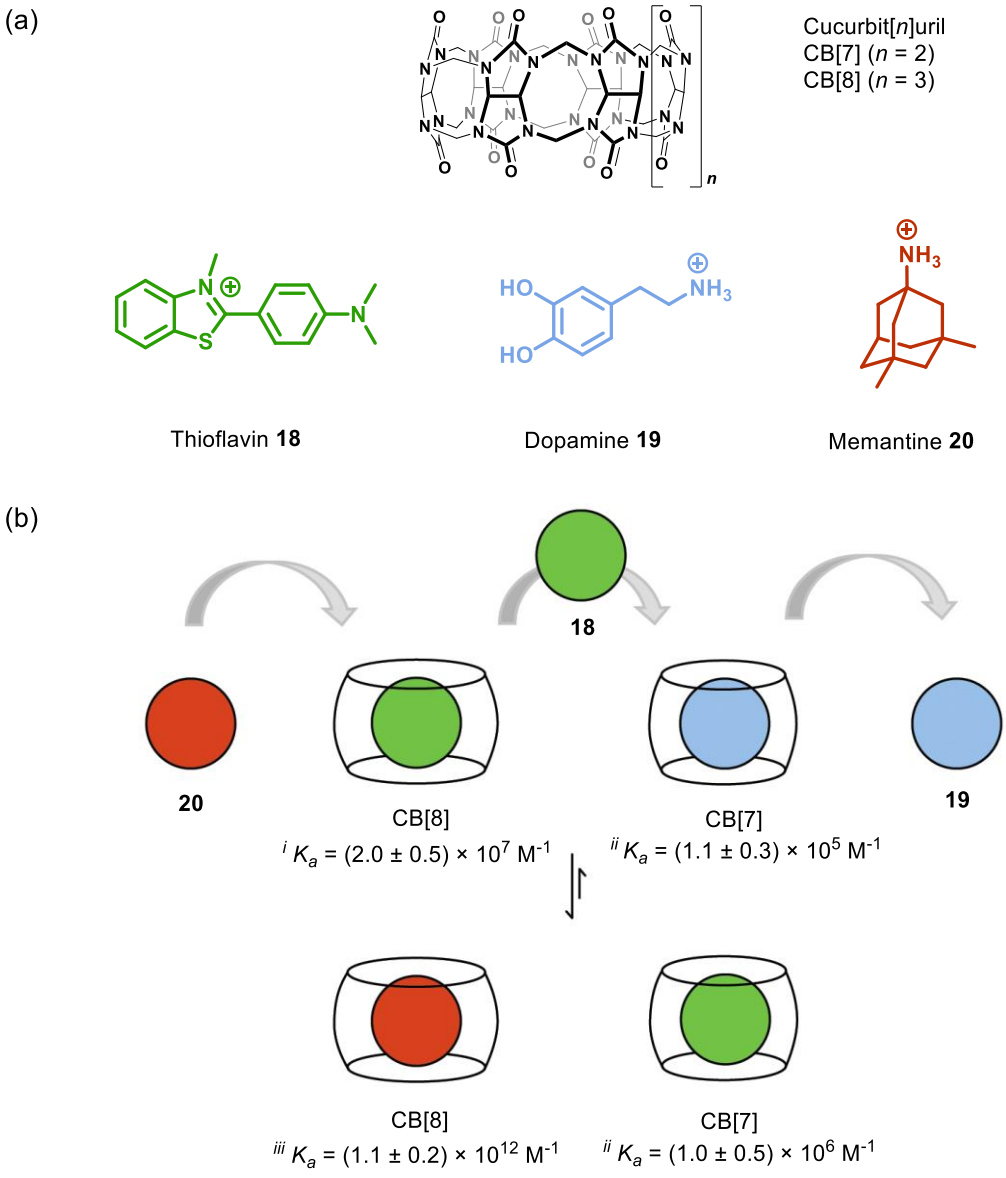

Figure 8. Cascade type system using host-guest interactions; (a) structures of the host and guest molecules in the cascade system; (b) red circle is memantine trigger **20**, green, thioflavin mediator **18**, and blue, the dopamine released guest **19**; [i] apparent K_a value obtained from competition experiment with CB[7] for a limited quantity of thioflavin; [ii] values measured by isothermal titration calorimetry (ITC) in water (298 K); [iii] value taken from reference [41]. Figure reproduced from [40].

Host-guest interactions work well here for the development of a biomimetic signalling cascade, however for the desired development of reconfigurable polymers the unique properties of HBMs promise to be more appropriate. Not only are HBMs able to possess all the properties of the self-sorting systems in this section, they have also been shown to be able to form some of the most complex synthetic systems,[33] and can be incorporated into polymers.[6]

1.2.1 Multiple hydrogen bonding arrays

In recent years utilising HBMs has emerged as a promising strategy for developing complex synthetic supramolecular self-sorting systems.[42, 43] Multiple hydrogen bonding arrays are able to simultaneously and sequentially reconfigure (Figure 9), switching between numerous different states of molecular recognition.

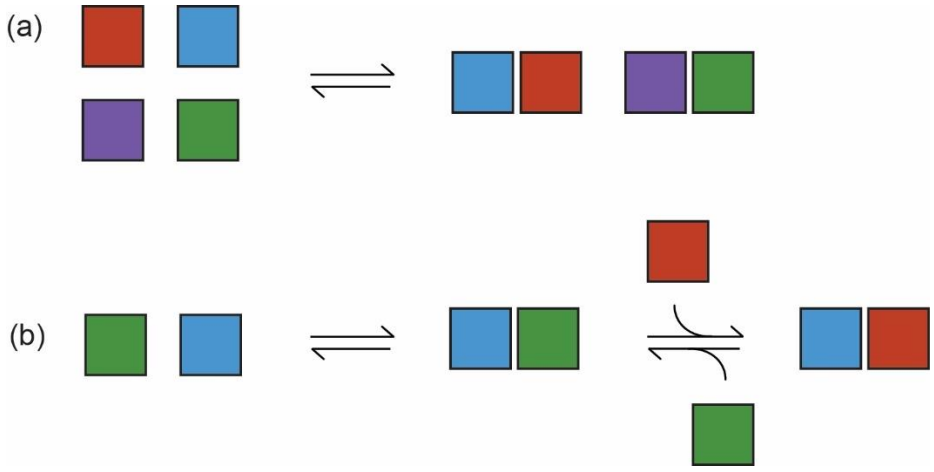

Figure 9. Schematic where each coloured block represents a HBM; (a) simultaneous self-sorting; (b) sequential self-sorting. Adapted from [4].

For example, Coubrough and co-workers presented a self-sorting system utilising six linear HBMs.[33] The chosen motifs were able to exhibit both promiscuous and high-fidelity molecular recognition which led to a complex self-sorting network. The presence or absence of the different components provided multiple pathways to unique self-sorted configurations. The network of self-sorting described in this work consisted of molecules able to form hydrogen bonded dimers, some linked by three hydrogen bonds and some by four. The molecules used within the network were dialkylaminoureidopyrimidinone **21** (AUPy), amidonapthyridone **22** (NAPyO), diamidonaphthyridine **23** (DAN), ureidopyrimidinone **17** (UPy), ureidoimidazole **7** (UIM) and amidoisocytosine **8** (AIC) (Figure 10a). These molecules were shown to follow seven different pathways to forming the same four hydrogen-bonding dimers with various 'pathway interchange' points where one route could be switched for another.

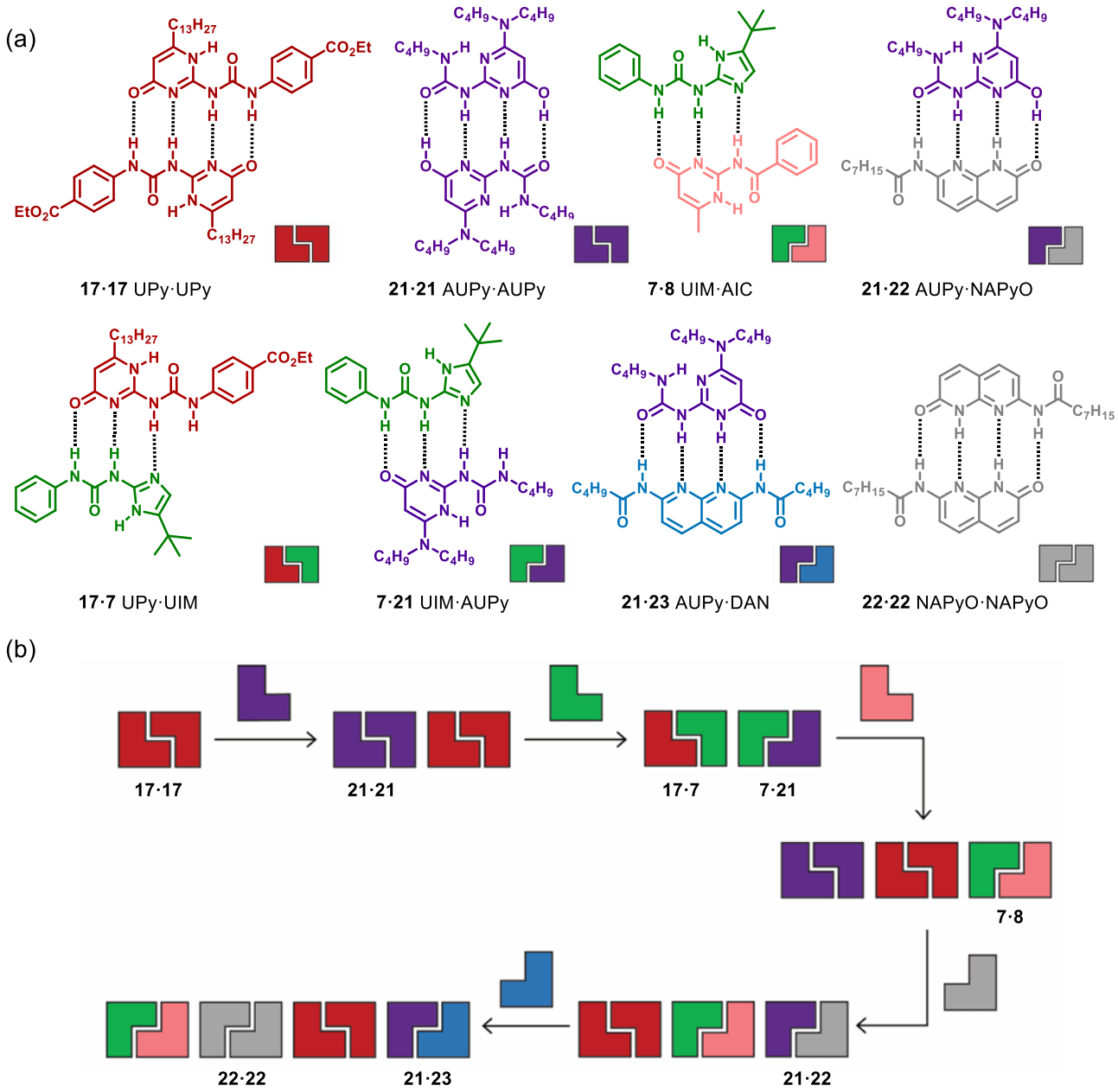

Figure 10. (a) HBM dimer interactions and their block representations. Red blocks represent UPy, blue AUPy, green UIM, pink AIC, grey NAPyO and purple DAN; (b) self-sorting pathway where each new dimer is labelled within the diagram. To simplify the diagram, accurate stoichiometries have been excluded. Adapted from [33].

One example of such a pathway (Figure 10b) begins with a UPy homodimer, followed by addition of AUPy to result in narcissistic self-sorting of UPy and AUPy into their respective homodimers. Upon addition of UIM the formation of UPy·UIM and AUPy·UIM heterodimers was observed. The consecutive introduction of AIC resulted in heterodimer formation with UIM (AIC·UIM) and simultaneous reformation of the UPy and AUPy homodimers. Next the formation of an AUPy·NAPyO heterodimer alongside the UPy homodimer and UIM·AIC heterodimer occurred *via* addition of NAPyO. Finally, addition of DAN disrupted the

AUPy·NAPyO complexation, forming an AUPy·DAN heterodimer. This resulted in a final configuration of four components, AUPy·DAN, UIM·AIC, NAPyO·NAPyO and UPy·UPy.

This system is a step toward a more accurate mimic of the bimolecular associations that occur in multicomponent protein assemblies. The incorporation of this kind of hydrogen bonding array into synthetic macromolecules would be a step further toward achieving complex biomimetic systems that can be readily reconfigured.

1.2.2 Stimuli responsive self-sorting

To add an orthogonal element of control to supramolecular self-sorting systems, stimuli responsive species can be incorporated. One example of this kind of system was reported by Schoder and Schalley, in this work cucurbit[8]uril complexes could be altered by changing the pH or redox conditions of the system.[44] The cyclic guest species was capable of complexation redox-responsive ethyl viologen **24** and pH responsive phenylpyridinium **25**. The self-sorting pathway in its initial state comprised of CB[8] complexed with two protonated 4-phenylpyridinium **25a** molecules with ethylviologen **24a** free within the system (Figure 11). Upon deprotonation phenylpyridinium **25b** was able to pair with ethylviologen **24a** resulting in a 1:1:1 complex with CB[8]. When electrons were made available within the system, ethylviologen **24a** was reduced to **24b**, and a 2:1 complex in which CB[8] holds two viologen radical cations as guests was subsequently observed. The system was reversible upon either pH or redox stimulus, resulting in a level of control difficult to achieve without the presence of a stimuli responsive element.

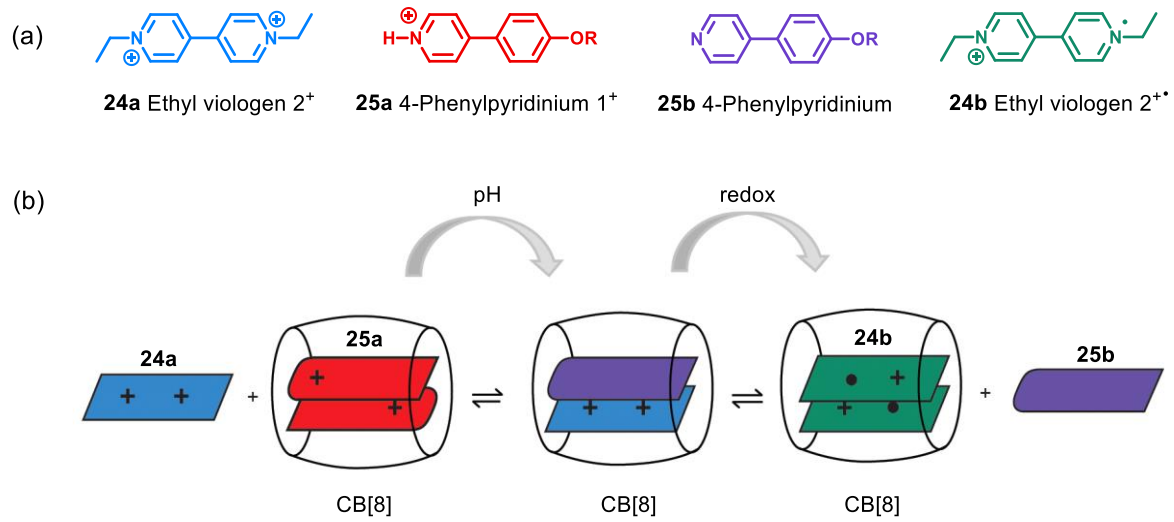

Figure 11. (a) Structures of ethyl viologen **24** and phenyl pyridinium **25** guest molecules; (b) schematic representing pH and redox responsive self-sorting system in water. CB[8] represents the host molecule, blue represents ethylviologen guest in the 2+ oxidation state **24a**, red represents protonated 4-phenlypyridinium **25a**, purple is deprotonated 4-phenlypyridinium **25b** and green is an ethylviologen radical cation **24b**. Reproduced from [44].

Another example of a pH responsive system has been reported by the Wilson group; here HBMs were used.[45] The system was studied by proton nuclear magnetic resonance (^{1}H NMR) and contained a pH responsive HBM capable of changing recognition preference in response to protons. In acidic conditions, proton responsive UIM **7**, underwent a change in array from *DDA* to *DDD*, due to protonation at its imidazole moiety (Figure 12). In this protonated state, UIM preferentially complexed with *AAA* motif benzoisoquinolino-napthypyridine (BB1) **26** over AIC **8** (*AAD*). This work demonstrates that control can be added to a hydrogen bonding self-sorting network and changes can be brought about in the system by an orthogonal stimulus rather than by addition of new components to the system.

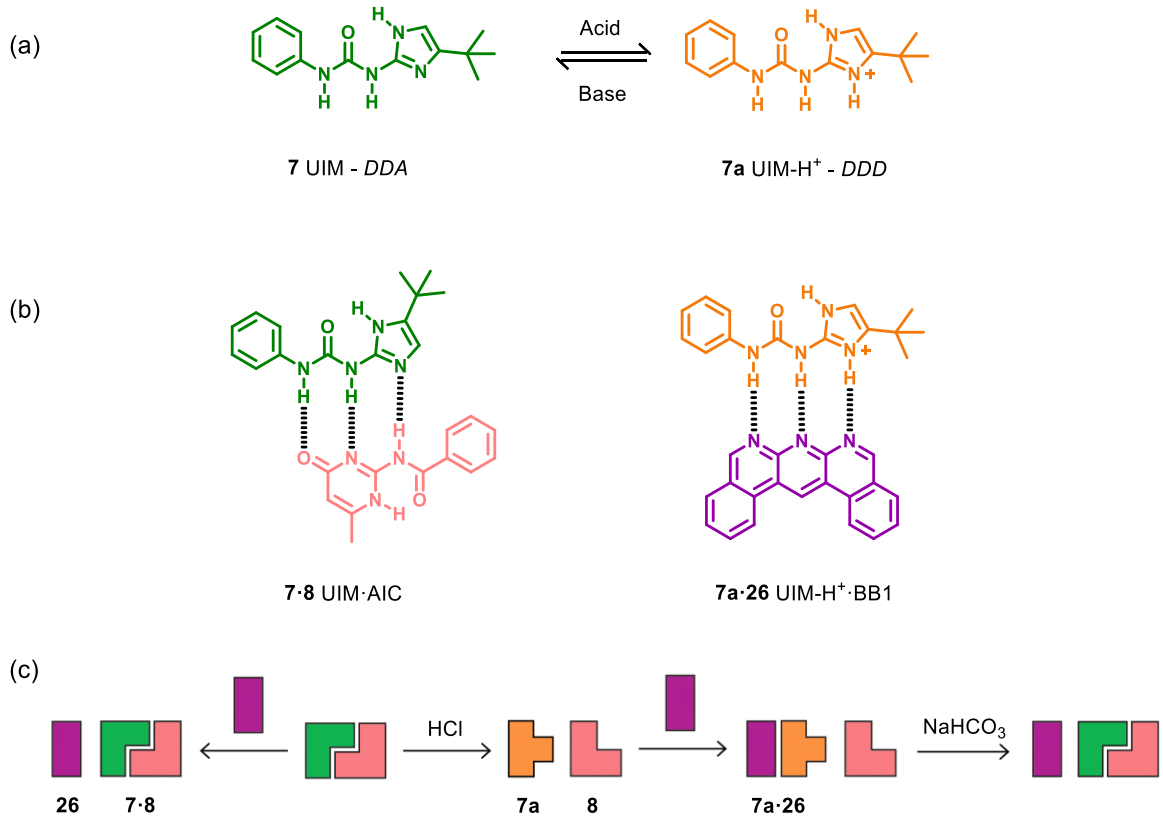

Figure 12. (a) Reversible protonation of the UIM motif, changing the array from *DDA* to *DDD*; (b) Binding observed between UIM **7** and AIC **8**, and UIM-H$^+$ **7a** and BB1 **26**; (c) Self-sorting pathway of UIM, AIC and BB1 in $CDCl_3$ with the addition of HCl and $NaHCO_3$. Adapted from [45].

In addition to the pH responsive system described above, the Wilson group also incorporated an external light stimulus into a self-sorting cascade (Figure 13).[8] This cascade used social self-sorting to sequentially sort four HBMs (UPy **17**, AIC **8**, UIM **7** and DAN **23**) upon the introduction of new binding partners. The AIC* motif **8a** contains a light cleavable moiety, when light is introduced to the system, the motif becomes available as the binding partner **8**.

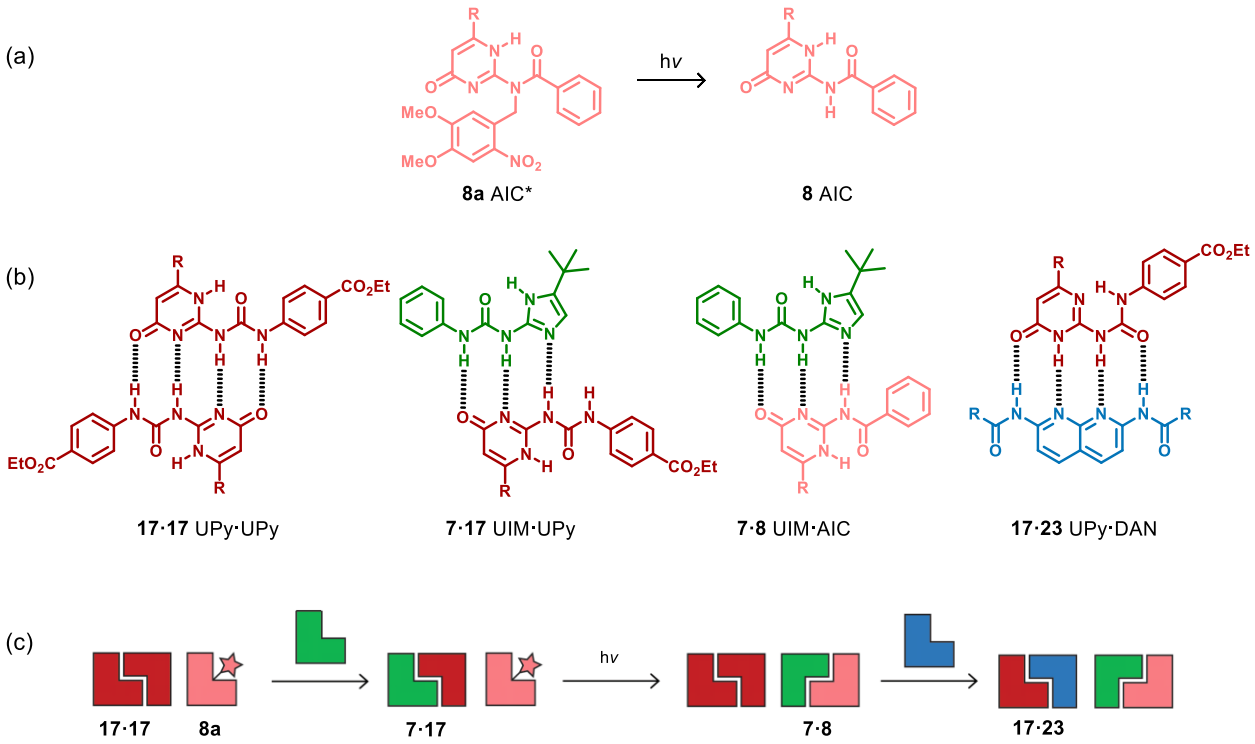

Figure 13. (a) Light responsive cleavage of *o*-nitro-4,5-dimethoxybenzyl group from AIC* **8a** resulting in AIC **8**; (b) binding partners observed within the cascade, UPy·UPy **17·17** homodimer, UIM·UPy **7·17**, UIM.AIC **7·8**, and UPy·DAN **17·23**; (c) schematic representing light responsive self-sorting cascade. Adapted from [8].

Whilst a light stimulus could be favourable over pH, as no chemicals need to be added to the system which may interfere with other binding partners, this example is not reversible like the pH responsive system. In order to add a reversible light responsive element to the system a photoresponsive molecule could be incorporated that does not result in cleavage of a moiety but rather, a reversible change that could temporarily release a new binding component into the system. Photoresponsive molecules of this nature are discussed further in section 1.4.

1.3 Polymeric materials

Many of nature's macromolecules are comparable to synthetic polymers, for example nucleic acids, proteins and polysaccharides are natural polymeric materials.[46] It is therefore of interest to use synthetic polymers for the creation of advanced biomimetic materials. Polymeric materials are also relatively easily accessible synthetically and can be prepared to encompass a wide range of properties.[47]

1.3.1 Covalent polymer synthesis

Within this research a combination of the properties of both supramolecular self-sorting systems and controlled structure polymers are investigated. Combining the reversibility of supramolecular interactions with covalently bonded polymers will allow for the development of complex architectures capable of controlled reconfiguration.

Conventionally, polymers are synthesised by the formation of covalent bonds between monomers upon an appropriate initiation step. The initiation process can be brought about by anions, cations or radicals, depending on the monomer used.[48] Once the polymerisation has been initiated, the polymeric species can begin to grow by addition of monomers to the initiator species, this results in the long chain-like molecules that we class as polymers. Within this process termination events can also occur, either by the recombination of two radical species or by disproportionation within one radial species. Once termination has taken place, the resulting non-radical species can be classed as 'dead', and it no longer takes part in the polymerisation process.

The majority of polymers produced industrially are made by the free radical polymerisation (FRP) method, this method is a chain-growth polymerisation in which unsaturated monomers are converted into a carbon-carbon backbone polymer using a radical initiator. Whilst the FRP method is used extensively in industry, and has relatively non-demanding reaction conditions, it lacks the level of control needed for more advanced and complex materials. In FRP the rate of propagation of the chain is not easily controlled, there are often undesirable chain-transfer and termination events which leads to poorly defined polymers with high dispersity (*Đ*) in chain lengths.[49] These issues may be exacerbated by the addition of complex monomer species; therefore, an alternative method of polymerisation was desirable for this work. There are many other, well-established, methods of polymerisation which offer greater control over the products they produce.

Polymers with more complex structures can be produced by living polymerisations. A polymerisation is determined as 'living' when it proceeds without chain-breaking reactions, this allows chains to continue to grow until the monomer is exhausted. In an ideal living polymerisation there are no irreversible termination events and the chain end remains active, meaning polymerisation can restarted by addition of more monomer. As all the polymer chains are initiated at the same time and propagate throughout the reaction, *Đ* is usually low, conversion is generally high, and most chains will contain the same composition of monomers. In practice, there are usually some termination events that take place in most polymerisations. Because of these termination events it can be difficult to classify some methods as true living polymerisations but polymerisation methods that have some living character generally produce well defined products.[50]

One of the methods that is classed as a living polymerisation is anionic polymerisation, here electrophilic monomers, for example styrene, are used with nucleophilic initiators, for example butyl lithium. As there is no formal termination stage, this method of polymerisation produces low *Đ* materials, and the active chain end means more monomer can be added post-polymerisation to restart polymerisation. Whilst there are these advantages, the reaction conditions of anionic polymerisation are much more demanding and there is a limited choice of monomers compared with FRP.[49]

An alternative method of polymerisation, which has been well documented for the production of advanced materials is, reversible-deactivation radical polymerisation (RDRP). RDRP methods are considered to mimic living polymerisations, whilst also benefiting from the versatility of a free radical polymerisations.[51] These methods are able to produce polymers with low molar mass dispersity, predictable molecular weights and a capacity for continued chain growth.[52] There are a few different methods of polymerisation that can be classed as RDRP, these include nitroxide-mediated polymerisation (NMP), atom transfer radical polymerisation (ATRP) and reversible addition-fragmentation chain transfer (RAFT). NMP uses a nitroxide initiator and has been shown to produce polymers with very low *Đ*, NMP can, however, suffer from hydrogen transfer side reactions and requires high temperature and long reaction times.[53] ATRP uses an alkyl halide initiator, and also requires an organometallic catalyst, which usually consists of copper with amine ligands. ATRP has been shown to produce complex polymer architectures with a wide variety of monomers.[54-56] One drawback of ATRP is that it often requires the use of organometallic catalysts at high concentrations, this could prevent any polymeric species produced from being used for biological applications. The type of RDPR used in this work is RAFT; this method is known to have good solvent compatibility and functional group tolerance.[57,58] Additionally, RAFT is capable of producing a

wide range of well-defined polymeric structures including linear block copolymers, branched polymer architectures and cross-linked networks.[59-62]

The mechanism for RAFT polymerisation proceeds as demonstrated in Figure 14; the first step in the polymerisation process is (a) initiation, this step requires the generation of a radical initiator which activates the polymerisation. Next, propagation occurs (b) and radical polymer chains of length *n* are generated. Following on from (b), is the pre-equilibrium RAFT propagation step (c) where the chain transfer reagent (CTA) or RAFT agent (often a thiocarbonylthio compound) is introduced. In this step the polymeric radical, $P_n^{\bullet}$, reacts with the RAFT agent forming an intermediate radical, this is followed by fragmentation to give a polymeric thiocarbonylthio species and a new radical $R^{\bullet}$. This radical is able to react with more monomer to form a new propagating radical with a chain length *m* in reinitiation (d). This stage is followed by the main equilibrium RAFT propagation (e); here there is a rapid equilibrium between the active propagating radicals $P_n^{\bullet}$ and $P_m^{\bullet}$ and the dormant thiocarbonylthio compounds, which means the majority of chains should grow to the same length. Once the polymerisation is complete, most chains will retain thiocarbonylthio end groups, hence the comparison to a living polymerisation. Although these chains have the potential to be extended upon addition of more monomer, radical-radical termination of the chains can also occur resulting in a small number of dead chains (f).[52, 63]

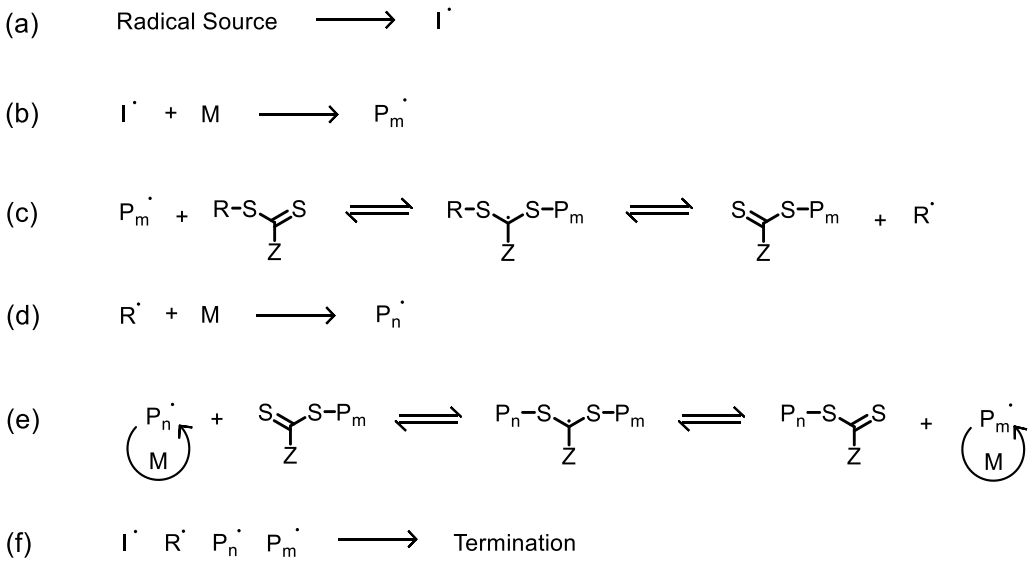

Figure 14. Mechanism for reversible-addition fragmentation chain transfer polymerisation.[52]

1.3.2 Supramolecular polymers

Supramolecular polymers (SPs) are macromolecules that, unlike controlled structure polymers, are constructed by non-covalent, reversible interactions. These materials exhibit properties that include self-healing, shape memory, and actuation.[64-68] Due to the dynamic nature of the non-covalent interactions that hold them together polymers also offer tremendous potential as stimuli responsive materials; temperature, pH, redox control and light have all been harnessed to regulate SP assembly.[69-73] To date, SPs have been used for a range of applications including adhesion, inkjet printing, tissue engineering and drug delivery.[74-78]

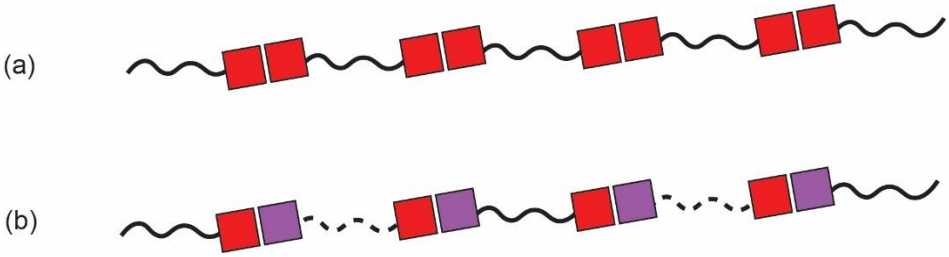

Figure 15. (a) Schematic representing an AA type linear supramolecular polymer consisting of one polymer linked by homodimer HBMs; (b) schematic representing an AB type linear supramolecular polymer comprising of two different polymer types linked by heterodimer HBMs.

HBM homodimers and heterodimers have been widely used for supramolecular polymer assembly (Figure 15).[12, 79-83] One of the first documented SPs was from Lehn *et al*.[84]; this work used complementary triple HBMs in the form of ditopic tartaric acid functionalised with 2,6-diamidopyridine **27** or uracil **28** (Figure 16). The chiral building blocks formed thermotropic liquid crystalline polymer **29** through linear hydrogen bonding. Though these SPs were not particularly stable or complex, the work underpinned the beginning of a new class of polymeric materials.

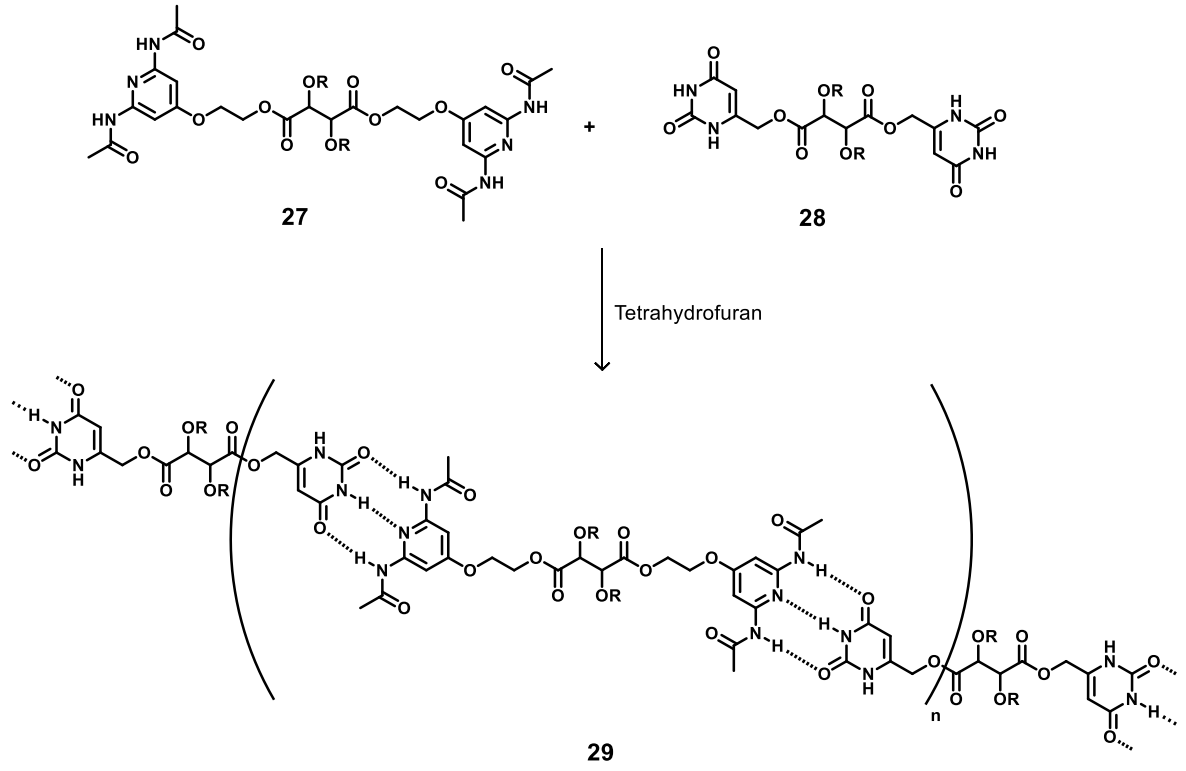

Figure 16. Linear supramolecular polymer **29** constructed from complementary triply hydrogen bonded units presented by Lehn and co-workers. Adapted from [84].

Development of SPs progressed further when Meijer and co-workers introduced the quadruple hydrogen bonding UPy motif **17**.[12] Due to the high UPy·UPy dimerisation constant (>10^5 M^{-1}), SPs with increased stability and higher degrees of polymerisation could be achieved. Ditopic UPy motifs, linked by alkyl chains, were shown to assemble into stable linear polymers in dilute chloroform solutions (Figure 17a,b). The SPs underwent viscosity changes that were dependent on both concentration and temperature. Additionally, when a monofunctional UPy molecule was added to the system, viscosity of the solution was reduced. This observation indicated end-capping of the SP chains, decreasing the degree of polymerisation and subsequently viscosity (Figure 17c). Since the UPy motif can take part in both homo- and heterodimer interactions this motif has been employed in a wide range of both A·A and A·B type linear SPs.[85-87]

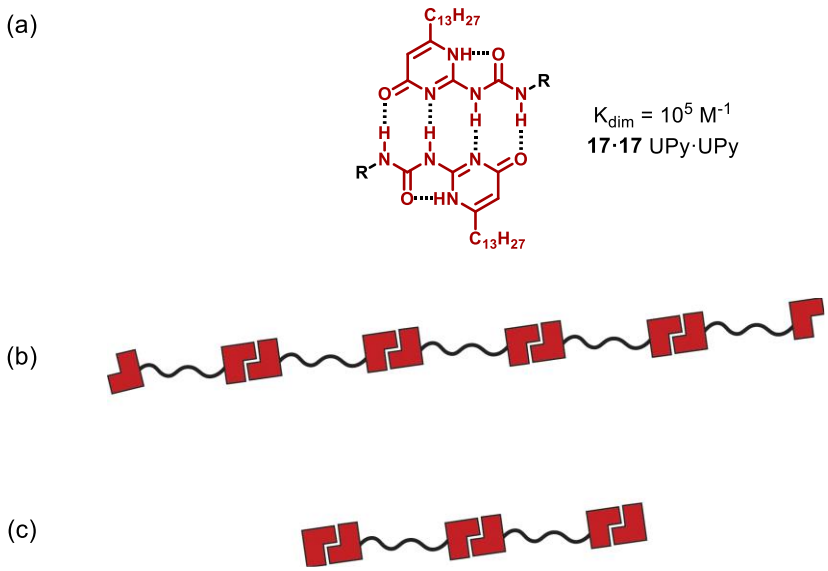

Figure 17. (a) UPy·UPy hydrogen bonding dimer **17·17** and its association constant; (b) representation of the SP polymers formed from dimeric UPy monomers; (c) representation of the chain capped polymers formed when monofunctional UPy is added to the dimeric UPy SPs. Adapted from [12].

In addition to linear polymers, Yan and co-workers demonstrated an example of SPs crosslinked by UPy motifs. This work aimed to fabricate skin-inspired thin film gold electrodes for use in wearable and implantable electronics (Figure 18).[88] The design consisted of two polymer blocks of poly(tetramethylene glycol) and poly(tetraethylene glycol) with incorporated UPy quadruple HBMs. The material exhibited a high resistance to fractures, the ability to stretch to 52 times its original length and was able to hold a weight 16,000 times greater than its own. The material could also be cut into two pieces, then self-heal when put back into contact. These properties are attributed to the strong binding of the UPy dimers, illustrating the kind of complex supramolecular polymers that can be constructed from hydrogen bonding motif interactions.

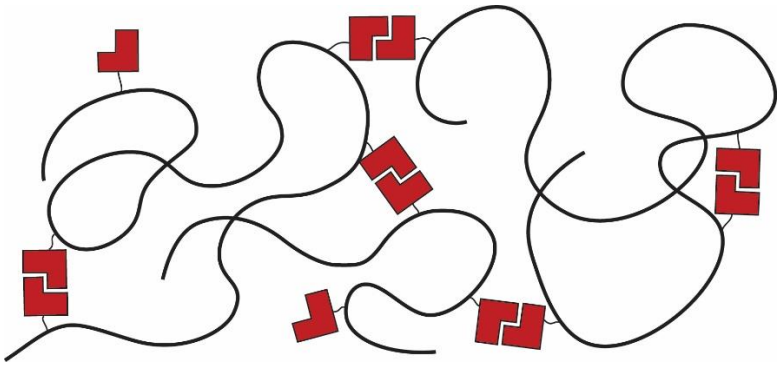

Figure 18. Schematic representing a supramolecular polymer network linked by UPy·UPy hydrogen bonding dimers **17·17**.

1.3.3 Synthesis of hydrogen bonding polymers

To develop complex materials with new and varied properties, polymers can be designed to consist of both covalent polymer chains, and supramolecular functionality. One route to creating such materials is *via* synthesis of covalent polymers with incorporated HBMs, this can be achieved using RAFT polymerisation.[57, 89] A successful example was reported by Wang and co-workers.[90] In this work, block copolymers were synthesised; this kind of polymer is a class of copolymer where chemically distinct monomer units are grouped into discrete blocks. For this example, butyl acrylate was polymerised first to produce poly(butyl acrylate) (PBA) **30**, then a diaminopyridine acrylamide (DAD) co-monomer **31** was added to produce block copolymer **32**.[90]

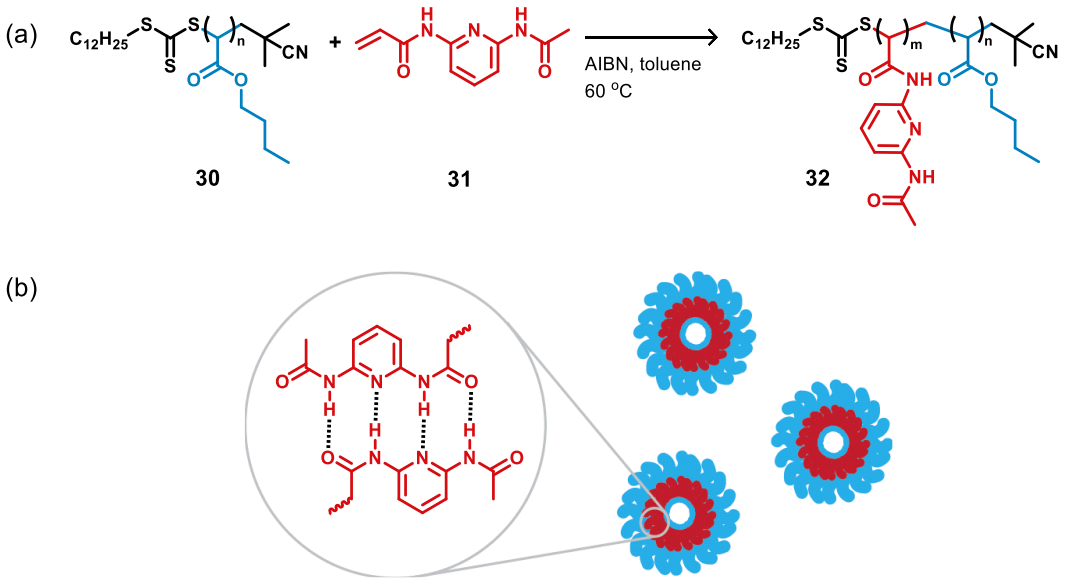

Figure 19. (a) Synthesis of PBA-b-PDAD block copolymer **32** upon addition of a DAD **31** (purple) acrylamide monomer to PBA (blue) macro-CTA **30**; (b) Formation of vesicles in chloroform containing *DADA*·*ADAD* hydrogen bonding within the vesicle walls. Adapted from [87].

The PBA-*b*-PDAD copolymer **32** had well-controlled molecular weight and the hydrogen bonding polymer blocks were able to form self-complementary *ADAD*·*DADA* interactions in chloroform. These homodimer interactions were thought to be responsible for the observed formation of spherical vesicles (Figure 19). This hypothesis was supported by the loss of vesicular aggregation upon introduction of maleimide to the system. The maleimide molecule contains a complementary *ADA* HBM and resulted in social self-sorting, disrupting the homodimer interactions. This kind of work demonstrates that covalent polymers can be adapted to contain HBMs, and that RAFT is a suitable mechanism for the polymerisation of HBM functionalised co-monomers.

Although it is evident that hydrogen bonding covalent polymers can be produced using RAFT, it is important to consider that the addition of a HBM to a conventional monomer species has the potential to change the behaviour of the monomer in polymerisation. Recent work from the Wilson group found that the length of the linker between the HBM and polymerisable moiety can impact the reactivity of the monomer.[91] It was discovered that the functionalisation of a monomer without a linker between the HBM and the conventional monomer can result in the preferential polymerisation of the functionalised monomer over the unfunctionalised monomer. It is likely that this arises due to the electron withdrawing properties of the HBM which aid stabilisation of the radicals formed within the RAFT polymerisation mechanism (Figure 20a). Adding a linker between the HBM and the monomer can prevent this from occurring, and is especially important when synthesising random copolymers, as without the linker the HBM functionalised monomer will be favoured over the conventional monomer and the sequence distribution of the monomers will not be random (Figure 20b,c).

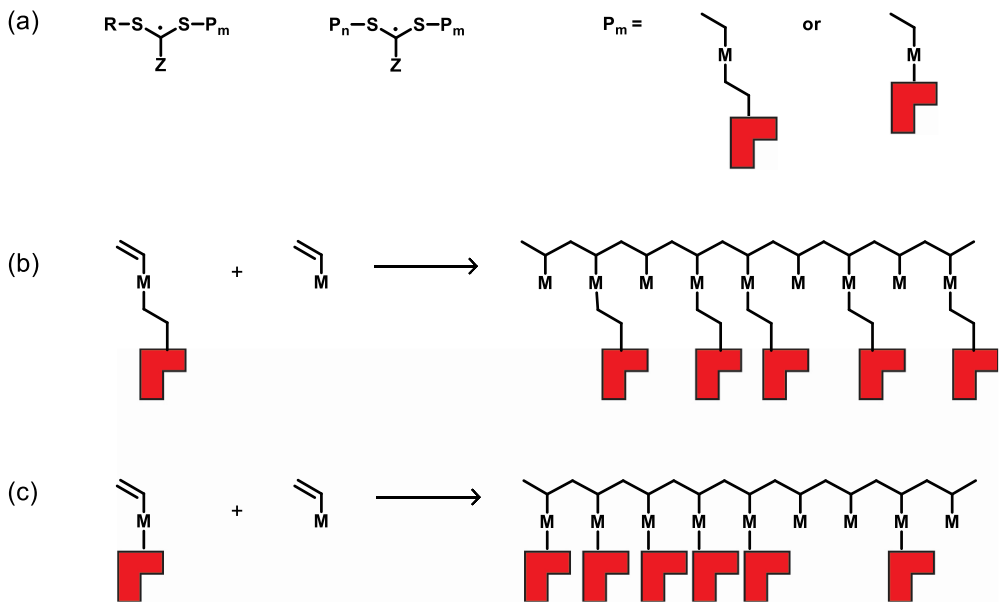

Figure 20. (a) Structures of radical species formed in the RAFT polymerization mechanism. R and Z represent RAFT agent substituents. P_m represents polymerised HBM-comonomer, either with or without an extended linker between the polymerisable moiety (M) and the hydrogen bonding functionality (red blocks); (b) Schematic showing polymerisation of a HBM functionalised co-monomer with a two-carbon linker and the resulting random copolymer; (c) Schematic showing polymerisation of a HBM functionalised co-monomer without a linker and the resulting gradient copolymer.

Another factor to consider is the potential for radical trapping to occur due to the addition of a hydrogen bonding moiety. Previous work has indicated the styrene-AIC co-monomer may act as a radical trapping agent.[92] This can hinder the RAFT process by producing an excess of radicals leading to 'dead' polymer chains, i.e. the chains are no longer able to grow. An

alternative explanation which was also considered was that, the co-monomer could be capping the end of the polymer chains. This is seen in radical trap-assisted atom transfer radical coupling (RTA-ATRC).[93] Using this co-monomer it was difficult to achieve above 6% weight of HBM co-monomer incorporation in the final polymer.

Alternatively, UIM has been used in a methyl methacrylate (MMA) co-monomer and did not show any radical trapping properties; in these polymerisations the *Đ* of the polymers with the incorporated HBM were not significantly different compared to the unfunctionalised polymers.[92] The radical trapping effects are therefore, seen in some HBMs, but not all and such effects will need to be monitored when incorporating any new HBM into polymers. To achieve well controlled polymerisation with high conversion and low *Đ* it is necessary that the co-monomer chosen does not produce significant radical trapping effects.

1.3.4 Reconfigurable polymers

To add a layer of complexity to the materials previously described in this section, orthogonal triggers can be added to develop reconfigurable polymer architectures. One example of such polymers was reported by Sun and co-workers. Here, reversible covalent bonds were utilised to allow for segments of a polymer to be disconnected and reconnected, transforming its structure.[94] Diels-Alder reactions were used to provoke macromolecular reconfiguration within the polymer architectures. A linear amphiphilic block copolymer and hyperbranched polymer were able to 'metamorphosise' into comb, star, and hydrophobic block copolymer configurations. To achieve this, a block copolymer of poly(ethylene glycol) and poly(methyl acrylate) centrally linked by a furan–maleimide cycloadduct **33** was synthesised. The cycloadduct could be broken apart by a retro Diels-Alder reaction, splitting the copolymer into two separate homopolymers. Upon addition of anthracene functionalised polystyrene, due to the more thermodynamically stable anthracene-maleimide cycloadduct **34**, a new hydrophobic copolymer was synthesised. This methodology was used with not only end functionalised polystyrene, but also with a styrene polymer that contained pendent anthracene moieties and a symmetric tri-anthracene core reagent, producing comb and star polymer reconfigurations (Figure 21). Due to the use of covalent linkages, rather than non-covalent these polymeric reconfigurations were not completely reversible. Nevertheless, this work demonstrates the kind of macromolecular reconfiguration that can be achieved by the incorporation of dynamic linkages within polymers.

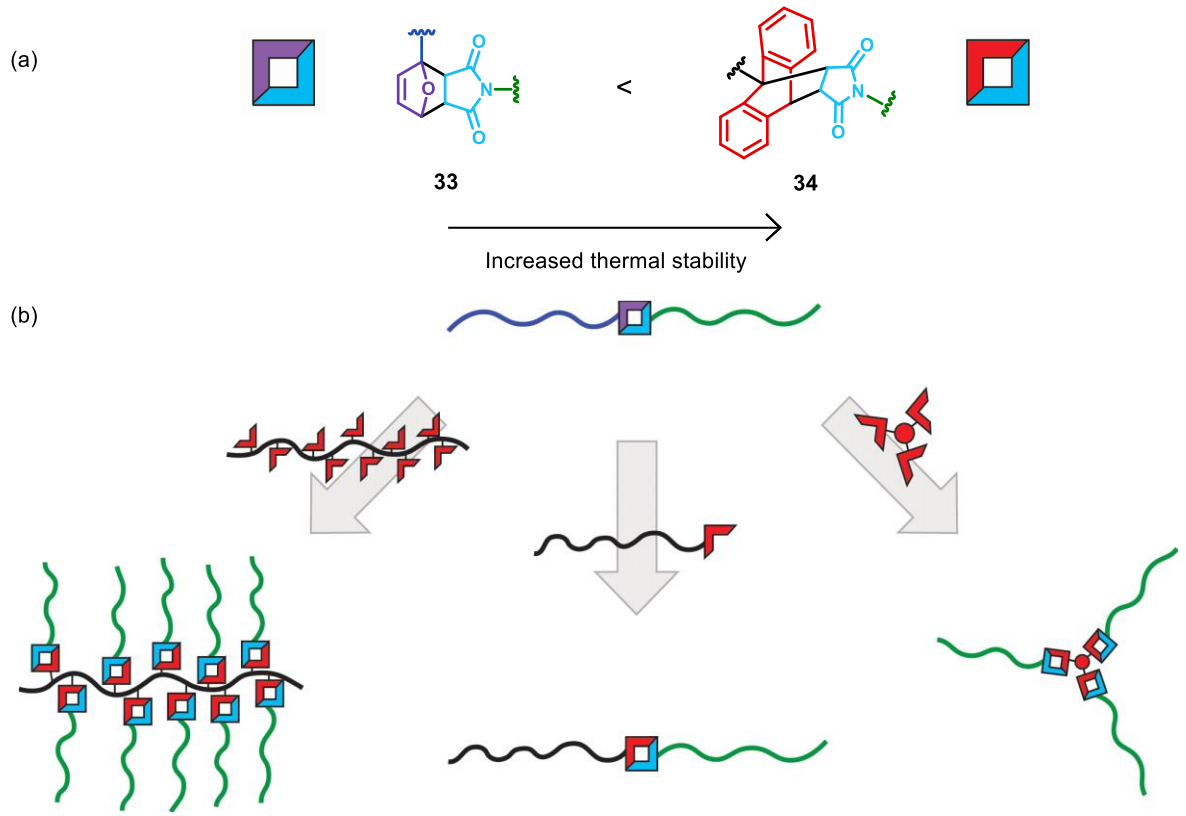

Figure 21. (a) Furan-malemide cycloadduct **33** and anthracene-malemide cycloadduct **34** and the blocks that represent them in the schematic below; (b) Schematic representing reconfigurable polymers starting from a block copolymer of poly(ethylene glycol) (blue polymer) and poly(methyl acrylate) (green polymer) centrally linked by a furan (purple blocks)–maleimide (blue blocks) cycloadduct. The addition of anthracene (red blocks) functionalised styrene (black polymer) results in formation of new polymer structure (left to right: comb polymer, hydrophobic block copolymer, star polymer). Adapted from [92].

An example of polymers which reconfigure by use of non-covalent interactions was reported from Yagai *et al.* In this work, photoresponsive SPs, incorporating both hydrogen-bonding and *π*-*π* stacking interactions were described (Figure 22).[95] Photoresponsive diarylethene molecules were utilised to polymerise and de-polymerise supramolecular copolymers in response to ultraviolet (UV) and visible-light triggers. In its open structure, formed after visible-light irradiation, diarylethene **35** complexed with dimeric stacks of perylene bismide **36**. The conformation adopted by **35a** in this complex resulted in the formation of polymeric helical nanoaggregates. Upon UV light irradiation, diarylethene **35b** continued to form a complex with two **36** guest molecules, however due to the restricted conformation of the closed structure, only dimeric nano-aggregates were formed. This work is a good example of the kind of morphological changes that can be achieved by incorporating both non-covalent interactions and stimuli responsive elements into polymeric materials.

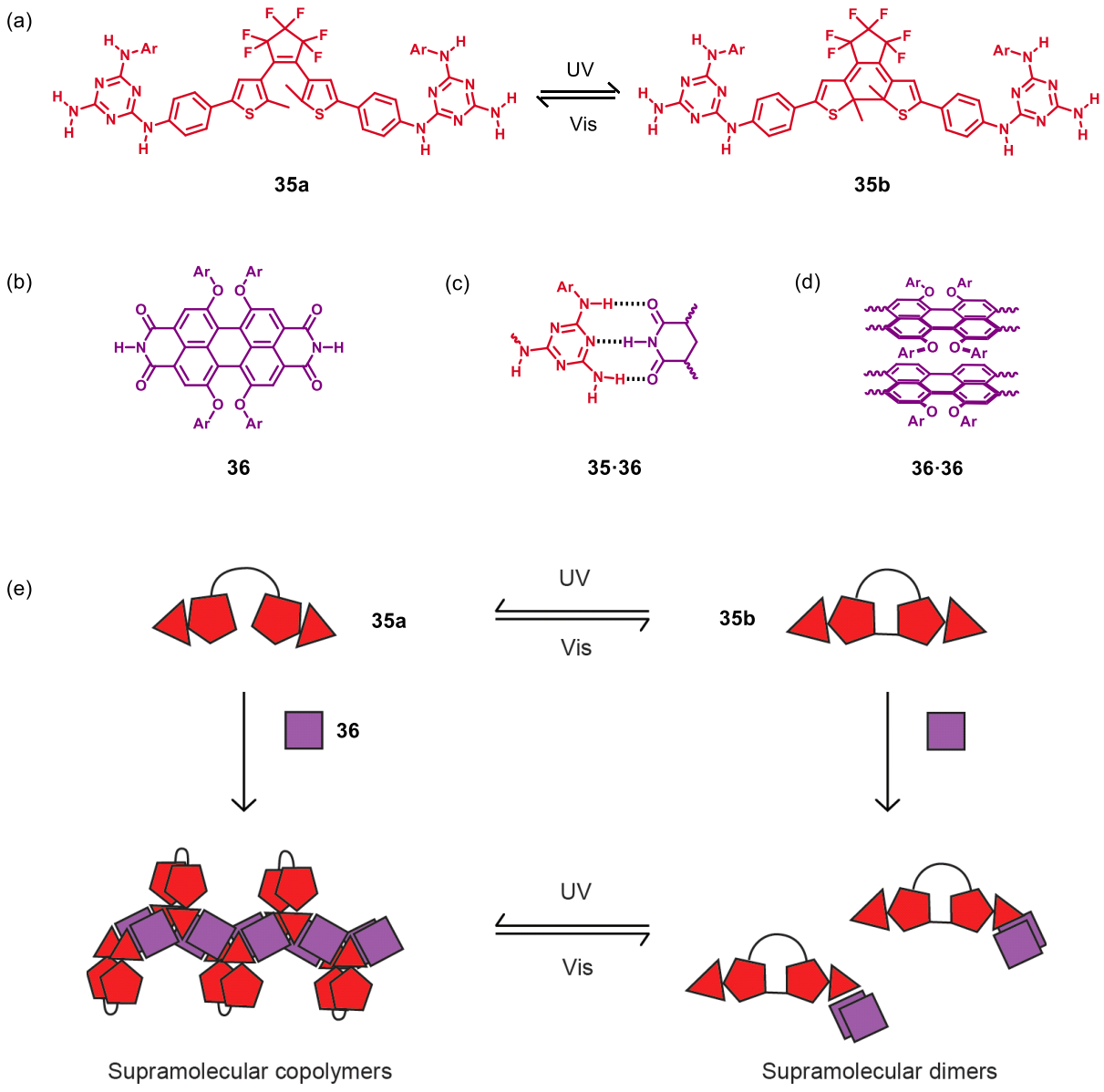

Figure 22. (a) Diarylethene receptor molecule able to switch between open **35a** and closed **35b** states using UV and visible light; (b) ditopic perylene bisimide guest molecule **36**; (c) hydrogen bonding interaction between receptor molecule **35** and guest molecule **36**; (d) *π*-*π* stacking interaction between two **36** guest molecules; (e) schematic representing supramolecular copolymers reversibly reconfigured upon irradiation with UV/visible light. adapted from [91].

Another example of reconfigurable polymer systems was presented by Zhan and co-workers.[96] Here, visible-light responsive hydrogen-bonded SPs were constructed by the self-assembly of ditopic UPy molecules **37** where the HBMs were bridged with a central azobenzene (Figure 23). The architectures and properties of the SPs formed were dependent on the dominant azobenzene isomer. In the *E* isomer, linear SPs were formed, whereas in the *Z* isomer cyclic dimers were preferred at low concentrations and folded SPs formed at high concentrations. The behavior of the *Z* isomer was indicative of a ring-chain polymerisation mechanism. A reversible visible-light initiated sol-gel transformation was observed when

switching between the *Z* and *E* isomers respectively. This work effectively demonstrates that reconfiguration of polymer architectures can result in a change in material properties.

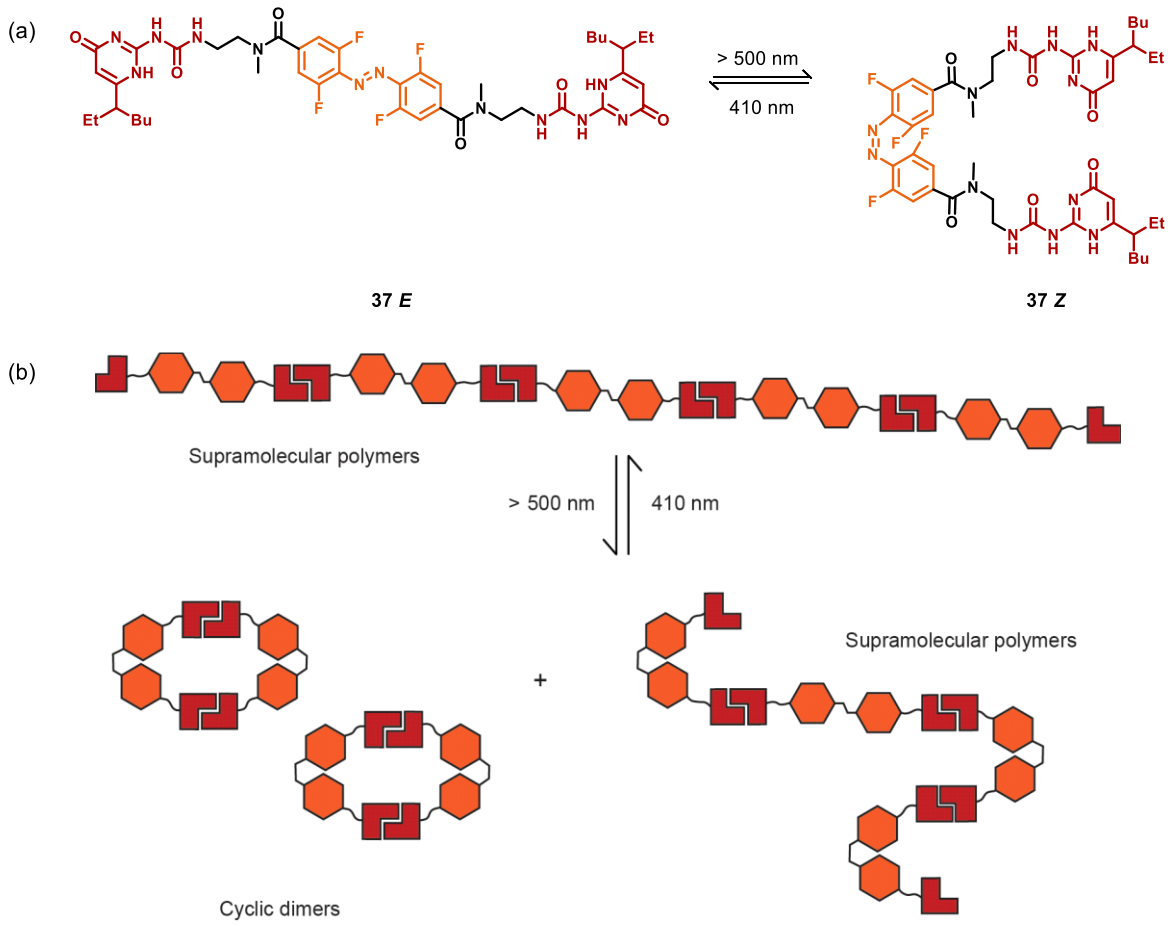

Figure 23. (a) *E* and *Z* isomers of **37** ditopic UPy molecule with central photoresponsive azobenzene; (b) schematic representing photoresponsive reconfigurable SPs produced by Zhan and co-workers.[93]

1.4 Photoresponsive molecules

Whilst using hydrogen bonding alone has been shown to allow complex reconfigurations,[4, 33, 51, 94, 97] we are still far from the advanced materials of natural life. A multicomponent system encompassing self-sorting cascades, supramolecular polymers, polymer self-assembly as well as a stimuli responsive element is therefore of interest.

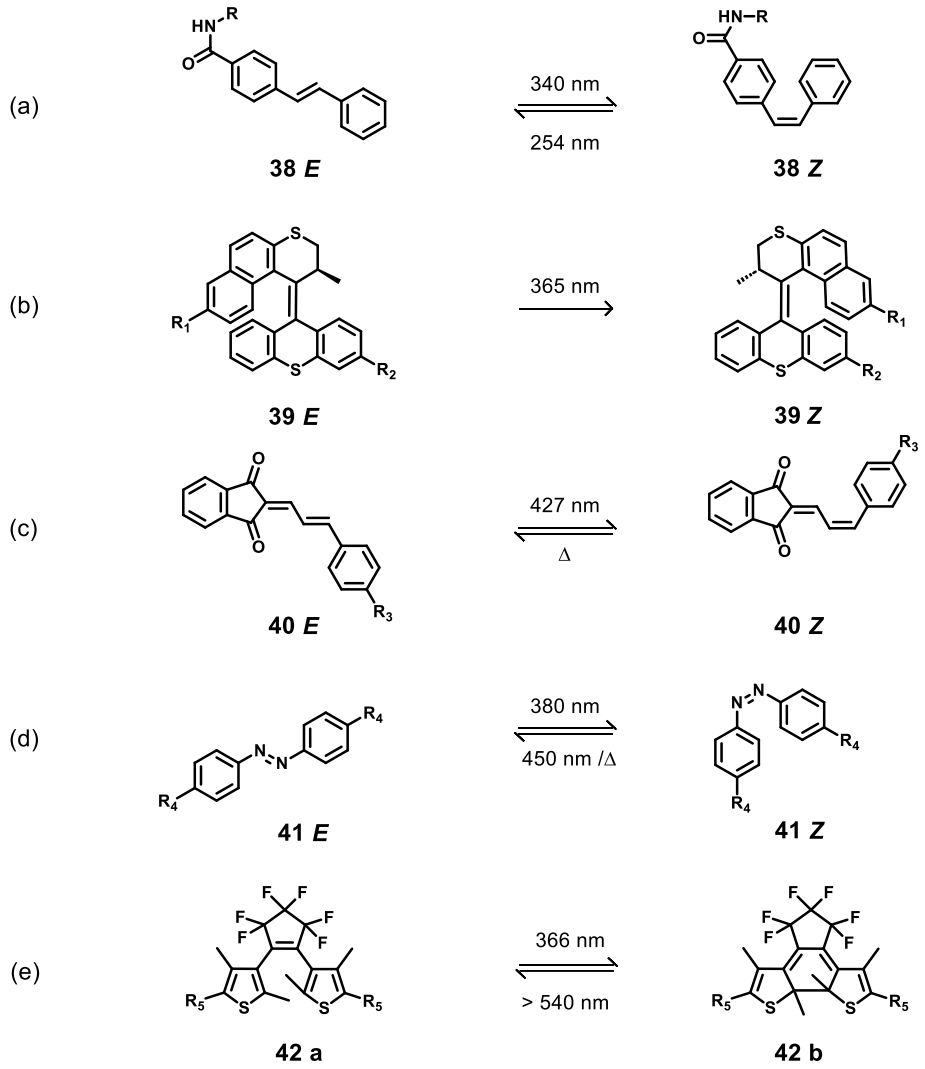

Figure 24. Examples of molecules used in the literature to bring about changes in systems in response to a light stimulus; (a) stilbene **38** capable of photoisomerisation upon irradiation with UV light [102]; (b) 'overcrowded' alkene **39** capable of photoisomerisation irreversibly under UV light [100]; (c) butadiene **40** able to be photoisomerised by visible light [104]; (d) azobenzene **41** able to be photoisomerised by UV light [105]; (e) dithienylethene **42** able to ring-close under UV light and ring-open under visible light.[101]

Stimuli responsive polymer based systems have already been reported within the fields of drug delivery,[98] biosensing,[99] and smart materials.[100] In these examples different kinds of stimuli, including pH, temperature and mechanical force have been used. An alternative, and

potentially more favourable stimuli, to those already mentioned, is light. Light is one of the most desirable stimuli due to its ability to induce a fast response and be remotely activated and controlled without introducing any extra chemicals to the system.[101, 102] In order to harness the potential of a light stimulus, a photoresponsive species needs to be incorporated into the system. Some examples of such photoresponsive molecules include dithienylethenes, stilbenes, alkenes, butadienes and azobenzenes.[103-109] These molecules will undergo a change in conformation/configuration if a particular wavelength of light is introduced into the system where they are present (Figure 24). Photoresponsive molecules have also been reported within supramolecular architectures as being able to effect remarkable responses such as, reversible polymerisation,[104, 105] development of complex supramolecular assemblies,[106] and formation of gels, liquid crystals and well-defined aggregation states.[107-110]

1.4.1 Azobenzenes

Azobenzenes are a class of photoresponsive molecules that can be used in stimuli responsive self-sorting systems.[97] Their ability to photoisomerise between structurally distinct *E* and *Z* isomers (Figure 25a), as well as being highly fatigue-resistant, is what makes them interesting for use within such systems.[111] The previously mentioned example from Tan *et al.*, showed switching between linear and folded SPs. Additionally, azobenzene moieties within SPs have been reported to be instrumental in reconfigurations responsible for switching a system between gel and solution,[112, 113] and reversible self-assembly of block-copolymers.[114]

There are some drawbacks associated with the use of azobenzenes, one being that the unfunctionalised species do not show complete conversion between isomers. The half-life of most *Z* isomer derivatives at room temperature is only a few hours.[102] This makes polymers of near pure *Z* isomers hard to synthesise and study. Additionally, it is typically observed that once isomerisation to the *Z* isomer has occurred, the reversal to the *E* isomer is also incomplete. This is because of the visible region n→π^* bands in both the *E* and *Z* isomers overlapping.[101] As well as the difficulties in producing pure isomers, there are also limits to the practicality of the use of azobenzenes in biological and materials sciences. This is due to the use of UV light, which is necessary to induce isomerisation *via* $\pi \rightarrow \pi^*$ excitation, but also has the potential to interfere with and destroy the surrounding environment.[101]

One solution to the issues associated with azobenzene switching capabilities is to modify the molecule so that n→π^* bands of the *E* and *Z* isomers are separated.[115] Bléger *et al.* synthesised a range of *ortho*-fluorinated azobenzenes (*o*-fluoroazobenzenes) and found that the addition of fluorine atoms resulted in a photoresponsive species with larger separation in the n→π^* band between isomers.[101] This was noted to be due to the *ortho*-fluorine atoms

reducing the electron density in the N=N bond which in turn lowers the n-orbital energy. These *o*-fluoroazobenzenes (**44**, Figure 25b) were able to switch back and forth from *E* to *Z* upon irradiation with visible light. The species also showed the ability to selectively switch between isomers with high to complete levels of photoconversion, as well as showing half-lives of almost 2 years in the *Z* isomer at 25 °C.

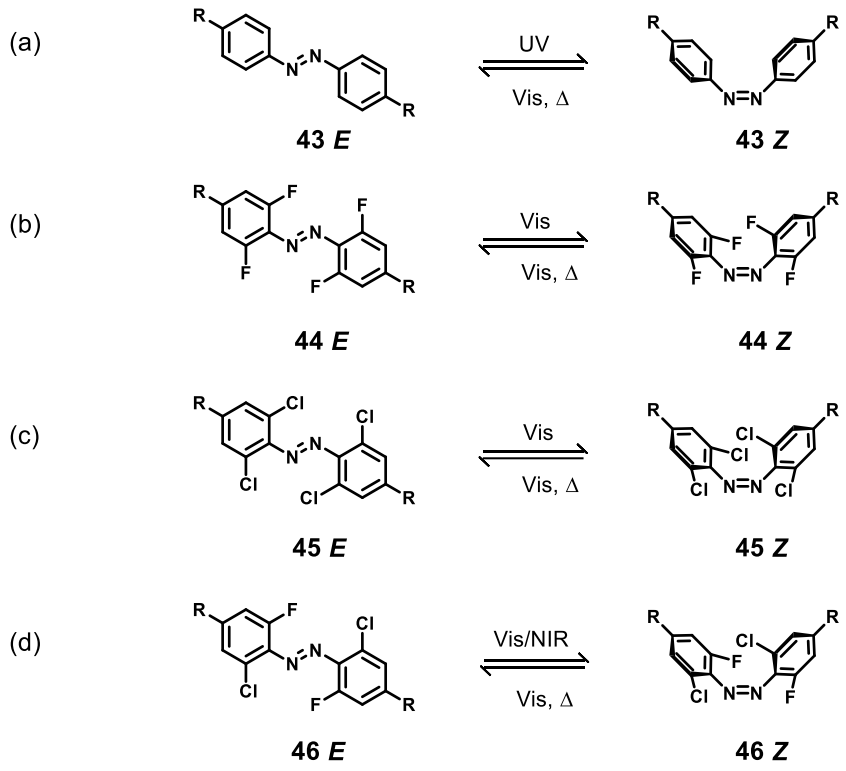

Figure 25. (a) Azobenzene **43** photoisomerised from *E*→*Z* by UV light and *Z*→*E* by visible light or heat [108]; (b) o-fluoroazobenzene **44** switched between the *E* and *Z* isomers upon irradiation with visible light[98]; (c) *o*-chloroazobenzene **45** switched between the *E* and *Z* isomers upon irradiation with visible light [113,114]; (d) *o*-chlorofluoroazobenzene **46** switched between the *E* and *Z* isomers upon irradiation with visible light or near-infrared light (NIR).[115]

As well as *o*-fluoroazobenzenes, there has been increasing interest in further red-shifted azobenzenes. Since *ortho*-chlorinated azobenzenes (*o*-chloroazobenzenes) (**45**, Figure 25c) also split the n→*π** bands, they have been studied for this purpose.[116,117] The splitting of the n→*π** in *o*-chloroazobenzenes has been attributed to the chlorine atoms facing toward the nitrogen lone pairs, this repulsive interaction is said to destabilise the n-orbital which, in turn, decreases the energy gap to the *π** orbital. The structure of the *Z* isomer allows the chlorine atoms to face in the opposite direction to the nitrogen lone pairs, hence why it becomes more favourable than the unsubstituted version.[118] Irradiating with visible light at the far ends of the n→*π** bands in *o*-chloroazobenzenes is able to produce significant *Z* content when using bright light sources and continuous irradiation, the literature states that the *Z* isomer is stable for around 20 hours at 70 °C.[118] There have also been investigations into substituting two of

the fluorine atoms in *o*-fluoroazobenzenes for chlorines (**46**, Figure 25d), the n→*π** separation in these *o*-chlorofluoroazobenzenes was even greater and when the excitation band tails were irradiated efficient photoswitching was observed. After prolonged exposure to light at 660 nm the *Z* isomer was observed in high quantities with a thermal half-life of 16 hours at 70 °C.[118] This is particularly interesting as 660 nm is in the near-infrared region which falls within the bio-optical window.

1.4.2 Foldamers

Foldamers can be generally defined as oligomers or polymers that adopt well defined biomimetic and abiotic secondary, tertiary and quaternary structures.[119, 120] They have been used to recognise small molecules or biomacromolecules.[121-127] Regulation of foldamer function through switching is feasible where folding is driven by co-operative non-covalent interactions; several stimuli have been used to switch between unfolded and folded forms[128] including acid/base,[129] cations,[130] anions,[131, 132] redox state[133] and light.[134] In this work, we aimed to use photo-responsive foldamers to initiate reconfigurations in hydrogen-bonding polymers.

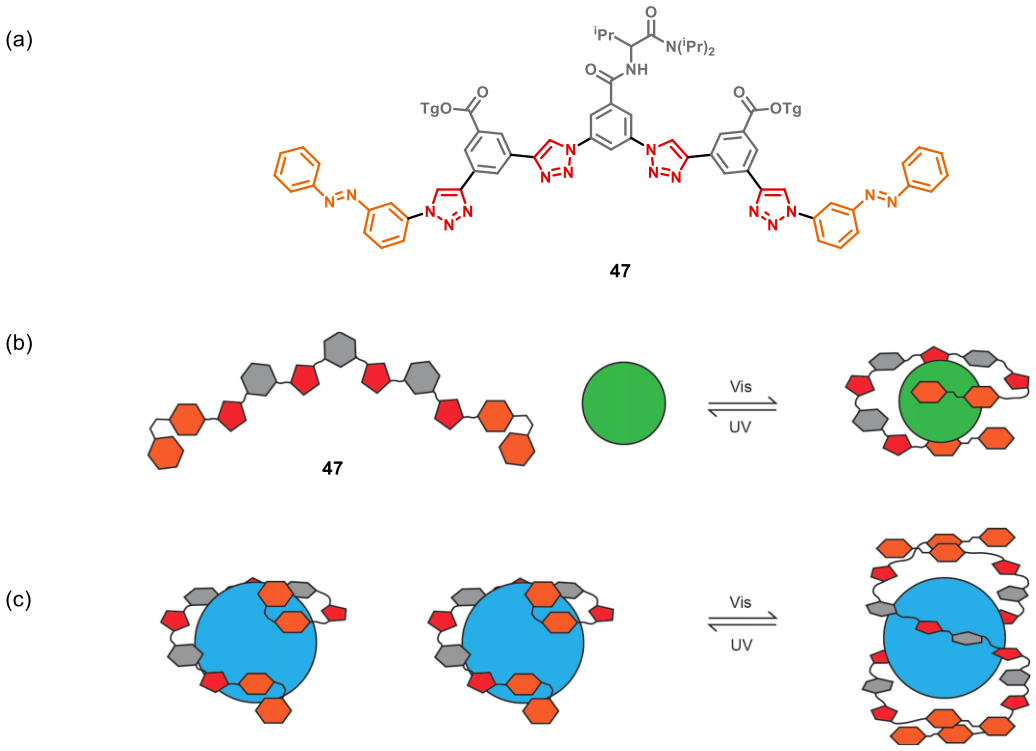

Figure 26. (a) Structure of photoresponsive foldamer **47**; (b) schematic representing the folding and unfolding of foldamer **47** in the presence of a small anion guest (Cl^-, Br^-, NO_2^-, I^-, NO_3^-); (c) schematic representing the folding and unfolding of foldamer **47** in the presence of a large anion guest (SCN^-, BF_4^-, ClO_4^-, ReO_4^-, PF_6^-, SgF_6^-). Adapted from [131].

An example a photoresponsive foldamer was recently reported by Parks and co-workers.[134] In this work, a foldamer was constructed with two terminal azobenzenes (Figure 26a). Anion guests were used as allosteric regulators, with different sized guests controlling foldamer quaternary structure. With no guest, an extended conformation with no defined structure was adopted by foldamer **47**. When a small anionic guest was introduced, single helices were observed, upon UV irradiation the anionic guest was released (Figure 26b). Larger anions guests resulted in photoresponsive switching between chiral double helices and racemic single helices (Figure 26c). This work demonstrated the significant structural changes that can be achieved by using photoresponsive foldamers.

Another photoresponsive foldamer molecule that utilises the properties of a central *o*-fluoroazobenzene moiety was reported (**48**, Figure 27).[135] This foldamer also incorporates triple HBMs in the form of pyridylurea (*ADD*) and amidonaphthyridine (*DAA*). These HBMs are able to interact narcissistically whilst the azobenzene is in the *Z* configuration and become available to socially self-sort when the azobenzene is in the *E* configuration.

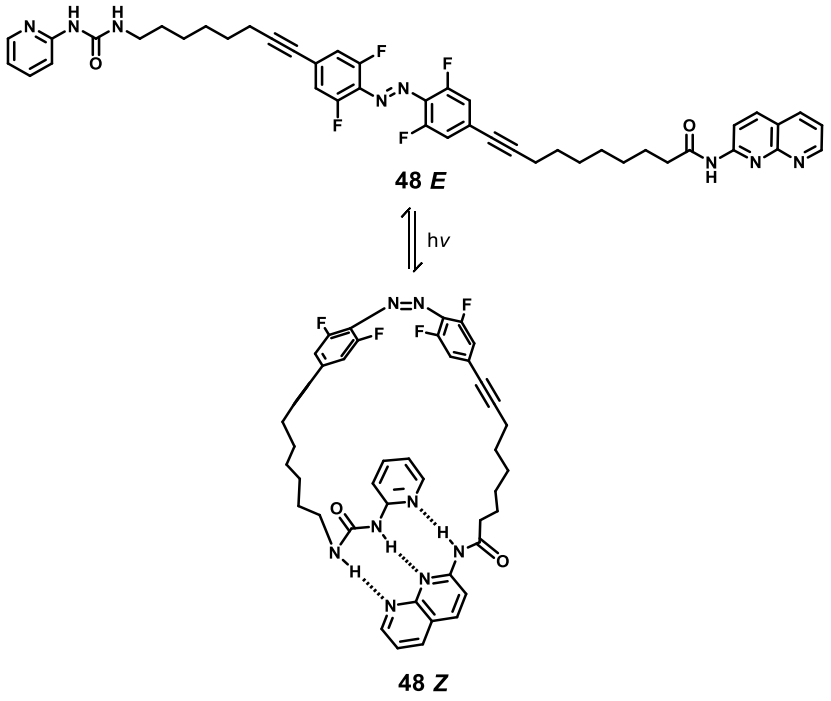

Figure 27. Foldamer **48** reported by Opie and co-workers. Adapted from [132].

Linked by flexible alkyl chains, foldamer **48** was shown by NMR and size exclusion chromatography to form a globular folded structure linked by the *ADD·DAA* HBMs when in the *Z* confirmation. This molecule showed promising results as a photoswitch with good isomeric ratios of the photostationary states. The *Z* isomer showed 80% conversion after excitation with visible light at $\lambda > 510$ nm for 10 minutes, and the *E* isomer, 85% after irradiation at $\lambda =$

410 nm for 15 minutes. Due to its stability in each confirmation, and readily incorporated hydrogen-bonding recognition patterns, this foldamer design was of interest for use in this project.

1.5 Conclusion and Project Aims

Supramolecular polymers have transformed materials chemistry.[136-139] Such polymers offer tremendous potential as stimuli responsive materials, due to the dynamic nature of the non-covalent interactions that hold them together. This work focuses on producing polymeric structures with tuneable functionality *via* incorporation of photoresponsive molecules into hydrogen-bonding supramolecular polymers. Whilst single chain folded supramolecular polymers have been reported,[140, 141] the development of self-assembled foldamers is less explored.[142-146] Therefore, the self-assembly of photoresponsive hydrogen-bonding foldamers was explored in this work. Using foldamers presents the opportunity to exploit the folded and unfolded configurations to bring about changes in polymer architecture.

This chapter has introduced the topic of hydrogen bonding motifs, the factors that control their interactions and their use in self-sorting supramolecular systems. Additionally, polymeric materials and photoresponsive molecules have been described with appropriate literature examples. The following chapters discuss the avenues taken toward achieving stimuli-responsive reconfigurable polymers. Chapter 2 examines the syntheses of photoresponsive hydrogen-bonding foldamers with the aim to use such molecules as both monomeric units for supramolecular polymers, and to regulate polymer architecture. In addition to the syntheses, the photoisomerisation and characterisation of such foldamers is detailed. Chapter 3 details efforts to develop reversibly assembled supramolecular polymers formed by the hydrogen bonding foldamers synthesised in chapter 2. Here, multistate supramolecular assemblies that reconfigure in response to visible light are reported. Finally, chapter 4 discusses the synthesis and development of HBM functionalised covalent polymers. In addition to the synthetic efforts, reconfigurations of these polymers are explored, by the addition of photoresponsive foldamers to the systems.

The overall aim of this work is to develop polymeric systems which can reconfigure their architectures in response to external stimuli. To achieve this, polymers with incorporated hydrogen bonding motifs and photoresponsive azobenzenes will be utilised. Developing polymers able to alter their material properties in response to light stimulus will provide a platform to achieve a new generation of complex ‘smart’ materials which can reconfigure using self-sorting.

2. Synthesis and characterisation of photoresponsive hydrogen-bonding foldamers

Folding is a process nature uses for many important biological processes including controlling the conformation of its macromolecules, enzyme catalysis, information storage and replication in nucleic acids, and energy capture and conversion.[147] To develop mimics of the well-defined conformations formed by biopolymers in nature, synthetic foldamer molecules can be used.

In this work, we sought to use light as a stimuli to regulate foldamer conformation and therefore assembly due to its ability to induce a fast response and remote activation/control without recourse to the addition of further reagents.[148] We selected azobenzenes; commonly used photoswitches that benefit from the ability to switch rapidly and without photo-fatigue.[102, 111, 149-151,150,151] Whilst unsubstituted azobenzenes are photoisomerised under UV light, *o*-tetrafluorinated azobenzenes are effectively isomerised using visible light. In addition, *o*-tetrafluorinated azobenzenes have been shown to exhibit long half-lives (over 2 years) in the less thermodynamically favourable *Z* isomer and are synthetically relatively easy to access.[101] A molecule incorporating a visible light activated photoswitch and two complementary hydrogen bonding motifs would provide the key elements for the development of a stimuli responsive foldamer capable of further self-assembly.

As described in chapter 1, Opie and co-workers designed a scaffold comprising a central *o*-tetrafluorinated azobenzene moiety appended with pyridylurea (Pyr) and amidonaphthyridine (NAP) triple HBMs (Figure 28).[135] These HBMs were shown to associate intramolecularly when the azobenzene adopts the *Z* configuration but could not engage in intermolecular hydrogen-bonding with the azobenzene in the *E* configuration. The *Z* isomer showed 80% conversion after excitation with visible light at $\lambda > 510$ nm, and the *E* isomer, 85% after irradiation at $\lambda = 410$ nm. This foldamer design was deemed of interest for our research due to the high ratios of the photostationary sates (PSSs) after irradiation and the reported excellent stability of each confirmation.

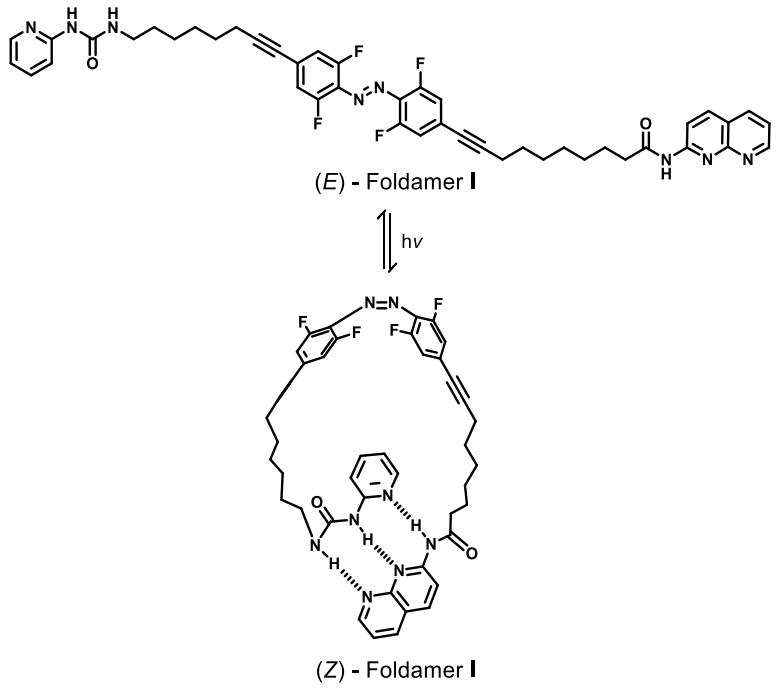

Figure 28. *E* and *Z* isomers of photoswitchable hydrogen-bonding foldamer **I** (previously **48**) reported by Opie and co-workers.[132]

2.1 Synthesis of hydrogen bonding foldamers

Due to the relatively low Pyr·NAP **11·12** dimerisation affinity (K_a ~ 30 M^{-1}).[27] We considered the possibility that formation of a supramolecular from foldamer **I** may be unlikely. Therefore, alternative HBMs, which dimerise with higher association constants, were considered for incorporation into the same photoresponsive scaffold (Figure 29).

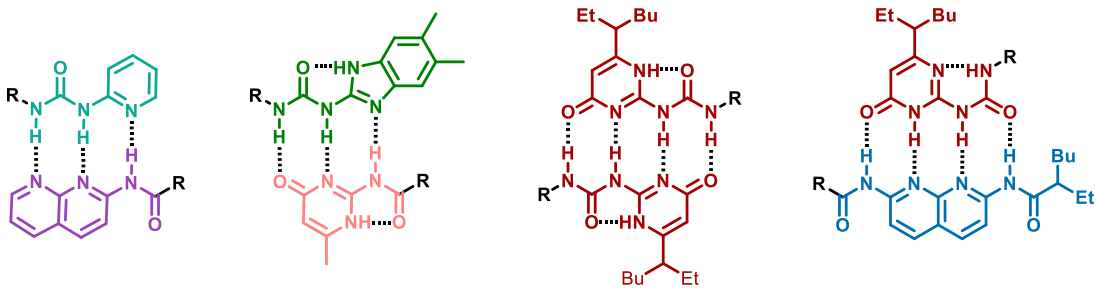

Figure 29. Hydrogen bonding motifs proposed for use in foldamers, and their association constants. Literature K_a and K_{dim} values determined by ^{1}H NMR titration in $CDCl_3$.[18, 27, 145]

This led to the design of three novel foldamers. Foldamer **II** contained uriedobenzimidazole (UIM) and aminocisocytosine (AIC) HBMs. Although the donor-acceptor patterns are the same

as foldamer **I**, the HBMs in foldamer **II** are preorganised for binding and able to exhibit conformer independent hydrogen bonding (Figure 30). In contrast, foldamer **I** contains an intramolecular hydrogen bond which disfavours heterodimerisation, meaning the association constant for the interaction of UIM·AIC **7·8** is likely to be greater than that of Pyr·NAP **11·12**.[152, 153] For foldamers **III** and **IV**, quadruple HBMs that exhibit association constants ~ 10^6 M^{-1} were selected.[154] Foldamer **III** contained two ureidopyrimidinone (UPy) motifs, and foldamer **IV** contained UPy and diamidonaphthyridine (DAN) motifs.

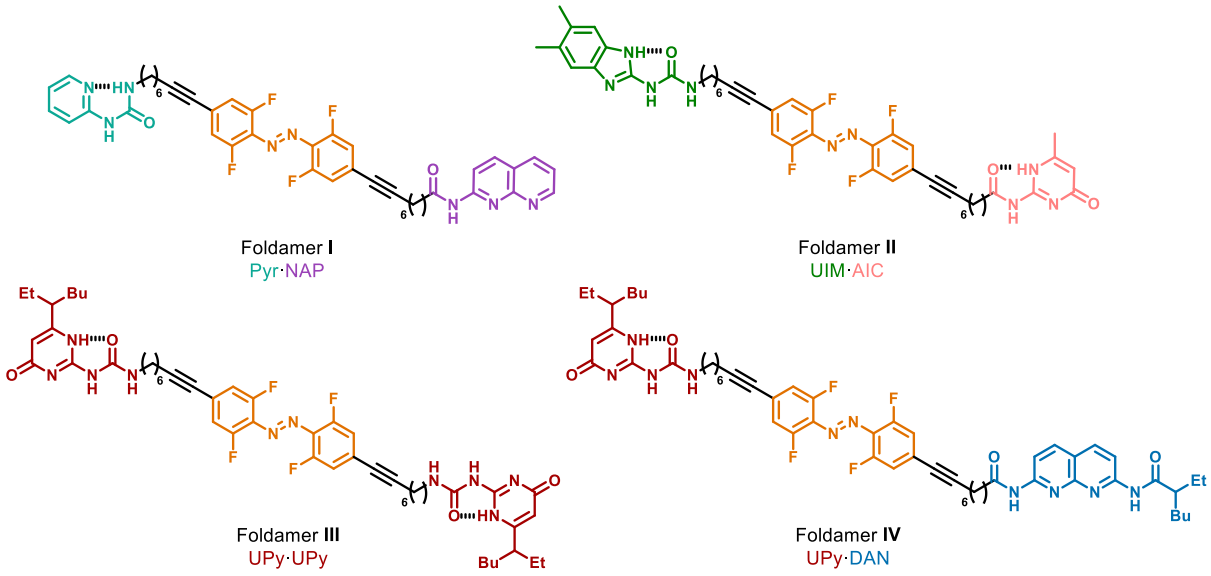

Figure 30. Structures of foldamers **I**-**IV**. Foldamer **I** from Opie et al.[132] Foldamers **II**, **III** and **IV** designed in this work.

2.1.1 NAP·Pyr foldamer I

The convergent synthesis of foldamer **I** (Scheme 1) was adapted from the pre-established synthetic procedure described by Opie and co-workers.[135] The *o*-tetrafluorinated azobenzene **52** was obtained by oxidation of bromoaniline **49** to the corresponding nitrosobenzene **50** and subsequent Baeyer-Mills reaction with 2,6-difluoro-4-iodoaniline **51**.[155] Each hydrogen bonding alkyne linker was obtained by preparation of 8-noynoic acid **52** from 7-bromoheptanoic acid **53**. For pyridyl urea linker **56**, an isocyanate was generated *in-situ* from 8-noynoic acid **54** by reaction with diphenylphosphoryl azide, upon addition of 2-aminopyridine **55**, linker **56** was afforded. Aminonapthyridine **59** was prepared from 2,6-diaminopyridine **57** and then used to prepare naphthyridine linker **60** *via* an amide coupling reaction, with 8-noynoic acid **54**. Finally, two successive Sonogashira reactions gave **61** and then foldamer **I**. The only minor change made from the literature procedure was switching coupling agent HBTU for EDC when synthesising alkyne **60**; this alteration aided purification.

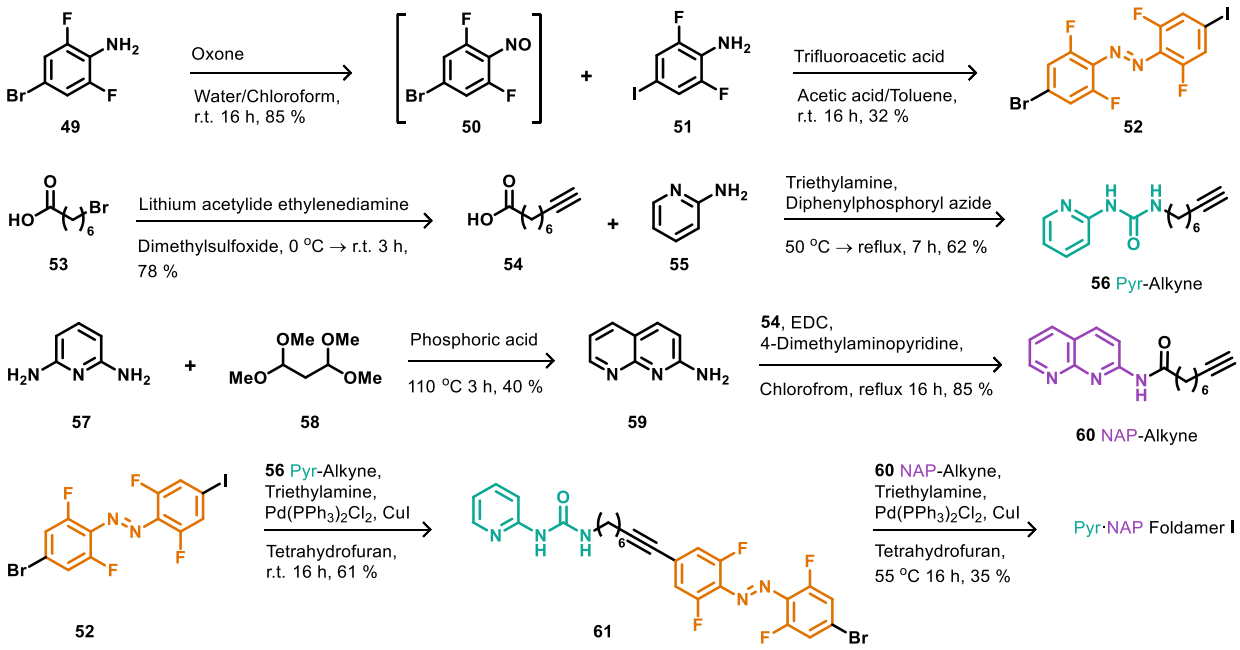

Scheme 1. Synthesis of foldamer **I**, conitaing pyridylurea (Pyr) and amidonaphthyridine (NAP) triple hydrogen bonding motifs.[132]

2.1.2 UIM·AIC foldamer II

Synthesis of UIM·AIC foldamer **II** was attempted *via* a similar route to foldamer **I** (Scheme 2). Here, alkyne **63** was synthesised by amide coupling of 8-noynoic acid **54** with amine **62**. Alkyne **66** was prepared *via* the addition of **65** to *in-situ* generated isocyanate **64**. Finally, two successive Sonogashira reactions gave **67** and then foldamer **II**. Although high-resolution mass spectrometry (HRMS) analysis provided evidence that UIM.AIC foldamer **II** was synthesised, the purification of the foldamer presented a significant challenge. It was not possible to identify a suitable solvent system that would both dissolve the foldamer and give separation from the starting material. Foldamer **II** therefore, could not be isolated.

Due to the hydrogen bonding motifs in foldamer **II** exhibiting the same array of acceptors and donors as those in foldamer **I**, the synthesis of this foldamer was explored no further given the availability of alternative ditopic photoswitchable HBM foldamers for characterisation (foldamer **IV**). Instead, efforts turned to the synthesis of quadruple hydrogen bonding foldamers which would have an even greater variation in association constant between the hydrogen bonding moieties when compared to Pyr·NAP foldamer **I**.

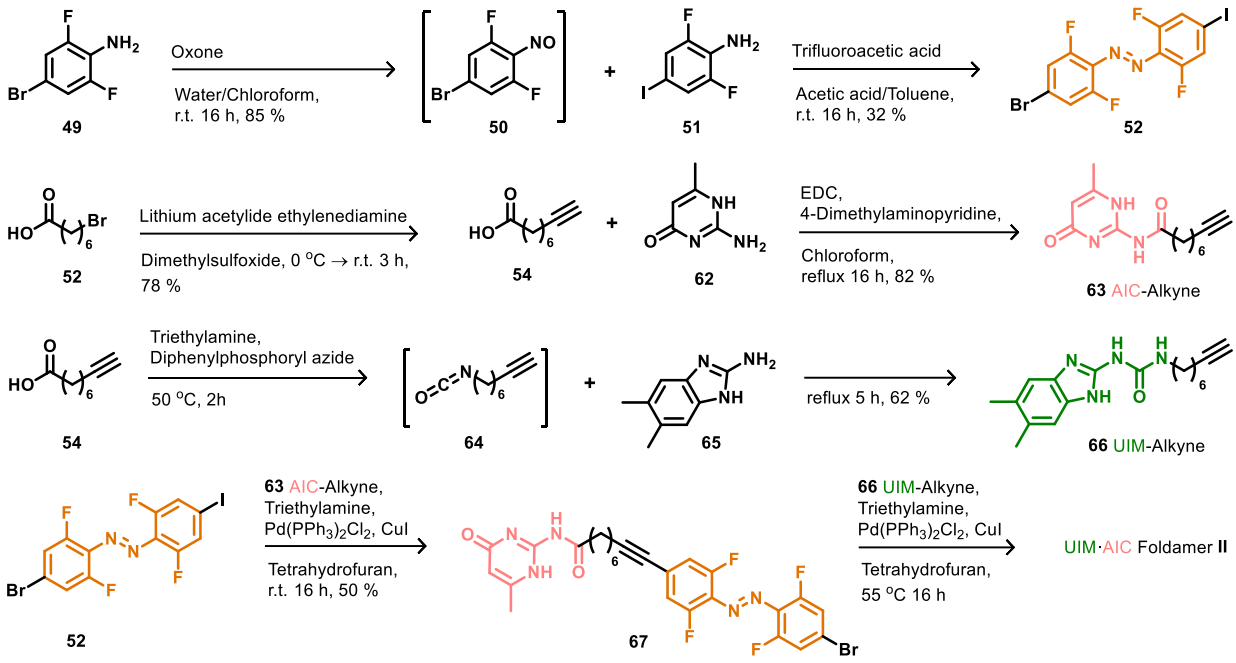

Scheme 2. Attempted synthesis of foldamer **II**, conitaing the ureidoimidazole (UIM) and aminoisocytosine (AIC) hydrogen bonding motifs.

2.1.3 UPy·UPy foldamer III

Despite being symmetrical, foldamer **III** was synthetically more challenging. It was possible to synthesise the UPy-functionalised alkyne **69** *via* a similar route to that followed for urea linkers **63** and **66** (Scheme 3). In an attempt to improve yields and reduce the number of synthetic steps, diiodo-*o*-tetrafluorinated azobenzene **70** was synthesised from aniline **51**. However, upon attempting a double Sonogashira coupling, foldamer **III** was produced only in low yield and could not practicably be isolated.

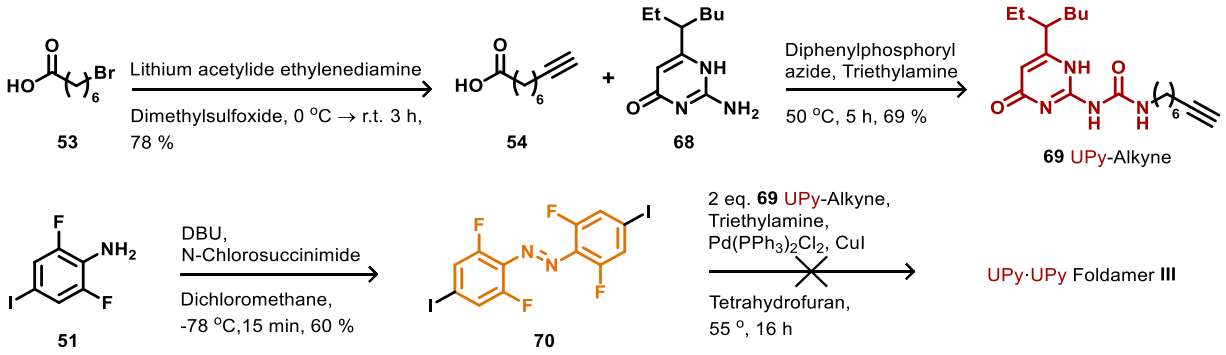

Scheme 3. Attempted procedure for the synthesis of UPy·UPy foldamer **III** using diiodo-azobenzene **70**.

To explore if the reactivity of the diiodo-*o*-fluorinatedazobenzene **70** was associated with low yield of foldamer **III**, the synthesis was carried out using *o*-tetrafluorinated azobenzene **52** in multiple steps (Scheme 4). The first coupling was successful, producing **71** in 60% yield. The

second Sonogashira reaction was, however, much less successful with very little conversion to product observed (~1 %, determined by ^{1}H NMR).

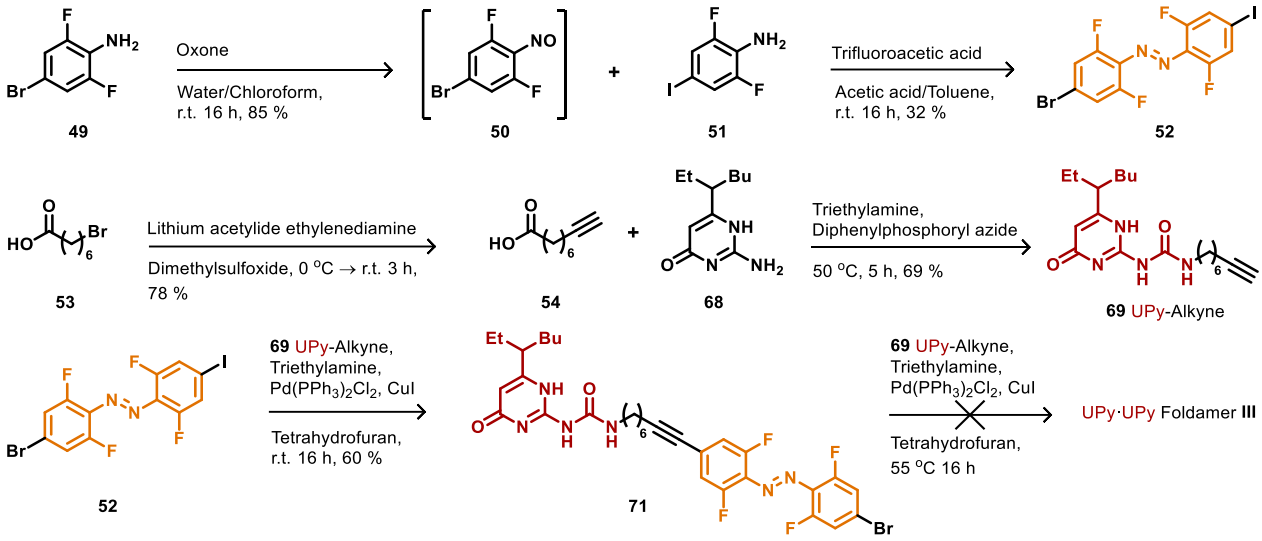

Scheme 4. Attempted procedure for the synthesis of UPy·UPy foldamer **III** using iodobromo-azobenzene **52**.

In order to circumvent the unsuccessful Sonogashira reaction, 8-nonynoic acid functionalised azobenzene **72** was synthesised. A Curtius rearrangement between azobenzene **72** and **68** was attempted but foldamer **III** was not produced (Scheme 5).

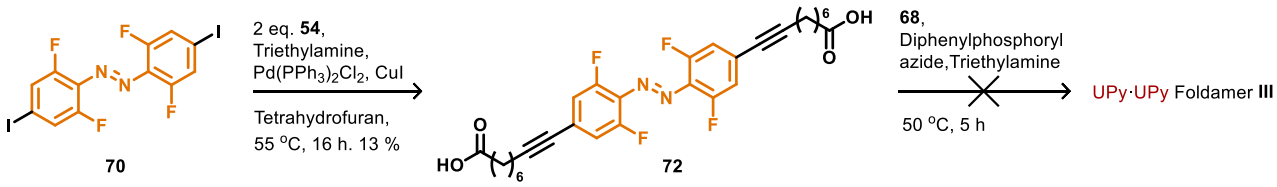

Scheme 5. Attempted synthesis of UPy·UPy foldamer **III** performing a Sonogashira reaction first, then a Curtius rearrangement.

The next avenue explored was the synthesis of UPy-aniline **73** at the outset of the synthetic procedure, then *via* the same route as diiodo-azobenzene **70**, the synthesis of foldamer **III** was attempted (Scheme 6). Crude ^{1}H NMR analysis provided evidence of foldamer **III** formation. However, conversion to product was minimal, and difficult purification further worsened this.

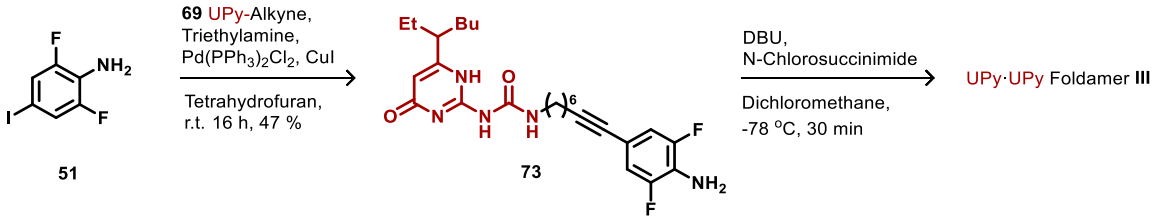

Scheme 6. Attempted synthesis of UPy·UPy foldamer **III** synthesising UPy-aniline **73** first, then the azobenzene moiety.

After some consideration, we hypothesised that the low conversion to product in the original approach (Scheme 6) was associated with homo and heteroassociation between **69** and **71** observed and that such interactions might sterically impede appropriate orientation for coupling to occur (Figure 31). The more facile synthesis of foldamer **I** is congruent with this theory with a much weaker association occurring between Pyr·NAP than UPy·UPy dimerisation. Another potential challenge identified was the low reactivity of bromide substrates in Sonogashira reactions. To test our hypotheses and further explore the conditions required for synthesis of foldamer **III**, a screen of alternative solvents and catalysts was performed (Scheme 7). Polar solvents were selected to suppress hydrogen bonding interactions between UPy functionalised molecules **69** and **71**. Catalysts were selected by examination of the literature. [156,157]

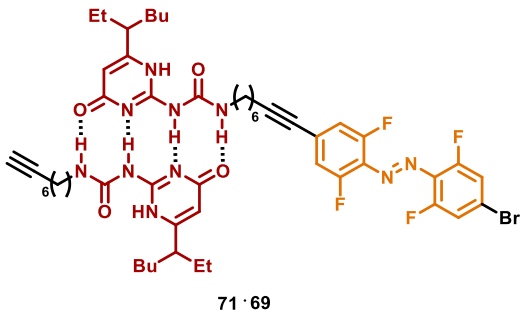

Figure 31. Proposed hydrogen bonding interaction between UPy alkyne **69** and UPy azobenzene **71** that may prevent UPy·UPy foldamer **III** synthesis.

Studies from Shilz and Plenio found that the presence of electron-withdrawing groups at the *ortho* positions on aryl bromides accelerate the rate of the Sonogashira coupling.[156] This electronic effect was thought to be more important than any moderate steric bulk at the aryl bromide. The presence of fluorine groups, which may be acting in an electron-donating manner, on our aryl bromide, could be a factor that reduced Sonogashira reaction rate. Although the use of *ortho*-fluorine atoms was unavoidable in this case, another factor identified to influence product yield was the choice of phosphine ligand. It was established that a combination of Na_2PdCl_4, with a relatively sterically bulky phosphine (tBu_3P) was most suitable

for sterically unhindered acetylene substrates.[156] Since our acetylene fitted this category, this catalyst combination was tested in our screen.

Another palladium catalyst identified, was the bidentate $PdCl_2(dppf).CH_2Cl_2$ complex. Bidentate ligands have been reported to exclude halides from the coordination sphere, supress β-hydride elimination and favour reductive elimination.[157] For these reasons, it was of interest to also trial a bidentate palladium-ligand complex in the Sonogashira screen.

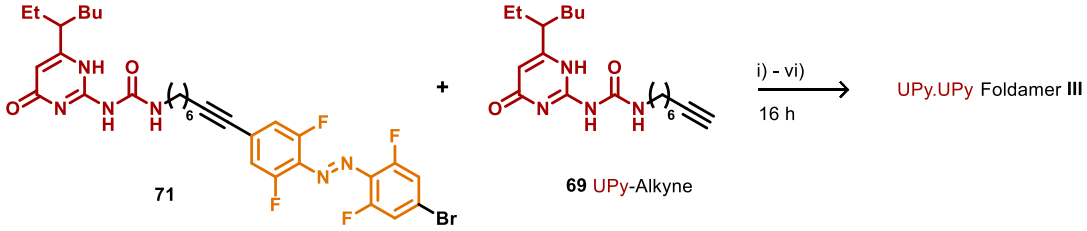

Entry	Solvent	Temp. (°C)	Pd catalyst	Cu catalyst	Base	Product
i)	THF	60	$Pd(PPh_3)_2Cl_2$	CuI	NEt_3	N
ii)	DMF	60	$Pd(PPh_3)_2Cl_2$	CuI	NEt_3	Y
iii)	NEt_3	60	$Pd(PPh_3)_2Cl_2$	CuI	NEt_3	Y
iv)	THF	60	$PdCl_2(dppf).CH_2Cl_2$	CuI	NEt_3	N
v)	DMF	60	$PdCl_2(dppf).CH_2Cl_2$	CuI	NEt_3	Y
vi)	$HN(^iPr)_2$	80	$Pd(t\text{-}Bu_3P)_2$ Na_2PdCl_4	CuI	$HN(^iPr)_2$	Y

Scheme 7. Screen of conditions to optimise the synthetic procedure for the formation of UPy·UPy foldamer **III**. Products identified by HRMS, but not isolated at this stage.

Upon completion of the screening, it was established that product could be obtained under the reaction conditions v) and vi). However, in the case of foldamer **III** synthesis it was significantly harder to isolate the foldamer from the catalysts used in v) and vi), than it was for the $Pd(PPh_3)_2Cl_2$ catalyst. Therefore, yields could not be improved by changing the palladium catalyst.

Reactions carried out in competitive solvents (dimethylformamide, triethylamine and diisopropylethylamine) yielded product, whereas those performed in tetrahydrofuran did not. Conditions iii) were selected to be repeated and scaled up. Despite the much better conversion in competitive solvents, yield of foldamer **III** was still relatively low at 13 %. This may be attributed to association of the unreacted **71** and **69** with foldamer **III** and the subsequent difficult purification of foldamer **III**. Despite the relatively low yield, sufficient quantities could be produced for subsequent characterisation.

2.1.4 UPy·DAN foldamer IV

UPy·DAN foldamer **IV** was synthesised *via* a procedure comparable to foldamer **III**. DAN alkyne linker **79** presented a more significant synthetic challenge than previous linkers. Following established routes, 2,6-diaminopyridine **57** underwent heterocycle formation to give naphthyridine **75**, which was followed by acylation to give **76**.[33] Amidonaphthyridine **78** could be yielded *via* the bromide functionalised naphthyridine intermediate **77**.[158] Linker **79** was produced *via* an amide coupling reaction with 8-noynoic acid **54** (Scheme 8). Although this synthetic procedure was successful, multiple steps resulted in poor yields, which could not be improved.

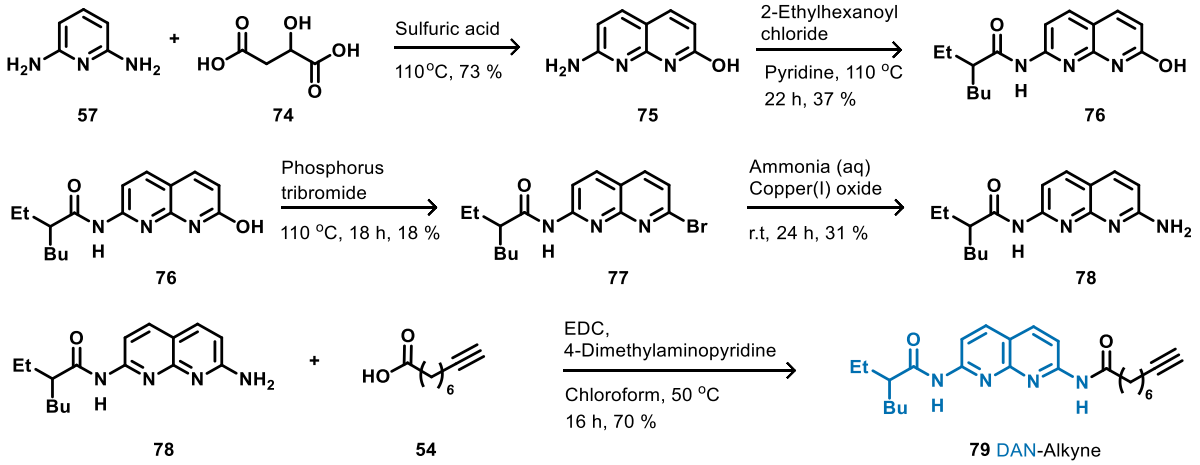

Scheme 8. Synthesis of DAN-alkyne **79** *via* bromo- naphthyridine **77**. Adapted from [33].

To bypass the low yielding reactions that produced naphthyridines **77** and **78**, chlorination of naphthyridine **75** was carried out (Scheme 9). An improved yield was achieved, and subsequently a Buchwald-Hartwig cross-coupling between naphthyridine **80** and *tert*-butyl carbamate was performed.[159] *In situ* thermal deprotection produced amidonaphthyridine **78** in a reasonable yield, and linker **79** could be obtained *via* an amide coupling with alkyne **54**.

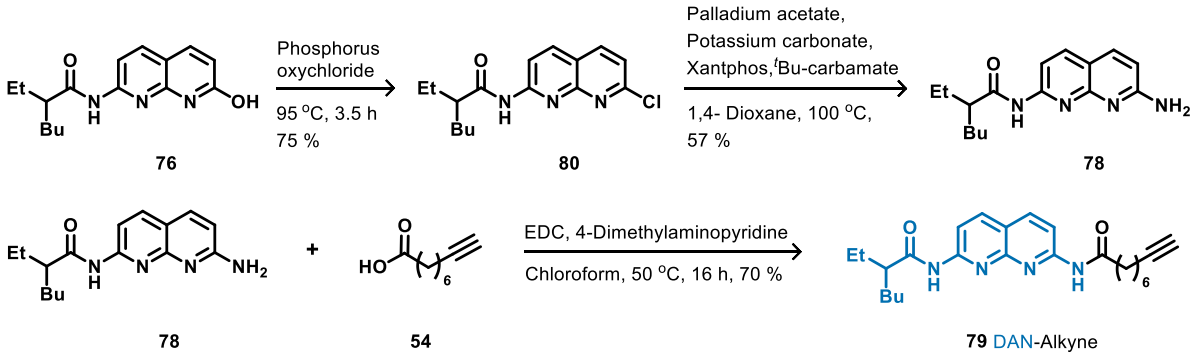

Scheme 9. Synthesis of DAN alkyne **79** *via* the chlorine substituted naphthyridine **80**.

Once linker **79** had been produced in suitable quantities, the reaction conditions required to produce foldamer **IV** could be considered. As the UPy·DAN interaction is of similar strength to that of the UPy·UPy interaction, it was considered highly likely that the same adverse interactions between substrates would be present. Therefore, the conditions used to synthesis foldamer **III** were also applied to the synthesis of foldamer **IV** (Scheme 10). Upon performing the Sonogashira reaction using DAN alkyne **79**, with a triethylamine solvent, foldamer **IV** could be produced with a yield of 10 %.

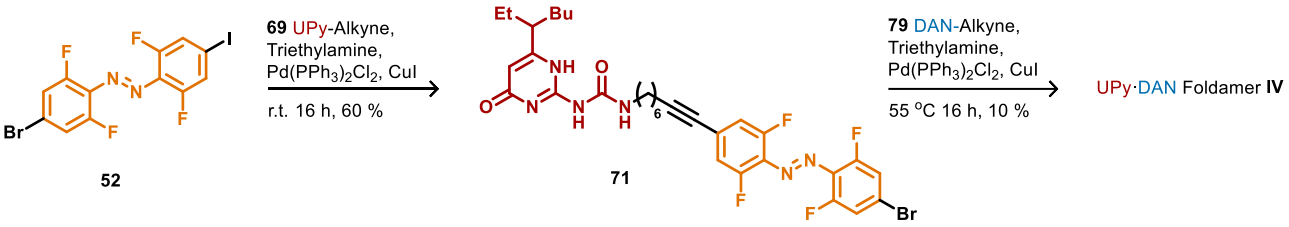

Scheme 10. Synthesis of foldamer **IV** contianing UPy and DAN hydrogen bonding motifs

2.2 Characterisation of photostationary states of hydrogen bonding foldamers

Proton and carbon NMR, infrared spectroscopy, and HRMS were used to confirm the successful syntheses of all foldamer targets (see experimental chapter 6). Upon confirmation that the characterisation matched that expected for each foldamer, efforts were directed toward assessing their photostationary states.

In accordance with previous studies on foldamer **I** samples were irradiated in the visible range under blue and green light to exploit the n→π* absorption bands of the photoresponsive azobenzene moiety.[135] The light source used was a high-power light-emitting diode (LED) system with LEDs of wavelengths 405 nm (blue) and 530 nm (green). Blue light was used to produce the *E* isomer of each foldamer, and green light was used to generate the *Z* isomer. To irradiate effectively, the foldamer solutions were made up in chloroform and transferred to a glass vial (aluminium foil covered) where they were stirred. Each sample was irradiated for 10 minutes at each wavelength. The samples were kept in darkness until analysed.

2.2.1 UV-Vis studies

Photoisomerisation behaviour of foldamers **I**, **II** and **III** were initially characterised using UV-Vis absorption spectroscopy. UV-Vis spectra were recorded after irradiation of 0.01 mM samples for 10 minutes (Figure 32).

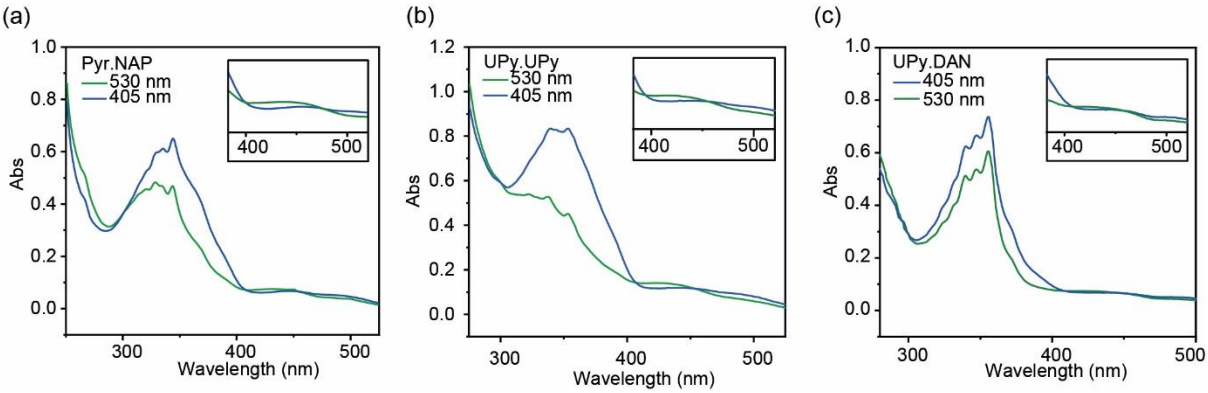

Figure 32. UV-Vis spectra of foldamers **I**, **II** and **IV** in (chloroform, 0.01 mM) after irradiation at 405 nm (blue) 530 nm (green), enlarged inset indicates the n→π* transition within the visible range; (a) Pyr·NAP foldamer **I**; (b) UPy·UPy foldamer **III**; (c) UPy·DAN foldamer **IV**.

For all foldamers, upon exposing blue light irradiated samples to green light the absorption maxima underwent a hypsochromic shift. Upon re-irradiation with blue light back-switching was achieved as evidenced by the corresponding bathochromic shift of the absorption maxima. This behaviour confirmed the photoisomerisation was occurring at the azobenzene moieties.

2.2.2 ^{1}H NMR studies

For ^{1}H NMR studies, solutions of each foldamer were prepared in anhydrous $CDCl_3$ (4 mM). Samples were irradiated for 10 minutes at each wavelength and kept in the dark until analysed. ^{1}H NMR spectra showed evidence of switching *via* a change of environment for key proton resonances within each foldamer (Figure 33). The ratio of *E*/*Z* isomers could be estimated from the integrals of the azobenzene protons, which show characteristic changes in chemical shift (δ) after irradiation. The distribution at the photo-stationary state for foldamer **I** was found to be 13:87 *Z*:*E* after irradiation at 405 nm and 85:15 *Z*:*E* after irradiation at 530 nm (Figure 33a). For foldamer **III** the distribution at the photo-stationary after irradiation at 405 nm and 27:73 *Z*:*E* and 71:29 *Z*:*E* after irradiation at 530 nm (Figure 33b). For foldamer **IV** the distribution at the photo-stationary after irradiation at 405 nm and 34:66 *Z*:*E* and 72:28 *Z*:*E* after irradiation at 530 nm (Figure 33c).

Interestingly, despite consistent concentrations and the photoisomerisable component being the same in each foldamer, there was some variation in the ratios of the isomers between foldamers. Foldamer **I** achieved the highest *E* and *Z* content after irradiation with blue and green light respectively (87% *E* and 85% *Z*). Foldamers **III** and **IV** both showed reduced switching to each isomer, foldamer **III** achieved 73% *E* and 71% *Z* and foldamer **IV** 66% *E* and 72% *Z*. This observation could be attributed to the differing association constants between the HBMs in each foldamer. As the association constant of dimerisation increases, the isomeric ratios decrease (Figure 33). This suggests that stronger interaction between the HMBs impedes the photoisomerisation in foldamers **III** and **IV**.

Upon the successful characterisation of the photostationary states, further ^{1}H NMR studies were carried out on samples of each foldamer across a range of concentrations. These studies were performed with the aim to characterise any supramolecular polymerisation of the foldamers. Concentration dependent ^{1}H NMR investigations, along with additional diffusion ordered spectroscopy (DOSY) and viscosity studies are discussed further in chapter 3.

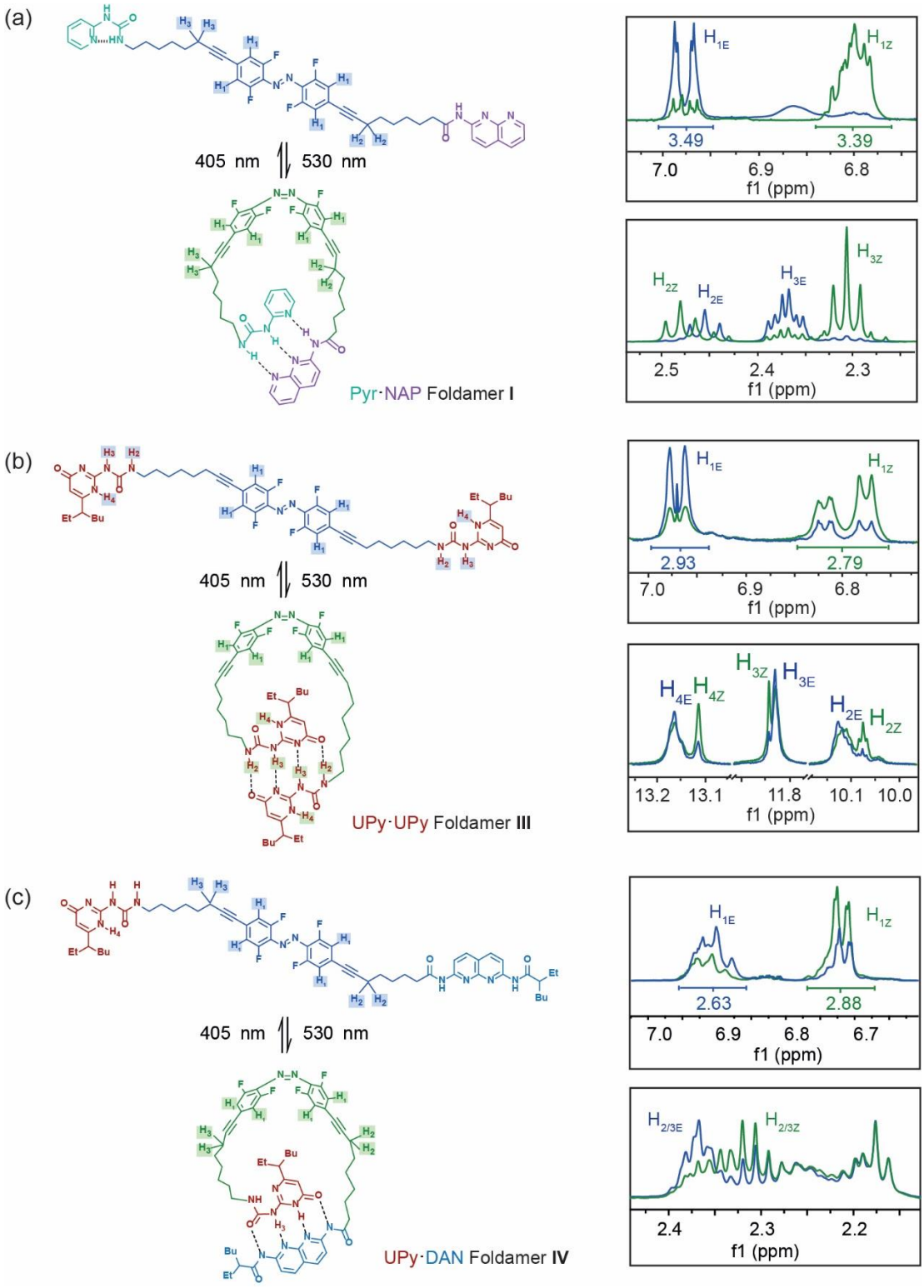

Figure 33. (a) Pyr·NAP foldamer **I** and its *E* (blue) and *Z* (green) isomers and ^{1}H NMR (500 MHz, $CDCl_3$, 298K, 4 mM) signals showing evidence of switching between isomers after irradiation (Integrals used to calculate PSSs ratios); (b) UPy·UPy foldamer **III** and its *E* (blue) and *Z* (green) isomers and ^{1}H NMR (500 MHz, $CDCl_3$, 298K, 4 mM) signals showing evidence of switching between isomers after irradiation (integrals used to calculate PSSs ratios); (c) UPy·DAN foldamer **IV** and its *E* (blue) and *Z* (green) isomers and ^{1}H NMR (500 MHz, $CDCl_3$, 298K, 4 mM) signals showing evidence of switching between isomers after irradiation (integrals used to calculate PSSs ratios).

2.5 Conclusions

Opie and co-worker's NAP·Pyr foldamer **I** was synthesised and the photostationary states characterised by ^{1}H NMR and UV-Vis spectroscopy. In an effort to develop novel hydrogen bonding foldamers with differing recognition patterns, designs for foldamers **II** - **IV** were proposed. The syntheses of these foldamers presented significant challenges. UIM·AIC foldamer **II** was determined to be not viable for use in this work due to its lack of solubility in relevant solvents for purification. In addition to this, the low association constant between the triple hydrogen bonded UIM·AIC motifs made this foldamer less desirable for use in reconfigurable polymer systems within other themes of the project. Efforts were therefore directed toward producing quadruple hydrogen bonded foldamers **III** and **IV**. Multiple synthetic routes to UPy·UPy foldamer **III** produced no product or very low yields. It was theorised that a combination of aryl bromide substrates with low reactivity and quadruple hydrogen bonding reagents were the cause of unsuccessful Sonogashira reactions. A screen of reaction conditions confirmed that the hydrogen bonding reagents were likely to be a contributing factor in the challenging syntheses. Sonogashira reactions carried out in solvents that prevented hydrogen bonding interactions between reagents yielded product. Although efforts were made to find more suitable palladium-based catalysts for the aryl bromide substrates in these Sonogashira reactions, no such catalyst was found at this stage. Upon the successful synthesis of foldamer **III**, the photostationary states were characterised by ^{1}H NMR and UV-Vis spectroscopy. UPy·DAN foldamer **IV** presented its own challenges in the form of the synthesis of the DAN alkyne substrate **77**. Although this synthesis required more steps than that of the other alkyne substrates used, the route was optimised to provide sufficient quantities for the synthesis of foldamer **IV**. Upon the successful synthesis of foldamer **IV**, the photostationary states were determined by ^{1}H NMR and UV-Vis spectroscopy. Comparison of the photostationary state ratios of each foldamer suggested that the strength of the hydrogen bonding interaction between the HBMs may impact photoisomerisation. In future, kinetic studies could be performed to further assess this behaviour and investigate the impact of the association constant on the ratio of photostationary states.

3. Visible-light driven multistate assembly of hydrogen bonding foldamers

Supramolecular polymers have transformed materials chemistry.[136-139] Such polymers offer tremendous potential as stimuli responsive materials, due to the dynamic nature of the non-covalent interactions that hold them together; supramolecular materials exhibit properties that include self-healing, shape memory, and actuation.[64-68] Moreover, supramolecular polymers have been used for a range of applications including adhesion, inkjet printing, tissue engineering and drug delivery.[74-78] Temperature, pH, redox control and light have all been harnessed to regulate supramolecular polymer assembly,[69-73] however, there remains a need to develop multistate systems that are responsive to external stimuli. Foldamers present one potential route to achieving such systems; their function can be regulated through folding driven by co-operative non-covalent interactions. Various stimuli have been used to switch between unfolded and folded forms[128] including acid/base,[129] cations,[130] anions,[131, 132] redox state[133] and light.[134] Whilst single chain folded polymers have been reported,[140, 141] the development of self-assembled foldamers is less explored.[142-146]

HBMs are one of the most versatile molecular recognition motifs used for supramolecular assembly.[12, 79-83] A number of light responsive hydrogen-bond assembled supramolecular polymers have been described.[96, 163-167] Notably, stilbene, dithienylethene and azobenzene photoswitches have been used to regulate assembly of self-complementary hydrogen-bond assembled supramolecular polymers (i.e. AA type). [96, 97, 109, 164, 165, 168] In general, for ditopic UPy monomers,[32] the concentration dependent ring-chain equilibria[169-171] has been shown to bias assembly in favour of lower molecular weight cyclic oligomers for the *cis* or closed form whilst the *trans* or open form is biased towards chain extended polymers. There are few reports on visible light responsive hydrogen-bond assembled supramolecular polymers,[96] and similarly, no examples of light responsive supramolecular polymers assembled *via* heterodimerisation (i.e. AA + BB or AB type).

In this work, we detail the multistate visible-light responsive supramolecular assemblies that can formed from the folded and unfolded structures of hydrogen bonding foldamers **I**, **III** and **IV** (Figure 34). In each case, the *Z* and *E* photostationary states are biased toward cyclic or extended conformations respectively, leading to different discrete hydrogen-bonded rings and supramolecular polymer assemblies dependent on concentration, foldamer concentration and hydrogen-bond dimerisation affinity.

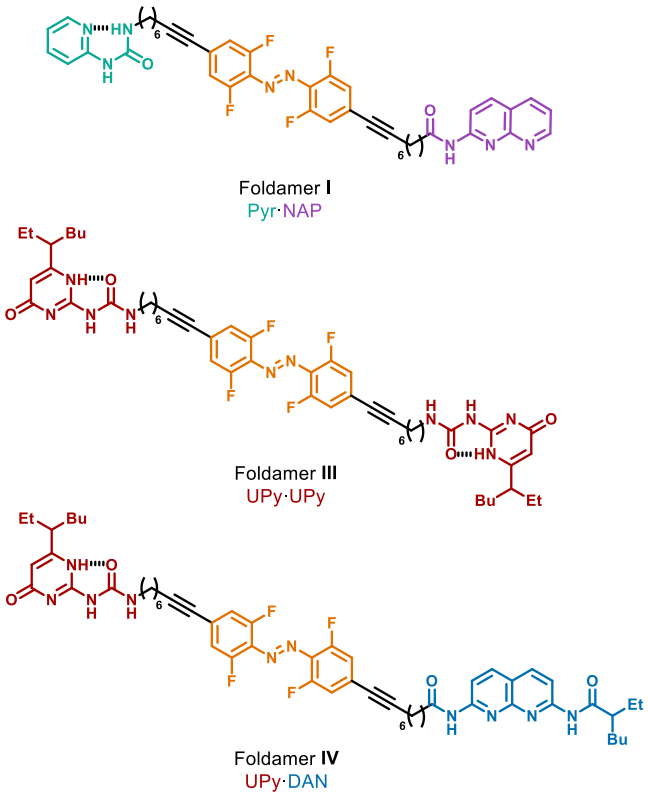

Figure 34. Structures of foldamers **I**, **III** and **IV**. Foldamer **I** from Opie et al.[132] Foldamers **III** and **IV** designed in this work.

3.1 Analyses of supramolecular polymer assembly

After confirming their switching capabilities (chapter 2), the propensity for foldamers **I**, **III** and **IV** to form supramolecular polymers was investigated. It was expected that relatively low Pyr·NAP dimerisation affinity (K_a ~ 30 M^{-1})[27] in foldamer **I** would mean it was unlikely that large assemblies could be formed from this foldamer. The formation of a supramolecular polymer from foldamers **III** and **IV** was considered to be more likely due to the higher association constants between the HBMs they contained. The UPy·UPy interaction present in foldamer **III** has been established to have a dimerisation constant of at least K_{dim}= 10^6 M^{-1}.[32] The UPy·DAN dimerisation in foldamer **IV** is favoured over UPy homodimerisation by a 20:1 ratio and this was considered promising as a supramolecular synthon to assemble the first visible light responsive AB type hydrogen-bonded supramolecular polymer.

To investigate the formation of supramolecular assemblies of each foldamer, concentration dependent DOSY NMR studies were performed. The inversely proportional relationship between diffusion coefficient and molecular weight was utilised to identify the size of the species formed by each foldamer.[172] In addition to this, viscometry studies were performed to identify changes in the physical properties of each sample which would indicate polymer formation.[173]

3.1.1 DOSY NMR studies

^{1}H DOSY NMR studies were performed for each foldamer. Initially, samples of each foldamer were prepared at 4 mM and spectra for each isomer were obtained (Figure 35). At this concentration, only negligible change in diffusion coefficient (D) was observed for foldamer I upon photoswitching. This indicated no significant change in size of the species, suggesting that the respective photostationary states are monomeric. In contrast, foldamers **III** and **IV** exhibited a lower D in the *E* form than in the *Z* form suggesting a difference in molecular weight. This observation could be attributed to the formation of cyclic dimers from the *E* isomers of foldamers **III** and **IV** (see section 3.2 for proposed structures).

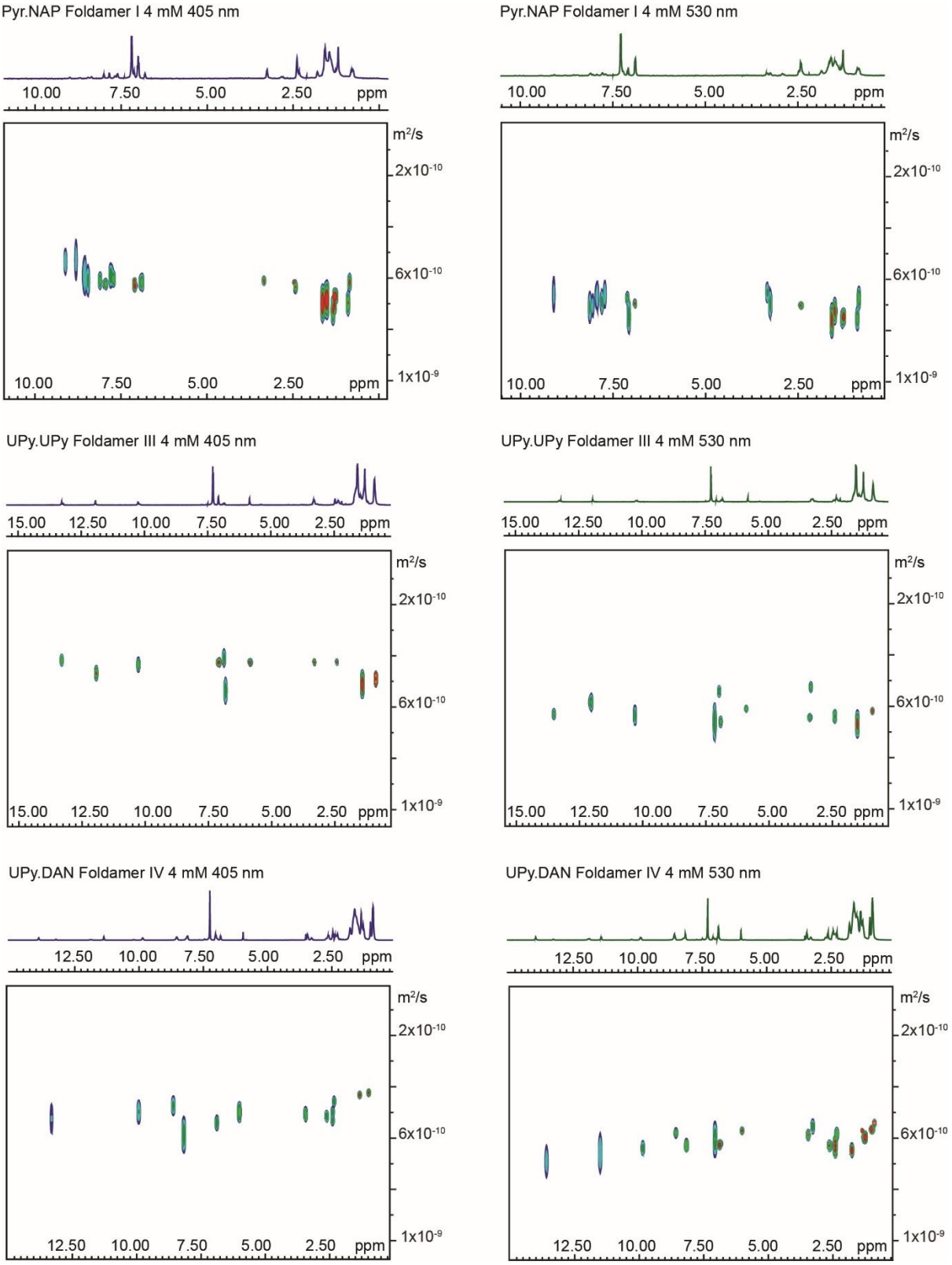

Figure 35. ^{1}H DOSY spectra of foldamer **I**, **III** and **IV** at 4 mM concentrations; Left- blue light irradiated *E* isomer samples; Right- green light irradiated *Z* isomer samples; Top- Pyr·NAP foldamer **I**; Middle- UPy·UPy foldamer **III**; Bottom – UPy·DAN foldamer **IV**.

Next, DOSY spectra were acquired at a range of concentrations of each foldamer (4 - 56 mM (see appendix B for spectra)). As concentration increased, there was a decrease in D for all foldamers indicating an increase in size of the species (Figure 36a, 4a, 5a). For foldamer **I**, at low concentrations (< 24 mM) D decreased slightly for the *Z* isomer, whilst for the *E* isomer a similar trend was observed; D values were consistently slightly smaller for the *E* isomer than those for the *Z* isomer (Figure 36a). Whilst these data imply limited chain elongation at lower concentrations this minor difference might be associated with the proclivity for the *Z* isomer to favour cyclic monomers and the *E* isomer to favour extended oligomers.

At higher concentrations of foldamer **I** (> 24 mM) the behaviour differed, with the size of both the *E* and *Z* isomers both increasing to a comparable degree. This indicated a switch in the ring-chain equilibria towards a chain preference. From these data, it was possible to calculate an approximate degree of polymerisation, and subsequently molecular weight (M_w), for each isomer at each concentration. Assuming only monomeric species were present at 4 mM, degree of polymerisation (DP) could be calculated the using the diffusion coefficients according to the following formula: $DP = (D_{monomer}/D)^3$.[165] Conversion to M_w and plotting against concentration (Figure 36b), provides evidence to indicate both (*E*)-foldamer **I** and (*Z*)-foldamer **I** undergo concentration dependent step-growth oligomerisation.[48]

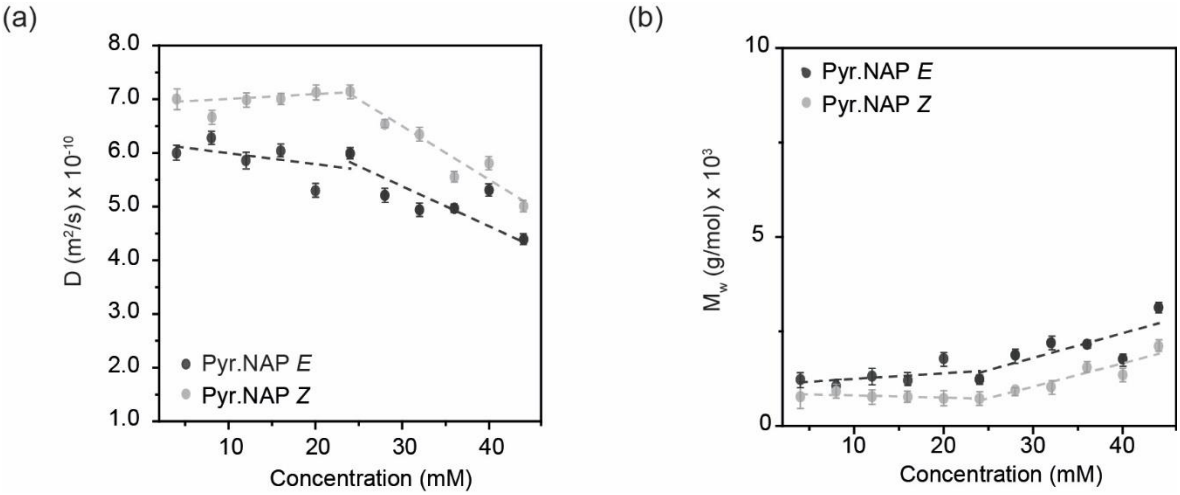

Figure 36. (a) Concentration dependent diffusion coefficient of foldamer **I** (Pyr·NAP *E*, dark grey and Pyr·NAP *Z*, light grey); (b) variation with concentration of approximate molecular weight of each isomer of foldamer **I**. Diffusion coefficients obtained from fitting data in Topspin Dynamics Center, errors estimated using the standard deviation from the fitting.

For foldamer **III**, there were more pronounced differences between the D values for the *E* and *Z* photostationary states at all concentrations (Figure 37a) when compared to foldamer **I**. Blue irradiated foldamer **III** was found to have lower D than green light irradiated (*Z*)-foldamer **III** (which exhibited D values in a similar range to foldamer **I** in the low concentration regime).

This implies a more pronounced difference in the assembly state for the *E* and *Z* states of foldamer **III**. For low concentration samples of foldamer **III** (< 24 mM) D was approximately constant for the *Z* isomer. When converted to M_w, the D values for the *E* isomer imply a species double the size of the *Z* isomer. A small increase in size can be observed with concentration, suggesting only moderate chain extension. Taken together, these data suggest at low concentration foldamer **III** switches between a monomeric macrocycle for the *Z* isomer and small hydrogen-bonded oligomers (likely dimers) for the *E* isomer.

At higher concentrations of foldamer **III** (> 24 mM) the D values for *Z* isomer solutions decreased moderately, indicating a switch in the ring-chain equilibria from cyclic species to oligomers. For the *E* isomer, the D values decreased more rapidly than those for the *Z* isomer indicating a switch from cyclic oligomers to supramolecular polymers. When converted to molecular weight and plotted against concentration (Figure 37b), it is evident that the species formed by (*E*)-foldamer **III** are significantly larger than any observed for the foldamer **I** or (*Z*)-foldamer **III**. This suggests step-growth polymerisation occurs for (*E*)-foldamer **III** and oligomerisation for (*Z*)-foldamer **III** at higher concentrations.

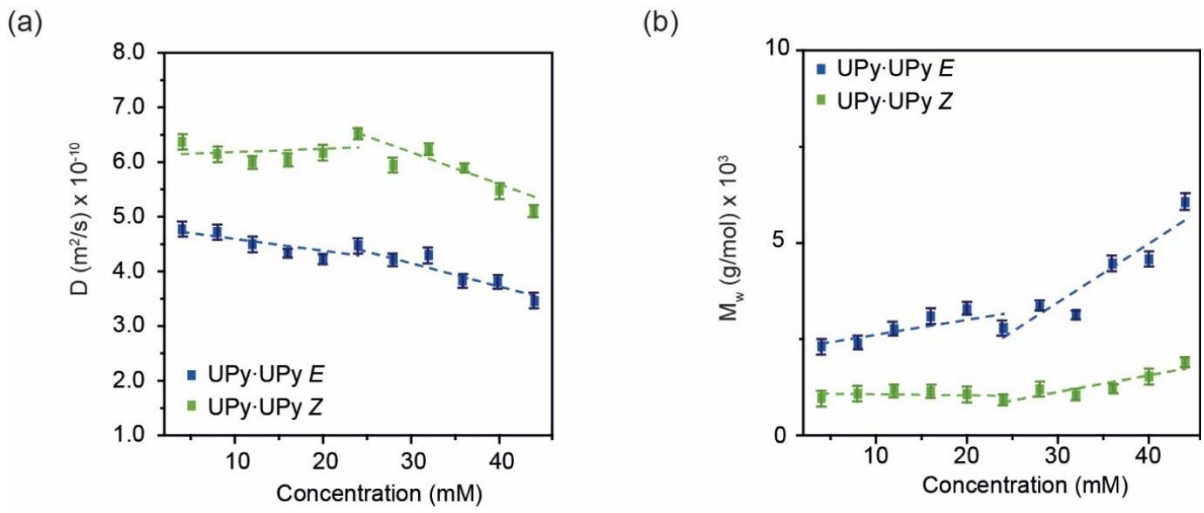

Figure 37. (a) Concentration dependent average diffusion coefficient of foldamer **III** (UPy·UPy *Z*, light green and UPy·UPy *E*, blue); (b) variation with concentration of approximate molecular weight of each isomer of foldamer **III**. Diffusion coefficients obtained from fitting data in Topspin Dynamics Center, errors estimated using the standard deviation from the fitting.

For foldamer **IV**, more complex behaviour was observed. As for foldamer **III**, differences between the D values for the *E* and *Z* photostationary states were observed at all concentrations (Figure 38a). At 4 mM, blue irradiated (*E*)-foldamer **IV** was found to have lower D than green light irradiated (*Z*)-foldamer **IV**. When converted to M_w the D values for the *E* isomer imply a species double the size of the *Z* isomer indicating the latter is monomeric whilst the former is dimeric at low concentration; this recapitulates the behaviour of foldamer **III**.

As concentration increases the D value for the *Z* isomer undergoes only small changes until ~ 24 mM and then decreases at first dramatically and then from ~ 32 mM with a shallower gradient. For the *E* isomer D decreases significantly up to ~ 24 mM and then at a shallower gradient. Thus, the DOSY data imply two phases in the concentration dependent behaviour for the *E* isomer of foldamer **IV** and three phases in the concentration dependent behaviour of the *Z* isomer foldamer **IV**. These phases are not as pronounced in the M_w v concentration plots (Figure 38b) derived from the DOSY data but may be interpreted to arise from the concentration dependent variation in the UPy·DAN and UPy·UPy speciation and associated chain stoppering effect.[171] Alternatively, if the diffusion coefficient recorded for (*Z*)-foldamer **IV** at 32 mM is discounted as an outlier, the data could be interpreted as showing just two phases in concentration dependent behaviour. Taken together, these data suggest the assembly state switches to supramolecular polymers >~ 24mM. As for foldamer **III**, (*E*)-foldamer **IV** and (*Z*)-foldamer **IV** assemble to different extents or states, but both appear to form larger assemblies which can be attributed to the higher UPy·DAN affinity.

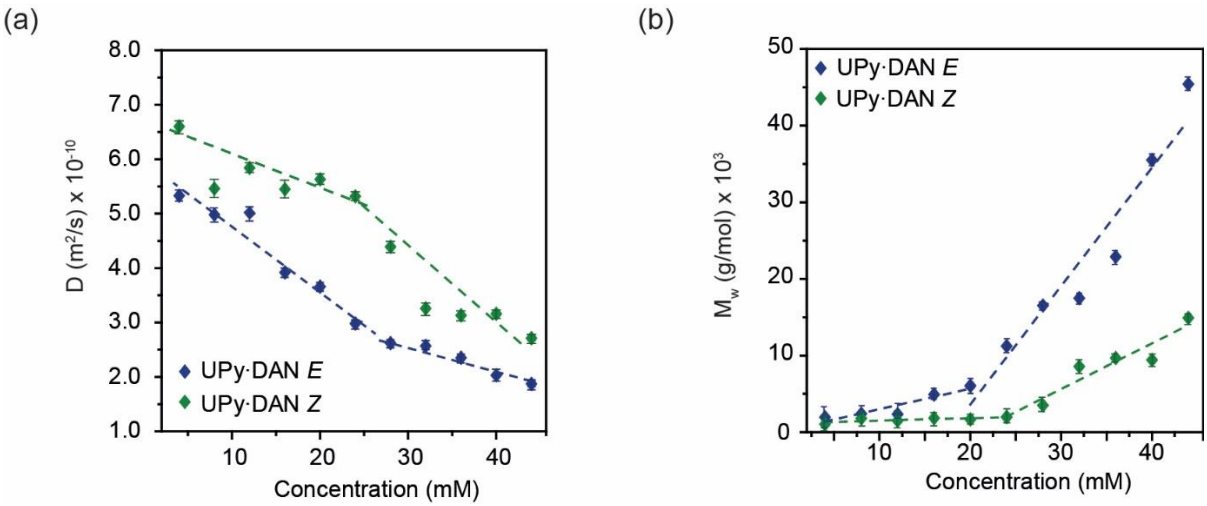

Figure 38. (a) Concentration dependent average diffusion coefficients foldamer **IV** (UPy·DAN *Z*, dark green and UPy·DAN *E*, dark blue; (b) variation with concentration of approximate molecular weight of each isomer of foldamer **IV**. Diffusion coefficients obtained from fitting data in Topspin Dynamics Center, errors estimated using the standard deviation from the fitting.

3.1.2 Viscosity studies

To further assess the physical properties of foldamers **I**, **III** and **IV**, viscosity measurements were performed on solutions of each foldamer using a micro-Ostwald viscometer. A double-logarithmic plot of the specific viscosity *versus* concentration was obtained for each isomer of each foldamer (Figure 39).

(*Z*)-Foldamer **I** exhibited only minor changes in viscosity between concentrations 4 mM-24 mM with a slope of ~ 1.0, suggesting small cyclic species were present. Above 24 mM the slope increased to ~ 1.5, indicating an increase in molecular weight.[174] The viscosities of (*E*)-foldamer **I** increased steadily with concentration with a slope of 1.2, indicative of concentration dependent oligomerisation – an inflection in the double-logarithmic plot denoting a switch from in ring-chain bias is more difficult to perceive. Nonetheless, these findings were generally in agreement with the DOSY NMR results.

In solutions of (*Z*)-foldamer **III**, below 24 mM a constant viscosity with a slope of 1.7 was observed. Above 24 mM, the slope increased to 4.0, indicating oligomerisation. In comparison to DOSY NMR data, which indicated a small increase in size, the viscosities measured for foldamer **III** suggest a more significant increase in molecular weight in both concentration regimes. The viscosities for (*E*)-foldamer **III** increased more steadily with concentration with a slope of 2.6, indicative of concentration dependent polymerisation across the concentration gradient; an inflection point for the critical concentration denoting transition from the cyclic to oligomeric regime in the double logarithmic plot can be perceived (Figure 39).

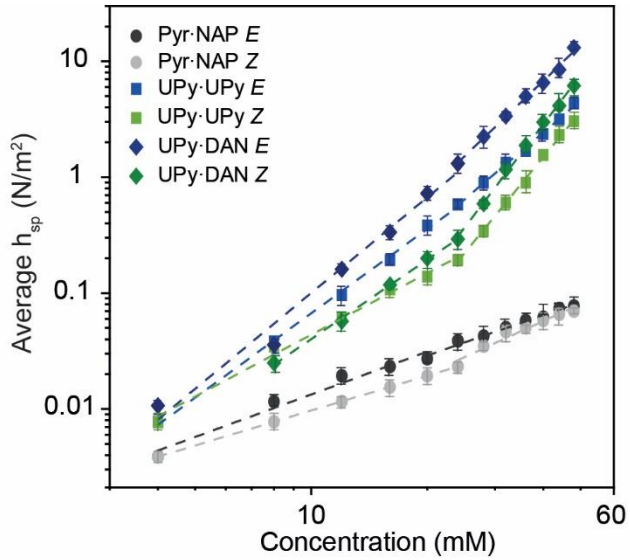

Figure 39. Average specific viscosity of foldamer **I** (Pyr·NAP *E*, dark grey and Pyr·NAP *Z*, light grey), foldamer **III** (UPy·UPy *Z*, light green and UPy·UPy *E*, blue) foldamer **IV** (UPy·DAN *Z*, dark green and UPy·DAN *E*, dark blue) at concentrations 4 mM- 56 mM. Solutions prepared in chloroform. Errors estimated using the standard deviation across four replicates.

For solutions of (*Z*)-foldamer **IV**, below 24 mM a constant viscosity with a slope of 2.3 was observed. Above the critical concentration the slope changes to 4.4. The viscosities for (*E*)-foldamer **IV** below 24 mM increased steadily with concentration with a slope of 2.7. An inflection point for the critical concentration denoting transition from the cyclic to oligomeric regime in the double logarithmic plot was observed ~ 24 mM at which point the slope increased

to 3.2 (Figure 39). These data indicate similar ring-chain behaviour to that observed for foldamer **III** with the *Z* isomer exhibiting a greater tendency than the *E* isomer towards ring formation below the critical concentration (24 mM) and then above the critical concentration, both isomers polymerising with the *E* isomer forming more viscous assemblies. In each case the *E* and *Z* isomers of foldamer **IV** are more viscous than the corresponding *E* and *Z* isomers of foldamer **III** in the higher concentration regime.

Finally, to demonstrate reversible property switching, multiple cycles of irradiation were carried out at three concentrations (4mM, 32 mM and 56 mM) for foldamer **III** (Figure 40a) and foldamer **IV** (Figure 40b). In both cases the variation in viscosity was negligible at 4mM, more significant at 32 mM and most significant at 56 mM. It was possible to switch the viscosities of foldamer **III** from approximately 7 N/m^2 to approximately 6 N/m^2 foldamer **IV** from approximately 11 N/m^2 to approximately 22 N/m^2 through 10 cycles of irradiation under blue and green light demonstrating robust nature of the physical property photoswitching. The greater variation in viscosity for foldamer **IV** is consistent with the interpretation that foldamer **IV** can form larger assemblies that foldamer **IV** driven by the higher affinity of the UPy·DAN interaction in comparison to the UPy·UPy interaction.

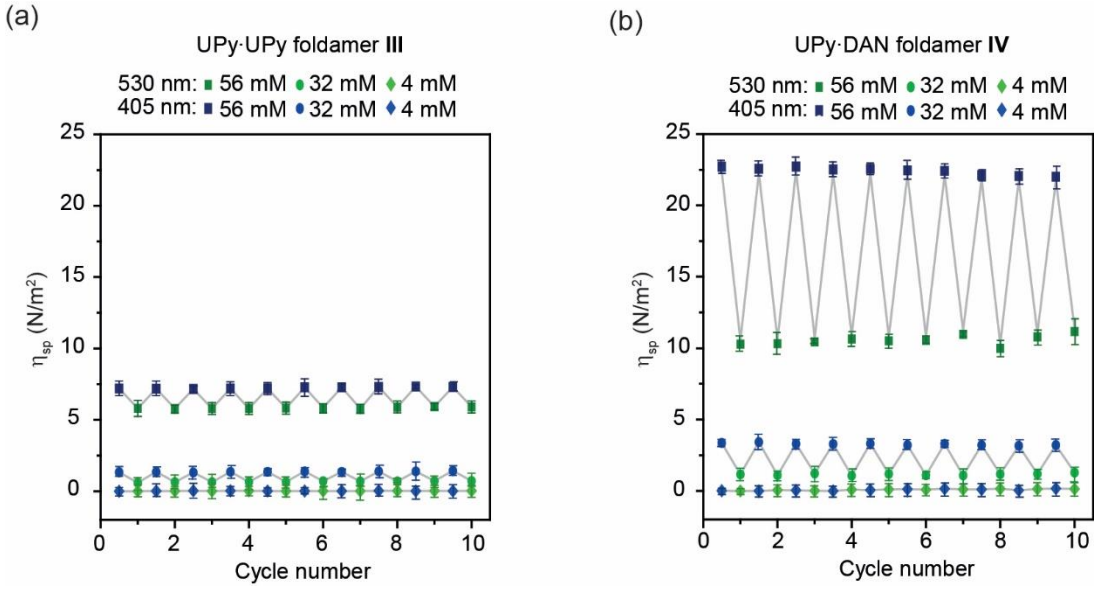

Figure 40. (a) Specific viscosity of foldamer **III** in response to ten successive cycles of light irradiation at 56, 32 and 4 mM concentrations (UPy·UPy *Z,* light green and UPy·UPy *E*, blue); and, (b) specific viscosity of foldamer **IV** in response to ten successive cycles of light irradiation at 56, 32 and 4 mM concentrations (UPy·DAN *Z*, dark green and UPy·DAN *E*, dark blue). Errors estimated using the standard deviation across four replicates.

3.2 Multi-state supramolecular assemblies

The data obtained from DOSY NMR and viscosity studies suggest multi-state assemblies can be formed by each foldamer. In low concentration samples of Pyr·NAP foldamer **I** there was little change observed in with viscosity or D, these findings suggest the foldamer forms monomeric structures; (*Z*)-foldamer **I** forms cyclic monomeric species and (*E*)-foldamer **I** forms monomeric linear species (Figure 41). At high concentrations, both the DOSY and viscosity data indicated a switch in the ring-chain equilibria from cyclic species to chain extended oligomers. Both (*E*)-foldamer **I** and (*Z*)-foldamer **I** form short oligomers rather than supramolecular polymers which likely derives from the moderate strength for the triply hydrogen-bonded heterodimerisation.

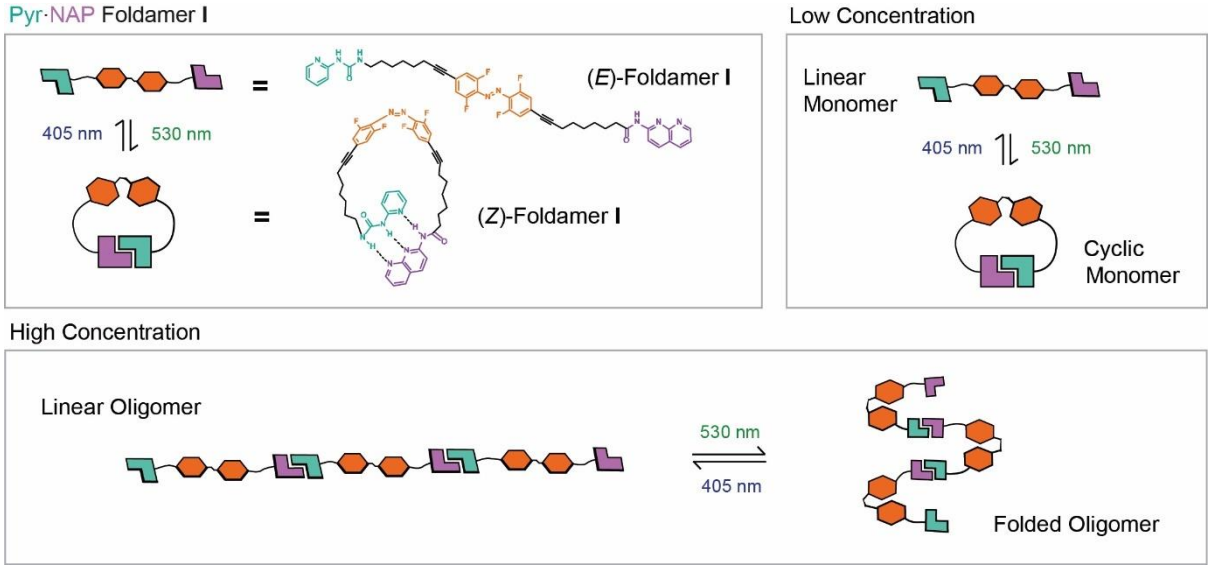

Figure 41. Schematic representing the architectures formed by the *E* and *Z* isomers of Pyr·NAP foldamer **I** at high and low concentrations. At low concentrations foldamer **I** switches between monomeric cyclic and linear structures in response to green/blue light. At high concentration foldamer **I** switiches between short linear and folded supramolecular oligomers in response to green/blue light.

Both DOSY and viscosity data indicated that UPy·UPy foldamer **III** can form significantly larger molecules than foldamer **I**. This behaviour can be attributed to the increased strength of the quadruply hydrogen-bonded homodimerisation. Although it was evident larger species could be formed by foldamer **III**, there was some discrepancy between the DOSY and viscosity data. The viscosity measurements suggest a more significant increase in molecular weight in both concentration regimes. A possible explanation for this is due to the folded shape of (*Z*)-foldamer **III** (Figure 42). Viscosity, depends also on solvation[175] and shape[176] for instance single stranded DNA has lower intrinsic viscosity than double stranded DNA, however at low ionic strength this trend can be reversed. Therefore, the data can be interpreted to indicate

(*Z*)-foldamer **III** indeed assembles but to give shorter more compact and rigid structures. Given diffusion coefficient is correlated with the hydrodynamic radius of a spherical molecule, differences in shape between oligomers of (*Z*)- and (*E*)-foldamer **III** are unlikely to be accounted for. This relationship, defined by the Stokes–Einstein equation, provides a reasonable explanation for the discrepancy between the DOSY and viscosity data.[177]

Taken together, the DOSY and viscosity measurements suggest the assembly state of foldamer **III** at low concentration differs between the *E* and *Z* states. This could be attributed to the formation of a folded macrocycle for the *Z* isomer and cyclic hydrogen-bonded oligomers (likely dimers) for the *E* isomer. At high concentrations larger macromolecules are formed, in these systems it was possible to switch between folded supramolecular oligomer (Z)-foldamer **III** and linear supramolecular polymer (*E)*-foldamer **III** in response to visible light (Figure 42).

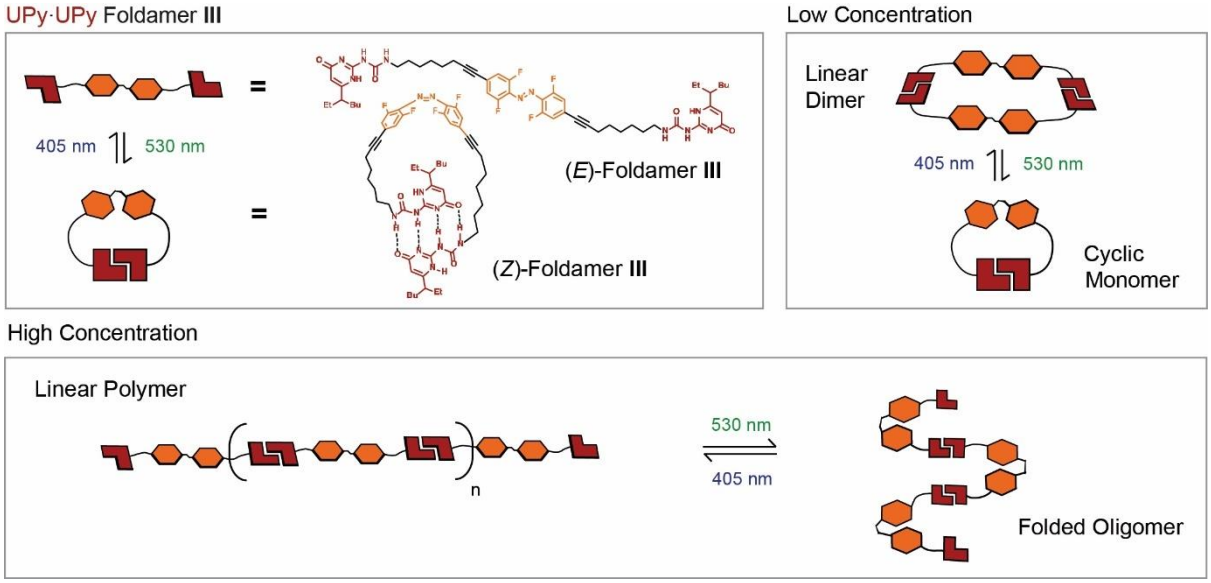

Figure 42. Schematic representing the architectures formed by the *E* and *Z* isomers of UPy.UPy foldamer **III** at high and low concentrations. At low concentrations foldamer **III** switches between monomeric and dimeric cyclic structures in response to green/blue light. At high concentration foldamer **III** switiches between linear supramolecular polymer and folded supramolecular oligomers in response to green/blue light.

For UPy·DAN foldamer **IV**, both the DOSY and viscometry data indicated formation of the largest assemblies yet. This can be attributed to the high UPy·DAN heterodimerisation affinity. In the low concentration regime, the data for foldamer **IV** indicate similar ring-chain behaviour to that observed for foldamer **III** with the *Z* isomer exhibiting a tendency towards monomeric ring formation and the *E* isomer a tendency to form dimeric species (Figure 43). The DOSY data for foldamer **IV** indicates an additional phase in the concentration dependent behaviour for foldamer **IV**, likely arising from UPy·UPy interactions (see before). Despite this, above the critical concentration point, both isomers of foldamer **IV** polymerise. As for foldamer **III**, (*E*)-

foldamer **IV** and (*Z*)-foldamer **IV** assemble to different extents or states, but both form larger species than foldamer **III** (Figure 43).

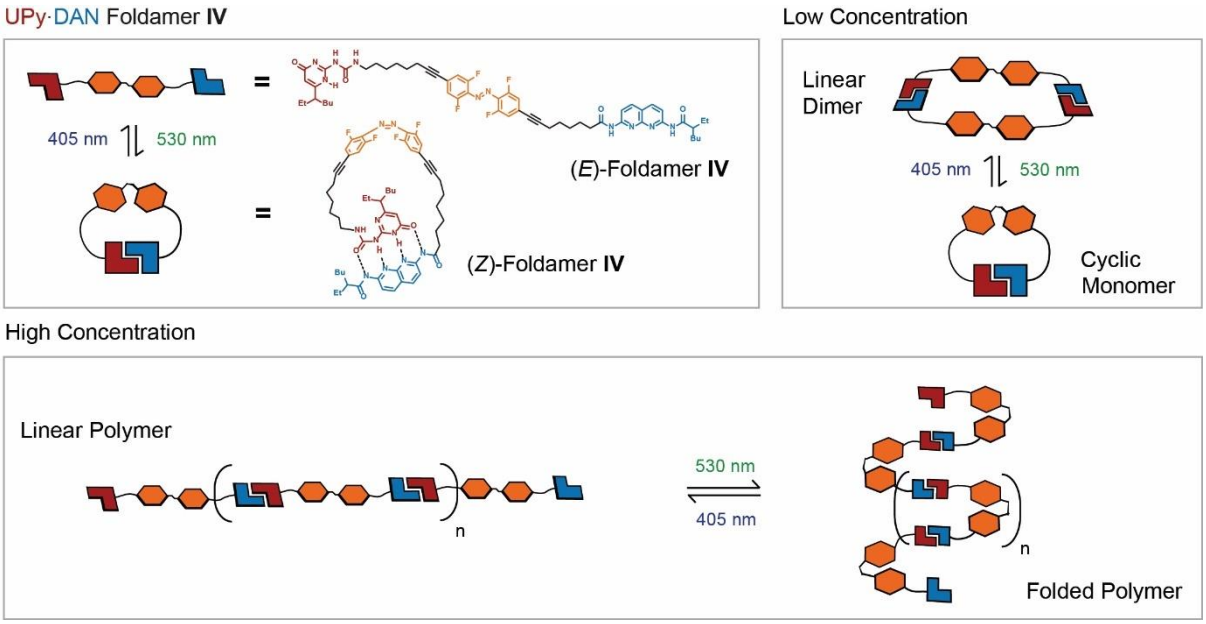

Figure 43. Schematic representing the architectures formed by the *E* and *Z* isomers of UPy·DAN foldamer **IV** at high and low concentrations. At low concentrations foldamer **IV** switches between monomeric and dimeric cyclic structures and some linear oliogmers in response to green/blue light. At high concentration foldamer **IV** switiches between linear supramolecular polymer folded supramolecular polymer in response to green/blue light.

3.3 Conclusions

The photoresponsive oligomerisation and polymerisation behaviours of the *E* and *Z* isomers of foldamers **I**, **III** and **IV** have been characterised by DOSY NMR and viscosity studies. At concentrations below 24 mM, a cyclic hydrogen-bonded monomer dominates for (*Z*)-foldamer **I** whereas the linear non-hydrogen-bonded form is preferred for (*E*)-foldamer **I**. At concentrations above 24 mM (*Z*)-foldamer **I** undergoes a shift in the ring-chain equilibria toward a chain preference, forming folded supramolecular oligomers. (*E*)-foldamer **I** forms linear oligomers where the number of repeat units is proportional to the concentration. Foldamer **III** is able to form significantly larger molecules than foldamer **I** due to the higher association constant between the HBMs. From viscosity and DOSY studies, it appears that below 24 mM foldamer **III** is able to switch between linear oligomers and cyclic monomers and dimers. Above 24 mM larger macromolecules begin to be formed, in these systems it was possible to switch between folded supramolecular oligomer (*Z*)-foldamer **III** and linear supramolecular polymer (*E*)-foldamer **III** in response to visible light. The four different states; cyclic monomer or dimer at low concentration and linear or folded polymer at high concentration uniquely represent an example of multistate switching. Foldamer **IV**, incorporating a quadruply hydrogen-bonded heterodimer represents the first photoswitchable AB type hydrogen-bonded supramolecular polymer. Taken together, this visible light responsive multistate switching offers opportunities for regulation of more complex functions, an objective that could be pursued in future research.

4. Towards reconfigurable hydrogen-bonding covalent polymers

Covalent main-chain polymers are used to develop materials for an enormous range of applications; including coatings, packaging, medical devices, electronics, cosmetics and many more.[178] The incorporation of non-covalent interactions into polymer chains can diversify these properties even further. Additionally, orthogonal triggers can be added to polymeric systems with the intention to develop complex architectures capable of controlled reconfiguration.[69-73]

To develop stimuli responsive reconfigurable polymer systems, we proposed the synthesis of covalent main-chain polymers functionalised with hydrogen bonding motifs complementary to those present in our foldamer molecules discussed in chapter 3. It was hypothesised that bringing together hydrogen-bonding foldamers with hydrogen-bonding functionalised covalent polymers would lead to novel supramolecular polymer systems capable of undergoing stimuli-responsive reconfigurations. The syntheses and behaviours of hydrogen bonded foldamers are discussed in chapters 2 and 3. This chapter details firstly, the synthesis of covalently linked polymers with incorporated hydrogen bonding motifs, and secondly, the supramolecular interaction between a hydrogen-bonding foldamer and hydrogen-bonding polymer.

The method of covalent polymer synthesis selected for this work was reversible RAFT. RAFT has been established to have good solvent compatibility and functional group tolerance, producing a wide variety of polymer architectures, including polymers with incorporated HBMs.[57, 89, 90] Here we used RAFT with the aim to incorporate a range of HBMs into well controlled polymers. To achieve such polymers multiple methods of functionalisation were trailed. Pre-polymerisation methods such as monomer and RAFT agent functionalisation, as well as post-polymerisation functionalisation were investigated.

Upon the synthesis of suitable hydrogen-bonding covalent polymers, we aimed to incorporate these polymers into systems which could undergo reconfigurations facilitated by supramolecular interactions. The addition of photoresponsive foldamers to these systems was of interest to incorporate an element of spatial-temporal control. This work ultimately aimed to bring about photoresponsive switching within polymeric systems that would effect a change in physical properties. The results discussed in this chapter indicate that it is possible to develop polymers which can reconfigure *via* supramolecular self-sorting.

4.1 Pendent functionalised polymers

The preparation of covalent polymers functionalised with HBMs, was initially explored *via* the synthesis of comonomers with HBM functionality. The use of comonomers would provide an opportunity to develop copolymers with differing ratios of incorporated HBM functionality in the main chain. It was important to consider the structure of these monomers due to previous work having established that the addition of a HBM to a conventional monomer species has the potential to alter the reactivity of the monomer during polymerisation. Hydrogen-bonding comonomers can lead to unwanted aggregation and phase septation, as well as a difference in the stability of the radical species formed during RAFT polymerisation.[93, 91] In an effort to prevent this, incorporation levels of the comonomers were kept low, and to aid stabilisation of the radical species, a 2 carbon linker was used between the HBM and the conventional monomer moieties.

4.1.1 Comonomer synthesis

Comonomers were designed and synthesised to include a MMA polymerisable moiety. For triple hydrogen-bonding UIMMMA comonomer **82** a reaction between **65** and 2-isocyanatoethyl methacrylate **81** was performed. This method produced good yields of comonomer and could also be used to synthesise triple hydrogen-bonding comonomer PyrMMA **83** and quadruple hydrogen-bonding comonomer UPyMMA **84**.

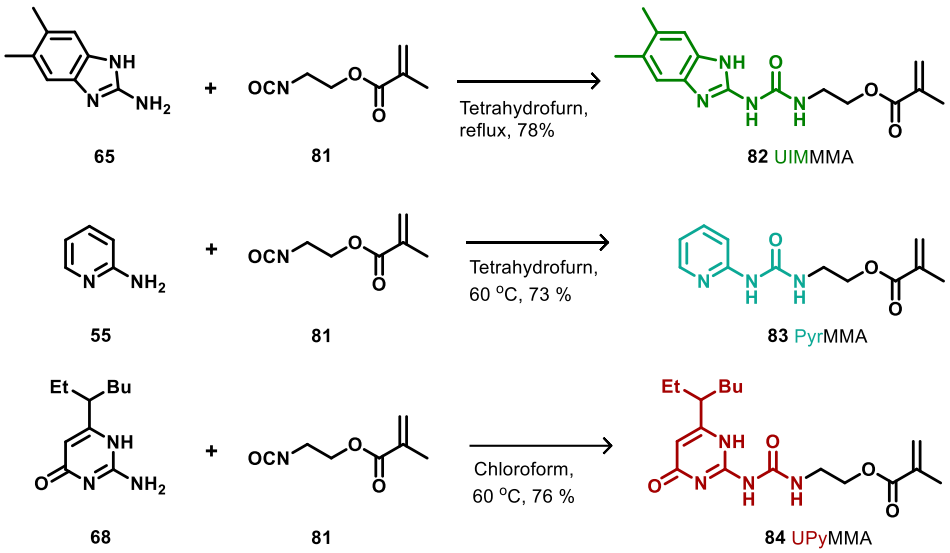

Scheme 11. Syntheses of triple hydrogen bonding comonomers **82** UIMMMA and **83** PyrMMA and quadruple hydrogen bonding comonomer **84** UPyMMA.

4.1.2 Polymer Synthesis

Upon the successful synthesis of multiple HBM comonomers, their compatibility with the RAFT polymerisation mechanism was investigated. All polymerisations were carried out by Dr Yasmeen Jhons, these polymerisations are nevertheless discussed here to demonstrate the viability of the comonomers in the development of hydrogen-bonding covalent polymers. To develop such polymers, HBM comonomers were polymerised along with unfunctionalised MMA to give copolymers. The synthesis of copolymers, rather than homopolymers, would help to maintain a well-controlled polymer structure in the case that the HBM comonomers had a negative impact on the RAFT polymerisation mechanism.

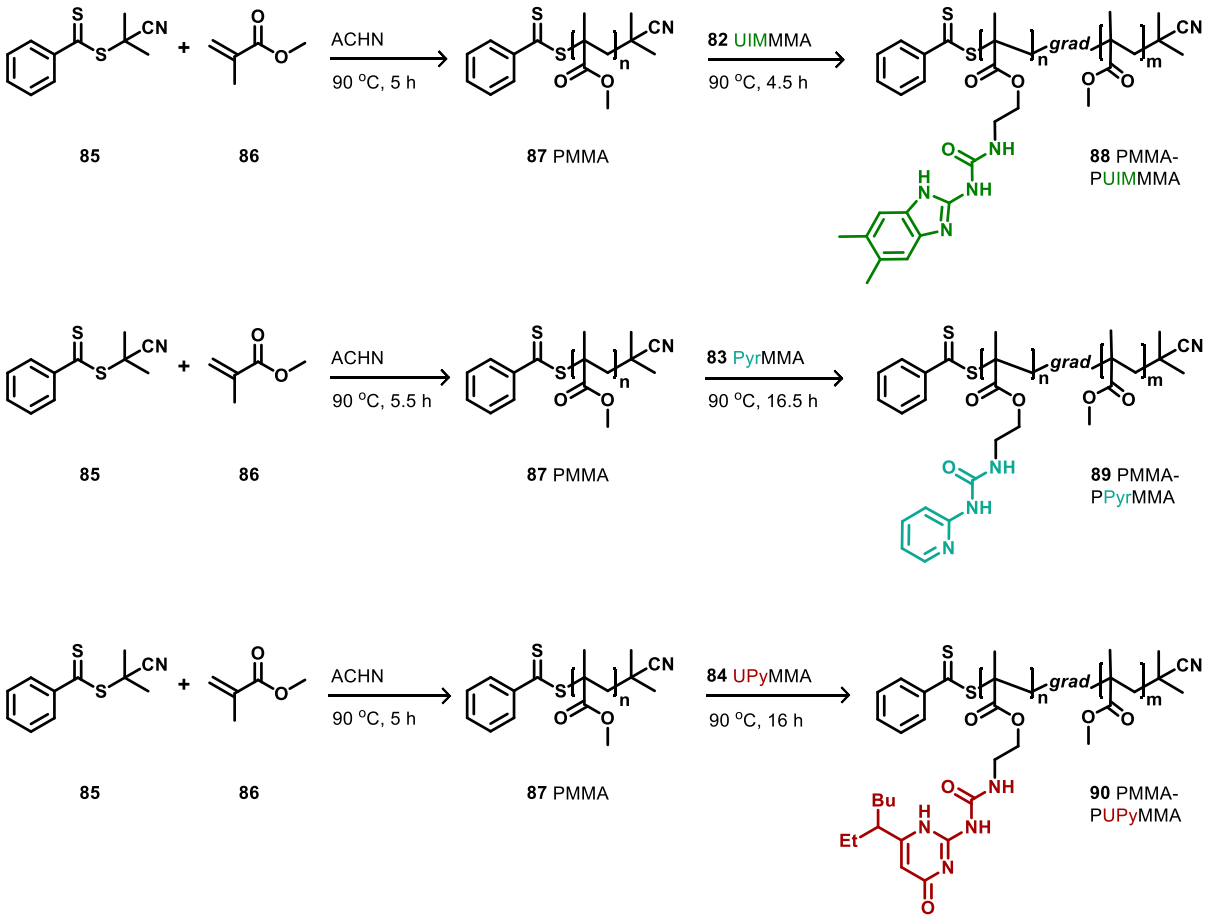

Scheme 12. *Top*- RAFT polymerisation of MMA **86** using 2-cyanopropan-2-yl benzodithioate (CPD) RAFT agent **85** and 1,1′-azobis(cyclohexanecarbonitrile) (ACHN) initiator and subsequent attempted gradient (*grad*) copolymerisation of UIMMMA **82**; *Middle*- RAFT polymerisation of MMA **86** using CPD RAFT agent **85** and ACHN initiator and subsequent *grad* copolymerisation of PyrMMA **83**; *Bottom*- RAFT polymerisation of MMA **86** using CPD RAFT agent **85** and ACHN initiator and subsequent *grad* copolymerisation of UPyMMA **84**. All polymerisations carried out in n,n-dimethylformamide. Polymerisations performed by Dr Yasmeen Jhons.

Synthesis of gradient copolymer **88** was attempted by initially polymerising MMA **86**, when conversion to PMMA reached close to 80 %, UIMMMA **82** was added (Scheme 12). Comonomer **82** suffered from poor solubility in solvents suitable for MMA polymerisation, and

was only capable of dissolving in n,n-dimethylformamide at high temperatures (90 °C). Gel permeation chromatography (GPC) analyses of PMMA **87** and copolymer **88** were performed. The data obtained for homopolymer **87** indicated a well-controlled polymerisation (Figure 44a), whereas data for copolymer **88** indicated that some uncontrolled free radical polymerisation had taken place alongside RAFT polymerisation (Figure 44b). This was likely caused by the high temperatures required to use comonomer **82**. Due to PyrMMA **83** displaying the same donor/acceptor pattern, and having greater solubility, this comonomer was used as an alternative to comonomer **82**.

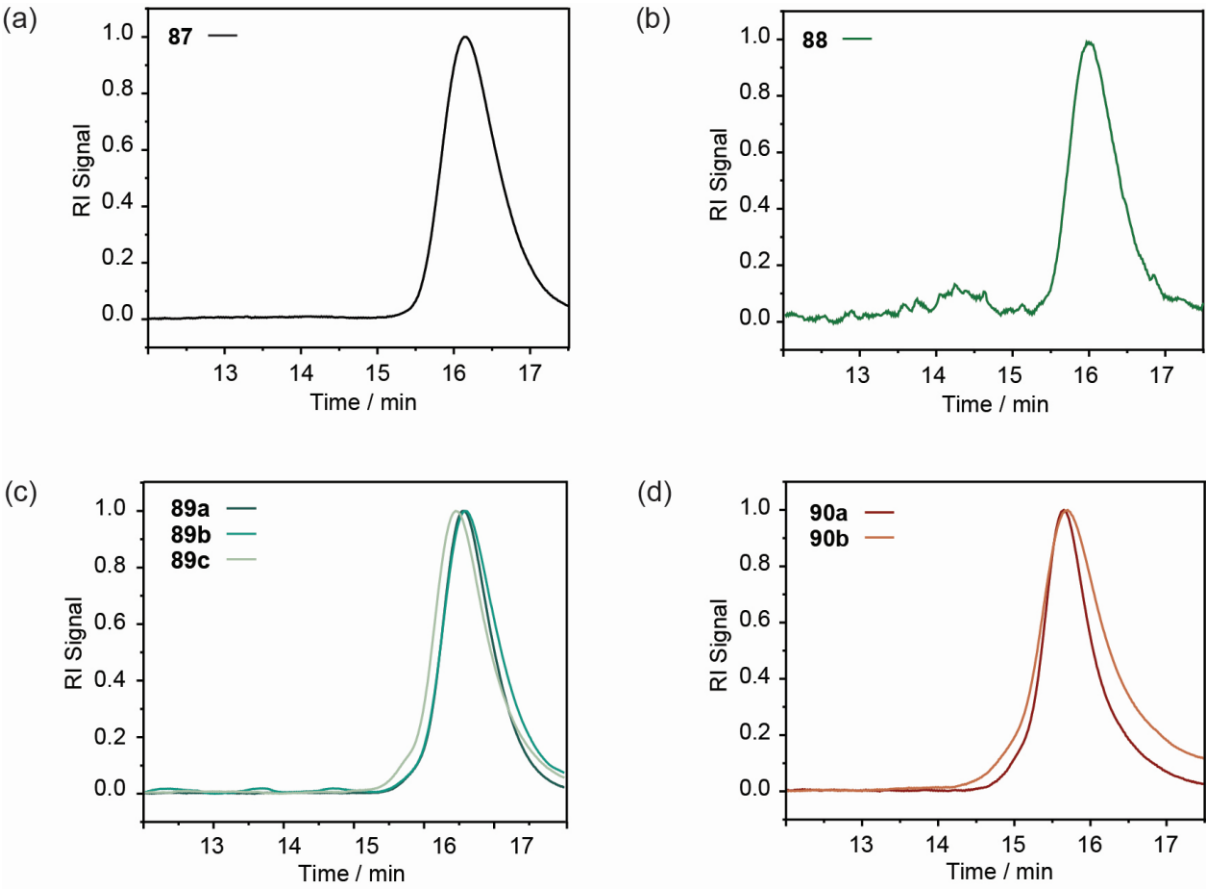

Figure 44. (a) PMMA **87** GPC trace, before addition of any HBM comonomers; (b) GPC trace of PMMA-PUIMMMA **88**. Peaks with retention time ~14-15 min indicated FRP; (c) GPC traces of PMMA-PPyrMMA **89a-c**; (d) GPC traces of PMMA-PUPyMMA **90a-b** . Data acquired by Dr Yasmeen Jhons.

To incorporate PyrMMA **83** and UPyMMA **84** into polymers gradient copolymerisations were performed (Scheme 12). MMA was polymerised first to give PMMA **87**, when conversion to PMMA reached close to 80 %, hydrogen bonding comonomers were added. For both polymers, various short block lengths were targeted with degrees of polymerisation (DP) ranging from 1 to 10 units. GPC data indicated that these polymerisations were well controlled (Figure 44c, d). Further analyses by NMR and GPC provided evidence that comonomers **83**

and **84** could be successfully incorporated into PMMA to give hydrogen-bonding copolymers **89** and **90** (Table 1).

Polymer	HBM DP	% MMA conversion	% HBM conversion	PMMA / PHBM	M_n (NMR) (g mol^{-1})	M_n (GPC) (g mol^{-1})	$Đ$ (GPC)
87	-	87	-	-	10550	10800	1.13
88	5	80	78	78: 3.9	8950	8700	1.18
89a	1	80	76	67: 1.6	7100	5430	1.19
89b	2	80	74	60: 3.0	6750	4967	1.23
89c	3	79	84	33: 4.6	4450	5581	1.29
90a	10	81	63	105: 12	15500	8100	1.25
90b	5	73	73	245: 7	27400	14400	1.24

Table 1. Data from homopolymerisation of PMMA **87** and gradient polymerisations of PMMA-PUIMMMA **88**, PMMA-PPyrMMA **89**, and PMMA-PUPyMMA **90**. For PMMA-PMMAPyr **89a** n = 1, **89b** n = 2, **89c** n = 3. For PMMA-PMMAUPy **90a** n = 10, **90b** n = 75 Data acquired by Dr Yasmeen Jhons.

The polymerisations performed here, showed that our HBM comonomers can be incorporated into covalent polymers by using RAFT. The polymerisation data indicates that comonomers PyrMMA **83** and UPyMMA **84** are more suitable for polymerisation than UIMMMA **82**. It was possible to produce gradient copolymers with relatively low dispersity, however when compared with PMMA homopolymer, the HBM copolymers all show an increase in dispersity (Table 1). This suggests that there was some loss of control in the polymerisations when the HBM comonomers were introduced. To investigate if there was a potential route to produce HBM functionalised polymers while maintaining well controlled polymerisation, the syntheses of end-functionalised polymers were explored.

Additional experiments performed on PMMA-PUPyMMA **90** polymers found that hydrogen-bonded cross-linked networks could be formed. These networks could be broken down in response to the addition of a competitive DAN HBM. This work was performed by Dr Yasmeen Jhons, therefore it is not discussed further in this thesis.

4.2 End functionalised polymers

In addition to main-chain functionalised polymers it was also desirable to develop a range of end-chain functionalised hydrogen-bonding polymers. One motivation behind the syntheses of end-functionalised polymers was to find a method of incorporation that had less impact on the polymer synthesis than the use of HBM comonomers. In addition to this, producing polymers with HBM functionality at different positions, would provide a wider range of possible reconfigurations. End functionalised polymers provide the opportunity to alter polymer structure at the terminus rather than in the main-chain, potentially leading to reconfigurable hydrogen-bonded block copolymers or a change in polymer molecular weight *via* a hydrogen-bonded chain extension.

To develop such polymers, two avenues were explored, firstly pre-polymerisation functionalisation and secondly post-polymerisation functionalisation. As with the monomers mentioned previously it was essential to incorporate the HBM functionality with a suitable linker between itself and the polymerisation-active moieties (especially for pre-polymerisation incorporation). In this case, to reduce the number of synthetic steps required, alkyne HBMs used for foldamer syntheses (chapter 2) could be utilised in azide click reactions to add functionality to the end of polymers.

4.2.1 Pre-polymerisation functionalisation

The first method used to add HBM functionality to polymers was through pre-polymerisation functionalisation of RAFT agents. A benefit of adding functionalisation in this way, is that incorporation is likely to be more complete than for post-polymerisation. Hydrogen bonding RAFT agents were synthesised *via* azide click reaction (Scheme 13). Alkynes **60**, **69** and **79** were linked to azide functionalised RAFT agent **91** by triazole ring formation. NAP-RAFT agent **92**, UPy-RAFT Agent **93** and DAN-RAFT agent **94** were all successfully synthesised in reasonable yields.

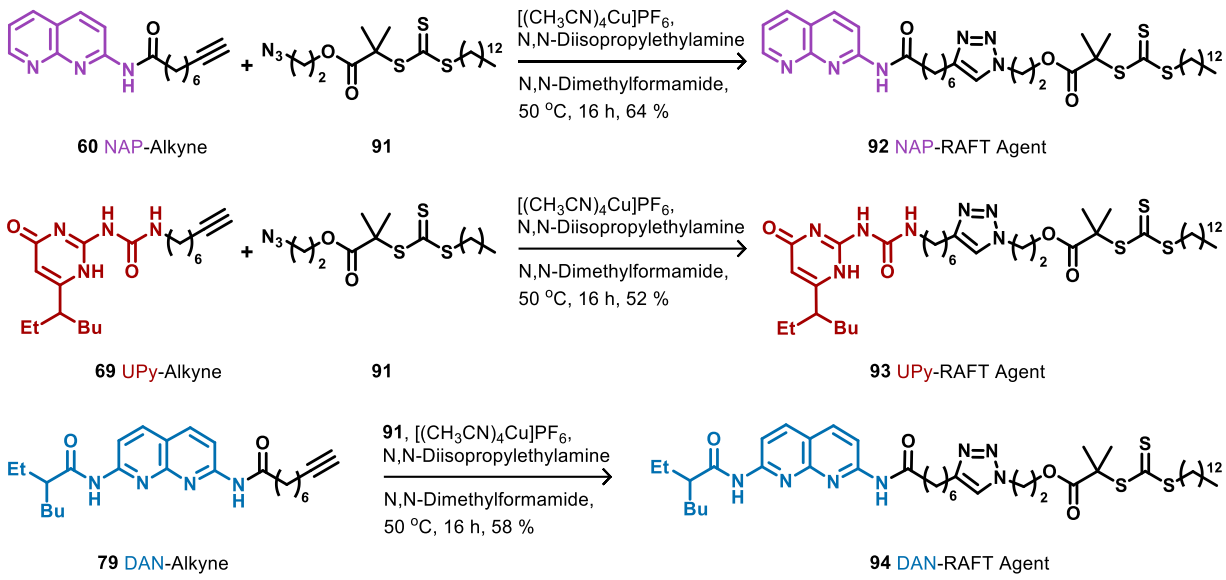

Scheme 13. Click chemistry syntheses of NAP-RAFT agent **92**, UPy-RAFT agent **93** and DAN-RAFT agent **94**.

Once a range of suitable hydrogen bonding RAFT agents had been synthesised, their ability to function as chain transfer agents was assessed. Studies performed by Dr Yasmeen Jhons determined that RAFT agent **91** was better suited to the polymerisation of methyl acrylate (MA) than MMA. Therefore, the viability of each HBM RAFT agent was tested by polymerisation of MA **95** (Scheme 14).

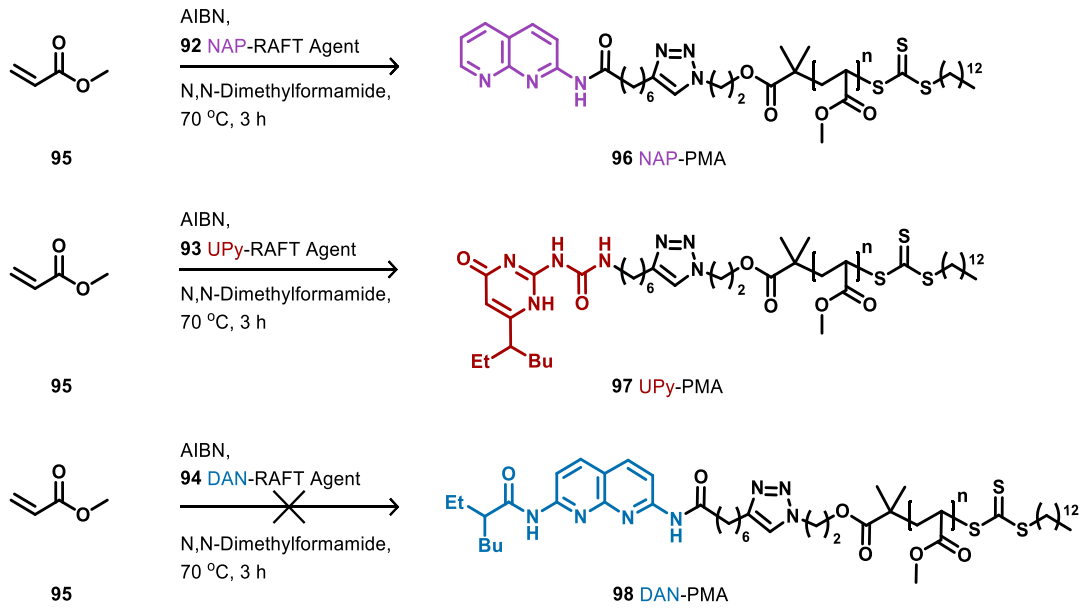

Scheme 14. RAFT polymerisations of MA **95** using NAP-RAFT agent **92**, UPy-RAFT agent **97**, and DAN-RAFT agent **98**. Polymerisations performed by Dr Yasmeen Jhons.

Analyses of each polymerisation was conducted *via* ^{1}H NMR and GPC (Table *2*). NAP-RAFT agent **92** was able to produce reasonably low dispersity polymers ($Đ$ = 1.19), however conversion from monomer to polymer was low after 3 hours, only reaching 31 %. This

suggested that the addition of the NAP HBM had an adverse impact on polymerisation, potentially through trapping of radical species. UPy-RAFT agent **93** also produced reasonably low dispersity polymers (*Đ* = 1.18), however using this RAFT agent, conversion was high at 84 %. RAFT agent **93**, was therefore deemed suitable to be used to produce UPy end-functionalised polymers. When polymerisation of methyl acrylate was attempted using DAN-RAFT agent **94** no evidence of polymerisation could be observed in crude ^{1}H NMR analysis after 3 hours. Upon purification, ^{1}H NMR analysis indicated only oligomerisation had taken place (approximately 3 repeat units). The low DP indicated that DAN-RAFT agent **94** was not suitable for this polymerisation, potentially acting as a radical trap, preventing the polymerisation from taking place.

Polymer	RAFT agent	% MA conversion	DP	M_n (NMR) (g mol^{-1})	M_n (GPC) (g mol^{-1})	$Đ_{(GPC)}$
96	**92** NAP	31	24	2800	3700	1.19
97	**93** UPy	84	148	13500	18200	1.18
98	**94** DAN	-	3	1100	-	-

Table 2. Data from polymerisations of MA **95** using RAFT agents **92**, **93** and **94**. Full analyses could not be carried out for polymer **98** due to unsuccessful polymerisation. Data acquired by Dr Yasmeen Jhons.

4.2.2 Post-polymerisation functionalisation

An alternative route to achieving end functional HBM polymers was to add functionality post-polymerisation. Here, polymerisations were carried out using azide functionalised RAFT agent **91**. The azide group was maintained in the polymerised structure, allowing for an azide click reaction to be performed using DAN-alkyne **79** (Scheme 15).

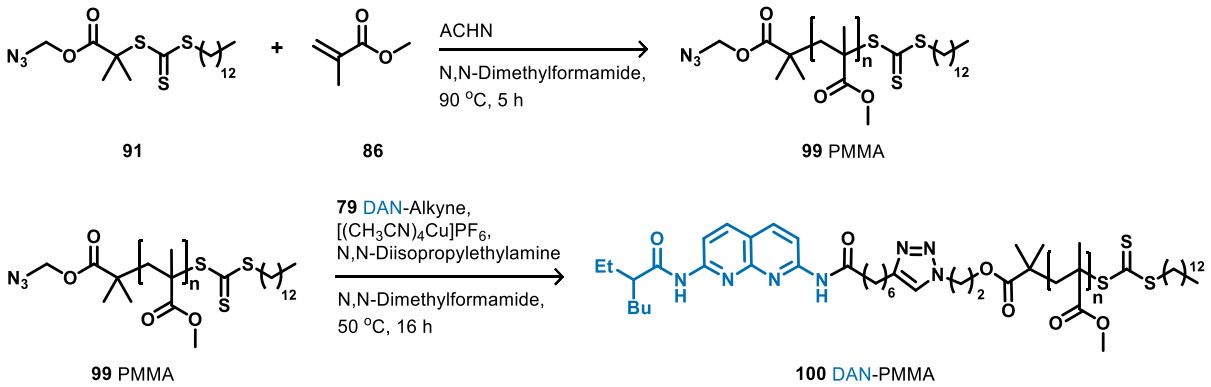

Scheme 15. Synthesis of PMMA **99** using azide RAFT agent **91** and post-polymerisation azide click reaction producing DAN-PMMA **100**.

For this work, PMMA was selected over PMA due to it being easier to purify after the addition of the HBM end group. Due to RAFT agent **91** not being well suited for the polymerisation of MMA, the polymers synthesised had a higher dispersity than desirable (Table 3).

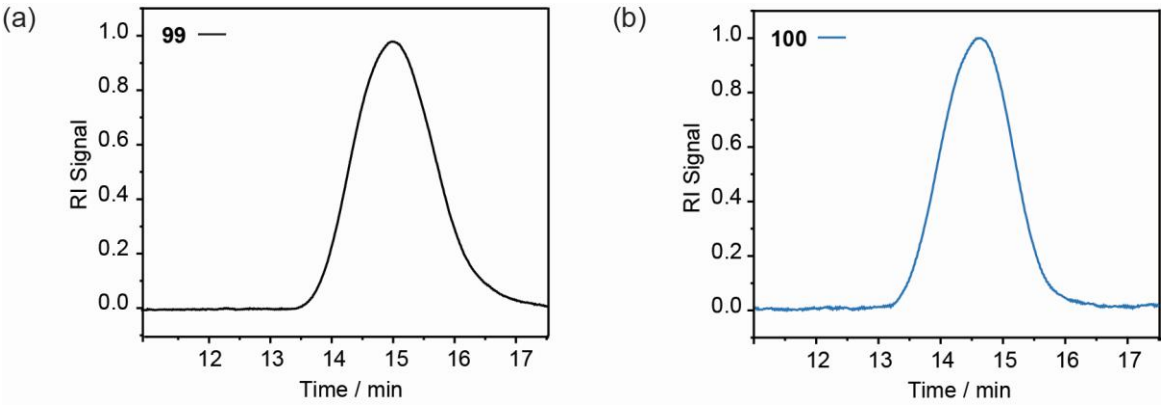

Figure 45. (a) GPC trace of PMMA **99** (pre-functionalisation); (b) GPC trace of DAN-PMMA **100** (post-functionalisation). Data for polymer **99** acquired by Dr Yasmeen Jhons.

Analyses of polymers **99** and **100** by GPC showed that there was a shift to higher molecular weight and lower dispersity after addition of the HBM (Figure 45.). This change was likely due to the additional purification performed after functionalisation; a size exclusion column was used to obtain polymer **98** which would have also resulted in the removal of some of the shorter polymer chains in the sample.

Polymer	% MMA conversion	$M_{n\,(GPC)}$ (g mol^{-1})	$Đ_{(GPC)}$
99	99	24600	1.52
100	99	31200	1.32

Table 3. Data for polymerisation of PMMA **99** and post-polymerisation functionalised DAN-PMMA **100**. M_n could not be obtained by NMR analysis due to overlapping signals. Data for polymer **99** acquired by Dr Yasmeen Jhons.

Analyses by NMR were more challenging; it was not possible to perform end group analysis due to overlapping RAFT agent and polymer proton environments. Despite this, NMR could still be used to calculate conversion and to provide structural information. The spectrum obtained for DAN-PMMA **100** could be used to confirm the incorporation of DAN functionality *via* key proton environments (Figure 46). Due to the overlapping RAFT agent and polymer signals, it was not possible to calculate the exact quantity of DAN successfully incorporated into DAN-PMMA **100**. However, using the integrals of the DAN proton environments identified, an approximate M_n of 32,000 g mol^{-1} was calculated. This M_n was similar to that obtained by GPC, suggesting that incorporation of the DAN HBM was close to complete.

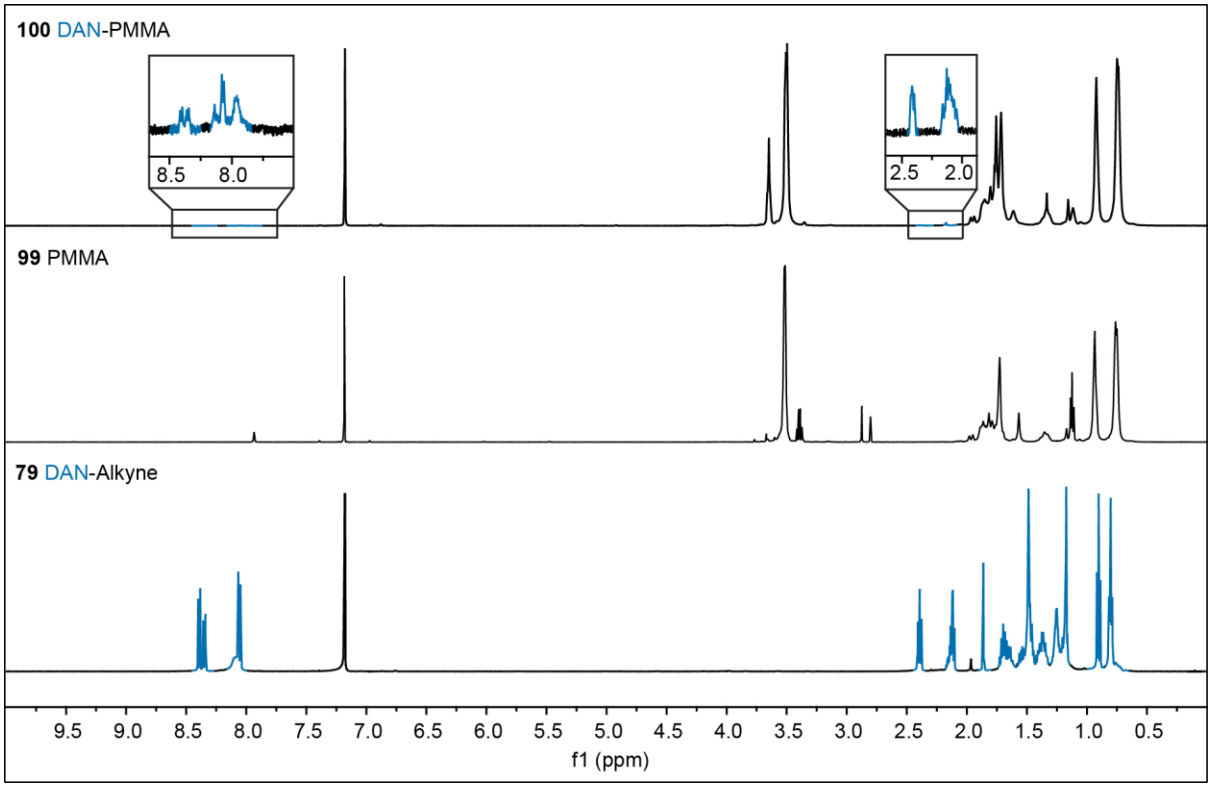

Figure 46. ^{1}H NMR spectra for DAN-Alkyne **79**, PMMA **99** and DAN-PMMA **100**. Insets show signals which indicate DAN HBM functionality has been incorporated into PMMA **100**. Spectrum for PMMA **99** acquired by Dr Yasmeen Jhons.

While there were some difficulties in the analyses of polymers **99** and **100**, post-polymerisation functionalisation benefits from no interference between HBM functionality and the mechanism of polymerisation. This method was therefore deemed to be effective for incorporation of HBMs which cannot be tolerated in the RAFT polymerisation mechanism.

4.3 Reconfigurable covalent polymers

To develop a photoresponsive reconfigurable polymer system using HBM functionalised polymers, DAN-PMMA polymer **100** and UPy·UPy foldamer **III** were selected. It was theorised that the *Z* isomer of UPy·UPy foldamer **III** would be unable to interact with DAN-PMMA **100**, with the two UPy HBMs preferentially hydrogen-bonding intramolecularly. Upon photoisomerisation, the UPy motifs no longer preferentially bind intramolecularly, and therefore become available to bind to the polymer's terminal DAN motifs. This interaction between foldamer and polymer would bring about a change a molecular weight of the polymer, effectively doubling the size of each chain *via* central hydrogen bonded linkages.

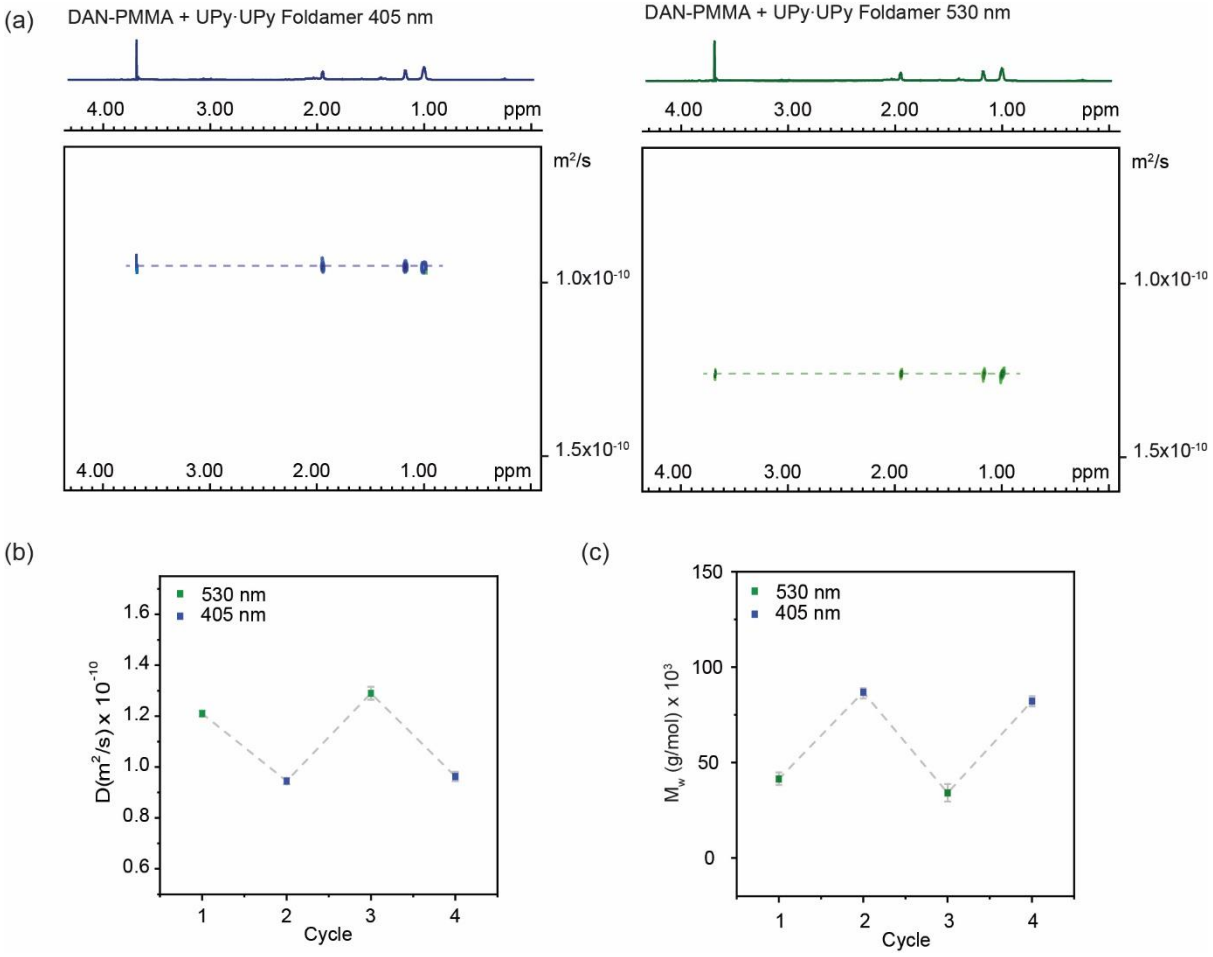

Figure 47. (a) DOSY spectra for DAN-PMMA **100** and UPy·UPy foldamer **III** after irradiation at 405 nm (blue) and 530 nm (green); (b) Diffusion coefficient of DAN-PMMA **100** and UPy·UPy foldamer **III** after 2 cycles of green and blue light irradiation; (c) molecular weight of DAN-PMMA **100** and UPy·UPy foldamer **III** after 2 cycles of green and blue light irradiation. Diffusion coefficients obtained from fitting data in Topspin Dynamics Center, errors estimated using the standard deviation from the fitting.

DOSY NMR studies were performed to assess this behaviour. To prevent the formation of supramolecular polymer from UPy·UPy foldamer **III**, samples of DAN-PMMA **100** and

UPy·UPy foldamer **III** were prepared at low concentrations (8 mM and 4 mM respectively). A 2:1 stoichiometry of polymer to foldamer was used so that each UPy motif in the ditopic foldamer could interact with one terminal DAN motif on each polymer chain. Initially, samples were exposed to green light (530 nm) for 10 minutes, then DOSY NMR was performed. This process was repeated after exposure to blue light (405 nm) for 10 minutes. A reduction in diffusion coefficient was observed after blue light irradiation, to confirm this behaviour was reversible, irradiation was performed using each wavelength again, and DOSY spectra recorded. The data obtained showed good evidence of a reversible change in diffusion coefficient upon irradiation (Figure 47). When converted to molecular weight it became clear that the species approximately doubles in size after blue light irradiation. These data confirm that, in this system, UPy·UPy foldamer **III** can undergo isomerisation from *Z* to *E*, resulting in a reversible interaction with DAN-PMMA **100** which effects a change in molecular weight of the polymer (Figure 48).

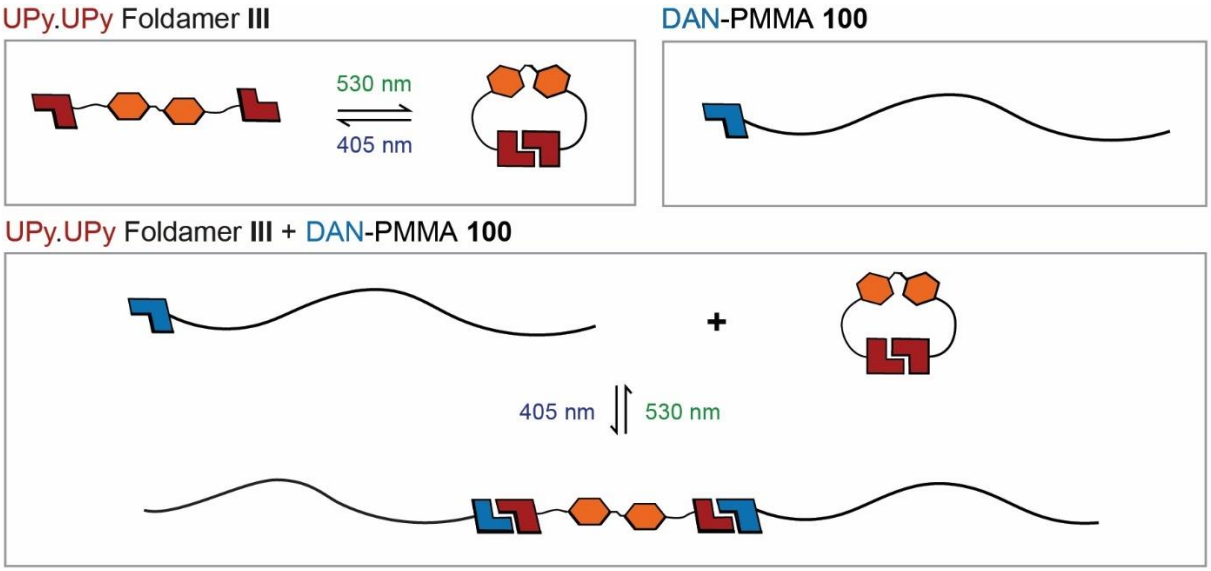

Figure 48. Schematic showing the reversible rearrangement of DAN-PMMA **100** and UPy·UPy foldamer **III** in response to blue and green light.

4.4 Conclusions

Hydrogen-bonding comonomers UIMMMA **82**, PyrMMA **83** and UPyMMA **84** were all successfully synthesised. Using these monomers pseudo-block copolymerisations were attempted. PMMA-PUIMMMA **88** could not be produced in a controlled manner due to poor solubility, however PMMA-PPyrMMA **89** and PMMA-PUPyMMA **90** were synthesised successfully. This method provided a range of PMMA copolymers with differing ratios of pendent HBM functionality. To add terminal hydrogen-bonding functionality both pre- and post- polymerisation techniques were investigated. NAP-RAFT agent **92**, UPy-RAFT agent **93** and DAN-RAFT agent **94** were synthesised and each tested in the polymerisation of MA. It was discovered that UPy-RAFT agent **93** worked well as a chain-transfer agent producing UPy-PMA **97**. However, NAP-RAFT agent **92** resulted in low conversion to polymer, and DAN-RAFT agent **94**, produced no polymer (only short oligomers). It was thought that the structures of these two RAFT agents likely provide a trap for radical species which are required for the polymerisations to progress. To circumvent this issue, PMMA was synthesised to contain functionality that allowed for post-polymerisation addition of HBMs. This method successfully produced DAN-PMMA **100**. Due to the established complementary UPy·DAN interaction, a reconfigurable polymer system using DAN-PMMA **100** and UPy·UPy foldamer **III** was proposed. Through DOSY NMR experiments, it was possible to determine that a change in polymer molecular weight could be initiated by photoisomerisation of UPy·UPy foldamer **III**. Future work should focus on characterising this polymer/foldamer system further. Viscosity measurements of the solutions after irradiation at each wavelength should be assessed to give further support to the DOSY evidence showing change in molecular weight. In addition to this, in future, a wide range of interactions could be explored between the other hydrogen-bonding polymers synthesised in this chapter, and the foldamers synthesised in chapter 2. These interactions could lead to the formation of complex reconfigurable polymer systems where significant changes in the material properties could be brought about in a reversible photoresponsive manner.

5. Summary and Future Work

5.1 Thesis Summary

The overall aim of this work was to develop reconfigurable polymers *via* the introduction of supramolecular self-sorting capabilities into polymeric materials. To achieve this, the design and syntheses of hydrogen-bonding photoresponsive foldamers were investigated. A range of hydrogen bonding motifs were investigated for use in these foldamers and three foldamers with different hydrogen bonding motifs were successfully synthesised. Next, the photoresponsive behaviours of the NAP·Pyr, UPy·UPy and UPy·DAN foldamers were tested using visible light irradiation. It was found that each could be isomerised effectively using blue and green light to produce their *E* and *Z* isomers respectively. Following on from these studies, the abilities of each foldamer to oligomerise and/or polymerise in response to light stimuli were evaluated. The studies revealed that the behaviour of each foldamer differed with both concentration and light stimulus. Additionally, the strength of the hydrogen bonding motifs used in the foldamer was found to be of paramount importance to the size of the supramolecular oligomers or polymers formed. At high concentrations both the UPy·UPy and UPy·DAN foldamers were able to form supramolecular polymers. These polymers altered their size and properties in response to visible light. Finally, the syntheses of hydrogen bonding motif functionalised covalent polymers were explored. To achieve such polymers, a range of hydrogen bonding monomers and RAFT agents were synthesised and their suitability to produce well controlled covalent polymers was tested. Multiple hydrogen bonding monomers were successfully incorporated into gradient copolymers. It was also possible to use hydrogen bonding RAFT agents to polymerise homopolymers, however this was unsuccessful for the DAN hydrogen bonding motif. Alternatively, it was discovered that the DAN motif could incorporated into polymers post-polymerisation. The resulting polymer was combined with the complementary UPy·UPy foldamer, which, upon irradiation, brought about a change in molecular weight of the polymer.

5.2 Future Directions

The work completed in chapter 2 was successful in synthesising three hydrogen bonding foldamers. In future work, the structures of these foldamers could be optimised for their use in supramolecular polymers. This could be achieved by exploring different linker chain lengths, alternative hydrogen bonding motifs, and different photoresponsive moieties. For example, the use of *o*-chlorofluoroazobenzenes may be of interest to develop near-infrared responsive foldamers for biological applications. Additionally, studies of the kinetic photoswitching behaviors of the foldamers, and the impact hydrogen bonding strength has on this could be of interest. To build upon the work completed in chapter 3, microscopy experiments could be used to distinguish the characteristics of the materials further. Techniques such as atomic force microscopy and transmission electron microscopy could be used for studying the surface morphologies and any assemblies taking place on the nanoscale. Moreover, to develop polymeric materials which reconfigure to bring about significant changes in their physical properties, a combination of the foldamer systems described in chapter 3 could be combined with the hydrogen bonding polymers from chapter 4. This idea was explored briefly at the end of chapter 4 (section 3), showing that interactions can take place between hydrogen bonding foldamers and polymers, whilst maintaining their ability to isomerise and subsequently self-soft. These experiments could be expanded upon in future by using polymers with lower dispersities, and lower molecular weight so that the hydrogen bonding interactions present can be monitored by proton NMR. It could also be of interest to explore the addition of foldamers into polymer systems where both hydrophobic and hydrophilic polymers are present. This could present an opportunity to develop a system where light-initiated self-assembly into nanoparticles could be explored.

6. Experimental

6.1 General Considerations

Solvents and reagents were purchased from Sigma Aldrich, Fluorochem or Fisher Scientific and used without further purification unless otherwise stated. Where anhydrous solvents or reagents were required, tetrahydrofuran was obtained from the in-house solvent purification system Innovative Inc. PureSolv® (dried over activated alumina), anhydrous triethylamine was purchased from Fluorochem and anhydrous dimethylsulfoxide from Sigma Aldrich. All non-aqueous reactions were carried out in oven-dried glassware under a nitrogen atmosphere with magnetic stirrer bars, unless otherwise stated. All work-up and purification procedures were carried out using reagent-grade solvents under ambient atmosphere. Analytical thin layer chromatography was performed on Merck Kieselgel 60 F_{254} 0.25 mm pre-coated aluminium plates and visualised by UV quenching (λ_{max}=254 nm). Flash chromatography was carried out using Merck Kieselgel 60 silica gel. High-performance liquid chromatography (HPLC) was performed with an Agilent Technologies 1290 Infinity analytical preparative system equipped with a Kinetex EVO C18 reverse-phase column (φ 21.2 x 250 mm).

Infra-red (IR) spectra were obtained using a PerkinElmer Fourier transform IR spectrometer in which absorption maxima (ν_{max}) are expressed in wavenumbers (cm^{-1}). High-resolution mass spectrometry (HRMS) was performed using a Bruker maXis Impact QTOF mass spectrometer, with an electrospray ionisation (ESI) source. UV-Vis absorption spectra were recorded on an Agilent Technologies Cary Series UV-Vis spectrophotometer.

For NMR experiments anhydrous chloroform-*d* was purchased from Sigma Aldrich. All ^{1}H NMR spectra were acquired on Bruker AVANCE spectrometers, operating at 400 MHz or 500 MHz for ^{1}H, 100 MHz or 125 MHz for ^{13}C and 375 MHz for ^{19}F. NMR spectra were obtained at 298 K and referenced using residual solvent signals as internal standards unless stated otherwise. The spectrometers used for 1D experiments were either a two-channel Bruker AV3HD NMR spectrometer operating at 9.4 T (400 MHz ^{1}H) equipped with a 5 mm BBO probe or a two-channel Bruker AV-NEO NMR spectrometer operating at 11.7 T (500 MHz ^{1}H) equipped with a 5 mm DCH cryoprobe. DOSY spectra were obtained using a four-channel Bruker AV-NEO NMR spectrometer operating at 11.7 T (500 MHz ^{1}H) and equipped with 5mm TXI probe (δ = 0.002 s, Δ = 0.0999). Chemical shifts are expressed in parts per million (ppm) and the following abbreviations are used: s (singlet), d (doublet), t (triplet), q (quartet), m (multiplet) and br (broad).1D and 2D NMR spectra can be found appendices A and B respectively.

6.2 Compound Synthesis

1-(4-Bromo-2,6-difluorophenyl)-2-(2,6-difluoro-4-iodophenyl)diazene – 52

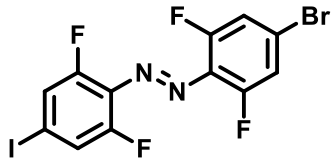

Procedure adapted from literature.[135] 2,6-Difluoro-4-bromoaniline **49** (0.85 g, 4.06 mmol, 1.0 eq) was dissolved in chloroform (10 mL) and stirred. Oxone (5.00 g, 8.13 mmol, 2.0 eq) was dissolved in water (40 mL) and added to the chloroform solution dropwise. The biphasic mixture was stirred for 16 h and the product extracted into chloroform (3 x 20 mL). The combined organic extracts were washed with 1 M hydrochloric acid solution (2 x 20 mL), saturated sodium bicarbonate solution (2 x 20 mL), water (2 x 20 mL) and brine (2 x 20 mL), then dried with magnesium sulfate, filtered and concentrated to give a brown solid. Without further purification the crude product was suspended in a mixture of toluene, acetic acid and trifluoroacetic acid (1:1:0.17), then 2,6-difluoro-4-iodo-analine **51** (0.88 g, 3.45 mmol, 0.85 eq) was added. The reaction was stirred for 16 h then concentrated to give a brown solid. The product was isolated *via* column chromatography (SiO_2, 6:4 hexane: dichloromethane), then crystallised from ethanol, to give the title compound **52** as red needles (0.51 g, 1.10 mmol, 38 %). ^{1}H NMR (500 MHz, chloroform-*d*) δ 7.53 – 7.46 (m, 2H, 2 x ArI-*H*), 7.30 (dd, 2H, J 6.9, 4.9 Hz, 2 x ArBr-*H*); ^{13}C NMR (100 MHz, chloroform-*d*) δ 156.6 (d), 153.9 (d), 134.1 (t), 130.8 (t), 122.5 (dd), 116.8 (dd), 94.7 (t); ^{19}F NMR (375 MHz, chloroform-*d*) δ -118.6 (d), -119.5 (d); Rf 0.57 (60:40 hexane: dichloromethane); IR v_{max} (solid state) = 3476.9, 3366.7, 2345.9, 1595.2 cm^{-1}; ESI-HRMS *m/z* found 458.8613 $[M + H]^+$ $C_{12}H_5BrF_4IN_2$ requires 458.8611.

8-Nonynoic acid – 54

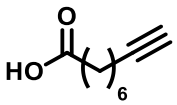

Procedure adapted from literature.[135] 7-Bromoheptanoic acid **53** (1.9 g, 9.1 mmol, 1 eq) in anhydrous dimethyl sulfoxide (3 mL) was added to suspension of lithium acetylide ethylenediamine complex (3.3 g, 36.4 mmol, 4 eq) in anhydrous dimethyl sulfoxide (30 mL) dropwise at 0 °C over 30 min. After stirring at 0 °C for 1 h, the solution was warmed to room temperature, and stirred for a further 2 h. The reaction mixture was quenched by pouring onto 10% sulfuric acid solution (225 mL) at 0 °C. The aqueous phase was extracted with hexane (3 x 100 mL) and the combined organic fractions were dried over sodium sulfate, filtered and

concentrated to give the title compound **54** as a light pink liquid (1.09 g, 7.1 mmol, 78%). ^{1}H NMR (400 MHz, chloroform-*d*) δ 11.45 (s, 1H, COO*H*), 2.31 (t, *J* 7.5 Hz, 2H, C*H*$_2$COOH), 2.14 (td, *J* 7.0, 2.6 Hz, 2H, C*H*$_2$CCH), 1.91 (t, *J* 2.6 Hz, 1H, CH$_2$CC*H*), 1.60 (p, *J* 7.5 Hz, 2H, C*H*$_2$), 1.53 – 1.21 (m, 6H C*H*$_2$C*H*$_2$C*H*$_2$); ^{13}C NMR (100 MHz, chloroform-*d*) δ 180.3, 84.3, 68.2, 33.9, 28.3, 28.1, 28.0, 24.3, 18.1; Rf 0.74 (1:1 hexane: ethyl acetate); IR ν_{max} (solid state) = 3300.7, 2935.7, 2116.9, 1703.6 cm^{-1}; ESI-HRMS *m/z* found 153.0913 $[M - H]^-$ $C_9H_{13}O_2$ requires 153.0921.

1-(Oct-7-yn-1-yl)-3-(pyridin-2-yl)urea – 56 (Pyr alkyne)

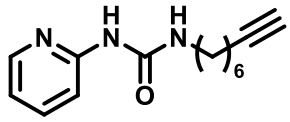

Procedure adapted from literature.[135] Triethylamine (0.18 mL, 1.31 mmol, 1 eq) and diphenylphosphoryl azide (0.28 mL, 1.31 mmol, 1 eq) were added to a solution of 8-nonynoic acid **54** (0.20 g. 1.31 mmol, 1 eq) in acetonitrile (5 mL). After stirring for 2 h at 50 °C, 2-aminopyridine **55** (0.12 g, 1.31 mmol, 1 eq) was added, and the solution was heated to reflux for 5 h. The solution was concentrated, and the residue purified by column chromatography (SiO_2, 1:1 hexane: ethyl acetate) to give the title compound **56** as a white solid (0.20 g, 0.82 mmol, 62 %). ^{1}H NMR (500 MHz, chloroform-*d*) δ 9.36 (s, 1H, N*H*), 8.67 (s, 1H, N*H*), 8.18 (ddd, 1H, *J* 5.2, 1.9, 0.9 Hz, Pyr-*H*), 7.76 – 7.48 (m, 1H, Pyr-*H*), 6.97 – 6.76 (m, 2H, 2 x Pyr-*H*), 3.41 (m, 2H, NHCONH-C*H*$_2$), 2.22 (m, 2H, HCC-C*H*$_2$), 1.96 (td, 1H, *J* 2.7, 0.9Hz, CC*H*), 1.70 – 1.61 (m, 2H, C*H*$_2$), 1.61 – 1.54 (m, 2H, C*H*$_2$), 1.53 – 1.39 (m, 4H, 2 x C*H*$_2$); ^{13}C NMR (125 MHz, chloroform-*d*) δ 156.2, 153.5, 145.7, 138.4, 112.0, 84.6, 68.2, 39.8, 29.9, 28.4, 28.4, 26.5, 18.4; Rf 0.49 (1:1 hexane: ethyl acetate); IR ν_{max} (solid state) = 3244.4, 2919.0, 1678.9 cm^{-1}; ESI-HRMS *m/z* found 246.1610 $[M + H]^+$ $C_{14}H_{20}N_3O$ requires 246.1601.

1,8-Naphthyridin-2-amine – 59

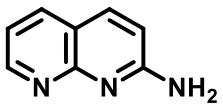

Procedure adapted from literature.[135] 2,6-Diaminopyridine **57** (5.0 g, 46.0 mmol, 1 eq) was suspended in polyphosphoric acid (30 g). After stirring at 90 °C for 1 h, 1,1,3,3-tetramethoxypropane **58** (7.9 mL, 48.0, 1.05 eq) was added dropwise over 15 min. The solution was heated to 110 °C and stirred for 4 h. After cooling to room temperature, chloroform (180 mL) and water (90 mL) were added. A solution of 10 N sodium hydroxide (180 mL) was used to quench the reaction at 0 °C, the resulting brown precipitate was removed *via* filtration and washed with chloroform. The organic extracts were combined, dried with sodium

sulfate, filtered, and concentrated. The residue was purified by column chromatography (SiO_2, 9:1 dichloromethane: methanol) to give the title compound **59** as a yellow powder (2.67 g, 18.4 mmol, 40 %). ^{1}H NMR (400 MHz, chloroform-*d*) δ 8.88 (dd, 1H, *J* 4.4, 2.0 Hz, Ar*H*), 7.97 (dd, 1H, *J* 7.9, 2.0 Hz, Ar*H*), 7.89 (d, 1H, *J* 8.7 Hz, Ar*H*), 7.22 (dd, 1H, *J* 7.9, 4.4 Hz, Ar*H*), 6.82 (d, 1H, *J* 8.7 Hz, NH_2-Ar*H*), 5.27 (br s, 2H, NH_2); ^{13}C NMR (125 MHz, chloroform-*d*) δ 159.4, 156.6, 152.9, 138.4, 136.3, 118.4, 117.6, 112.6; Rf 0.38 (9:1 dichloromethane: methanol); IR v_{max} (solid state) = 3314.5, 3161.5, 1617.5 cm^{-1}; ESI-HRMS *m/z* found 146.0711 $[M + H]^+$ $C_8H_8N_3$ requires 146.0713.

***N*-(1,8-Naphthyridin-2-yl)non-8-ynamide – 60 (NAP alkyne)**

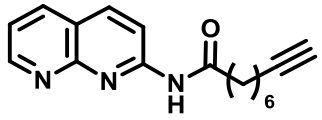

Procedure adapted from literature.[135] EDC (1.29 g. 8.3 mmol, 1.2 eq) was added to a solution of 8-nonynoic acid **54** (1.28 g, 8.3 mmol, 1.2 eq) and 4-dimethylaminopyridine (1.26 g, 10.3 mmol, 1.5 eq) in chloroform (50 mL). After stirring for 30 min, **59** (1.00 g, 6.9 mmol, 1 eq) was added, and the solution was stirred at 50 °C for 16 h. Chloroform was then removed by rotary evaporation, and the crude material redissolved in ethyl acetate (50 mL), and washed with 1M hydrochloric acid (2 x 20 mL), saturated sodium bicarbonate solution (2 x 20 mL) and brine (20 mL). After drying over sodium sulfate and concentration in vacuo, title compound **60** was afforded as a white solid (2.34 g, 7.9 mmol, 85 %). ^{1}H NMR (500 MHz, chloroform-d) δ 9.62 (s, 1H, N*H*), 9.07 (dd, 1H, J 4.3, 1.8 Hz, Ar*H*), 8.63 (d, 1H, J 8.9 Hz, Ar*H*), 8.30 (d, 1H, J 8.9 Hz, Ar*H*), 8.23 (d, 1H, J 8.0 Hz, Ar*H*), 7.51 (dt, 1H, J 11.2, 5.6 Hz, Ar*H*), 2.60 (t, 2H, J 7.4 Hz, HNCOCH_2), 2.22 (td, J 6.9, 2.6 Hz, 2H, HCC-CH_2), 1.97 (t, 1H, J 2.6 Hz, CC*H*), 1.82 (p, 2H, J 7.5 Hz, CH_2), 1.63 – 1.54 (m, 2H, CH_2), 1.49 (ddt, 4H, J 11.0, 8.5, 5.5 Hz, 2 x CH_2);^{13}C NMR (125 MHz, chloroform-*d*) δ 172.8, 154.0, 153.8, 153.6, 139.9, 136.9, 121.1, 120.6, 115.4, 84.5, 68.3, 37.9, 28.6, 28.4, 28.2, 25.0, 18.3; Rf 0.30 (ethyl acetate); IR v_{max} (solid state) = 3291.3, 2932.3, 1695.6 cm^{-1}; ESI-HRMS m/z found 282.1608 [M + H]+ $C_{17}H_{20}N_3O$ requires 282.1601.

1-(8-(4-((4-Bromo-2,6-difluorophenyl)diazenyl)-3,5-difluorophenyl)oct-7-yn-1-yl)-3-(pyridin-2-yl)urea – 61

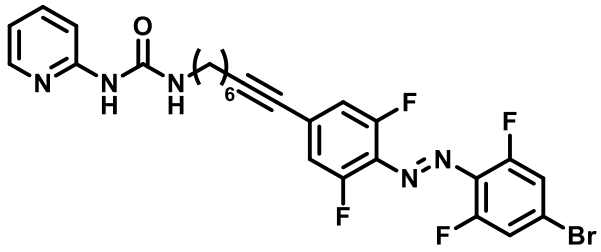

Procedure adapted from literature.[135] Azobenzene **52** (1.70, 3.71, 1.0 eq), copper iodide (5 mol%), bis(triphenylphosphine)palladium(II) dichloride (2 mol%), and Pyr alkyne **56** (1.00 g, 4.08 mmol, 1.1 eq) were added to an oven dried flask. The flask was evacuated and back-filled with nitrogen three times, before anhydrous tetrahydrofuran (20 mL) was added. Anhydrous triethylamine (2.59 mL, 18.6 mmol, 5 eq) was prepared *via* three freeze, pump thaw cycles then added to the reaction mixture. The solution was stirred under nitrogen at room temperature for 16 h. The solvent was removed, and the crude red solid purified *via* column chromatography (SiO_2, 1:1 hexane: ethyl acetate). The resulting red solid was crystallised from acetonitrile to give the title compound **61** as an orange powder (1.30 g, 2.26 mmol, 61 %). ^{1}H NMR (400 MHz, chloroform-*d*) δ 9.24 (s, 1H, N*H*), 8.17 (dd, 1H, *J* 5.4, 2.1 Hz, Pyr*H*), 7.74 – 7.57 (m, 1H, Pyr*H*), 7.32 – 7.27 (m, 2H, 2 x Br-AB-*H*), 7.13 – 7.02 (m, 2H, 2 x AB-*H*), 6.98 – 6.78 (m, 2H, 2 x Pyr*H*), 3.42 (td, 2H, *J* 7.0, 5.6 Hz, NHCONH-CH_2), 2.47 (t, 2H, *J* 7.0 Hz, CC-CH_2), 1.70 (dd, 4H, *J* 14.1, 7.1 Hz, 2 x CH_2), 1.59 – 1.41 (m, 4H, 2 x CH_2); ^{13}C NMR (125 MHz, chloroform-*d*) δ 156.5 (dd), 155.8, 154.4 (d), 153.1, 145.4, 138.8, 130.9 (q), 128.4 (t), 124.0 (t), 116.9 – 116.4 (m), 116.1 – 115.3 (m), 112.1, 96.2, 78.9 (t), 39.8, 29.8, 28.4 (d), 26.5, 19.5; ^{19}F NMR (375 MHz, chloroform-*d*) δ -118.9 (d), -120.6 (d); Rf 0.29 (1:1 hexane: ethyl acetate); IR ν_{max} (solid state) = 3219.1, 3118.5, 2920.9, 2856.7, 2232.6, 1677.8 cm^{-1}; ESI-HRMS *m/z* found 576.1041 $[M + H]^+$ $C_{26}H_{23}BrF_4N_5O$ requires 576.1017.

9-(4-((2,6-Difluoro-4-(8-(3-(pyridin-2-yl)ureido)oct-1-yn-1-yl)phenyl)diazenyl)-3,5-difluorophenyl)-*N*-(1,8- naphthyridin-2-yl)non-8-ynamide – Foldamer I

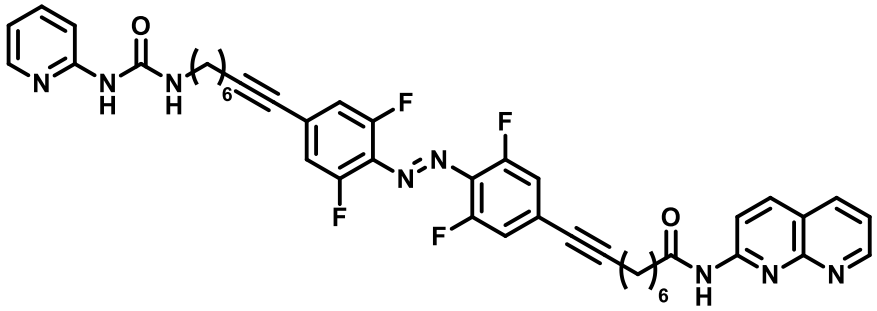

Procedure adapted from literature.[135] **61** (0.20 g, 0.35 mmol, 1.0 eq), bis(triphenylphosphine)palladium(II) dichloride (2 mol%), copper iodide (5 mol%) and NAP alkyne **60** (0.10 g 0.35 mmol, 1.0 eq) were added to an oven dried flask. The flask was evacuated and back-filled with nitrogen three times, before anhydrous tetrahydrofuran (100 mL) was added. Anhydrous triethylamine (0.24 mL, 1.75 mmol, 5.0 eq) was prepared *via* three freeze, pump thaw cycles then added to the reaction mixture. The solution was stirred under nitrogen at room temperature for 16 h. The solvent was removed, and the crude red solid purified *via* column chromatography (SiO_2, ethyl acetate). The resulting red solid was further purified by reverse phase HPLC (50-60 % MeCN in H_2O) the product was isolated by lyophilisation to afford foldamer **I** as an orange powder (0.10 g, 0.12 mmol, 35 %). *E* isomer - ^{1}H NMR (500 MHz, chloroform-*d*) δ 8.96 (s, 1H, N*H*), 8.83 (s, 1H, N*H*), 8.51 (d, 1H, *J* 8.9 Hz, Nap-*H*), 8.31 – 7.90 (m, 4H, 2 x Nap-*H,* 2 x Pyr-*H*), 7.82 – 7.70 (m, 1H, Nap-*H*), 7.47 – 7.23 (m, 2H, Nap-*H*, Pyr-*H*), 7.04 – 6.90 (m, 5H, 4 x AB-*H*, Pyr-*H*), 3.29 (q, 2H, *J* 6.4 Hz, NHCONH-C*H*$_2$), 2.47 (t, 2H, *J* 7.5 Hz, CONH-C*H*$_2$), 2.38 (m, 4H, 2 x CC-C*H*$_2$), 1.75 (q, 2H, *J* 7.4 Hz, C*H*$_2$), 1.57 (q, 6H, *J* 7.2 Hz), 1.46 – 1.35 (m, 8H, 4 x C*H*$_2$); *Z* isomer - ^{1}H NMR (500 MHz, chloroform-*d*) δ 10.32 (s, 1H, N*H*), 9.10 (s, 1H, N*H*), 9.04 (s, 1H, N*H*), 8.61 (t, 1H, *J* 9.3 Hz, Nap-*H*), 8.33 – 8.08 (m,4H, 2 x Nap-*H,* 2 x Pyr-*H*), 7.76 – 7.64 (m, 1H, Nap-*H*), 7.46 (m, 2H, Nap-*H*, Pyr-*H*), 7.10 – 7.03 (m, 2H, 2 x AB-*H*), 6.95 (dt, 1H, *J* 13.6, 6.1 Hz, Pyr-*H*), 6.87 (dd, 2H, *J* 7.8, 2.5 Hz, 2 x AB-*H*), 3.40 (q, 2H, *J* 6.6 Hz, NHCONH-C*H*$_2$), 2.56 (q, 2H, *J* 7.5 Hz, CONH-C*H*$_2$), 2.46 (td, 2H, *J* 7.1, 2.3 Hz, (Pyr)CC-C*H*$_2$), 2.40 (t, 2H, *J* 6.8 Hz, (Nap)CC-C*H*$_2$), 1.82 (q, 2H, *J* 6.6, 5.9 Hz, C*H*$_2$), 1.76 – 1.57 (m, 6H, 3 x C*H*$_2$), 1.57 – 1.37 (m, 8H, 4 x C*H*$_2$); ^{13}C NMR (125 MHz, chloroform-d_3) δ 172.7, 156.5, 154.7, 154.6, 154.4, 154.4, 153.2, 152.8, 152.3, 150.4, 147.1, 139.6, 139.5, 136.9, 136.9, 136.8, 136.7, 126.3, 126.3, 126.1, 116.8, 116.8, 115.9, 115.8, 115.7, 115.7, 115.3, 115.3, 115.2, 95.9, 94.8, 78.9, 78.5, 39.8, 37.6, 29.8, 28.7, 28.7, 28.4, 28.1, 28.1, 26.5, 25.1, 19.5, 19.3; ^{19}F NMR (375 MHz, chloroform-*d*) δ -119.7 (dd), -120.8 (d); Rf 0.39 (ethyl acetate); IR ν_{max} (solid state) = 3271.2, 3140.0, 3050.6, 2928.1,

2855.0, 2229.5, 1662.0 cm^{-1}; ESI-HRMS *m/z* found 777.3398 $[M + H]^+$ $C_{43}H_{41}F_4N_8O_2$ requires 777.3283.

***N*-(6-methyl-4-oxo-1,4-dihydropyrimidin-2-yl)non-8-ynamide – 63 (AIC linker)**

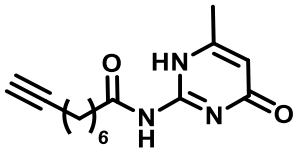

EDC (0.2 g. 1.3 mmol, 1.2 eq) was added to a solution of 8-noynoic acid **54** (0.2 g, 8.3 mmol, 1.2 eq) and 4-dimethylaminopyridine (0.2 g, 1.3 mmol, 1.5 eq) in tetrahydrofuran (20 mL). After stirring for 30 min, 6-methylisocytosine **62** (0.14 g, 1.1 mmol, 1 eq) was added, and the solution was stirred at 50 °C for 16 h. Tetrahydrofuran was then removed by rotary evaporation, and the crude material redissolved in ethyl acetate (30 mL) and washed with 1M hydrochloric acid (2 x 20 mL), saturated sodium bicarbonate solution (2 x 20 mL) and brine (20 mL). After drying over sodium sulfate and concentration the title compound **63** was afforded as a white solid (0.24 g, 0.9 mmol, 82 %). ^{1}H NMR (400 MHz, chloroform-*d*) δ 6.01 (d, *J* 0.7 Hz, 1H, Ar-C*H*), 2.52 (t, *J* 7.4 Hz, 2H, CH_2CONH), 2.24 (s, 3H, Ar-CH_3), 2.18 (m, 2H, CH_2CCH), 1.93 (t, *J* 2.6 Hz, 1H, *H*CC), 1.77 – 1.66 (m, 2H, CH_2), 1.58 – 1.49 (m, 2H, CH_2), 1.49 – 1.34 (m, 4H, CH_2CH_2); ^{13}C NMR (125 MHz, chloroform-*d*) δ 170.10, 133.07, 132.59, 126.77, 116.13, 115.56, 84.42, 68.36, 35.00, 28.53, 28.31, 28.19, 24.06, 18.34; Rf 0.19 (SiO_2, 1:1 hexane: ethyl acetate); ESI-HRMS *m/z* found 262.1544 $[M + H]^+$ $C_{14}H_{20}N_3O_2$ requires 262.1550.

1-(5,6-Dimethyl-1*H*-benzo[*d*]imidazole-2-yl)-3-(oct-7-yn-1-yl)urea – 66 (UIM alkyne)

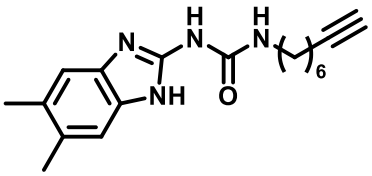

Triethylamine (1.18 mL, 8.5 mmol, 1.0 eq) and diphenylphosphoryl azide (1.70 mL, 8.5 mmol, 1.0 eq) were added to a solution of 8-noynoic acid **54** (1.30 g. 8.5 mmol, 1.0 eq) in tetrahydrofuran (50 mL). After stirring for 2 h at 50 °C, 2-amino-5,6-dimethylbenzimidazole **65** (1.50 g, 9.3 mmol, 1.1 eq) was added, and the solution was heated to reflux for 4 h. The solution was concentrated, and the residue purified by column chromatography (SiO_2, 9:1 ethyl acetate: methanol) to give the title compound **66** as a white solid (1.63 g, 5.2 mmol, 62 %).^{1}H NMR (500 MHz, dimethyl sulfoxide-d_6) δ 11.19 (s, 1H, N*H*), 9.64 (s, 1H, N*H*), 7.44 (s, 1H, N*H*), 7.11 (s, 2H, 2 x Ar-*H*), 3.16 (q, 2H, *J* 6.6 Hz, NHCONH-CH_2), 2.74 (q, 1H, *J* 2.9 Hz, CC*H*), 2.23 (s, 6H, 2 x Ar-CH_3), 2.15 (m, 2H, HCC-CH_2), 1.46 (m, 4H, 2 x CH_2), 1.34 (m, 4H, 2 x CH_2); ^{13}C NMR (125 MHz, dimethyl sulfoxide-d_6) δ 158.7, 143.5, 140.9, 135.9, 128.3, 123.8, 114.8,

105.1, 85.0, 71.7, 30.4, 29.9, 28.4, 28.3, 26.3, 20.3, 18.1; Rf 0.55 (9:1 ethyl acetate: methanol); IR ν_{max} (solid state) = 3291.9, 3066.4, 2859.0, 2116.6, 1721.7, 1642.4 cm^{-1}; ESI-HRMS *m/z* found 313.2029 $[M + H]^+$ $C_{18}H_{25}N_4O$ requires 313.2023.

9-(4-((4-Bromo-2,6-difluorophenyl)diazenyl)-3,5-difluorophenyl)-*N*-(6-methyl-4-oxo-1,4-dihydropyrimidin-2-yl)non-8-ynamide – 67

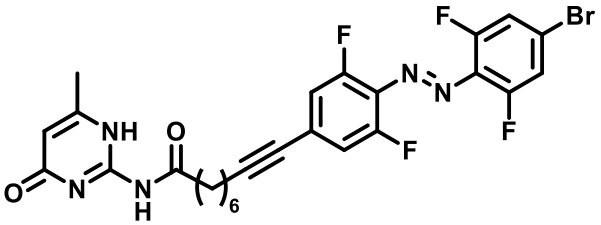

Azobenzene **52** (1.28 g, 2.78 mmol, 1.0 eq), bis(triphenylphosphine)palladium(II) dichloride (2 mol%), copper iodide (5 mol%) and AIC alkyne **63** (0.80 g, 3.06 mmol, 1.1 eq) were added to an oven dried flask. The flask was evacuated and back-filled with nitrogen three times, before anhydrous tetrahydrofuran (25 mL) was added. Anhydrous triethylamine (1.94 mL, 13.9 mmol, 5.0 eq) was prepared *via* three freeze, pump thaw cycles then added to the reaction mixture. The solution was stirred under nitrogen at room temperature for 16 h. The solvent was removed and the crude red solid purified *via* column chromatography (SiO_2, ethyl acetate) to afford the title compound **67** as and orange powder (0.82 g mmol, 50 %). ^{1}H NMR (400 MHz, dimethyl sulfoxide-d_6) δ 11.81 (s, 1H, N*H*), 11.59 (s, 1H, N*H*), 7.79 (d, 2H, *J* 9.6 Hz, AB-*H*), 7.41 (d, 2H, *J* 10.8 Hz, AB-*H*), 5.92 (s, 1H, Ar-*H*), 2.44 (d, 2H, *J* 7.4 Hz, CONH-CH_2), 2.13 (s, 3H, Ar-CH_3), 1.70 – 1.47 (m, 4H, 2 x CH_2), 1.37 (m, 4H, 2 x CH_2). ^{13}C NMR (100 MHz, chloroform-*d*) δ 174.21, 169.16, 165.66, 157.21 – 155.48 (m), 154.73, 154.18 (d), 132.12 (d), 128.53 (d), 116.24 (dd), 95.94, 78.94, 37.20, 29.30 – 28.33 (m), 28.09 (d), 24.66 (d), 19.45. Rf 0.48 (Ethyl acetate); IR ν_{max} (solid state) = 3291.9, 3066.4, 2859.0, 2116.6, 1721.7, 1642.4 cm^{-1}; ESI-HRMS *m/z* found 594.0979 $[M + H]^+$ $C_{26}H_{23}BrF_4N_5O_2$ requires 594.0945.

9-(4-((4-(8-(3-(5,6-dimethyl-1*H*-benzo[*d*]imidazole-2-yl)ureido)oct-1-yn-1-yl)-2,6-difluorophenyl)diazenyl)-3,5-difluorophenyl)-*N*-(6-methyl-4-oxo-1,4-dihydropyrimidin-2-yl)non-8-ynamide – Foldamer III

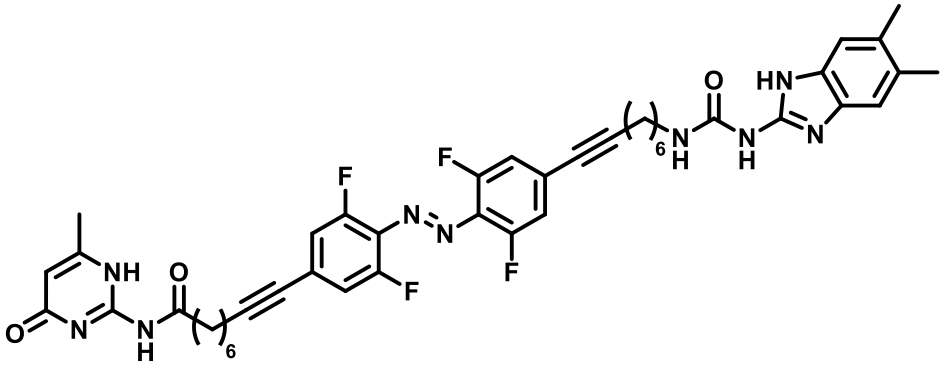

67 (0.60 g, 1.01 mmol, 1.0 eq), bis(triphenylphosphine) palladium(II) dichloride (2 mol %), copper iodide (5 mol %) and UIM alkyne **66** (0.32 g, 1.01 mmol, 1.0 eq) were added to an oven dried flask. The flask was evacuated and back-filled with nitrogen three times, before anhydrous tetrahydrofuran (20 mL) was added. Anhydrous triethylamine (0.71 mL, 5.06 mmol, 5.0 eq) was prepared *via* three freeze, pump thaw cycles then added to the reaction mixture. The solution was stirred under nitrogen at 55 °C for 16 h. The solvent was removed; however the crude red solid could not be purified at this stage. LC-MS *m/z* found 824.46 [M + H]+ $C44H46F_4N9O3$ requires 824.37.

1-(6-(heptan-3-yl)-4-oxo-1,4-dihydropyrimidin-2-yl)-3-(oct-7-yn-1-yl)urea – 69 (UPy alkyne)

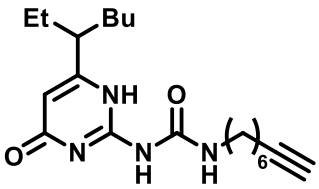

Triethylamine (0.17 mL, 1.20 mmol, 1 eq) and diphenylphosphoryl azide (0.24 mL, 1.20 mmol, 1 eq) were added to a solution of 8-nonynoic acid **54** (0.20 g. 1.30 mmol, 1 eq) in acetonitrile (6 mL). After stirring for 2 h at 50 °C, 2-amino-6-(1-ethylpentyl)-4(3*H*)-pyrimidinone **68** (0.25 g, 1.20 mmol, 1 eq) was added, and the solution was heated to reflux for 5 h. The solution was concentrated, and the residue purified by column chromatography (SiO_2, 1:1 hexane: ethyl acetate) to give the title compound **69** as a white solid (0.30 g, 0.83 mmol, 69 %). ^{1}H NMR (500 MHz, chloroform-*d*) δ 13.29 (s, 1H, N*H*), 11.95 (s, 1H, N*H*), 10.25 (s, 1H, N*H*), 5.86 (s, 1H, Ar*H*), 3.30 (td, 2H, *J* 7.5, 5.4 Hz, HNCONH-CH_2), 2.34 (m, 1H, EtBu-C*H*), 2.22 (td, 2H, *J* 7.0, 2.7 Hz, HCC-CH_2), 1.96 (t, 1H, *J* 2.7 Hz, CC*H*), 1.76 – 1.61 (m, 6H, 3 x CH_2), 1.56 (d,

2H, *J* 7.0 Hz, C*H*$_2$), 1.52 – 1.45 (m, 2H, C*H*$_2$), 1.44 – 1.23 (m, 6H, 3 x C*H*$_2$), 0.93 (dt, 6H, *J* 11.5, 7.3 Hz, 2 x C*H*$_3$); ^{13}C NMR (100 MHz, chloroform-*d*) δ 167.2, 155.5, 147.2, 139.3, 106.2, 84.1, 68.1, 45.4, 40.0, 32.9, 29.3, 29.2, 28.4, 28.2, 26.6, 26.5, 22.5, 18.3, 13.9, 11.7; Rf (0.77, 1:1 hexane: ethyl acetate); IR v_{max} (solid state) = 3246.7, 2935.6, 2496.7, 1693.6 cm^{-1}; ESI-HRMS *m/z* found 361.2598 [M + H]$^+$ $C_{20}H_{33}N_4O_2$ requires 361.2598.

1,2-Bis(2,6-difluoro-4-iodophenyl)diazene – 70

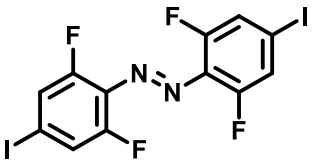

Procedure adapted from literature.[179] 2,6-Difluoro-4-iodoaniline **51** (2.04 g, 8.0 mmol, 1 eq) was dissolved in dichloromethane (60 mL), DBU (2.38 mL, 16.0 mmol, 2 eq) was added and the reaction stirred at room temperature for 5 min. The solution was cooled to -78 °C and NCS (2.14 g, 16.0 mmol, 2 eq) added. After stirring for 10 min a dark red solution formed. The reactions was then quenched using saturated sodium bicarbonate solution (60 mL) and warmed to room temperature. The organic layer was isolated, washed with water (200 mL) and 1M hydrochloric acid (200 mL), then dried with sodium sulfate, filtered and concentrated. The residue was purified by column chromatography (SiO_2, 60:40 hexane: dichloromethane) to provide the title compound **70** as red needles (1.82 g, 3.6 mmol, 60 %). ^{1}H NMR (400 MHz, dimethyl sulfoxide-d_6) δ 7.87 (d, *J* 8.8 Hz, 4H, 4 x Ar*H*); ^{13}C NMR (100 MHz, dimethyl sulfoxide-d_6) δ 156.00 (d), 153.37 (d), 131.82 – 126.92 (m), 123.02 (d), 102.06 – 93.78 (m); ^{19}F NMR (375 MHz, dimethyl sulfoxide-d_6) δ -120.58 (d); Rf 0.67 (60:40 hexane: dichloromethane); ESI-HRMS *m/z* found 506.8806 [M + H]$^+$ $C_{12}H_5F_4I_2N_2$ requires 506.8400.

1-(8-(4-((4-Bromo-2,6-difluorophenyl)diazenyl)-3,5-difluorophenyl)oct-7-yn-1-yl)-3-(6-(heptan-3-yl)-4-oxo-1,4-dihydropyrimidin-2-yl)urea – 71

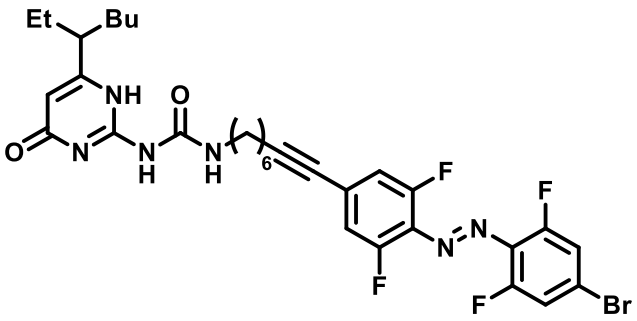

Azobenzene **52** (0.60 g, 1.39 mmol, 1.0 eq), bis(triphenylphosphine)palladium(II) dichloride (2 mol %), copper iodide (5 mol %) and UPy alkyne **69** (0.50 g, 1.39 mmol, 1.0 eq) were added to an oven dried flask. The flask was evacuated and back-filled with nitrogen three times,

before anhydrous tetrahydrofuran (20 mL) was added. Anhydrous triethylamine (0.97 mL, 6.95 mmol, 5.0 eq) was prepared via three freeze, pump thaw cycles then added to the reaction mixture. The solution was stirred under nitrogen at room temperature for 16 h. The solvent was removed, and the crude red solid purified via column chromatography (SiO_2, dichloromethane → dichloromethane: methanol (97:3)) to afford the title compound **71** as a red oil (0.58 g, 0.84 mmol, 60 %). ^{1}H NMR (500 MHz, chloroform-*d*) δ 13.24 (s, 1H, N*H*), 11.91 (s, 1H, N*H*), 10.22 (s, 1H, N*H*), 7.28 – 7.25 (m, 2H, 2 x AB-*H*), 7.21 – 6.89 (m, 2H, 2 x AB-*H*), 5.82 (s, 1H, Ar-*H*), 3.27 (m, 2H, NHCONH-CH_2), 2.43 (t, 2H, *J* 7.0 Hz, CC-CH_2), 2.30 (m, 1H, EtBu-C*H*), 1.64 (m, 6H, 3 x CH_2), 1.51 (m, 4H, 2 x CH_2), 1.47 – 1.37 (m, 2H, CH_2), 1.27 (m, 4H, 2 x CH_2), 0.88 (m, 6H, 3 x CH_3); ^{13}C NMR (125 MHz, chloroform-*d*) δ 173.1, 157.5 – 155.2 (m), 155.6, 154.8, 154.5 (d), 152.4, 148.8, 135.7, 131.0 (d), 124.0, 116.7 (d), 116.2 – 115.0 (m), 106.2, 96.3, 78.9, 45.4, 40.0, 32.9, 29.3, 28.6, 28.2, 27.2 – 25.3 (m), 22.5, 19.5, 13.9, 11.7; ^{19}F NMR (375 MHz, chloroform-*d*) δ -118.9 (d), -120.6 (d); Rf 0.50 (95:5 dichloromethane: methanol); IR v_{max} (solid state) = 3106.8, 2872.2, 2234.3, 1725.0, 1654.44, 1461.3 cm^{-1}; ESI-HRMS *m/z* found 693.2035 $[M + H]^+$ $C_{32}H_{36}BrF_4N_6O_2$ requires 693.1993.

9,9'-(Diazene-1,2-diylbis(3,5-difluoro-4,1-phenylene))bis(non-8-ynoic acid) – 72

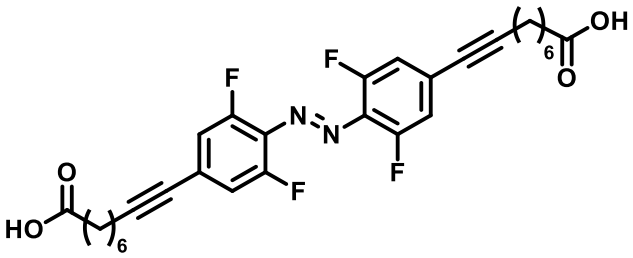

Azobenzene **70** (0.3 g, 0.65 mmol, 1.0 eq), bis(triphenylphosphine)palladium(II) dichloride (2 mol %), copper iodide (5 mol %) and 8-noynoic acid **54** (0.2 g, 1.30 mmol, 2.0 eq) were added to an oven dried flask. The flask was evacuated and back-filled with nitrogen three times, before anhydrous tetrahydrofuran (5 mL) was added. Anhydrous triethylamine (0.46 mL, 3.3 mmol, 5.0 eq) was prepared via three freeze, pump thaw cycles then added to the reaction mixture. The solution was stirred under nitrogen at 55 ^{o}C for 16 h. The solvent was removed and the crude red solid purified via column chromatography (SiO_2, 1:1 ethyl acetate: hexane → ethyl acetate) to afford the title **72** compound as a red solid (0.05 g, 0.08 mmol, 13 %). ^{1}H NMR (500 MHz, dimethyl sulfoxide-d_6) δ 12.02 (s, 2H, 2 x O*H*), 7.52 – 7.34 (m, 4H, 4 x AB-*H*), 2.28-2.21 (m, 8H, 2 x COOH-CH_2, 2 x CC-CH_2), 1.57 – 1.53 (m, 4H, 2 x CH_2), 1.46 – 1.42 (m, 4H, 2 x CH_2), 1.35 – 1.26 (m, 8H,4 x CH_2); ^{13}C NMR (125 MHz, dimethyl sulfoxide-d_6) δ 174.98 (d), 155.22 (dd), 130.80 (t), 128.34 (t), 116.52 (dd), 97.35, 78.45, 34.10, 28.43 (dd), 28.08, 24.81, 19.18; ^{19}F NMR (375 MHz, Chloroform-*d*) δ -118.52 (d), -119.73 (dd); Rf 0.75 (ethyl acetate); ESI-HRMS *m/z* found 559.2249 $[M + H]^+$ $C_{30}H_{31}F_4N_2O_4$ requires 559.5811.

1-(8-(4-Amino-3,5-difluorophenyl)oct-7-yn-1-yl)-3-(6-(heptan-3-yl)-4-oxo-1,4-dihydropyrimidin-2-yl)urea – 73

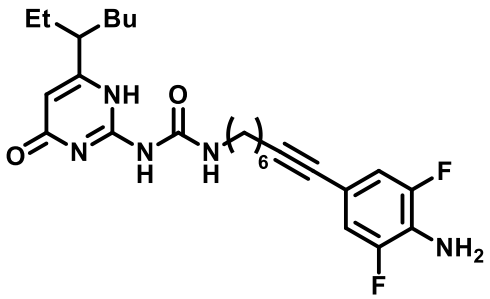

2,6-difluoro-4-iodoanaline **51** (0.24 g, 0.96 mmol, 1.0 eq), bis(triphenylphosphine)palladium(II) dichloride (2 mol%), copper iodide (5 mol%) and UPy alkyne **69** (0.38 g, 1.05 mmol, 1.1 eq) were added to an oven dried flask. The flask was evacuated and back-filled with nitrogen three times, before anhydrous tetrahydrofuran (20 mL) was added. Anhydrous triethylamine (0.67 mL, 4.79 mmol, 5.0 eq) was prepared via three freeze, pump thaw cycles then added to the reaction mixture. The solution was stirred under nitrogen at room temperature for 16 h. The solvent was removed and the crude solid purified by column chromatography (SiO_2, 95:5 dichloromethane: methanol) to give the title compound **73** as a red solid (0.14 g, 0.45 mmol, 47 %). ^{1}H NMR (500 MHz, chloroform-*d*) δ 13.26 (s, 1H, N*H*), 11.92 (s, 1H, N*H*), 10.23 (s, 1H, N*H*), 6.87 (dd, 2H, *J* 7.2, 1.9 Hz, 2 x An-*H*), 5.83 (s, 1H, Ar-*H*), 3.79 (s, 1H, NH_2), 3.30 - 3.35 (m, 2H, NHCONH-CH_2), 2.36 (t, 2H, *J* 7.1 Hz, CC-CH_2), 2.32 – 2.30 (m, 1H, EtBu-C*H*), 1.70-1.60 (m, 4H, 2 x CH_2), 1.49 – 1.39 (m, 6H, 3 x CH_2), 1.33 – 1.23 (m, 6H, 3 x CH_2), 0.92 – 0.87 (m, 6H, 2 x CH_3); ^{13}C NMR (125 MHz, chloroform-*d*) δ 175.56 (d), 154.66 – 154.41 (m), 151.63, 147.00, 139.41, 138.19, 125.62, 115.46, 51.14, 32.42, 29.74, 26.05, 22.74, 13.93, 12.01; ^{19}F NMR (375 MHz, chloroform-*d*) δ -132.79; Rf 0.32 (95:5 dichloromethane: methanol); ESI-HRMS *m/z* found 488.2836 $[M + H]^+$ $C_{26}H_{36}F_2N_5O_2$ requires 488.2832.

1,1'-(Diazene-1,2-diylbis(3,5-difluoro-4,1-phenylene)bis(oct-7-yne-8,1-diyl))bis(3-(6-(heptan-3-yl)-4-oxo-1,4-dihydropyrimidin-2-yl)urea) – Foldamer III

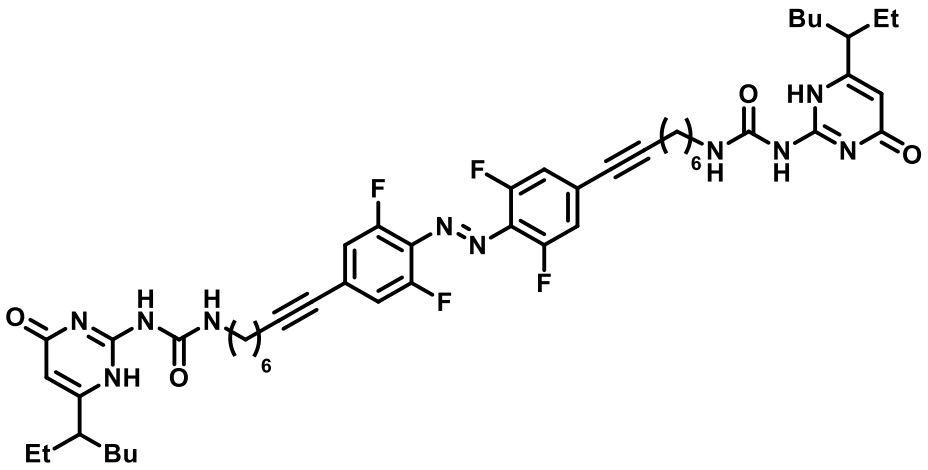

71 (0.05 g, 0.07 mmol, 1.0 eq), bis(triphenylphosphine)palladium(II) dichloride (10 mol%), copper iodide (25 mol%) UPy alkyne **69** (0.04 g, 0.11 mmol, 1.5 eq) were added to an oven dried flask. The flask was evacuated and back-filled with nitrogen three times and anhydrous triethylamine (5 mL), prepared via three freeze, pump thaw cycles, was added to the reaction mixture. The solution was stirred under nitrogen at 60 ^{o}C for 16 h. Upon cooling to room temperature, the solvent was removed, and the crude red solid suspended in a 1:1 mixture of dichloromethane and ethyl acetate. The reaction mixture was filtered through a plug of silica then concentrated. The residue was further purified via column chromatography (SiO_2, 97:2:1 dichloromethane: methanol: acetic acid) to provide foldamer **III** as red oil (0.01 g, 0.01 mmol, 13 %). (*E*-isomer) - ^{1}H NMR (500 MHz, chloroform-*d*) δ 13.17 (s, 2H, 2 x N*H*), 11.84 (s, 2H, 2 x N*H*), 10.15 (s, 2H, 2 x N*H*), 7.06 – 6.89 (m, 3H, 3 x AB-*H*), 6.85 – 6.67 (m, 1H, AB-*H*), 5.75 (s, 2H, 2 x Ar-*H*), 3.19 (q, *J* 6.6 Hz, 4H, 2 x NHCONH-CH_2), 2.40 – 2.26 (m, 4H, 2 x CC-CH_2), 2.16 (q, *J* 7.7, 7.2 Hz, 2H, 2 x EtBu-C*H*), 1.35 (m, 4H, 2 x CH_2), 1.20 (m, 12H, 6 x CH_2), 0.80 (dd, *J* 8.5, 5.1 Hz, 12H, 4 x CH_3); (*Z*-isomer) - ^{1}H NMR (500 MHz, chloroform-*d*) δ 13.14 (s, 2H, 2 x N*H*), 11.85 (s, 2H, 2 x N*H*), 10.11 (s, 2H, 2 x N*H*), 7.02 – 6.92 (m, 3H. 3 x AB-*H*), 6.76 (m, 2H, AB-*H*), 5.74 (s, 2H, 2 x Ar-*H*), 3.26 – 3.13 (m, 4H, 2 x NHCONH-CH_2), 2.40 – 2.25 (m, 4H, 2 x CC-CH_2), 2.22 – 2.14 (m, 2H, 2 x EtBu-C*H*), 1.37 – 1.34 (m, 4H, 2 x CH_2), 1.18 (m, 12H, 6 x CH_2), 0.83 – 0.77 (m, 12H, 4 x CH_3); ^{13}C NMR (125 MHz, chloroform-*d*) δ 173.2, 156.7, 156.5, 156.5, 155.5, 154.9, 154.5, 154.4, 131.2, 131.2, 131.1, 128.0, 127.9, 116.8, 116.6, 115.8, 115.8, 115.6, 115.2, 114.5, 106.2, 106.1, 96.6, 95.9, 94.9, 78.9, 45.4, 40.0, 32.9, 29.7, 29.3, 28.6, 28.3, 26.6, 26.5, 22.5, 19.5, 19.3, 13.9, 11.7; ^{19}F NMR (375 MHz, chloroform-*d*) δ -119.3 (d), -127.0 (d). Rf 0.59 (95:5 DCM: MeOH); IR ν_{max} (solid state) = 3218.1, 3031.9, 2858.7, 2234.1, 1694.9 cm cm^{-1}; ESI-HRMS *m/z* found 971.5277 $[M + H]^+$ $C_{52}H_{67}F_4N_{10}O_4$ requires 971.5238.

7-Amino-1,8-naphthyridin-2-ol – 75

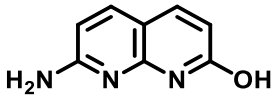

Procedure adapted from literature.[33] To, 2,6-diaminopyridine **57** (3.34g, 30.6 mmol, 1.0 eq) and D,L-malic acid **74** (4.51 g, 33.7 mmol, 1.1 eq), concentrated sulfuric acid (20 mL) was added dropwise at 0 °C. The reaction mixture was heated to 110 °C for 4 h. Upon cooling to 0 °C, aqueous ammonia solution was added dropwise until pH 9 was reached. The resulting brown precipitate was collected by vacuum filtration then washed with water and diethyl ether to afford the title compound **75** as a brown powder (3.58 g, 22.4 mmol, 73 %). ^{1}H NMR (500 MHz, dimethyl sulfoxide-d_6) δ 11.51 (br s, 1H, O*H*), 7.54 (m, 2H, 2 x Nap-*H*), 6.71 (s, 2H, NH_2), 6.24 (d, 1H, *J* 8.5 Hz, Nap-*H*), 6.01 (d, 1H, *J* 9.3 Hz, Nap-*H*);^{13}C NMR (125 MHz, dimethyl sulfoxide-d_6) δ 164.0, 160.9, 150.9, 139.9, 137.6, 115.4, 105.4, 105.4, 40.6, 40.5, 40.4, 40.3, 40.3, 40.2, 40.0, 39.8, 39.7, 39.5; Rf 0.59 (9:1 dichloromethane: methanol); IR v_{max} (solid state) = 3353.3, 3154.6, 3044.2, 1618.7 cm^{-1}; ESI-HRMS *m/z* found 162.0651 $[M + H]^+$ $C_8H_8N_3O$ requires 162.0662.

2-Ethyl-*N*-(7-hydroxy-1,8-napthyridin-2-yl)hexanamide – 76

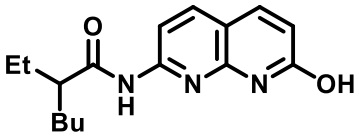

Procedure adapted from literature.[33] 2-Ethylhexnoyl chloride (2.6 mL, 15 mmol, 1.2 eq) was slowly added to a solution of **75** (2.0 g, 12.5 mmol, 1 eq) in dry pyridine (40 mL). The reaction mixture was heated to 110 °C for 22 h. Upon cooling to room temperature, the solvent was removed then the residue dissolved in dichloromethane (50 mL) then washed with 1M hydrochloric acid (2 x 25 mL), water (2 x 25 mL), saturated sodium bicarbonate solution (2 x 25 mL). The organic layer was dried with sodium sulfate, filtered and concentrated. The title compound was crystallised from acetone to give the title compound **76** as a cream powder (1.3 g, 4.6 mmol, 37 %). Synthesis repeated to provide a sufficient quantity for next step (1.0 g, 35 % and 3.4 g, 34 %). ^{1}H NMR (400 MHz, chloroform-*d*) δ 12.88 (br s, 1H, O*H*), 11.75 (s, 1H, N*H)*, 8.46 (d, 1H, *J* 8.7 Hz, Nap-*H*), 7.94 (d, *J* 8.7 Hz, 1H, Nap-*H*), 7.76 (d, 1H, *J* 9.4 Hz, Nap-*H*), 6.65 (d, 1H, *J* 9.4 Hz, Nap-*H*), 2.83 (m, 1H, EtBu-C*H*), 1.82 – 1.68 (m, 2H, CH_2), 1.66 – 1.47 (m, 2H, CH_2), 1.34 (m, 4H, 2 x CH_2), 0.97 (t, 3H, *J* 7.4 Hz, CH_3), 0.86 (t, 3H, *J* 7.1 Hz, CH_3); ^{13}C NMR (100 MHz, chloroform-*d*) δ 177.7, 165.2, 154.2, 148.7, 139.7, 139.0, 119.9, 111.3, 110.9, 48.6, 32.5, 29.7, 26.2, 22.9, 14.0, 11.9; Rf 0.74 (9:1 dichloromethane: methanol);

IR ν_{max} (solid state) = 3171.5, 2998.9, 2871.5, 1700.3, 1662.3 cm^{-1}; ESI-HRMS *m/z* found 288.1708 $[M + H]^+$ $C_{16}H_{22}N_3O_2$ requires 288.1707.

***N*-(7-Bromo-1,8-naphthyridin-2-yl)-2-ethylhexanamide – 77**

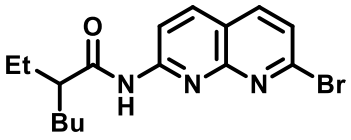

76 (5.73 g, 20 mmol, 1 eq) was suspended in phosphorus tribromide (37 mL, 399 mmol, 20 eq) under an inert atmosphere. The reaction was heated 110 °C for 16 h. Upon cooling to room temperature, the reaction mixture was diluted with dichloromethane (100 mL). The biphasic mixture was separated and the aqueous solution was extracted with dichloromethane (4 x 20 mL). The organic extracts were combined and washed with water (3 x 50 ml) and saturated sodium bicarbonate solution (3 x 50 mL). The organic layer was dried with sodium sulfate, filtered and concentrated. The title compound **77** was purified *via* column chromatography (SiO_2 98:2 dichloromethane: methanol) and was afforded as colourless powder (1.26 g, 3.6 mmol, 18 %). ^{1}H NMR (500 MHz, chloroform-*d*) δ 8.62 (d, 1H, *J* 8.9 Hz, Nap-*H*), 8.29 (s, 1H, N*H*), 8.19 (d, 1H, *J* 8.9 Hz, Nap-*H*), 7.96 (d, 1H, *J* 8.3 Hz, Nap-*H*), 7.54 (d, 1H, *J* 8.3 Hz, Nap-*H*), 2.29 – 2.19 (m, 1H, EtBu-C*H*), 1.80 – 1.69 (m, 2H, CH_2), 1.63 (dd, 2H, *J* 13.8, 7.3 Hz, CH_2), 1.37 – 1.31 (m, 4H, 2 x CH_2), 0.98 (t, 3H, *J* 7.4 Hz, CH_3), 0.88 (t, 3H, *J* 7.4 Hz, CH_3); ^{13}C NMR (125 MHz, chloroform-*d*) δ 175.82, 154.62, 154.31, 145.51, 139.37, 138.22, 125.57, 119.40, 115.77, 77.32, 77.06, 76.81, 50.74, 32.34, 29.69, 25.97, 22.74, 13.92, 11.96; Rf 0.6 (98:2 dichloromethane: methanol); ESI-HRMS *m/z* found 350.0875 $[M + H]^+$ $C_{16}H_{21}BrN_3O$ requires 350.0863.

***N*-(7-Amino-1,8-naphthyridin-2-yl)-2-ethylhexanamide – 78**

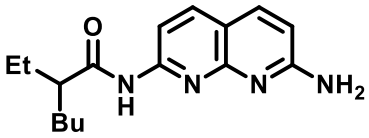

Method 1:

Procedure adapted from literature.[33] **77** (0.1 g, 0.29 mmol, 1.0 eq) was dissolved in a 1:1 mixture of 1,2-dimethoxyethane and ethylene glycol (2 mL). Copper (I) oxide (0.01 g, 0.09 mmol, 0.3 eq) and aqueous ammonia solution (0.1 mL, 2.9 mmol, 10.0 eq) were added, the flask was sealed, and the reaction was stirred at room temperature for 24 h. The flask was carefully unsealed and a 1:1 mixture of dichloromethane and water was added (8 mL), the reaction was stirred for a further 1 h, then diluted again with water (12 mL), and extracted with dichloromethane (3 x 15 mL). The extracts were combined and washed with water (2 x 12

mL), then dried with sodium sulfate, filtered, and concentrated. The residue was purified *via* column chromatography (SiO_2, ethyl acetate → ethyl acetate: methanol (9:1)) to afford the title compound **78** as a white powder (26 mg, 0.09 mmol, 31 %). ^{1}H NMR (500 MHz, chloroform-*d*) δ 8.25 (d, 1H, *J* 8.6 Hz, Nap-*H*), 8.06 (s, 1H, N*H*), 7.96 (d, 1H, *J* 8.6 Hz, Nap-*H*), 7.82 (d, 1H, *J* 8.6 Hz, Nap-*H*), 6.67 (d, 1H, *J* 8.6 Hz, Nap-*H*), 4.92 (s, 2H, NH_2), 2.19 (m, 1H, EtBu-*H*), 1.78 – 1.66 (m, 2H, C*H*$_2$), 1.64 – 1.57 (m, 2H, C*H*$_2$), 1.36 – 1.29 (m, 4H, 2 x C*H*$_2$), 0.97 (t, 3H, *J* 7.4 Hz, C*H*$_3$), 0.89 – 0.86 (m, 3H, C*H*$_3$); ^{13}C NMR (125 MHz, chloroform-*d*) δ 175.16, 164.81, 159.78, 152.96, 138.74, 137.94, 115.27, 110.58, 110.44, 51.18, 32.55, 29.78, 26.15, 22.77, 13.95, 12.05; Rf 0.31 (ethyl acetate); ESI-HRMS *m/z* found 287.1850 $[M + H]^+$ $C_{16}H_{23}N_4O$ requires 287.1866.

Method 2:

80 (0.5 g, 1.64 mmol, 1.0 eq), tert-butylcarbamate (0.3 mg, 2.62 mmol, 1.6 eq), potassium carbonate (0.45 g, 3.27 mmol, 2.0 eq), palladium(II) acetate (10 mg, 0.05 mmol, 0.03 eq) and xantphos (60 mg, 0.10 mmol, 0.06 eq) were suspended in 1,4-dioxane (10 mL). The reaction mixture was degassed via three freeze, pump, thaw cycles, then heated to 100 °C for 48 h. Upon cooling to room temperature the reaction mixture was diluted in ethyl acetate and filtered through celite. The solvent was evaporated in vacuo and the crude product was purified via column chromatography (SiO_2, ethyl acetate → ethyl acetate: methanol (9:1)) to afford the title **78** compound as a white solid (0.26 g, 0.93 mmol, 57 %). ^{1}H NMR (500 MHz, chloroform-*d*) δ 8.25 (d, 1H, *J* 8.6 Hz, Nap-*H*), 8.06 (s, 1H, N*H*), 7.96 (d, 1H, *J* 8.6 Hz, Nap-*H*), 7.82 (d, 1H, *J* 8.6 Hz, Nap-*H*), 6.67 (d, 1H, *J* 8.6 Hz, Nap-*H*), 4.92 (s, 2H, NH_2), 2.19 (m, 1H, EtBu-*H*), 1.78 – 1.66 (m, 2H, C*H*$_2$), 1.64 – 1.57 (m, 2H, C*H*$_2$), 1.36 – 1.29 (m, 4H, 2 x C*H*$_2$), 0.97 (t, 3H, *J* 7.4 Hz, C*H*$_3$), 0.89 – 0.86 (m, 3H, C*H*$_3$); ^{13}C NMR (125 MHz, chloroform-*d*) δ 175.16, 164.81, 159.78, 152.96, 138.74, 137.94, 115.27, 110.58, 110.44, 51.18, 32.55, 29.78, 26.15, 22.77, 13.95, 12.05; Rf 0.31 (ethyl acetate); ESI-HRMS *m/z* found 287.1850 $[M + H]^+$ $C_{16}H_{23}N_4O$ requires 287.1866.

***N*-(7-(2-Ethylhexanamido)-1,8-naphthyridin-2-yl)non-8-ynamide – 79 (DAN-Alkyne)**

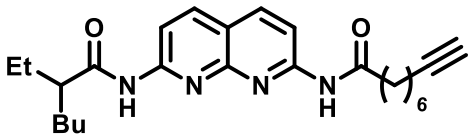

EDC (14 mg. 0.09 mmol, 1.2 eq) was added to a solution of 8-nonyoic acid **54** (12 mg, 0.08 mmol, 1.0 eq) and DMAP (15 mg, 0.12 mmol, 1.5 eq) in chloroform (5 mL). After stirring for 30 min, **78** (22 mg, 0.08 mmol, 1.0 eq) was added, and the solution was stirred at 60 °C for 16 h. Upon cooling to room temperature, the reaction mixture diluted with chloroform (5 mL)

and washed with 1M hydrochloric acid (2 x 5 mL), saturated sodium bicarbonate solution (2 x 5 mL) and brine (5 mL). The organic layer was collected, dried with sodium sulfate, filtered, and concentrated. The residue was suspended in hexane and filtered through silica and eluted with ethyl acetate: hexane (1:1). The solvent was removed to afford the title compound **79** as a colourless solid (23 mg, 0.06 mmol, 70 %). ^{1}H NMR (500 MHz, chloroform-*d*) δ 8.47 (d, 1H, *J* 8.8 Hz, Nap-*H*), 8.43 (d, 1H, *J* 8.8 Hz, Nap-*H*), 8.17 (br s, 2H, 2 x N*H*), 8.14 (dt, 2H, *J* 8.8, 0.6 Hz, 2 x Nap-*H*), 2.47 (t, 2H, *J* 7.5 Hz, NHCO-CH_2), 2.28 – 2.21 (m, 1H, EtBu-C*H*), 2.21 – 2.17 (m, 2H, HCC-CH_2), 1.94 (t, 1H, *J* 2.7 Hz, CC*H*), 1.81 – 1.72 (m, 4H, 2 x CH_2), 1.66 – 1.57 (m, 4H, 2 x CH_2), 1.45 (m, 2H, CH_2), 1.39 – 1.27 (m, 6H, 3 x CH_2), 0.98 (t, *J* 7.5 Hz, 3H, CH_3), 0.90 – 0.87 (m, 3H, CH_3); ^{13}C NMR (125 MHz, chloroform-*d*) δ 175.21, 171.9, 153.6, 153.6, 152.2, 138.9, 138.9, 118.3, 113.4, 113.2, 84.3, 68.2, 51.0, 37.8, 32.4, 31.5, 29.7, 29.6, 28.5, 28.3, 28.1, 26.0, 25.0, 22.6, 18.2, 13.8, 11.9; Rf 0.28 (1:1 ethyl acetate: hexane); IR ν_{max} (solid state) = 3311.0, 3136.7, 2929.9, 2857.2, 2117.1, 1773.3, 1694.1 cm^{-1}; ESI-HRMS *m/z* found 423.2756 [M + H] $^{+}$ $C_{25}H_{35}N_4O_2$ requires 423.2755.

***N*-(7-Chloro-1,8-naphthyridin-2-yl)-2-ethyl hexanamide – 80**

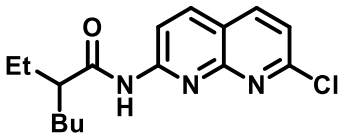

Procedure adapted from literature.[33] **76** (0.4 g, 1.4 mmol, 1.0 eq) was dissolved in phosphorus oxychloride (10 mL) and the solution was heated to 95 °C for 4 h. Upon cooling to room temperature, the reaction mixture was slowly poured onto ice cold water. The resulting mixture was extracted into dichloromethane (4 x 20 mL), the extracts were combined and washed with saturated sodium bicarbonate solution (3 x 20 mL), water (3 x 20 mL) and brine (20 mL). The organic extracts were dried with sodium sulfate, filtered and concentrated to afford the title compound **80** as a yellow crystalline solid (0.32 g, 1.05 mmol, 75 %). ^{1}H NMR (500 MHz, chloroform-*d*) δ 8.61 (d, 1H, J 8.8 Hz, Nap-*H*), 8.31 (s, 1H, N*H*), 8.21 (d, 1H, J 8.8 Hz, Nap-*H*), 8.08 (d, 1H, J 8.4 Hz, Nap-*H*), 7.41 (d, 1H, J 7.7 Hz, Nap-*H*), 2.33 – 2.17 (m, 1H, EtBu-C*H*), 1.81 – 1.68 (m, 2H, CH_2), 1.66 – 1.54 (m, 2H, CH_2), 1.33 (s, 4H, 2 x CH_2), 0.98 (t, 3H, J 7.4 Hz, CH_3), 0.87 (m, 3H, CH_3); ^{13}C NMR (125 MHz, chloroform-*d*) δ 175.6, 154.5 154.1, 153.8, 139.2, 138.8, 122.1, 119.2, 115.3, 51.1, 32.4, 29.7, 26.0, 22.8, 13.9, 12.0; Rf 0.70 (1:1 ethyl acetate: Hexane); IR ν_{max} (solid state) = 3176.2, 3128.2, 2958.5, 2857.9, 1693.9 cm^{-1}; ESI-HRMS *m/z* found 306.1362 [M + H]$^{+}$ $C_{16}H_{21}ClN_3O$ requires 306.1368.

9-(4-((2,6-Difluoro-4-(8-(3-(6-(heptan-3-yl)-4-oxo-1,4-dihydropyrimidin-2-yl)ureido)oct-1-yn-1-yl)phenyl)diazinyl-3,5-difluorophenyl-*N*-(7-(2-ethylhexanamido)-1,8-naphthyridin-2-yl)non-8-ynamide – Foldamer IV

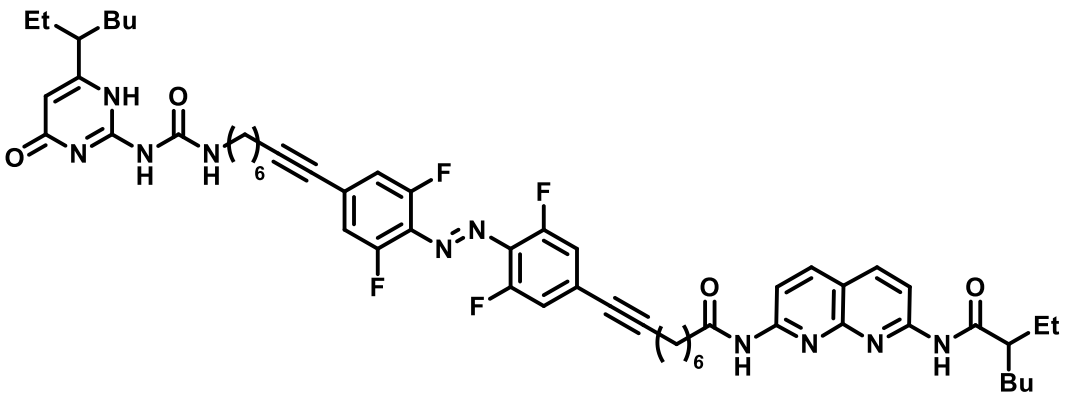

71 (0.23 g, 0.33 mmol, 1.0 eq), bis(triphenylphosphine)palladium(II) dichloride (2 mol%), copper iodide (5 mol%) and DAN alkyne **79** (0.14 g, 0.33 mmol, 1.0 eq) were added to an oven dried flask. The flask was evacuated and back-filled with nitrogen three times, before anhydrous triethylamine (10 mL), prepared via three freeze, pump thaw cycles was added to the reaction mixture. The solution was stirred under nitrogen at 60 °C for 16 h. The solvent was removed, the resultant crude solid was resuspended in dichloromethane then filtered through celite. The reaction mixture was concentrated, then triturated with methanol. The solids were collected by vacuum filtration then purified by column chromatography (SiO_2, dichloromethane: methanol: triethyl amine mixtures). Foldamer **IV** was afforded as a dark red oil (30 mg, 0.03 mmol, 10 %). (*E*-isomer) - ^{1}H NMR (500 MHz, chloroform-*d*) δ 13.84 (s, 1H, N*H*), 11.84 (br s, 2H, 2 x N*H*), 11.31 (s, 1H, N*H*), 9.81 (s, 1H, N*H*), 8.46 (dd, 2H, *J* 14.5, 8.8 Hz, 2 x Nap-*H*), 8.04 (d, 2H, , *J* 8.8 Hz, 2 x Nap-*H*), 6.98 -6.78 (m, 4H, 4 x AB-*H*), 5.90 (s, 1H, Ar-*H*), 3.42-3.35 (m, 2H, NHCONH-CH_2), 3.19 -3.11 (m, 1H, EtBu-C*H*), 2.55 -2.49 (m, 3H, EtBu-C*H*, NHCO-CH_2), 2.37 -2.33 (m, 6H, 2 x CC-CH_2, CH_2), 2.24 -2.17 (m, 6H, 3 x CH_2), 1.67-2.46 (m, 12 H, 6 x CH_2), 1.26 -1.18 (m, 10 H, 5 x CH_2), 0.90 (t, 3H, *J* 7.3, CH_3), 0.80 (dt, 9H, *J* 18.0, 9.1 Hz, 3 x CH_3); (*Z*-isomer) - ^{1}H NMR (500 MHz, chloroform-*d*) δ 13.85 (s, 1H, N*H*), 11.60 (br s, 2H, 2 x N*H*), 11.27 (s, 1H, N*H*), 9.77 (s, 1H, N*H*), 8.47 (dd, 2H, *J* 14.5, 8.8 Hz, 2 x Nap-*H*), 8.05 (d, 2H, , *J* 8.8 Hz, 2 x Nap-*H*), 7.07-6.76 (m, 4H, 4 x AB-*H*), 5.90 (s, 1H, Ar-*H*), 3.36 (m, 2H, NHCONH-CH_2), 3.20-3.14 (m, 1H, EtBu-C*H*), 2.66-2.54 (m, 3H, EtBu-C*H*, NHCO-CH_2), 2.55-2.51 (m, 6H, 2 x CC-CH_2, CH_2), 2.38-2.34 (m, 6H, 3 x CH_2), 2.28-2.09 (m, 12 H, 6 x CH_2), 1.75-1.62 (m, 10 H, 5 x CH_2), 0.90 (t, 3H, *J* 7.3, CH_3), 0.80 (dt, 9H, *J* 18.0, 9.1 Hz, 3 x CH_3); ^{13}C NMR (125 MHz, chloroform-*d*) δ ^{13}C NMR (100 MHz, $CDCl_3$) δ 170.9, 170.6, 165.1, 157.1, 156.7, 155.4, 155.3, 155.0, 150.8, 142.8, 139.4, 133.9 (d), 131.2, 129.7, 126.6 (d), 115.8, 115.6, 115.3, 115.1 - 114.9 (m), 114.2, 106.3, 87.0, 86.9, 79.7, 48.8, 41.8, 40.0, 37.2, 33.8, 32.4, 30.8, 29.8 - 29.5 (m), 28.7, 28.6 (d), 28.2 (d), 27.4, 26.7, 26.1, 25.3, 22.8 (d),

19.5, 19.2, 14.0 (d), 12.0; ^{19}F NMR (375 MHz, chloroform-*d*) δ -119.3 (d), -127.0 (d); Rf 0.50 (95:5 DCM: MeOH); IR ν_{max} (solid state) = 3191.1, 3053.0, 2857.3, 2229.9, 1697.2 cm^{-1}; ESI-HRMS *m/z* found 1033.5455 $[M + H]^+$ $C_{57}H_{69}F_4N_{10}O_4$ requires 1033.5434.

2-(3-(5,6-Dimethyl-1*H*-benzo[*d*]imidazol-2-yl)ureido)ethyl methacrylate – 82 (UIM MMA)

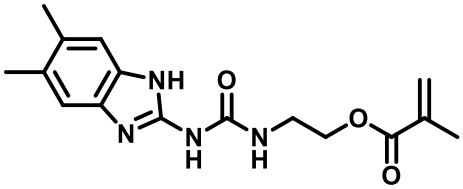

Procedure adapted from literature.[92] 2-Amino-5,6-dimethylbenzimidazole **65** (1.9 g, 11.8 mmol, 1.0 eq.) was dissolved in in anhydrous tetrahydrofuran (20 mL) and stirred at reflux under nitrogen for 1 h. 2-Isocyanatoethyl methacrylate **81** (2.00 mL, 14.2 mmol, 1.2 eq.) was added dropwise to the reaction mixture over 5 minutes and the reaction stirred at reflux for a further 18 h. The resulting precipitate was isolated and dried under vacuum. The resulting pale orange solid was triturated with methanol, filtered, and dried under vacuum to give the title compound **82** as colourless solid (2.92 g, 9.20 mmol, 78%). ^{1}H NMR (400 MHz, dimethyl sulfoxide-d_6) δ 9.92 (br s, 1H, N*H*), 7.60 (br s, 1H, N*H*), 7.14 (s, 2H, Ar-*H*), 6.15 (s, 1H, CCH*H'*), 5.75 (s, 1H, CC*H*H'), 4.23 (t, *J* 5.2 Hz, 2H, O-CH_2), 3.53 (dd, *J* 5.2, 10.6 Hz, 2H, CH_2-NH), 2.28 (s, 6H 2 x Ar-CH_3), 1.94 (s, 3H, CH_3); ^{13}C NMR (100 MHz, dimethyl sulfoxide-d_6) δ 171.7, 152.9, 147.8, 145.3, 143.7, 141.1, 139.7, 135.5, 133.8, 133.7, 131.2, 68.9, 43.4, 25.1, 23.2; IR ν_{max} (solid state) = 3291.9, 3066.4, 2859.0, 1681.8, 1642.4 cm^{-1}; ESI-HRMS *m/z* found 317.1955 $[M + H]^+$ $C_{16}H_{21}N_4O_3$ requires 317.1608.

2-(3-(Pyridin-2-yl)ureido)ethyl methacrylate – 83 (Pyr MMA)

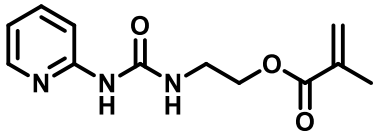

2-Aminopyridine **55** (1.0 g, 10.6 mmol, 1.0 eq.) was dissolved in anhydrous tetrahydrofuran (20 mL) and stirred at reflux under nitrogen for 1 h. 2-Isocyanatoethyl methacrylate **81** (1.8 mL, 12.8 mmol, 1.2 eq.) was added dropwise to the reaction mixture over 5 minutes and the reaction stirred at reflux for a further 16 h. Upon cooling, the solvent was removed, and the resulting residue purified by column chromatography (SiO_2, 98:2 dichloromethane: methanol) to give the title compound **83** as a colourless solid (1.93 g, 7.74 mmol, 73 %). ^{1}H NMR (500 MHz, chloroform-*d*) δ 9.70 (s, 1H, N*H*), 8.92 ((s, 1H, N*H*), 8.38 – 7.91 (m, 1H, Ar-*H*), 7.74 – 7.25 (m, 1H, Ar-*H*), 6.96 – 6.59 (m, 2H, 2 x Ar-*H*), 6.12 (dd, *J* 1.6, 1.0 Hz, 1H, CCH*H'*), 5.52

(t, *J* 1.6 Hz, 1H, CC*H*H'), 4.26 (t, *J* 5.6 Hz, 2H, O-CH_2), 3.66 (d, *J* 5.6 Hz, 2H, CH_2-NH), 1.90 (dd, *J* 1.6, 1.0 Hz, 3H, CH_3). ^{13}C NMR (125 MHz, chloroform-*d*) δ 167.2, 156.4, 153.4, 145.9, 138.3, 136.2, 125.76, 116.8, 112.1, 63.8, 38.7, 18.3. IR v_{max} (solid state) = 3238.7, 2924.1, 1678.4, 1640.7 cm^{-1}; Rf 0.51 (98:2 dichloromethane: methanol); ESI-HRMS *m/z* found 250.1308 $[M + H]^+$ $C_{12}H_{16}N_4O_3$ requires 250.1186.

2-(3-(6-(Heptan-3-yl)-4-oxo-1,4-dihydropyrimidin-2-yl)ureido)ethyl methacrylate – 84 (UPy MMA)

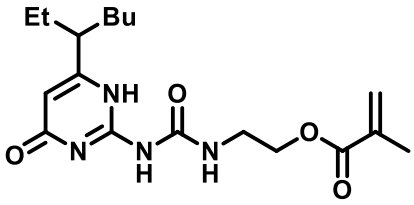

2-Amino-6-(1-ethylpentyl)-4(3*H*)-pyrimidinone **68** (0.6 g, 2.87 mmol, 1.0 eq.) was dissolved in anhydrous chloroform (25 mL) and heated to reflux under nitrogen for 1 h. 2-Isocyanatoethyl methacrylate **81** (0.41 mL, 2.87 mmol, 1.0 eq.) was added dropwise to the reaction mixture over 5 minutes and the reaction stirred at reflux for a further 16 h. Upon cooling, the solvent was removed, and the resulting residue purified by column chromatography (SiO_2, 95:5 dichloromethane: methanol) to give the title compound **84** as a colourless solid (0.79 g, 2.17 mmol, 76 %). ^{1}H NMR (400 MHz, chloroform-*d*) δ 13.10 (s, 1H, N*H*), 12.12 (s, 1H. N*H*), 10.49 (s, 1H, N*H*), 6.18 (s, 1H, Ar*H*), 5.79 (s, 1H, C=C*H*H), 5.53 (s, 1H, C=CH*H*), 4.28 (t, 2H, J 5.6 Hz, COOCH_2), 3.60 (q, 2H, J 5.6 Hz, NHCONH-CH_2), 2.31 (m, 1H, EtBu-C*H*), 1.93 (s, 3H, C=C-CH_3), 1.81 – 1.44 (m, 4H, 2 x CH_2), 1.42 – 1.12 (m, 4H, 2 x CH_2), 0.89 (m, 6H, 2 x CH_3); ^{13}C NMR (100 MHz, chloroform-*d*) δ 167.3, 164.4, 157.4, 148.8, 146.5, 139.4, 126.1, 106.3, 63.2, 38.8, 37.4, 32.9, 29.3, 26.6, 22.5, 18.3, 13.9, 11.7. Rf 0.53 (95:5 dichloromethane: methanol); IR v_{max} (solid state) = 3242.0, 2927.9, 1693.6, 1649.5 cm^{-1}; ESI-HRMS *m/z* found 365.2192 $[M + H]^+$ $C_{18}H_{29}N_4O_4$ requires 365.2183.

2-(4-(8-((1,8-Napthyridin-2-yl)amino)8-oxooctyl)1H-1,2,3-triazol-1-yl)ethyl-2-(((dodecylthio)carbonothioyl)thio)-2-methyl propanoate – 92 (NAP RAFT agent)

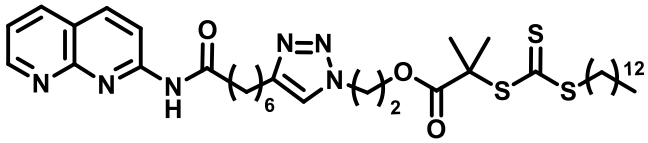

Nap alkyne **60** (0.37 g, 1.32 mmol, 1.0 eq.), 2- (dodecyl-thiocarbonothioylthio)-2-methylpropionic acid 3-azido-1-propanol ester **91** (1.1 mL, 2.63 mmol, 2.0 eq.) and tetrakis(acetonitrile)copper(I) hexafluorophosphate (0.05 g, 0.13 mmol, 0.1 eq.) were

dissolved in anhydrous n,n-dimethylformamide (10 mL). N,N-diisopropylethylamine (0.52 mL, 2.99 mmol, 2.3 eq.) was added and the reaction stirred under nitrogen at 50 °C for 16 h. Upon cooling to room temperature, the reaction mixture was diluted with dichloromethane (50 mL), then washed with 5 % lithium chloride solution (3 x 50 mL), dried with sodium sulfate, filtered, and concentrated in vacuo. The title compound was isolated via column chromatography (SiO_2, dichloromethane: methanol (99:1 → 90:10)) to give the title compound **92** as a yellow solid (0.62 g, 0.85 mmol, 64 %). ^{1}H NMR (500 MHz, Chloroform-*d*) δ 9.13 – 8.88 (m, 2H, 2 x Nap-*H*), 8.57 (d, 1H, *J* 8.9 Hz, Nap-*H*), 8.17 (m, 2H, 2 x Nap-*H*), 7.41 (dd, 1H, *J* 8.0, 4.3 Hz, Nap-*H*), 7.29 (s, 1H, triazole-*H*), 4.36 (t, 2H, *J* 6.9 Hz, (triazole) N-C*H*$_2$), 4.11 (t, 2H, *J* 5.8 Hz, COO-C*H*$_2$), 3.27 (t, 2H, *J* 7.5 Hz, (triazole) C-C*H*$_2$), 2.71 (t, 2H, *J* 7.5 Hz, SSCS-C*H*$_2$), 2.49 (t, 2H, *J* 7.5 Hz, NHCC-C*H*$_2$), 2.24 (p, 2H, *J* 6.6 Hz, NCH$_2$C*H*$_2$CH$_2$O), 1.77 (p, 2H, *J* 7.5 Hz, SCH$_2$*CH*$_2$), 1.70 (s, 6H, SC(C*H*$_3$)$_2$), 1.66-1.63 (m, 4H, 2 x C*H*$_2$), 1.46 – 1.40 (m, 4H, 2 x C*H*$_2$), 1.38-1.33 (m, 2H, C*H*$_2$), 1.27-1.23 (m, 16 H, 8 x C*H*$_2$), 0.87 (t, 3H, *J* 6.9 Hz, C*H*$_3$); ^{13}C NMR (125 MHz, Chloroform-*d*) δ 222.1, 172.8, 172.6, 154.8, 153.82 (d, 2 x C), 148.2, 139.6, 136.6, 120.9 (d, 2 x C), 115.4 (d, 2 x C), 62.5, 56.0, 46.9, 37.8, 37.1, 31.9, 29.8 – 29.2 (m, 2 x C), 29.1, 29.0 – 28.4 (m, 10 x C), 27.9, 26.1 – 24.4 (m, 2 x C), 22.7, 14.1; ESI-HRMS *m/z* found 729.3671 [M + H]+ $C_{37}H_{57}N_6O_3S_3$ requires 729.3649; Rf 0.3 (9.5:0.5 dichloromethane: methanol); IR ν_{max} (solid state) = 3238.3, 3122.0, 2920.5, 2850.8, 2219.6, 1726.7 cm^{-1}.

2-(4-(7-(3-(6-(Heptan-3-yl)4-oxo-1,4-dihydropyrimidin-2-yl)ureido)heptyl)-1*H*-1,2,3-triazol-1-yl)ethyl-2-(((dodecylthio)carbonothioyl)thio)-2-methyl propanoate – 93 (UPy RAFT agent)

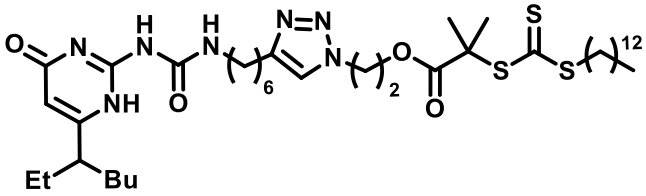

UPy alkyne **69** (0.4 g, 1.18 mmol, 1 eq), 2- (dodecyl-thiocarbonothioylthio)-2-methylpropionic acid 3-azido-1-propanol ester **91** (1.0 mL, 2.37 mmol, 2 eq), tetrakis(acetonitrile) copper(I) hexafluorophosphate (0.05g, 0.12 mmol, 0.1 eq) and diisopropylethylamine (0.47 mL, 2.72 mmol, 2.3 eq) were dissolved in n,n-dimethylformamide (10 mL) under an inert gas atmosphere. The suspension was stirred for 16 h at 50 ^{o}C. The reaction mixture was diluted with dichloromethane (25 mL) and washed with 5% LiCl solution (3 x 25 mL), then dried with sodium sulfate, filtered and concentrated to give a yellow oil. The product was isolated *via* column chromatography (SiO_2, dichloromethane: methanol (99:1 → 95:5)) to afford title compound **93** as a brown oil (0.5 g, mmol, 52 %). ^{1}H NMR (500 MHz, chloroform-*d*) δ 13.25

(s, 1H, N*H*), 11.91 (s, 1H, N*H*), 10.18 (s, 1H, N*H*), 7.26 (s, 1H, triazole-*H*), 5.82 (s, 1H, Ar-*H*), 4.43 – 4.32 (m, 2H, (triazole) N-CH_2), 4.12 (t, 2H, J 5.8 Hz, COO-CH_2), 3.28 – 3.24 (m, 4H, (triazole) C-CH_2, NHCONH-CH_2), 2.70 – 2.69 (m, 2H, SSCS-CH_2), 2.32 – 2.29 (m, 1H, EtBu-*H*), 2.24 (t, 2H, *J* 6.3 Hz, $NCH_2CH_2CH_2O$), 1.70 (s, 6H, SC(CH_3)$_2$), 1.69 – 1.49 (m, 10H, 5 x CH_2), 1.44 - 1.41 (m, 4H, 2 x CH_2), 1.37-1.34 (m, 2H, CH_2), 1.31 – 1.20 (m, 20H, 10 x CH_2), 0.92 – 0.83 (m, 9H, 3 x CH_3); ^{13}C NMR (125 MHz, chloroform-*d*) δ 222.0, 173.2, 172.8, 156.7, 155.5, 154.9, 148.4, 121.0, 106.2, 62.5, 55.9, 46.85, 45.4, 40.1, 37.1, 32.9, 31.9, 30.0 – 29.2 (m, 3 x C), 29.2 – 28.3 (m, 10 x C), 27.9, 26.8, 26.6, 25.7, 25.4, 22.7, 22.5, 14.0 (d, 2 x C), 11.7; ESI-HRMS *m/z* found 808.4691 $[M + H]^+$ $C_{40}H_{70}N_7O_4S_3$ requires 808.4646; Rf 0.4 (9.5:0.5 dichloromethane: methanol); IR ν_{max} (solid state) = 3217.7, 2923.6, 2853.4, 2094.6, 1734.1 cm^{-1}.

2-(4-(8-((7-(2-Ethylhexanamido)-1,8-napthyridin-2-yl)amino)-8-oxooctyl)-1*H*-1,2,3-triazol-1-yl)ethyl-2-(((dodecylthio)carbonothioyl)thio)-2-methyl propanoate – 94 (DAN RAFT agent)

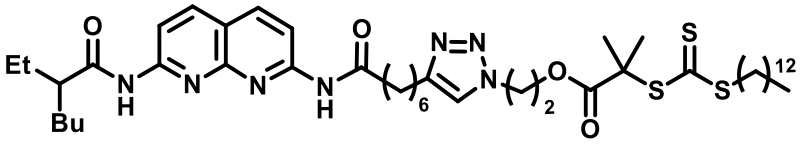

DAN alkyne **79** (0.06 g, 0.14 mmol, 1.0 eq.), 2- (dodecyl-thiocarbonothioylthio) -2-methylpropionic acid 3-azido-1-propanol ester **91** (0.12 mL, 0.28 mmol, 2.0 eq.) and tetrakis(acetonitrile)copper(I) hexafluorophosphate (0.005 g, 0.014 mmol, 0.1 eq.) were dissolved in anhydrous n,n-dimethylformamide (10 mL). N,N-diisopropylethylamine (0.06 mL, 0.33 mmol, 2.3 eq.) was added and the reaction stirred under nitrogen at 50 °C for 16 h. Upon cooling to room temperature, the reaction mixture was diluted with dichloromethane (25 mL), then washed with 5 % lithium chloride solution (3 x 20 mL), dried with sodium sulfate, filtered, and concentrated in vacuo. The title compound was isolated *via* column chromatography (SiO_2, dichloromethane: methanol (95:5)) to give the title compound **94** as a yellow solid (0.07 g, 0.08 mmol, 58 %). ^{1}H NMR (500 MHz, chloroform-*d*) δ 8.75 (s, 1H, N*H*), 8.61 (s, 1H, N*H*), 8.40 – 8.34 (m, 2H, 2 x Nap-*H*), 8.12 – 8.00 (m, 2H, 2 x Nap-*H*), 7.23 (s, 1H, triazole-*H*), 4.31 (t, 2H, *J* 6.9 Hz, (triazole) N-CH_2), 4.05 (m, 2H, COO-CH_2), 3.20 (t, 2H, *J* 7.4 Hz, (triazole)C-CH_2), 2.62 (m, 2H, SSCS-CH_2), 2.36 (t, 2H, *J* 7.4 Hz, CONH-CH_2), 2.17 (m, 3H, EtBuC*H*, $NCH_2CH_2CH_2O$), 1.63 (s, 6H, SC(CH_3)$_2$), 1.61 – 1.55 (m, 4H, 2 x CH_2), 1.34 – 1.26 (m, 6H, 3 x CH_2), 1.20 – 1.16 (m, 26H, 13 x CH_2), 0.86 (t, *J* 7.4 Hz, 3H, CH_3), 0.79 (dt, *J* 9.6, 6.7 Hz, 6H, 2 x CH_3); ^{13}C NMR (125 MHz, chloroform-*d*) δ 222.1, 175.8, 172.9, 171.2, 155.6, 154.1, 153.5, 148.3, 148.2, 139.2 (d, 2 x C), 121.3, 118.3, 113.8, 60.4, 50.7, 46.9, 37.7, 37.1, 32.4, 32.0,

31.6, 29.8-29.6 (d, 2 x C), 29.5-28.8 (m x 10 x C), 27.9, 26.0, 25.5-25.4 (d, 2 x C), 25.1, 22.7, 21.1, 14.3, 14.0, 12.0; ESI-HRMS *m/z* found 870.4840 $[M + H]^+$ $C_{45}H_{72}N_7O_4S_3$ requires 870.4802; Rf 0.3 (95:5 dichloromethane: methanol); IR ν_{max} (solid state) = 3139.5, 2923.0, 2852.8, 2222.7, 1732.8 cm^{-1}.

DAN-PMMA – 100

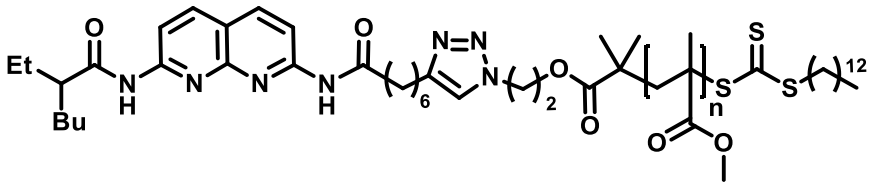

DAN alkyne **79** (0.01 g, 0.02 mmol, 1.0 eq.), azide-PMMA **99** (0.1 g, 0.02 mmol, 1.0 eq.) and tetrakis(acetonitrile)copper(I) hexafluorophosphate (0.7 mg, 0.002 mmol, 0.1 eq.) were dissolved in anhydrous n,n-dimethylformamide (10 mL). N,N-diisopropylethylamine (8 µL, 0.05 mmol, 2.3 eq.) was added and the reaction stirred under nitrogen at 50 °C for 16 h. Upon cooling to room temperature, the reaction mixture was diluted with dichloromethane (25 mL), then washed with 5 % lithium chloride solution (3 x 20 mL), dried with sodium sulfate, filtered, and concentrated in vacuo. The title polymer **100** was isolated by size exclusion chromatography (Bio-Bead S-X1 Resin, chloroform) to give polymer **98** as a pale-yellow solid (0.1 g). ^{1}H NMR (500 MHz, chloroform-*d*) δ 8.42 – 8.30 (m, 2 x Nap-*H*), 8.15 – 8.07 (m, 2 x Nap-*H*), 3.53 (s, PMMA O-CH_3), 3.53 (s, PMMA O-CH_3), 1.80 – 1.74 (m, PMMA CH_2), 0.95 – 0.78 (m, PMMA C-CH_3). Additional signals cannot be distinguished due to masking from polymer signals; IR ν_{max} (solid state) = 2994.2, 2853.8, 1724.6, 1678.8 cm^{-1}.

6.3 Photoisomerisation Studies

For irradiation of foldamer samples, a multiwavelength fiber coupled LED system was used. Green light (530 nm, 74 mW) was used for *E* to *Z* isomerisation and blue light (405 nm, 165 mW) was used for *Z* to *E* isomerisation. Irradiation was carried out at room temperature, with stirring, for 10 minutes. Samples were stirred magnetically in a glass vial covered with foil. After irradiation samples were transferred to NMR tubes and immediately transferred to the NMR sample changer.

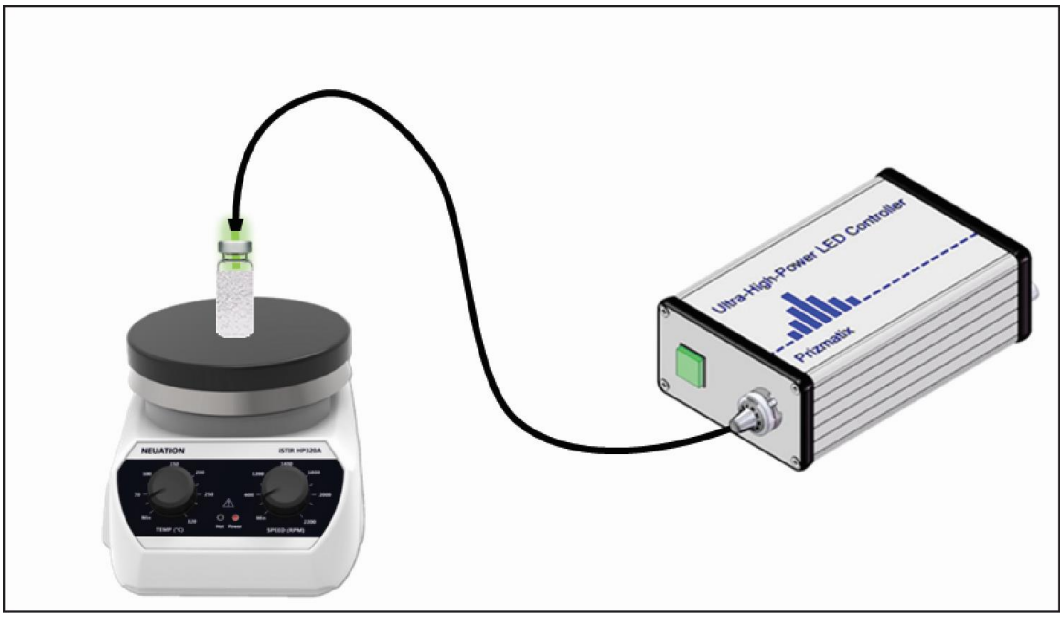

Figure 49. Representation of the equipment used for irradiation of samples.

6.3.1 DOSY NMR

DOSY spectra were obtained using a four-channel Bruker AV-NEO NMR spectrometer operating at 11.7 T (500 MHz ^{1}H) and equipped with 5mm TXI probe (δ = 0.002 s, Δ = 0.0999). Samples were prepared in Wilmad 500 MHz 5mm 528-PP-7 tubes using anhydrous deuterated chloroform purchased from Sigma Aldrich.

From the DOSY spectra obtained, reports were generated using the Bruker TopSpin Dynamics Centre software. Diffusion coefficient values were selected from the azobenzene proton peaks in the spectra. These peaks were selected as they showed clear evidence of switching after irradiation and were isolated from other proton environments in the spectra. Full spectra and data can be found in appendix B.

6.3.2 Viscometry

Viscosity measurements were carried out using a micro-Ostwald capillary viscometer purchased from VWR international. Solutions were prepared in anhydrous deuterated chloroform, irradiated, and then allowed to equilibrate to 298 K in a thermostatic water bath for 5 minutes. For each concentration, 4 readings were taken, and an average time was used to calculate the specific viscosity. See appendix C for data.

References

1. E. Frieden, *J. Chem. Educ.*, 1975, **52**, 754.
2. H. Lodish, A. Berk, C. A. Kaiser, M. Krieger and A. Bretscher, *Mol. Cell. Biol.*, Freeman, W. H. & Company, New York, 2016.
3. J. D. Watson and F. H. C. Crick, *Nature*, 1953, **171**, 737-738.
4. J. Nelson, *Structure and Function in Cell Signalling*, Wiley, Chichester, 2008.
5. H. Wang and S. C. Heilshorn, *Adv. Mater.*, 2015, **27**, 3717-3736.
6. R. McHale, J. P. Patterson, P. B. Zetterlund and R. K. O'Reilly, *Nat. Chem.*, 2012, **4**, 491-497.
7. J. W. Steed and J. L. Atwood, *Supramol. Chem.*, Wiley, Chichester, 2009.
8. M. L. Pellizzaro, K. A. Houton and A. J. Wilson, *Chem. Sci.*, 2013, **4**, 1825-1829.
9. D. Philp and J. F. Stoddart, *Angew. Chem., Int. Ed. Engl.*, 1996, **35**, 1154-1196.
10. A. Shahi and E. Arunan, *J. Chem. Sci.*, 2016, **128**, 1571-1577.
11. D. W. R. Balkenende, R. A. Olson, S. Balog, C. Weder and L. Montero de Espinosa, *Macromolecules*, 2016, **49**, 7877-7885.
12. R. P. Sijbesma, F. H. Beijer, L. Brunsveld, B. J. B. Folmer, J. H. K. K. Hirschberg, R. F. M. Lange, J. K. L. Lowe and E. W. Meijer, *Science*, 1997, **278**, 1601-1604.
13. D. A. Leigh, C. C. Robertson, A. M. Z. Slawin and P. I. T. Thomson, *J. Am. Chem. Soc*, 2013, **135**, 9939-9943.
14. J. Šponer, P. Jurečka and P. Hobza, *J. Am. Chem. Soc*, 2004, **126**, 10142-10151.
15. S. H. Kim and A. Rich, *Proc. Natl. Acad. Sci. U. S. A.*, 1968, **60**, 402-408.
16. Y. Kyogoku, R. C. Lord and A. Rich, *Proc. Natl. Acad. Sci. U. S. A.*, 1967, **57**, 250-257.
17. T. J. Murray and S. C. Zimmerman, *J. Am. Chem. Soc.*, 1992, **114**, 4010-4011.
18. W. L. Jorgensen and J. Pranata, *J. Am. Chem. Soc.*, 1990, **112**, 2008-2010.
19. S. C. C. van der Lubbe, F. Zaccaria, X. Sun and C. Fonseca Guerra, *J. Am. Chem. Soc.*, 2019, **141**, 4878-4885.
20. B. A. Blight, C. A. Hunter, D. A. Leigh, H. McNab and P. I. T. Thomson, *Nat. Chem.*, 2011, **3**, 244-248.
21. B. A. Blight, A. Camara-Campos, S. Djurdjevic, M. Kaller, D. A. Leigh, F. M. McMillan, H. McNab and A. M. Z. Slawin, *J. Am. Chem. Soc.*, 2009, **131**, 14116-14122.
22. P. L. A. Popelier and L. Joubert, *J. Am. Chem. Soc.*, 2002, **124**, 8725-8729.
23. W. E. Vallejo Narváez, E. I. Jiménez, E. Romero-Montalvo, A. Sauza-de la Vega, B. Quiroz-García, M. Hernández-Rodríguez and T. Rocha-Rinza, *Chem. Sci.*, 2018, **9**, 4402-4413.

24. O. J. Backhouse, J. C. R. Thacker and P. L. A. Popelier, *ChemPhysChem*, 2019, **20**, 555-564.
25. W. E. Vallejo Narváez, E. I. Jiménez, M. Cantú-Reyes, A. K. Yatsimirsky, M. Hernández-Rodríguez and T. Rocha-Rinza, *Chem. Commun.*, 2019, **55**, 1556-1559.
26. M. C. Etter, *Acc. Chem. Res.*, 1990, **23**, 120-126.
27. P. S. Corbin, S. C. Zimmerman, P. A. Thiessen, N. A. Hawryluk and T. J. Murray, *J. Am. Chem. Soc.*, 2001, **123**, 10475-10488.
28. L. V. Sudha and D. N. Sathyanarayana, *J. Mol. Struct.*, 1984, **125**, 89-96.
29. F. H. Beijer, H. Kooijman, A. L. Spek, R. P. Sijbesma and E. W. Meijer, *Angew. Chem., Int. Ed.*, 1998, **37**, 75-78.
30. C.-H. Chien, M.-k. Leung, J.-K. Su, G.-H. Li, Y.-H. Liu and Y. Wang, *J. Org. Chem.*, 2004, **69**, 1866-1871.
31. M. L. Pellizzaro, A. M. McGhee, L. C. Renton, M. G. Nix, J. Fisher, W. B. Turnbull and A. J. Wilson, *Chem. Eur. J.*, 2011, **17**, 14508-14517.
32. F. H. Beijer, R. P. Sijbesma, H. Kooijman, A. L. Spek and E. W. Meijer, *J. Am. Chem. Soc.*, 1998, **120**, 6761-6769.
33. H. M. Coubrough, S. C. C. van der Lubbe, K. Hetherington, A. Minard, C. Pask, M. J. Howard, C. Fonseca Guerra and A. J. Wilson, *Chem. Eur. J.*, 2019, **25**, 785-795.
34. Z. He, W. Jiang and C. A. Schalley, *Chem. Soc. Rev.*, 2015, **44**, 779-789.
35. A. Wu and L. Isaacs, *J. Am. Chem. Soc*, 2003, **125**, 4831-4835.
36. M. M. Safont-Sempere, G. Fernández and F. Würthner, *Chem. Rev.*, 2011, **111**, 5784-5814.
37. M. J. Mayoral, C. Rest, J. Schellheimer, V. Stepanenko and G. Fernández, *Chem. Eur. J.*, 2012, **18**, 15607-15611.
38. W. Jiang and C. A. Schalley, *Proc. Natl. Acad. Sci.*, 2009, **106**, 10425-10429.
39. N. Nayak and K. R. Gopidas, *ChemistrySelect*, 2016, **1**, 1028-1032.
40. P. Remón, D. González, M. A. Romero, N. Basílio and U. Pischel, *Chem. Commun.*, 2020, DOI: 10.1039/D0CC00217H.
41. J. Vázquez , P. Remón , R. N. Dsouza, A. I. Lazar, J. F. Arteaga, W. M. Nau and U. Pischel, *Chem. Eur. J.*, 2014, **20**, 9897-9901.
42. J.-F. Gohy, B. G. G. Lohmeijer and U. S. Schubert, *Chem. Eur. J.*, 2003, **9**, 3472-3479.
43. C. Xu, Y. Chen, H.-Y. Zhang and Y. Liu, *J. Photochem. Photobiol., A*, 2016, **331**, 240-246.
44. S. Schoder and C. A. Schalley, *Chem. Commun.*, 2017, **53**, 9546-9549.
45. H. M. Coubrough, B. Balonova, C. M. Pask, B. A. Blight and A. J. Wilson, *ChemistryOpen*, 2020, **9**, 40-44.

46. A. Kumar, A. Srivastava, I. Y. Galaev and B. Mattiasson, *Prog. Polym. Sci.*, 2007, **32**, 1205-1237.
47. A. S. Carlini, L. Adamiak and N. C. Gianneschi, *Macromolecules*, 2016, **49**, 4379-4394.
48. G. Odian, *Principles of Polymerization*, Wiley, New York, 2004.
49. in *Encyclopedia of Polymer Science and Technology*, DOI: 10.1002/0471440264.pst453.pub2, pp. 1-27.
50. D. A. Shipp, *Poly. Rev.*, 2011, **51**, 99-103.
51. A. D. Jenkins, R. G. Jones and G. Moad, *Pure Appl. Chem.*, 2009, **82**, 483.
52. S. Perrier, *Macromolecules*, 2017, **50**, 7433-7447.
53. R. B. Grubbs, *Polym. Rev.*, 2011, **51**, 104-137.
54. D. Samanta, S. McRae, B. Cooper, Y. Hu, T. Emrick, J. Pratt and S. A. Charles, *Biomacromolecules*, 2008, **9**, 2891-2897.
55. J. Nicolas, V. S. Miguel, G. Mantovani and D. M. Haddleton, *Chem. Commun.*, 2006, DOI: 10.1039/B609935A, 4697-4699.
56. R. M. Broyer, G. M. Quaker and H. D. Maynard, *J. Am. Chem. Soc.*, 2008, **130**, 1041-1047.
57. Y. Kang, A. Lu, A. Ellington, M. C. Jewett and R. K. O'Reilly, *ACS Macro Lett.*, 2013, **2**, 581-586.
58. M. R. Hill, R. N. Carmean and B. S. Sumerlin, *Macromolecules*, 2015, **48**, 5459-5469.
59. S. G. Roy, U. Haldar and P. De, *ACS Appl. Mater*, 2014, **6**, 4233-4241.
60. C. M. Schilli, M. Zhang, E. Rizzardo, S. H. Thang, Y. K. Chong, K. Edwards, G. Karlsson and A. H. E. Müller, *Macromolecules*, 2004, **37**, 7861-7866.
61. L. Kostka, L. Kotrchová, V. Šubr, A. Libánská, C. A. Ferreira, I. Malátová, H. J. Lee, T. E. Barnhart, J. W. Engle, W. Cai, M. Šírová and T. Etrych, *Biomaterials*, 2020, **235**, 119728.
62. A. Gregory and M. H. Stenzel, *Prog. Polym. Sci.*, 2012, **37**, 38-105.
63. G. Moad, E. Rizzardo and S. H. Thang, *Polymer*, 2008, **49**, 1079-1131.
64. Y. Yang and M. W. Urban, *Chem. Soc. Rev.*, 2013, **42**, 7446-7467.
65. Y. Chen and Z. Guan, *Chemical Communications*, 2014, **50**, 10868-10870.
66. A. Goujon, G. Mariani, T. Lang, E. Moulin, M. Rawiso, E. Buhler and N. Giuseppone, *J. Am. Chem. Soc*, 2017, **139**, 4923-4928.
67. T. Liu, S. Zou, C. Hang, J. Li, X. Di, X. Li, Q. Wu, F. Wang and P. Sun, *Polym. Chem.*, 2020, **11**, 1906-1918.
68. C. Li, A. Iscen, H. Sai, K. Sato, N. A. Sather, S. M. Chin, Z. Álvarez, L. C. Palmer, G. C. Schatz and S. I. Stupp, *Nat. Mater.*, 2020, **19**, 900-909.
69. S. Yagai and A. Kitamura, *Chem. Soc. Rev.*, 2008, **37**, 1520-1529.

70. Y. Li, T. Park, J. K. Quansah and S. C. Zimmerman, *J. Am. Chem. Soc*, 2011, **133**, 17118-17121.
71. B. J. Cafferty, R. R. Avirah, G. B. Schuster and N. V. Hud, *Chem. Sci.*, 2014, **5**, 4681-4686.
72. D. Görl, B. Soberats, S. Herbst, V. Stepanenko and F. Würthner, *Chem. Sci.*, 2016, **7**, 6786-6790.
73. F. Xu and B. L. Feringa, *Advanced Materials*, 2023, **35**, 2204413.
74. L. R. Hart, J. L. Harries, B. W. Greenland, H. M. Colquhoun and W. Hayes, *ACS Appl. Mater. Interfaces*, 2015, **7**, 8906-8914.
75. O. J. G. M. Goor, S. I. S. Hendrikse, P. Y. W. Dankers and E. W. Meijer, *Chem. Soc. Rev.*, 2017, **46**, 6621-6637.
76. Y. Ahn, Y. Jang, N. Selvapalam, G. Yun and K. Kim, *Angew. Chem., Int. Ed.*, 2013, **52**, 3140-3144.
77. C. A. Anderson, A. R. Jones, E. M. Briggs, E. J. Novitsky, D. W. Kuykendall, N. R. Sottos and S. C. Zimmerman, *J. Am. Chem. Soc*, 2013, **135**, 7288-7295.
78. R. Dong, Y. Zhou, X. Huang, X. Zhu, Y. Lu and J. Shen, *Advanced Materials*, 2015, **27**, 498-526.
79. L. Brunsveld, B. J. B. Folmer, E. W. Meijer and R. P. Sijbesma, *Chem. Rev.*, 2001, **101**, 4071-4098.
80. A. J. Wilson, *Soft Matter*, 2007, **3**, 409-425.
81. K. A. Houton and A. J. Wilson, *Polym. Int.*, 2014, DOI: 10.1002/pi.4837, n/a-n/a.
82. A. del Prado, D. González-Rodríguez and Y.-L. Wu, *ChemistryOpen*, 2020, **9**, 409-430.
83. A. Sikder, C. Esen and R. K. O'Reilly, *Acc. Chem. Res.*, 2022, **55**, 1609-1619.
84. C. Fouquey, J.-M. Lehn and A.-M. Levelut, *Adv. Mater.*, 1990, **2**, 254-257.
85. T. F. A. de Greef, G. Ercolani, G. B. W. L. Ligthart, E. W. Meijer and R. P. Sijbesma, *J. Am. Chem. Soc*, 2008, **130**, 13755-13764.
86. G. B. W. L. Ligthart, H. Ohkawa, R. P. Sijbesma and E. W. Meijer, *J. Am. Chem. Soc*, 2005, **127**, 810-811.
87. N. Oya, T. Ikezaki and N. Yoshie, *Polym. J.*, 2013, **45**, 955-961.
88. X. Yan, Z. Liu, Q. Zhang, J. Lopez, H. Wang, H.-C. Wu, S. Niu, H. Yan, S. Wang, T. Lei, J. Li, D. Qi, P. Huang, J. Huang, Y. Zhang, Y. Wang, G. Li, J. B. H. Tok, X. Chen and Z. Bao, *J. Am. Chem. Soc*, 2018, **140**, 5280-5289.
89. D. Wan, K. Satoh and M. Kamigaito, *Macromolecules*, 2006, **39**, 6882-6886.
90. S. Wang, M. Li, H. Zhang, X. Yang, X. Zhang, Y. Tao and X. Wang, *J. Polym. Sci., Part A: Polym. Chem.*, 2016, **54**, 1633-1638.

91. H. M. Coubrough, M. Reynolds, J. A. Goodchild, S. D. A. Connell, J. Mattsson and A. J. Wilson, *Polym. Chem.*, 2020, **11**, 3593-3604.
92. H. M. Coubrough, PhD thesis, University of Leeds, 2018.
93. E. M. Carnicom, J. A. Abruzzese, Y. Sidibe, K. D. Myers and E. S. Tillman, *Polymers*, 2014, **6**, 2737-2751.
94. H. Sun, C. P. Kabb, Y. Dai, M. R. Hill, I. Ghiviriga, A. P. Bapat and B. S. Sumerlin, *Nat. Chem.*, 2017, **9**, 817-823.
95. S. Yagai, K. Iwai, M. Yamauchi, T. Karatsu, A. Kitamura, S. Uemura, M. Morimoto, H. Wang and F. Würthner, *Angew. Chem., Int. Ed.*, 2014, **53**, 2602-2606.
96. T.-G. Zhan, M.-D. Lin, J. Wei, L.-J. Liu, M.-Y. Yun, L. Wu, S.-T. Zheng, H.-H. Yin, L.-C. Kong and K.-D. Zhang, *Polym. Chem.*, 2017, **8**, 7384-7389.
97. S. Tan, Y. Sha, T. Zhu, M. A. Rahman and C. Tang, *Polym. Chem.*, 2018, **9**, 5395-5401.
98. D. Zhang, L. Wang, X. Zhang, D. Bao and Y. Zhao, *J. Drug Deliv. Sci. and Tec.*, 2018, **45**, 281-286.
99. M. Toma, U. Jonas, A. Mateescu, W. Knoll and J. Dostalek, *J. Phys. Chem. C*, 2013, **117**, 11705-11712.
100. D. A. Davis, A. Hamilton, J. Yang, L. D. Cremar, D. Van Gough, S. L. Potisek, M. T. Ong, P. V. Braun, T. J. Martínez, S. R. White, J. S. Moore and N. R. Sottos, *Nature*, 2009, **459**, 68-72.
101. D. Bléger, J. Schwarz, A. M. Brouwer and S. Hecht, *J. Am. Chem. Soc*, 2012, **134**, 20597-20600.
102. A. A. Beharry, O. Sadovski and G. A. Woolley, *J. Am. Chem. Soc*, 2011, **133**, 19684-19687.
103. Z.-T. Shi, J.-J. Yu, Q. Zhang, M.-M. Li, W.-J. Liang, C.-X. Zhao and D.-H. Qu, *Chem. Commun.*, 2019, **55**, 10292-10295.
104. M. Takeshita, M. Hayashi, S. Kadota, K. H. Mohammed and T. Yamato, *Chem. Commun.*, 2005, DOI: 10.1039/B415114C, 761-763.
105. P. Kuad, A. Miyawaki, Y. Takashima, H. Yamaguchi and A. Harada, *J. Am. Chem. Soc*, 2007, **129**, 12630-12631.
106. K. Yamauchi, Y. Takashima, A. Hashidzume, H. Yamaguchi and A. Harada, *J. Am. Chem. Soc*, 2008, **130**, 5024-5025.
107. N. S. S. Kumar, S. Varghese, G. Narayan and S. Das, *Angew. Chem., Int. Ed.*, 2006, **45**, 6317-6321.
108. I. Willerich and F. Gröhn, *Angew. Chem., Int. Ed.*, 2010, **49**, 8104-8108.
109. W.-J. Liang, J.-J. Yu, Q. Zhang, C.-S. Ma, Z.-T. Shi and D.-H. Qu, *Polym. Chem.*, 2018, **9**, 4808-4812.

110. J. Wei and Y. Yu, *Soft Matter*, 2012, **8**, 8050-8059.
111. H. M. D. Bandara and S. C. Burdette, *Chem. Soc. Rev.*, 2012, **41**, 1809-1825.
112. W. A. Velema, M. C. A. Stuart, W. Szymanski and B. L. Feringa, *Chem. Commun.*, 2013, **49**, 5001-5003.
113. T. Suzuki, S. Shinkai and K. Sada, *Adv. Mater.*, 2006, **18**, 1043-1046.
114. Q. Jin, G. Liu, X. Liu and J. Ji, *Soft Matter*, 2010, **6**, 5589-5595.
115. H. A. Wegner, *Angew. Chem., Int. Ed.*, 2012, **51**, 4787-4788.
116. A. Rullo, A. Reiner, A. Reiter, D. Trauner, E. Y. Isacoff and G. A. Woolley, *Chem. Commun.*, 2014, **50**, 14613-14615.
117. S. Samanta, A. A. Beharry, O. Sadovski, T. M. McCormick, A. Babalhavaeji, V. Tropepe and G. A. Woolley, *J. Am. Chem. Soc.*, 2013, **135**, 9777-9784.
118. D. B. Konrad, G. Savasci, L. Allmendinger, D. Trauner, C. Ochsenfeld and A. M. Ali, *J. Am. Chem. Soc.*, 2020, **142**, 6538-6547.
119. S. Hecht and I. Huc, eds., *Foldamers: Structure, Properties, and Applications*, Wiley-VCH, Weinheim, 2007.
120. S. H. Gellman, *Acc. Chem. Res.*, 1998, **31**, 178-190.
121. J. W. Checco and S. H. Gellman, *Curr. Opin. Struct. Biol.*, 2016, **39**, 96-105.
122. T. A. Sobiech, Y. Zhong and B. Gong, *Org. Biomol. Chem.*, 2022, **20**, 6962-6978.
123. A. Barnard, K. Long, H. L. Martin, J. A. Miles, T. A. Edwards, D. C. Tomlinson, A. Macdonald and A. J. Wilson, *Angew. Chem., Int. Ed.*, 2015, **54**, 2960-2965.
124. Z. Hegedus, C. M. Grison, J. A. Miles, S. Rodriguez-Marin, S. L. Warriner, M. E. Webb and A. J. Wilson, *Chem. Sci.*, 2019, **10**, 3956-3962.
125. G. Guichard and I. Huc, *Chem. Commun.*, 2011, **47**, 5933-5941.
126. N. Chandramouli, Y. Ferrand, G. Lautrette, B. Kauffmann, C. D. Mackereth, M. Laguerre, D. Dubreuil and I. Huc, *Nat. Chem.*, 2015, **7**, 334.
127. K. Ziach, C. Chollet, V. Parissi, P. Prabhakaran, M. Marchivie, V. Corvaglia, P. P. Bose, K. Laxmi-Reddy, F. Godde, J.-M. Schmitter, S. Chaignepain, P. Pourquier and I. Huc, *Nat. Chem.*, 2018, **10**, 511-518.
128. D.-W. Zhang, X. Zhao and Z.-T. Li, *Acc. Chem. Res.*, 2014, **47**, 1961-1970.
129. C. Dolain, V. Maurizot and I. Huc, *Angew. Chem., Int. Ed.*, 2003, **42**, 2738-2740.
130. A. D. Peters, S. Borsley, F. della Sala, D. F. Cairns-Gibson, M. Leonidou, J. Clayden, G. F. S. Whitehead, I. J. Vitórica-Yrezábal, E. Takano, J. Burthem, S. L. Cockroft and S. J. Webb, *Chem. Sci.*, 2020, **11**, 7023-7030.
131. Y. Liu, F. C. Parks, E. G. Sheetz, C.-H. Chen and A. H. Flood, *J. Am. Chem. Soc*, 2021, **143**, 3191-3204.
132. D. P. Tilly, J.-P. Heeb, S. J. Webb and J. Clayden, *Nat. Commun.*, 2023, **14**, 2647.
133. J. Yin and V. B. Birman, *J. Org. Chem.*, 2022, **87**, 15744-15753.

134. F. C. Parks, Y. Liu, S. Debnath, S. R. Stutsman, K. Raghavachari and A. H. Flood, *J. Am. Chem. Soc.*, 2018, **140**, 17711-17723.
135. C. R. Opie, N. Kumagai and M. Shibasaki, *Angew. Chem., Int. Ed.*, 2017, **56**, 3349-3353.
136. J. D. Fox and S. J. Rowan, *Macromolecules*, 2009, **42**, 6823-6835.
137. T. Aida, E. W. Meijer and S. I. Stupp, *Science*, 2012, **335**, 813-817.
138. F. Huang and O. A. Scherman, *Chem. Soc. Rev.*, 2012, **41**, 5879-5880.
139. L. Yang, X. Tan, Z. Wang and X. Zhang, *Chem. Rev.*, 2015, **115**, 7196-7239.
140. L. Liu and S. H. Gellman, *Macromolecules*, 2020, **53**, 8141-8143.
141. J. Chen, E. S. Garcia and S. C. Zimmerman, *Acc. Chem. Res.*, 2020, **53**, 1244-1256.
142. F. C. Parks, E. G. Sheetz, S. R. Stutsman, A. Lutolli, S. Debnath, K. Raghavachari and A. H. Flood, *J. Am. Chem. Soc*, 2022, **144**, 1274-1287.
143. A. D. Peters, S. Borsley, F. della Sala, D. F. Cairns-Gibson, M. Leonidou, J. Clayden, G. F. S. Whitehead, I. J. Vitórica-Yrezábal, E. Takano, J. Burthem, S. L. Cockroft and S. J. Webb, *Chem. Sci.*, 2020, **11**, 7023-7030.
144. D. Bindl, P. K. Mandal, L. Allmendinger and I. Huc, *Angew. Chem., Int. Ed.*, 2022, **61**, e202116509.
145. Y. Huo and H. Zeng, *Acc. Chem. Res.*, 2016, **49**, 922-930.
146. H. Ito, M. Ikeda, T. Hasegawa, Y. Furusho and E. Yashima, *J. Am. Chem. Soc*, 2011, **133**, 3419-3432.
147. G. Guichard and I. Huc, *ChemComm*, 2011, **47**, 5933-5941.
148. F. Xu and B. L. Feringa, *Adv. Mater.*, 2023, **35**, 2204413.
149. S. Crespi, N. A. Simeth and B. König, *Nat. Rev. Chem.*, 2019, **3**, 133-146.
150. L. N. Lameijer, S. Budzak, N. A. Simeth, M. J. Hansen, B. L. Feringa, D. Jacquemin and W. Szymanski, *Angew. Chem., Int. Ed.*, 2020, **59**, 21663-21670.
151. J. Volarić, J. Buter, A. M. Schulte, K.-O. van den Berg, E. Santamaría-Aranda, W. Szymanski and B. L. Feringa, *J. Org. Chem.*, 2022, **87**, 14319-14333.
152. P. S. Corbin, S. C. Zimmerman, P. A. Thiessen, N. A. Hawryluk and T. J. Murray, *J. Am. Chem. Soc.*, 2001, **123**, 10475-10488.
153. W. L. Jorgensen and J. Pranata, *J. Am. Chem. Soc*, 1990, **112**, 2008-2010.
154. G. B. W. L. Ligthart, H. Ohkawa, R. P. Sijbesma and E. W. Meijer, *J. Am. Chem. Soc.*, 2005, **127**, 810-811.
155. A. Baeyer, *Ber. Dtsch. Chem.*, 1874, **7**, 1638-1640.
156. M. Schilz and H. Plenio, *J. Org. Chem.*, 2012, **77**, 2798-2807.
157. P. W. van Leeuwen, P. C. Kamer, J. N. Reek and P. Dierkes, *Chem. Rev.*, 2000, **100**, 2741-2770.

158. C. A. Anderson, P. G. Taylor, M. A. Zeller and S. C. Zimmerman, *J. Am. Chem. Soc.*, 2010, **75**, 4848-4851.
159. J. F. Hartwig, 1998, **37**, 2046-2067.
160. S. Yagai, T. Iwashima, K. Kishikawa, S. Nakahara, T. Karatsu and A. Kitamura, *Chem. Eur. J.*, 2006, **12**, 3984-3994.
161. S. Yagai, K. Ohta, M. Gushiken, K. Iwai, A. Asano, S. Seki, Y. Kikkawa, M. Morimoto, A. Kitamura and T. Karatsu, *Chem. Eur. J.*, 2012, **18**, 2244-2253.
162. L. Wei, S.-T. Han, T.-T. Jin, T.-G. Zhan, L.-J. Liu, J. Cui and K.-D. Zhang, *Chem. Sci.*, 2021, **12**, 1762-1771.
163. S.-L. Li, T. Xiao, W. Xia, X. Ding, Y. Yu, J. Jiang and L. Wang, *Chem. Eur. J.*, 2011, **17**, 10716-10723.
164. J.-F. Xu, Y.-Z. Chen, D. Wu, L.-Z. Wu, C.-H. Tung and Q.-Z. Yang, *Angew. Chem., Int. Ed.*, 2013, **52**, 9738-9742.
165. X. Liu, J.-F. Xu, Z. Wang and X. Zhang, *Polym. Chem.*, 2016, **7**, 2333-2336.
166. S. Tan, Y. Sha, T. Zhu, M. A. Rahman and C. Tang, *Polymer Chemistry*, 2018, **9**, 5395-5401.
167. W.-J. Liang, J.-J. Yu, Q. Zhang, C.-S. Ma, Z.-T. Shi and D.-H. Qu, *Polymer Chemistry*, 2018, **9**, 4808-4812.
168. S.-L. Li, T. Xiao, W. Xia, X. Ding, Y. Yu, J. Jiang and L. Wang, *Chem.--Eur. J.*, 2011, **17**, 10716-10723.
169. B. J. B. Folmer, R. P. Sijbesma and E. W. Meijer, *J. Am. Chem. Soc.*, 2001, **123**, 2093-2094.
170. A. T. ten Cate, H. Kooijman, A. L. Spek, R. P. Sijbesma and E. W. Meijer, *J. Am. Chem. Soc.*, 2004, **126**, 3801-3808.
171. O. A. Scherman, G. B. W. L. Ligthart, R. P. Sijbesma and E. W. Meijer, *Angew. Chem., Int. Ed.*, 2006, **45**, 2072-2076.
172. R. Neufeld and D. Stalke, *Chem. Sci.*, 2015, **6**, 3354-3364.
173. T. S. Rushing and R. D. Hester, 2003, **89**, 2831-2835.
174. F. Rodriguez, C. Cohen, C. K. Ober and L. A. Archer, *Principles of Polymer Systems*, CRC Press, New York, 6 edn., 2004.
175. T. Yamakita and A. Yoshimori, *J. Phys. Soc. Japan*, 2015, **84**, 043602.
176. S. E. Harding, *Prog. Biophys. Mol. Biol.*, 1997, **68**, 207-262.
177. P. Groves, *Polym. Chem.*, 2017, **8**, 6700-6708.
178. T. Aida and E. W. Meijer, *Isr. J. Chem.*, 2020, **60**, 33-47.
179. A. Antoine John and Q. Lin, *J. Org. Chem.*, 2017, **82**, 9873-9876.

Appendix A

^{1}H NMR Spectra

1-(4-Bromo-2,6-difluorophenyl)-2-(2,6-difluoro-4-iodophenyl)diazene **52**

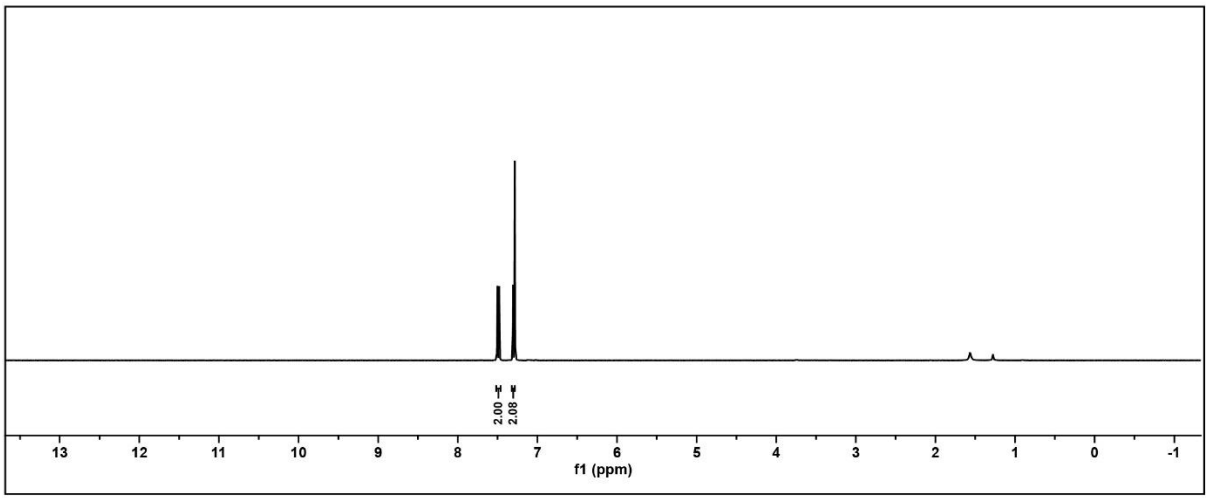

8-Nonynoic acid **54**

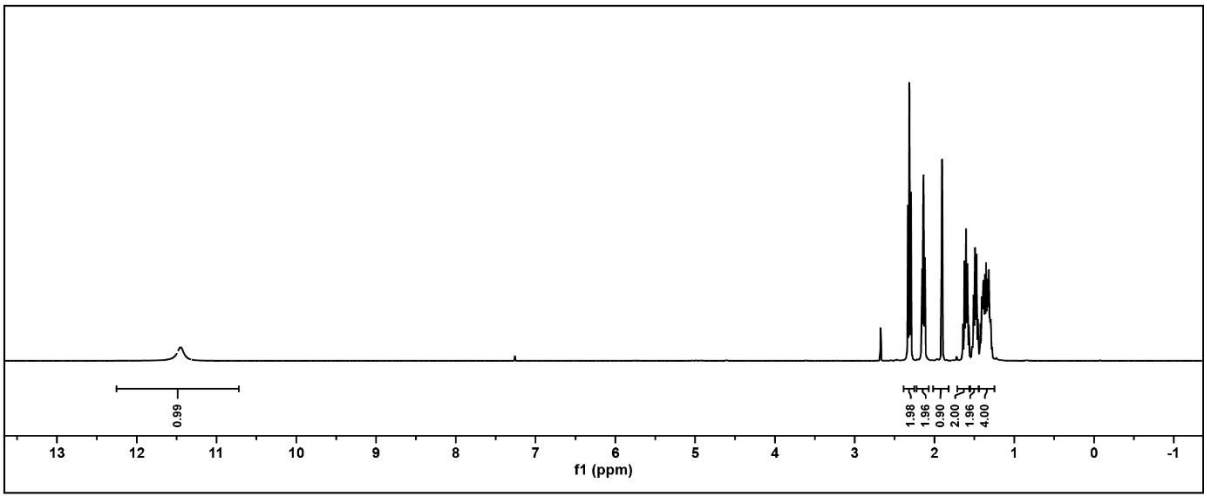

1-(Oct-7-yn-1-yl)-3-(pyridin-2-yl)urea **56**

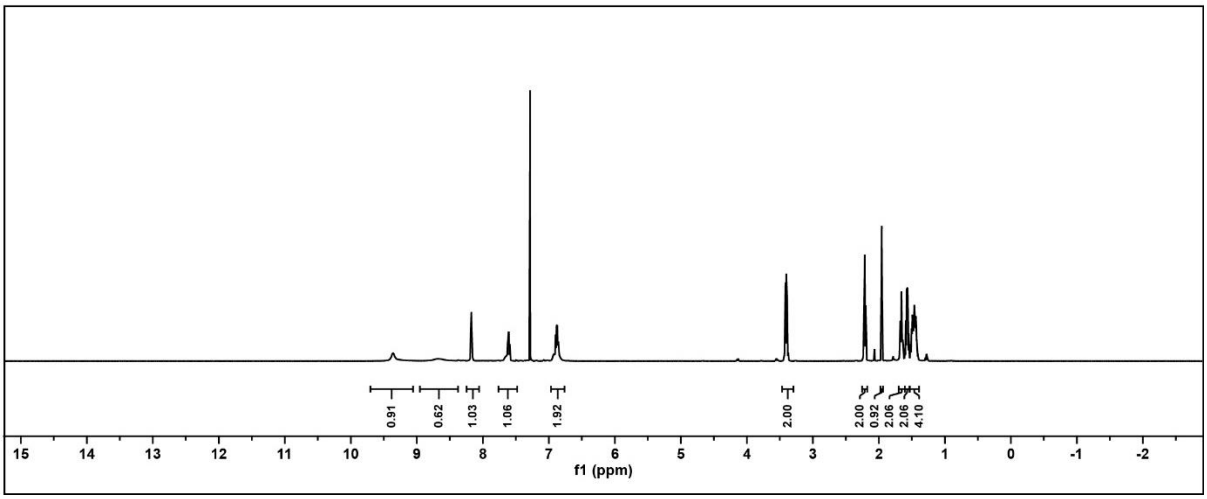

1,8-Naphthyridin-2-amine **59**

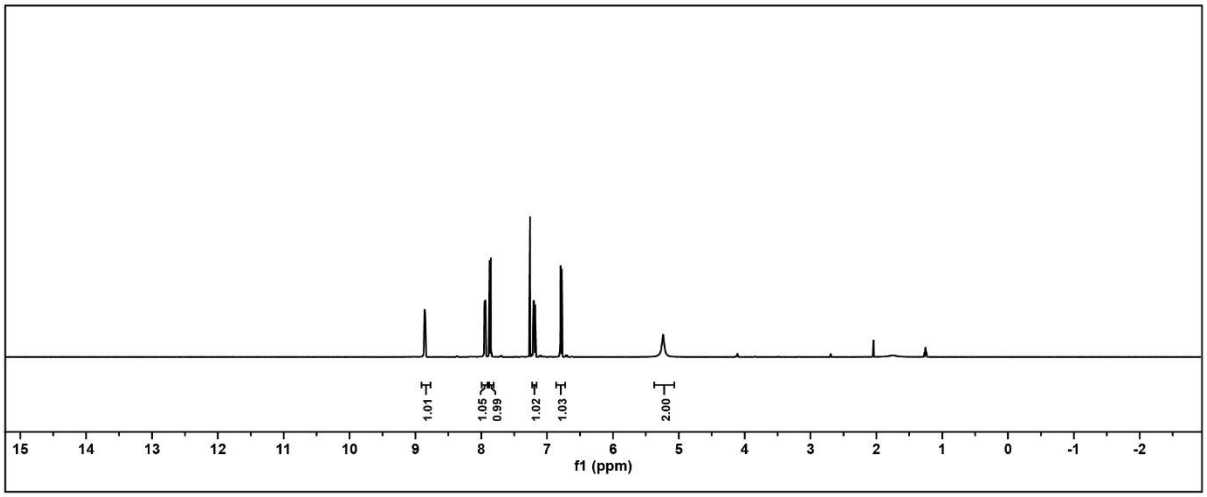

N-(1,8-Naphthyridin-2-yl)non-8-ynamide **60**

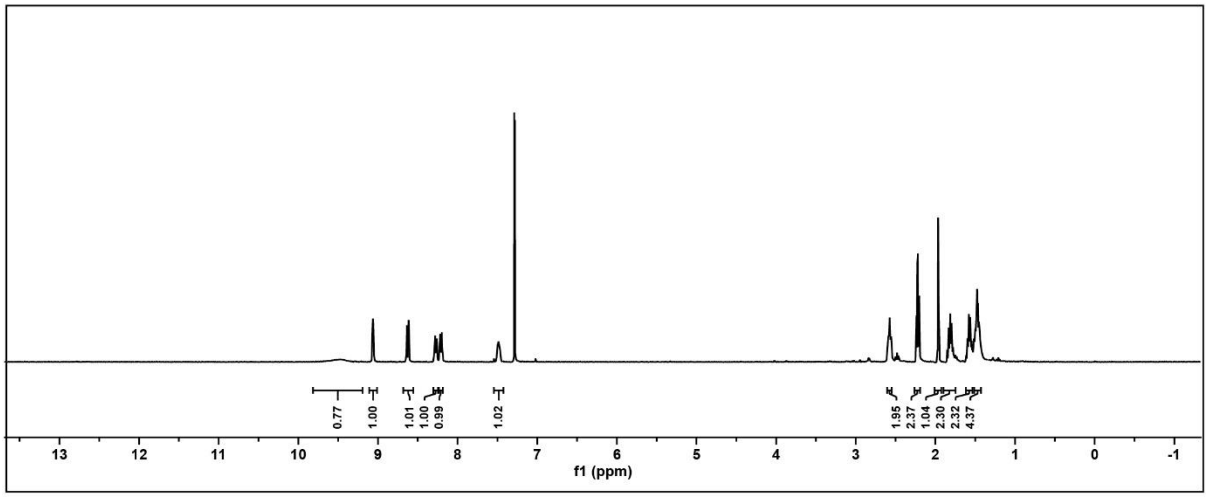

(*E*)-1- (8- (4-((4-Bromo -2,6- difluorophenyl)diazenyl)-3,5-difluorophenyl)oct7-yn-1-yl)-3-(pyridin-2-yl)urea **61**

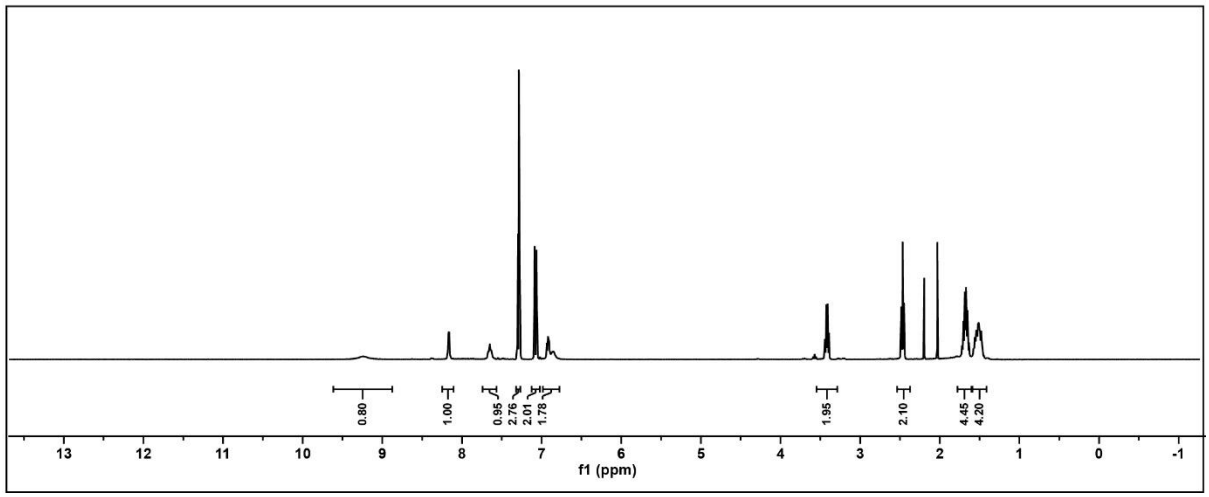

N-(6-Methyl-4-oxo-1,4-dihydropyrimidin-2-yl)non-8-ynamide **63**

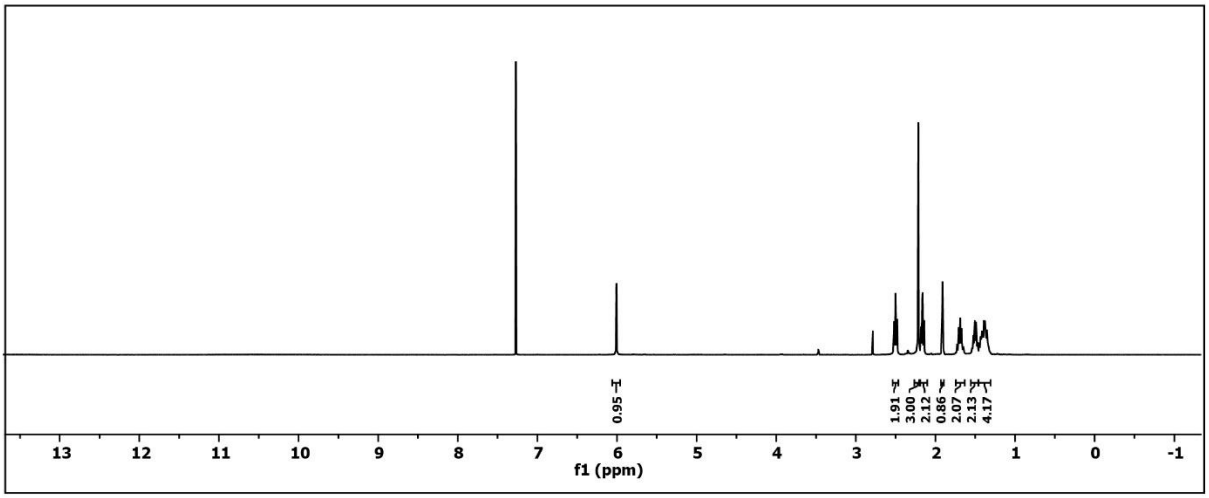

2-(3-(5,6-Dimethyl-1H-benzo[d]imidazol-2-yl)ureido)oct-7-yn **66**

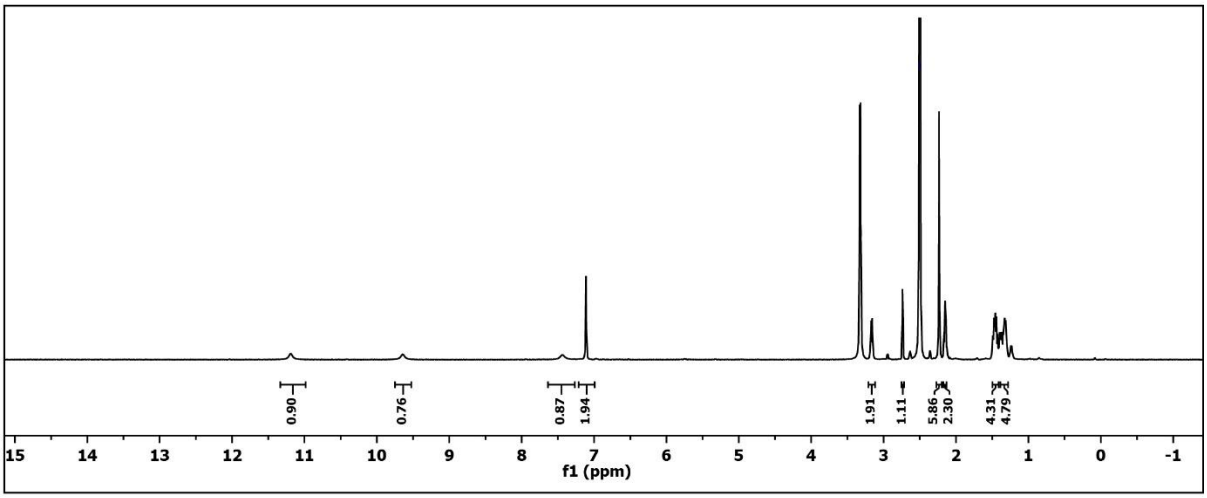

1-(8-(4-((4-Bromo-2,6-difluorophenyl)diazenyl)-3,5-difluorophenyl)-*N*-(6-methyl-4-oxo-1,4-dihydropyrimidin-2-yl))non-8-ynamide **67**

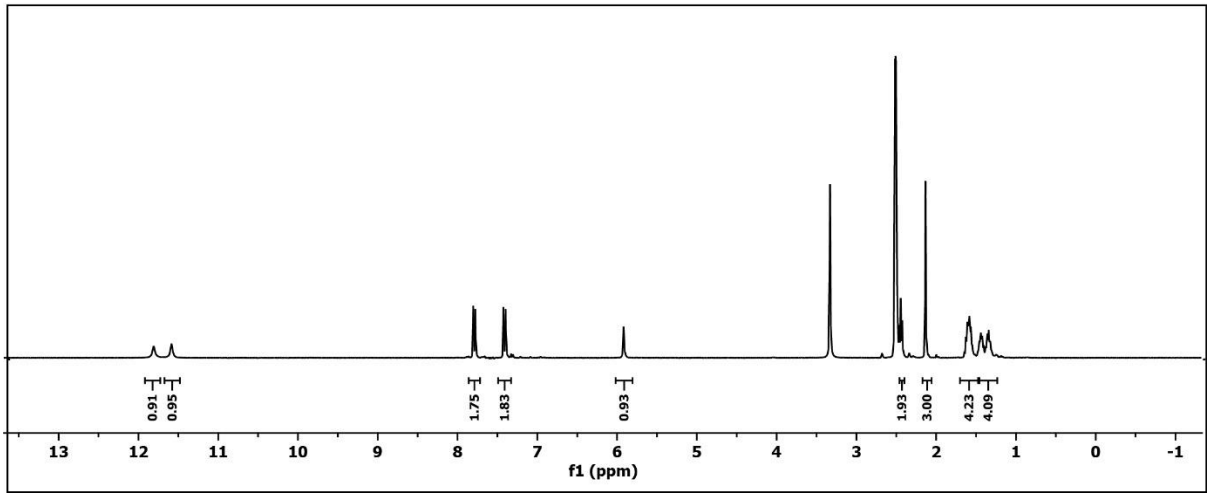

1-(Oct-7-yn-1-yl)-N-(4-(1-ethylpentyl)-1,6-dihydro-6-oxo-2-pyrimidinyl))urea **69**

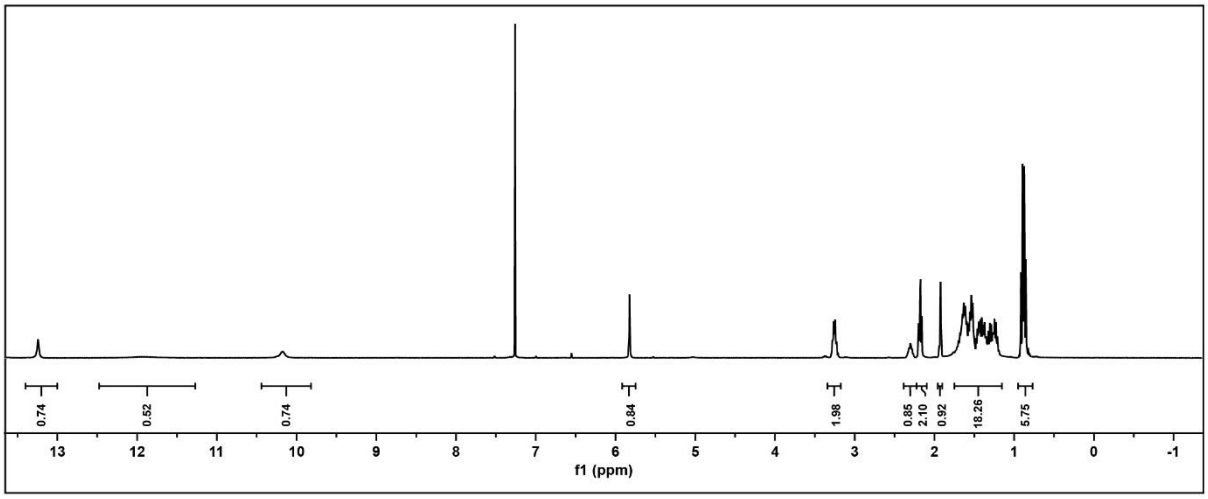

1,2-Bis(2,6-difluoro-4-iodophenyl)diazene **70**

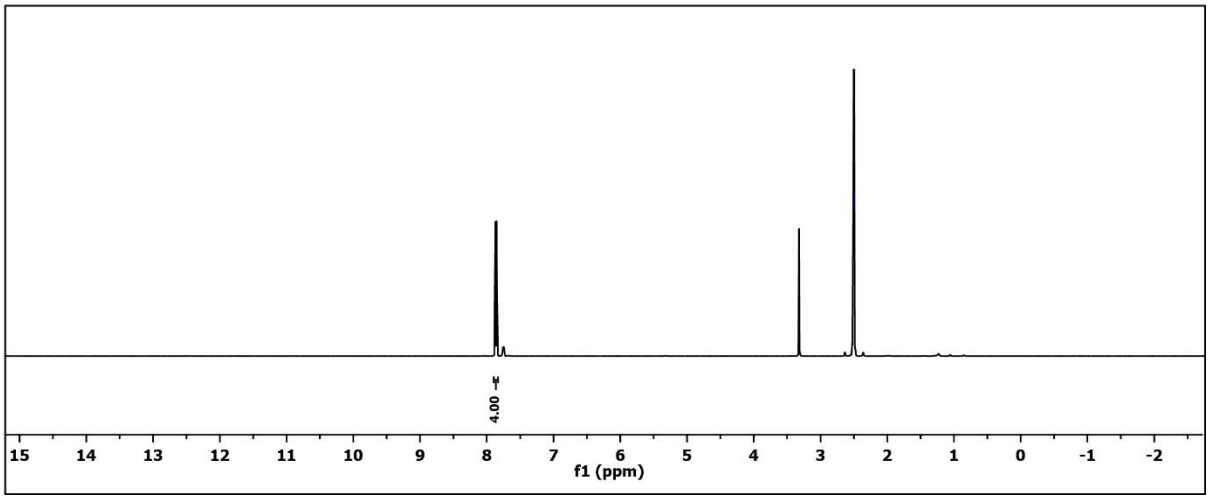

1-(8-(4-((4-Bromo -2,6- difluorophenyl) diazenyl)- 3,5-difluorophenyl) oct7-yn-1-yl)-*n*-(4-(1-ethylpentyl)-1,6-dihydro-6-oxo-2-pyrimidinyl))urea) **71**

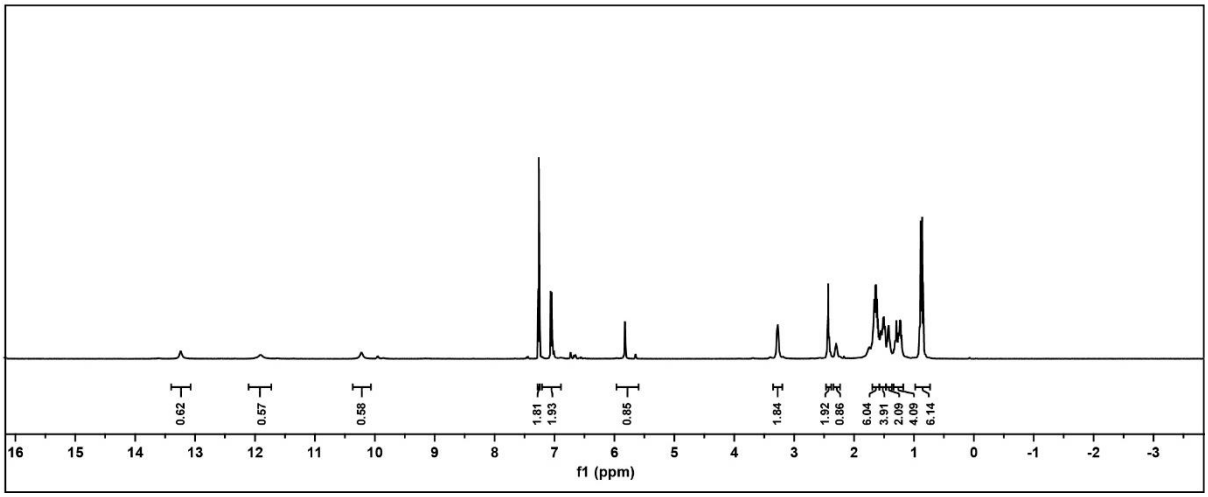

(*E*)-1,2-Bis(2,6-difluoro-4-1-(Oct-7-yn-1-yl)-acid)diazene **72**

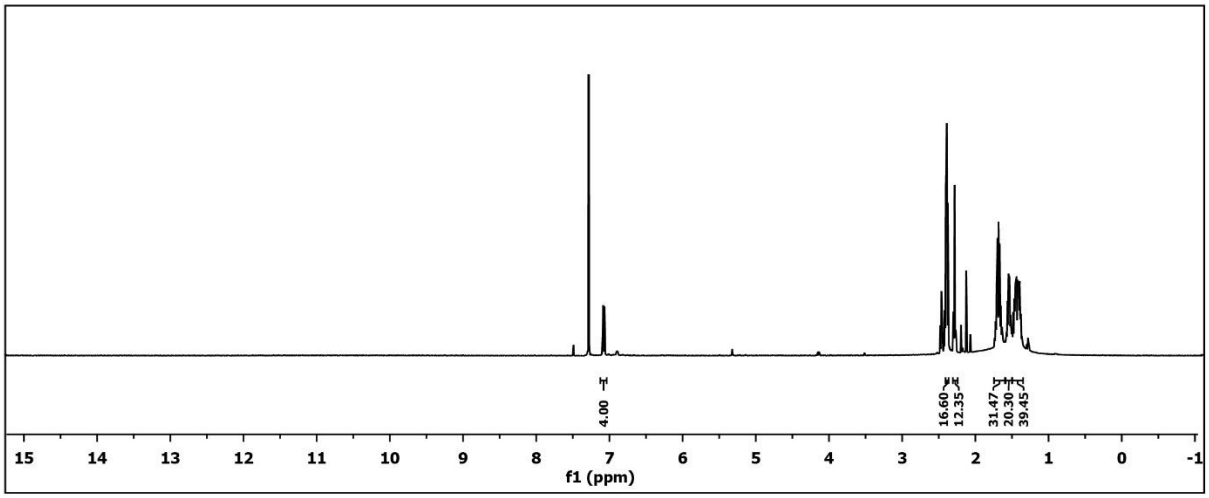

4-((2,6-Difluoroanaline)oct7-yn-1-yl)-*N*-(4-(1-ethylpentyl)-1,6-dihydro-6-oxo-2-pyrimidinyl))urea) **73**

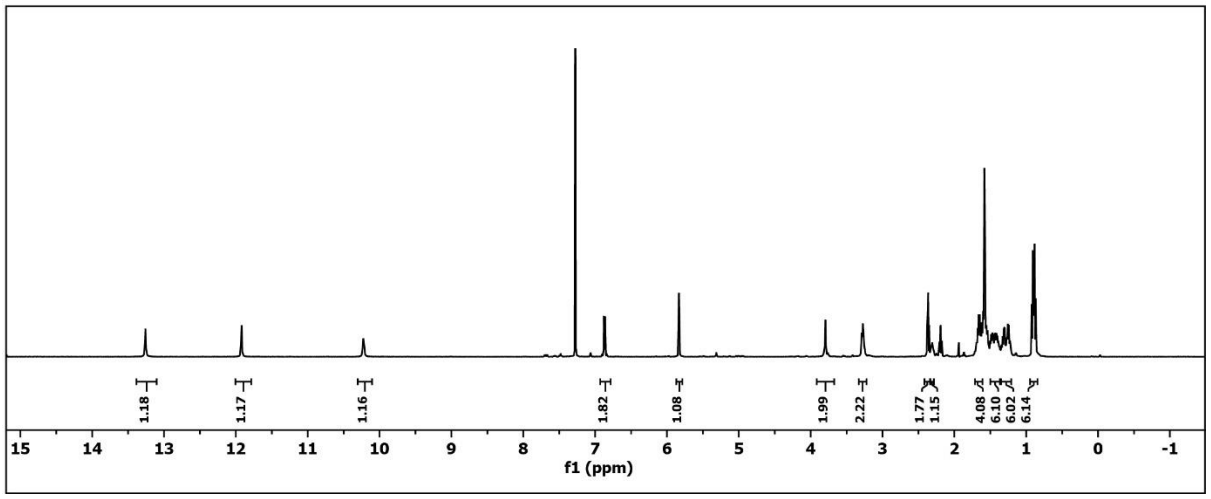

7-Hydroxy-1,8-naphthyridin-2-amine **75**

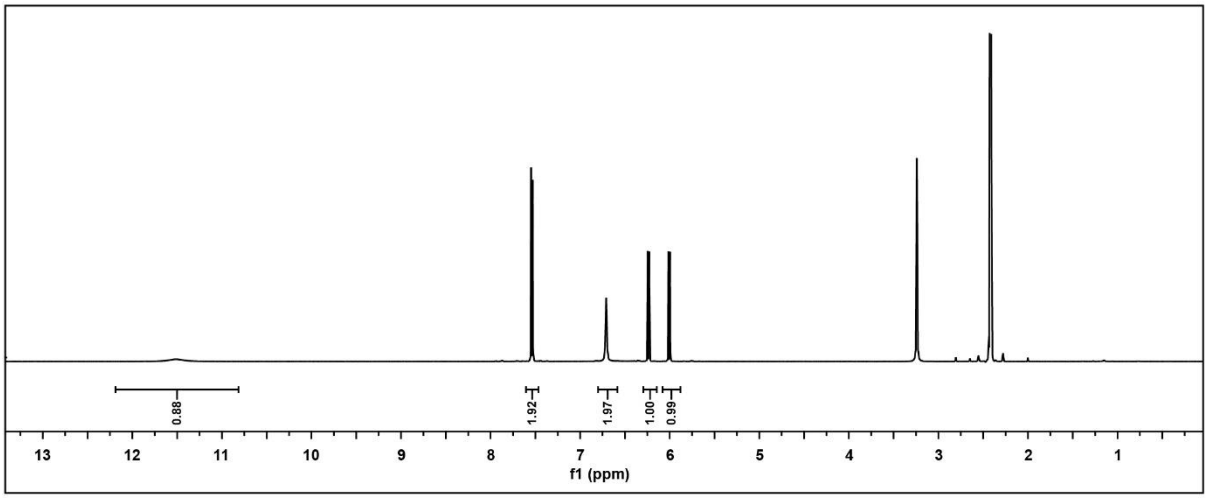

7-(2-Ethyl-hexanoyl)-amino-8H-(7-oxo-[1,8]-naphthyridine-2-yl) **76**

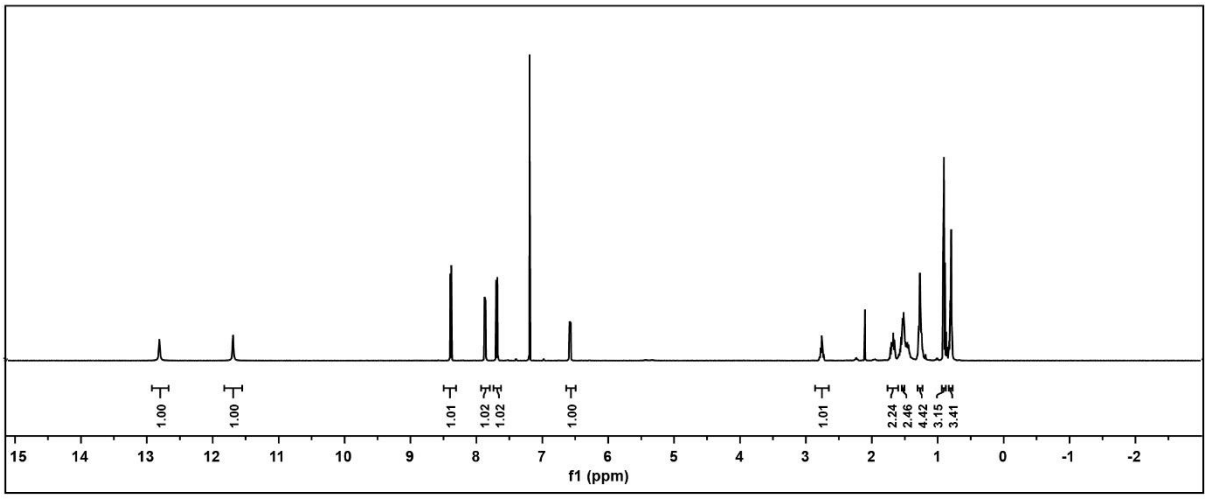

N-(7-Bromo-1,8-naphthyridin-2-yl)-2-ethylhexanamide **77**

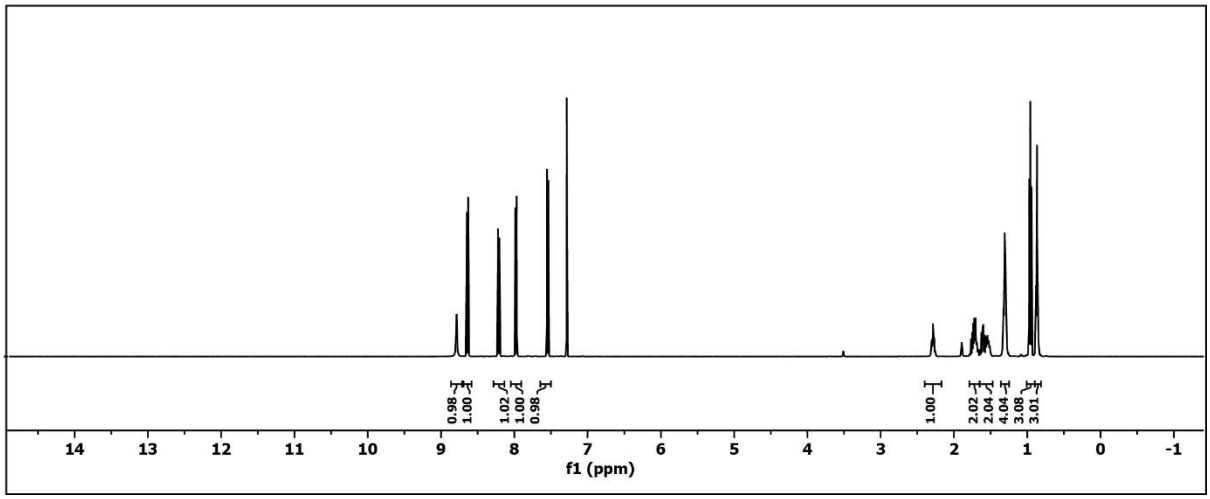

N-(7-Amino-1,8-naphthyridin-2-yl)-2-ethylhexanamide **78**

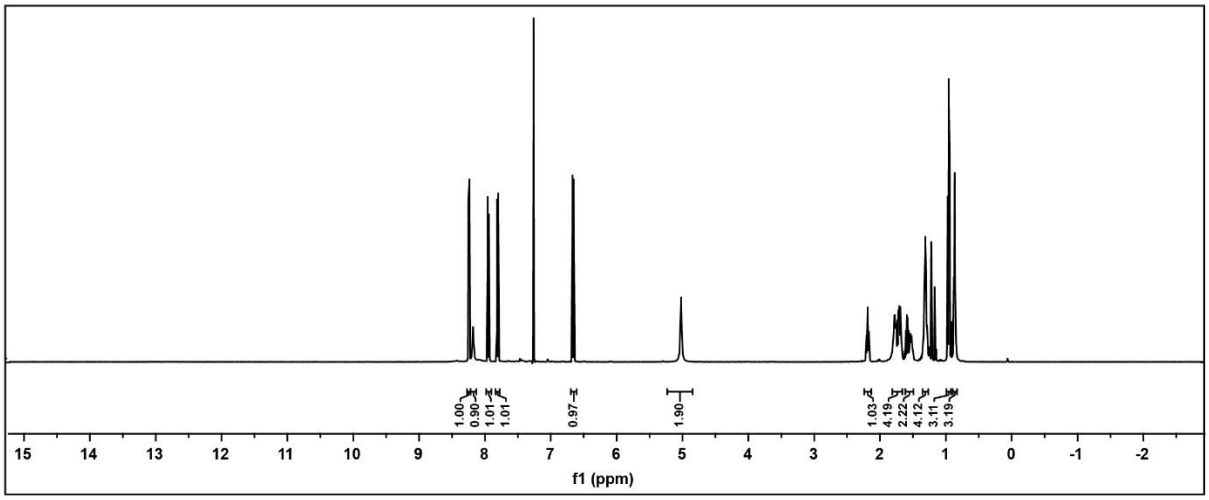

N-((1,8-Naphthyridin-2-yl)-2-ethylhexanamide)non-8-ynamide **79**

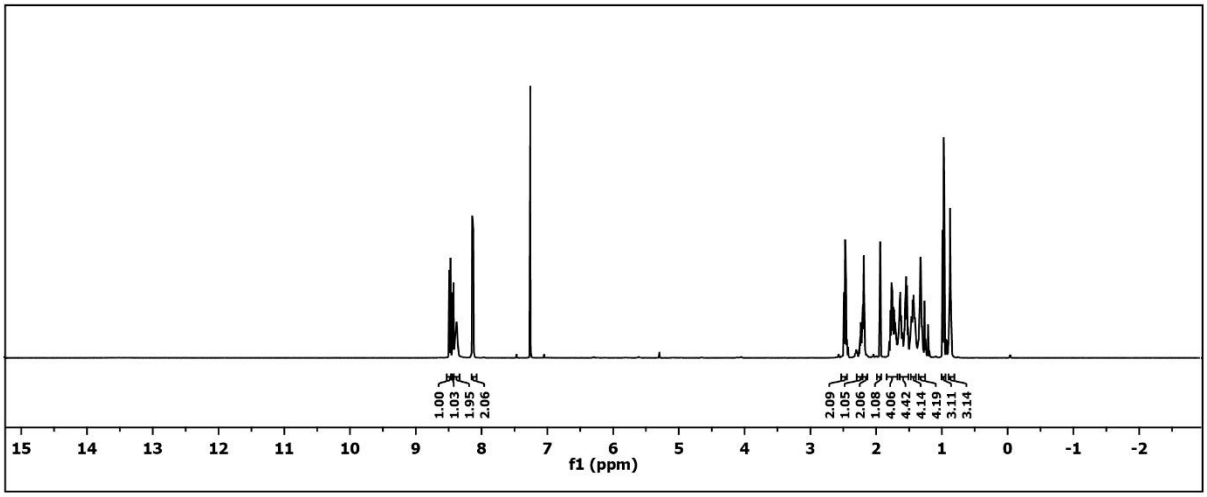

7-(2-Ethyl-hexanoyl)-amino-7-chloro-[1,8]-naphthyridine-2-yl **80**

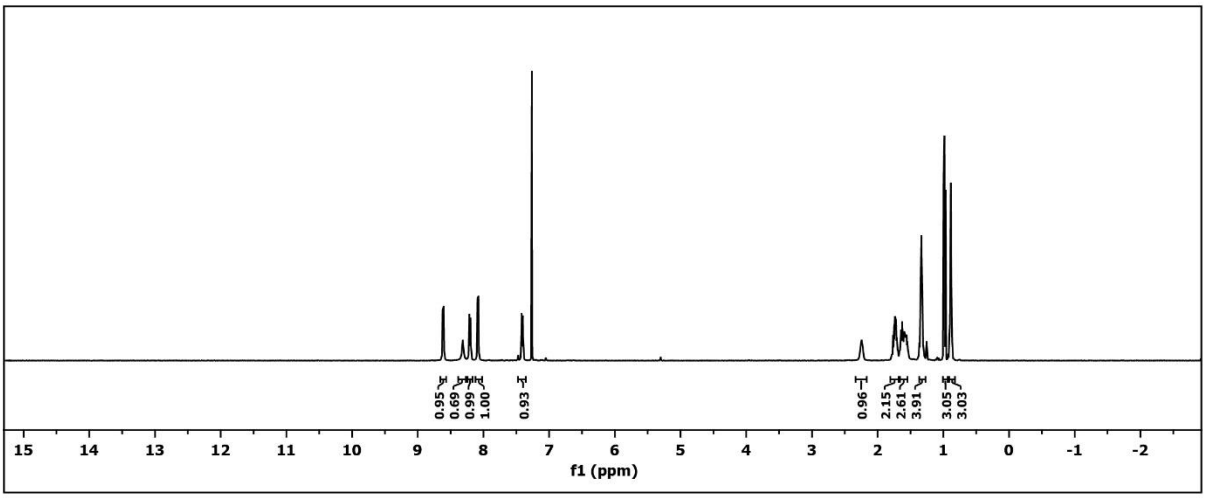

2-(3-(5,6-Dimethyl-1H-benzo[d]imidazol-2-yl)ureido)ethyl methacrylate **82**

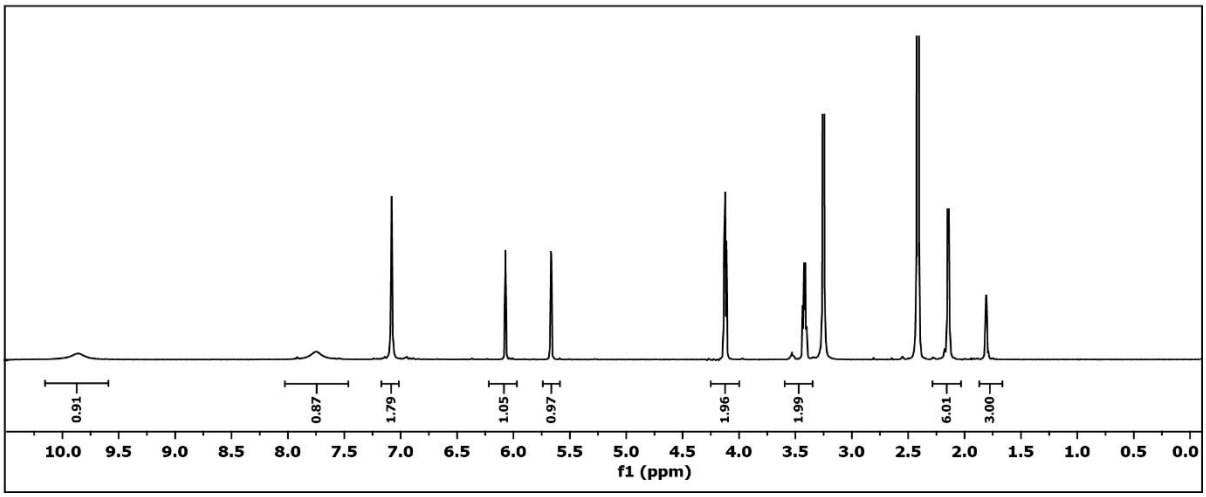

1-(Oct-7-yn-1-yl)-3-(pyridin-2-yl)ureido)ethyl methacrylate **83**

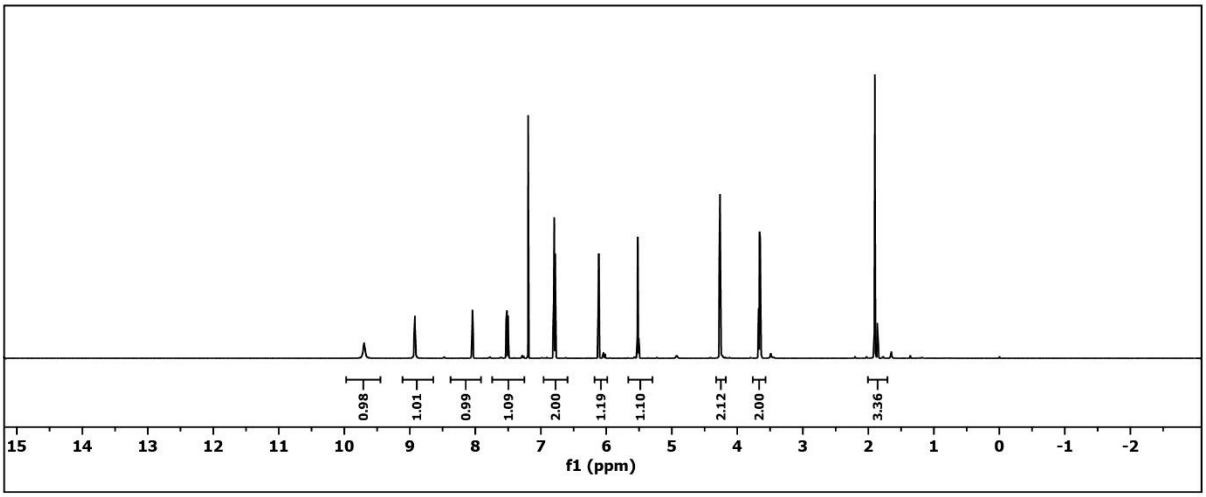

4-(1-Ethylpentyl)-1,6-dihydro-6-oxo-2-pyrimidinyl)ureido)ethyl methacrylate **84**

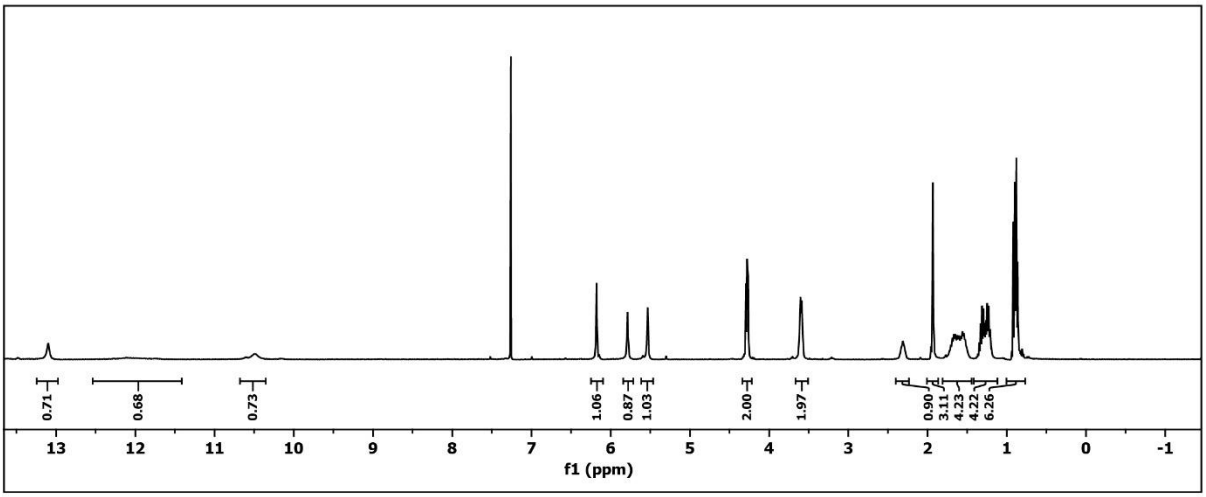

[1-[3-[2-[[(Dodecylthio)thioxomethyl]thio]-2-methyl-1-oxopropoxy]propyl]-1H-1,2,3-triazol-4-yl]-2-*N*-(1,8-naphthyridin-2-yl)oct-7-amide **92**

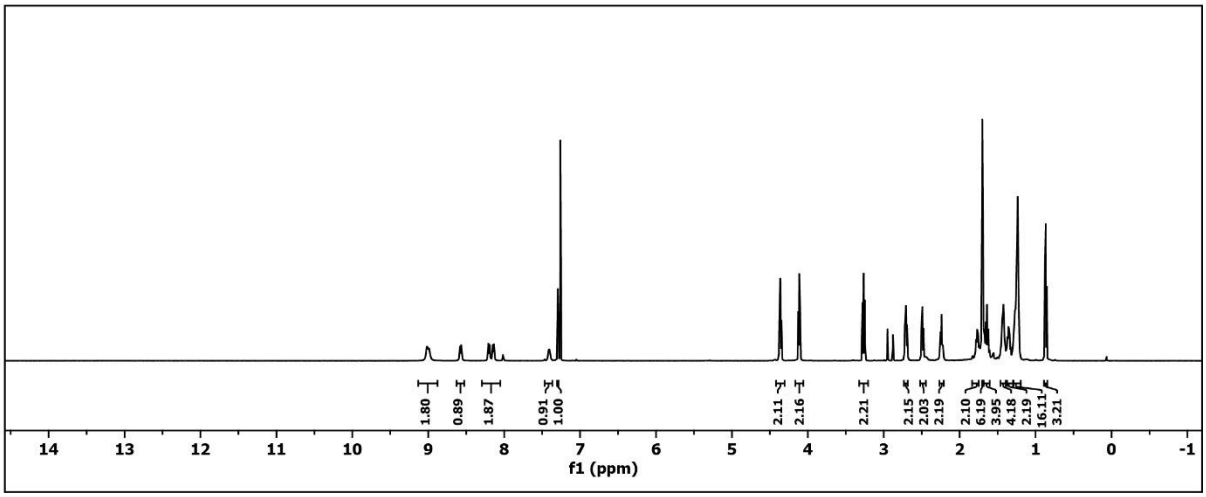

[1-[3-[2-[[(Dodecylthio)thioxomethyl]thio]-2-methyl-1-oxopropoxy]propyl]-1H-1,2,3-triazol-4-yl] -
2-(Oct-1-yl)-N-(4-(1-ethylpentyl)-1,6-dihydro-6-oxo-2-pyrimidinyl))urea **93**

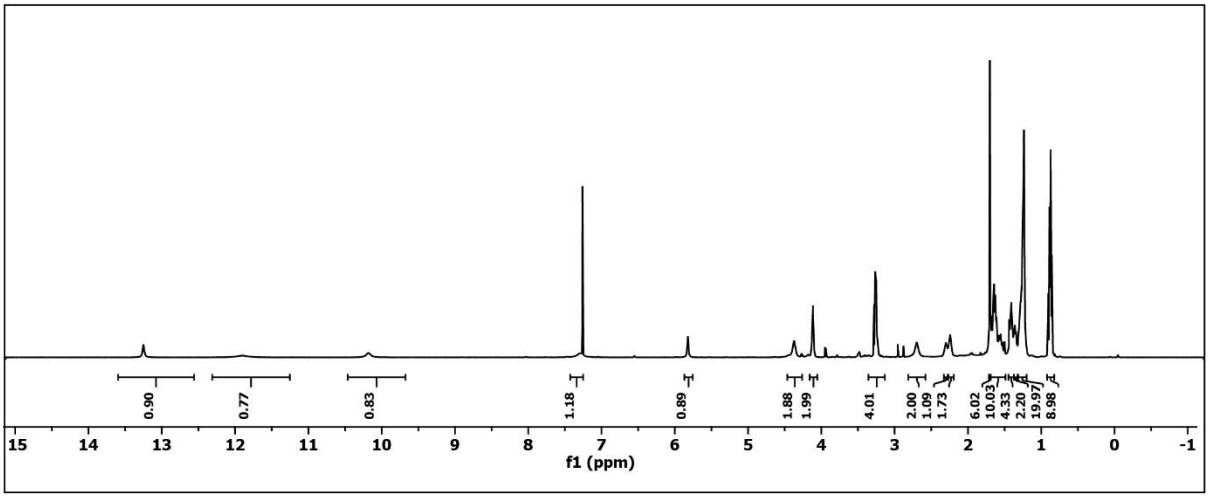

[1-[3-[2-[[(Dodecylthio)thioxomethyl]thio]-2-methyl-1-oxopropoxy]propyl]-1H-1,2,3-triazol-4-yl] -
2-((*N*-((1,8-naphthyridin-2-yl)-2-ethylhexanamide)oct-8-amide **94**

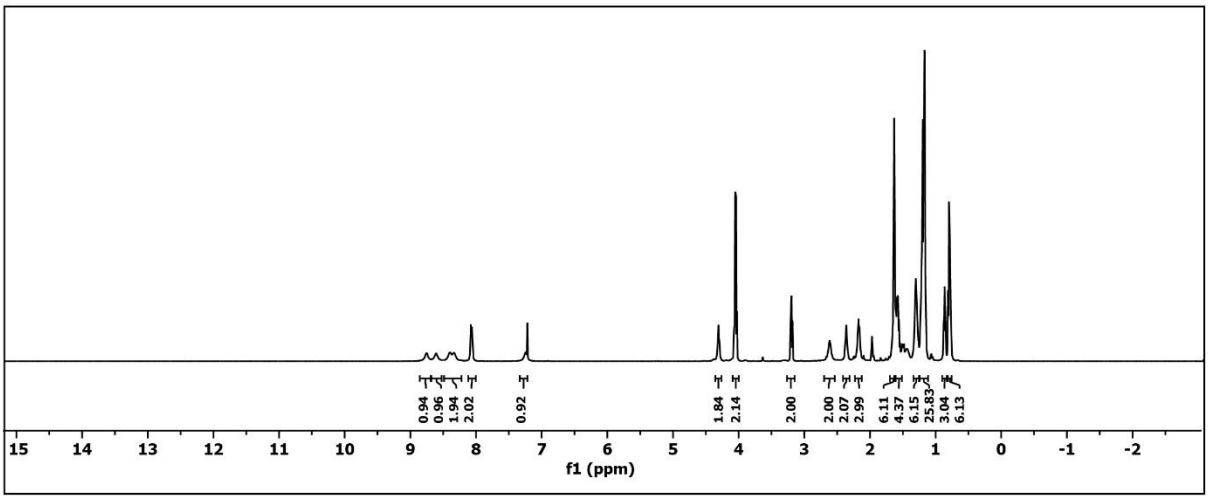

DAN-PMMA **100**

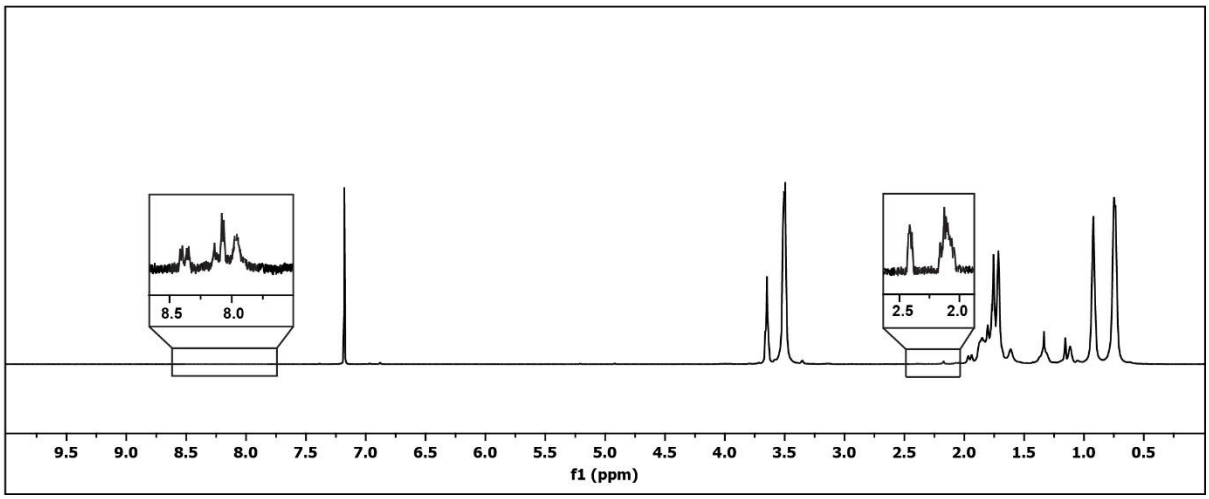

(*E*)-9-(4-((2,6-Difluoro-4-(8-(3-(pyridin-2-yl)ureido)oct-1-yn-1-yl)phenyl)diazenyl)-3,5-difluorophenyl)-N-(1,8- naphthyridin-2-yl)non-8-ynamide **Foldamer I**

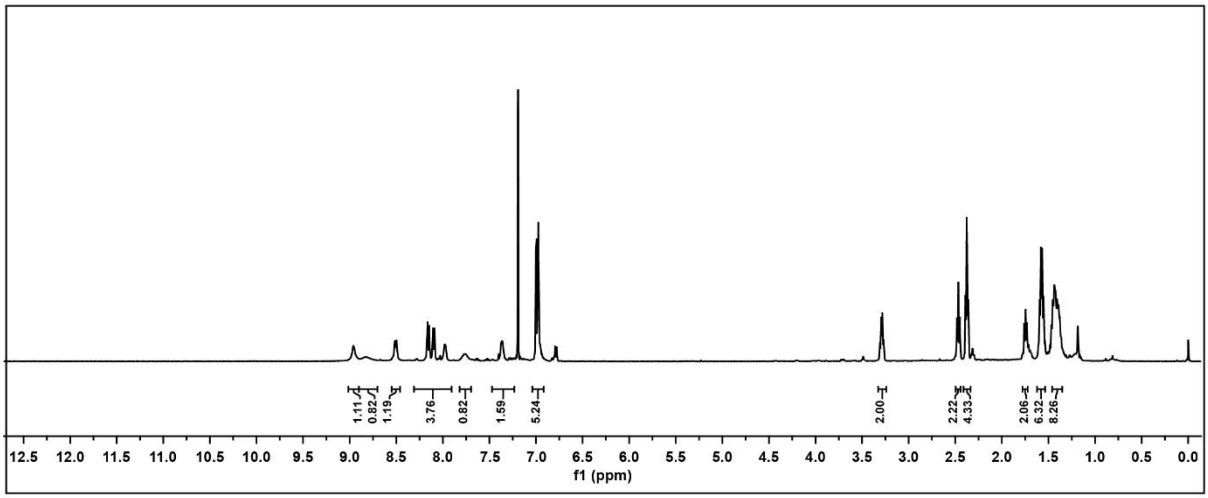

(*Z*)-9-(4-((2,6-Difluoro-4-(8-(3-(pyridin-2-yl)ureido)oct-1-yn-1-yl)phenyl)diazenyl)-3,5-difluorophenyl)-N-(1,8- naphthyridin-2-yl)non-8-ynamide **Foldamer I**

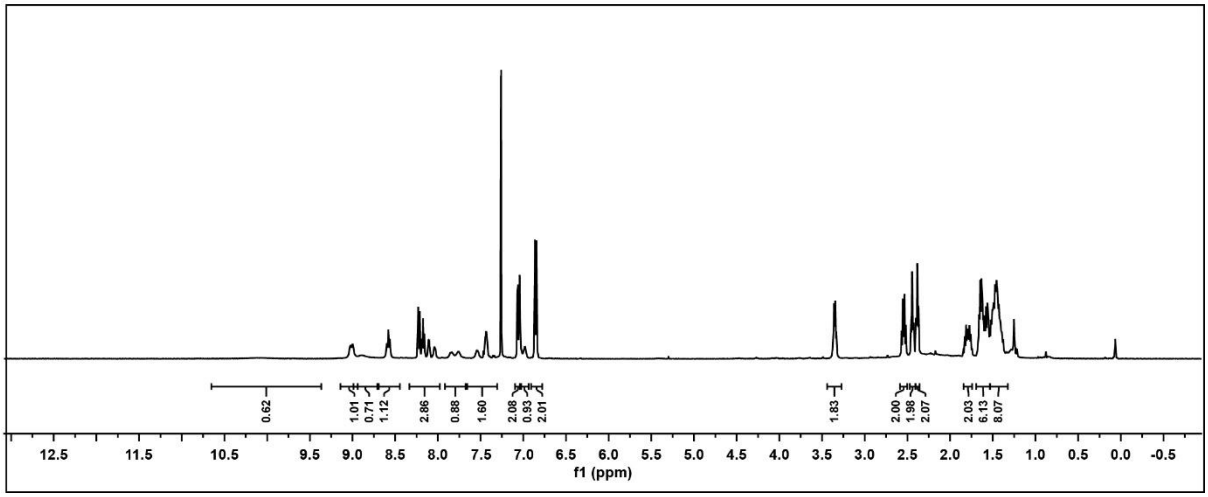

(*E*)-1,2-Bis(2,6-difluoro-4-1-(oct-7-yn-1-yl)-N-(4-(1-ethylpentyl)-1,6-dihydro-6-oxo-2-pyrimidinyl))urea)diazene **Foldamer III**

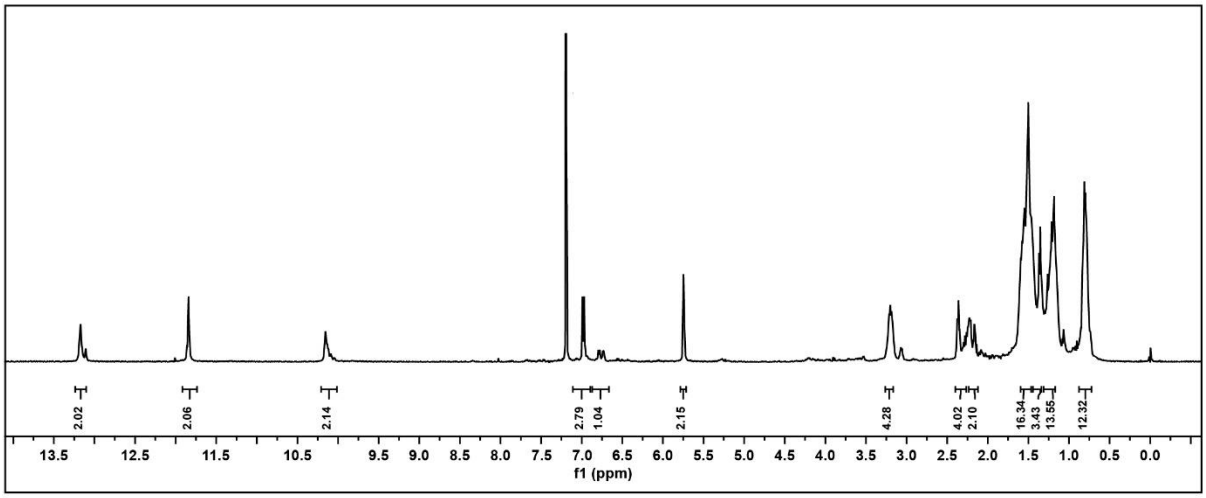

(*Z*)-1,2-Bis(2,6-difluoro-4-1-(oct-7-yn-1-yl)-N-(4-(1-ethylpentyl)-1,6-dihydro-6-oxo-2-pyrimidinyl))urea)diazene **Foldamer III**

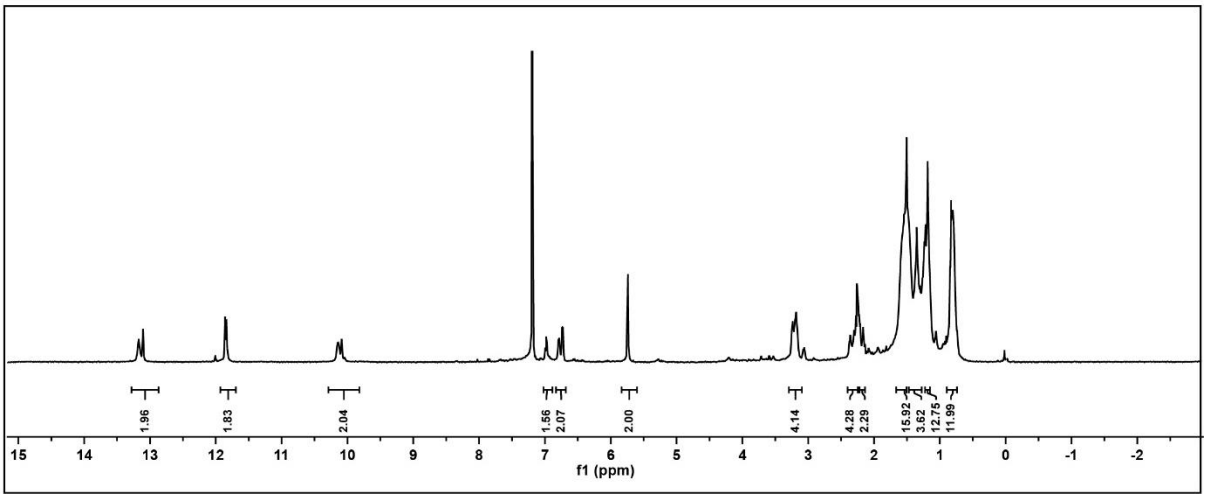

(*E*)- 9- (4- ((2,6-Difluoro - 4 - (oct-7-yn-1-yl) -N- (4-(1-ethylpentyl) - 1,6 - dihydro-6-oxo -2-pyrimidinyl)) urea) phenyl) diazenyl) - 3,5 - difluorophenyl) -N- ((1,8-naphthyridin-2-yl)-2-ethylhexanamide)non-8-ynamide **Foldamer IV**

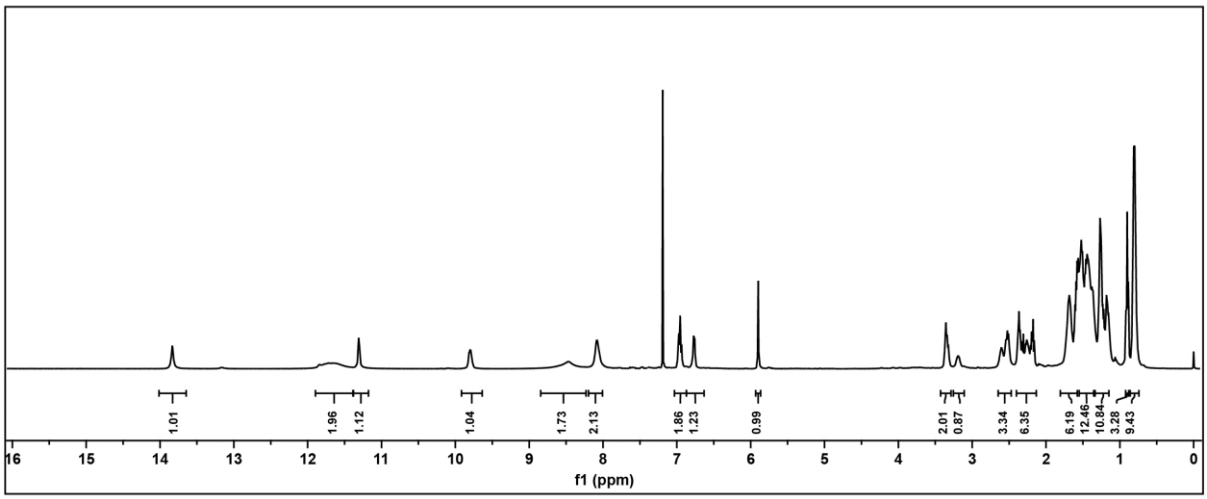

(*Z*)- 9- (4- ((2,6-Difluoro - 4 - (oct-7-yn-1-yl) -N- (4-(1-ethylpentyl) - 1,6 - dihydro-6-oxo -2-pyrimidinyl)) urea) phenyl) diazenyl) - 3,5 - difluorophenyl) -N- ((1,8-naphthyridin-2-yl)-2-ethylhexanamide)non-8-ynamide **Foldamer IV**

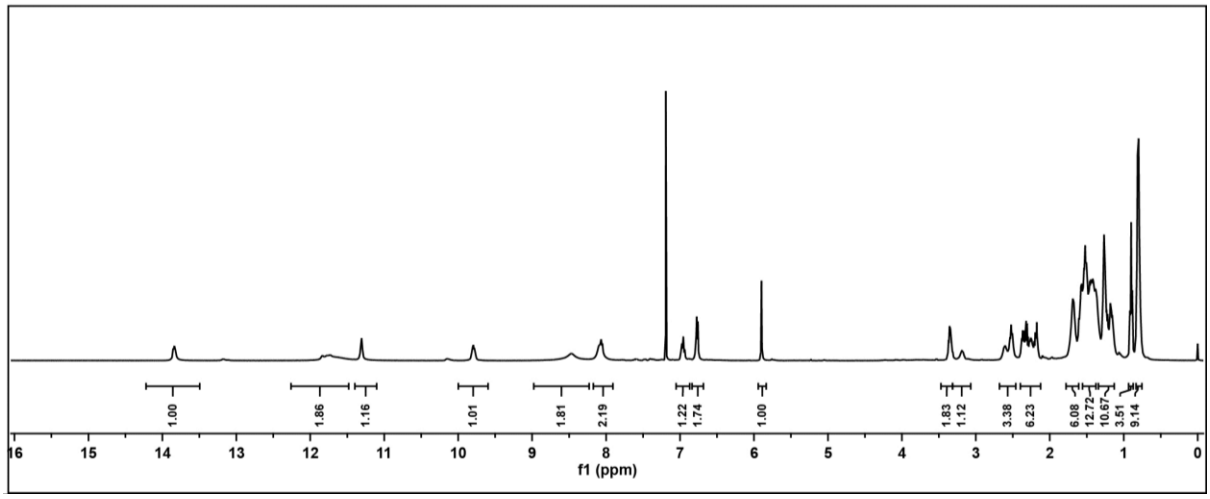

^{13}C NMR Spectra

1-(4-Bromo-2,6-difluorophenyl)-2-(2,6-difluoro-4-iodophenyl)diazene **52**

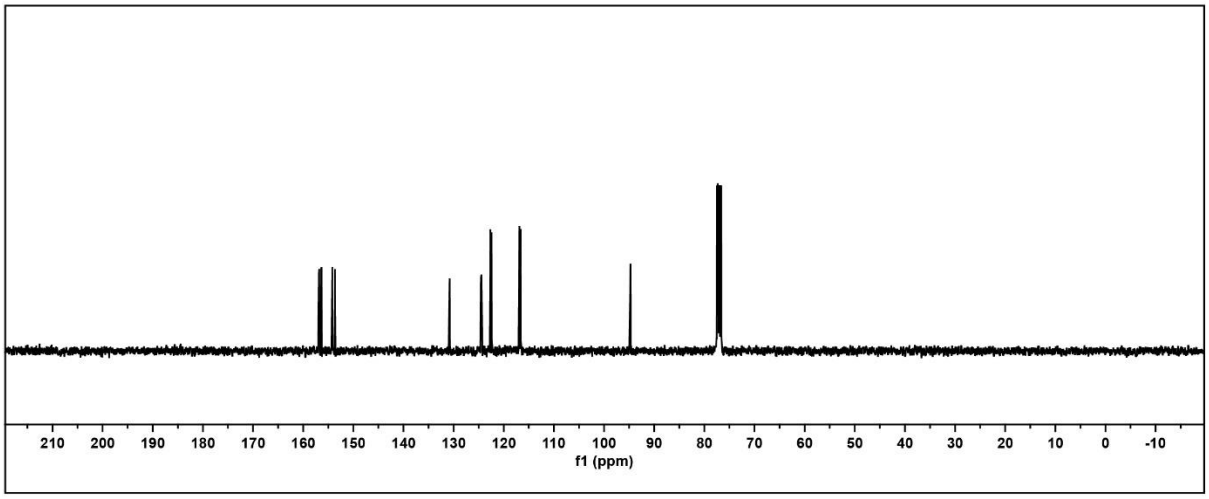

8-Noynoic acid **54**

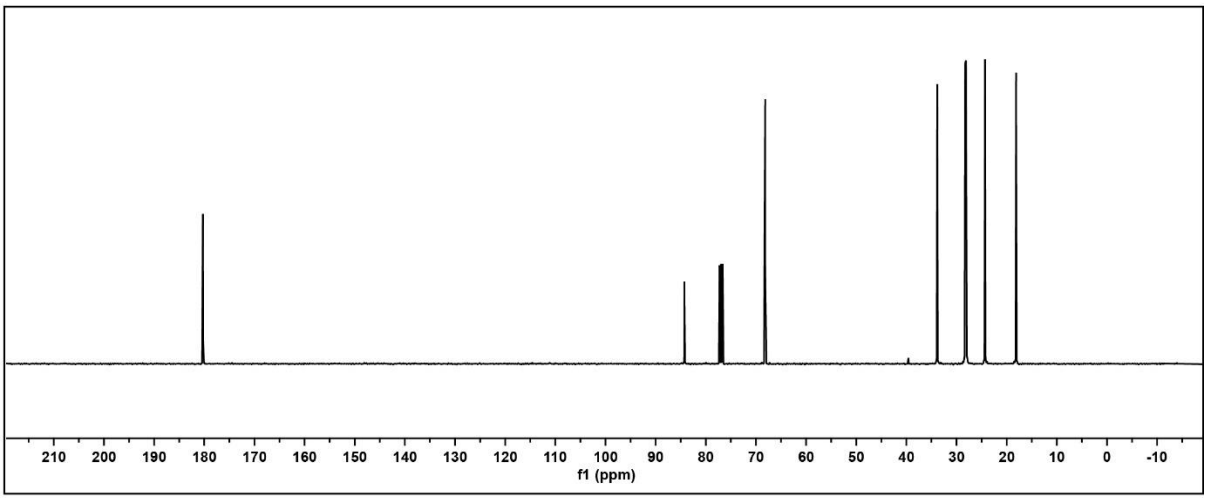

1-(Oct-7-yn-1-yl)-3-(pyridin-2-yl)urea **56**

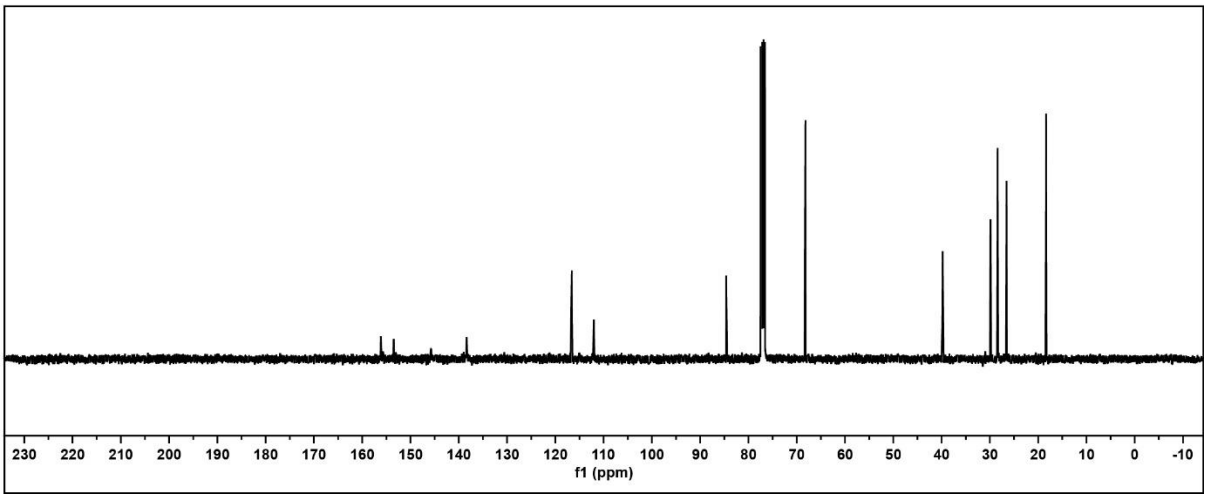

1,8-Naphthyridin-2-amine **59**

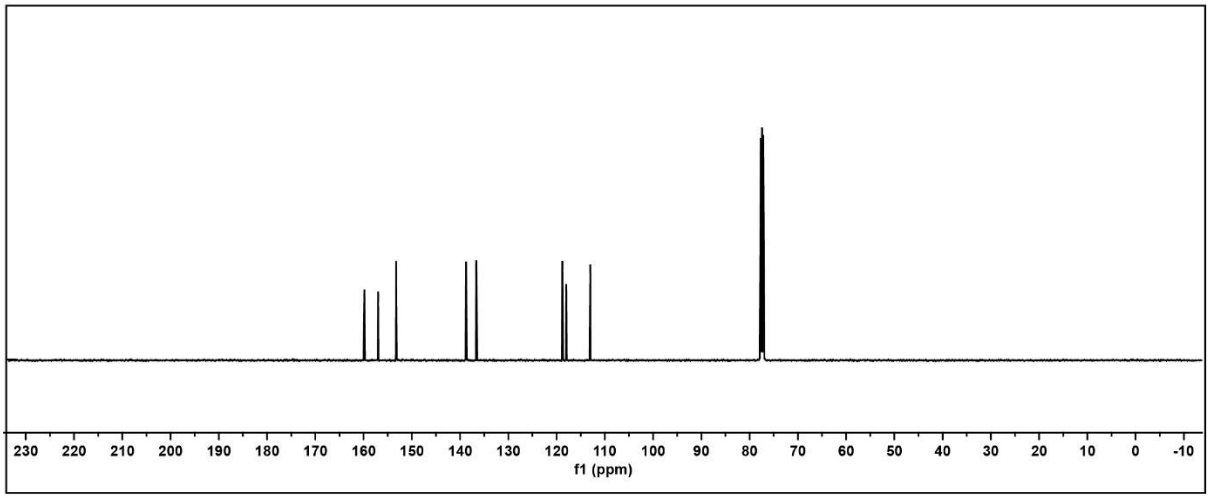

N-(1,8-Naphthyridin-2-yl)non-8-ynamide **60**

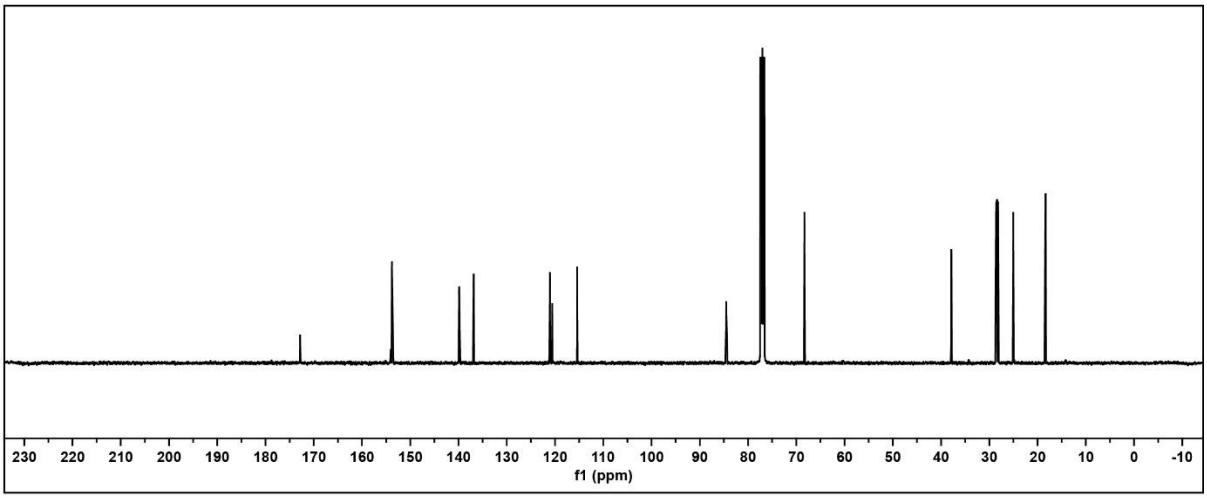

(*E*)-1- (8- (4-((4-Bromo -2,6- difluorophenyl)diazenyl)-3,5-difluorophenyl)oct7-yn-1-yl)-3-(pyridin-2-yl)urea **61**

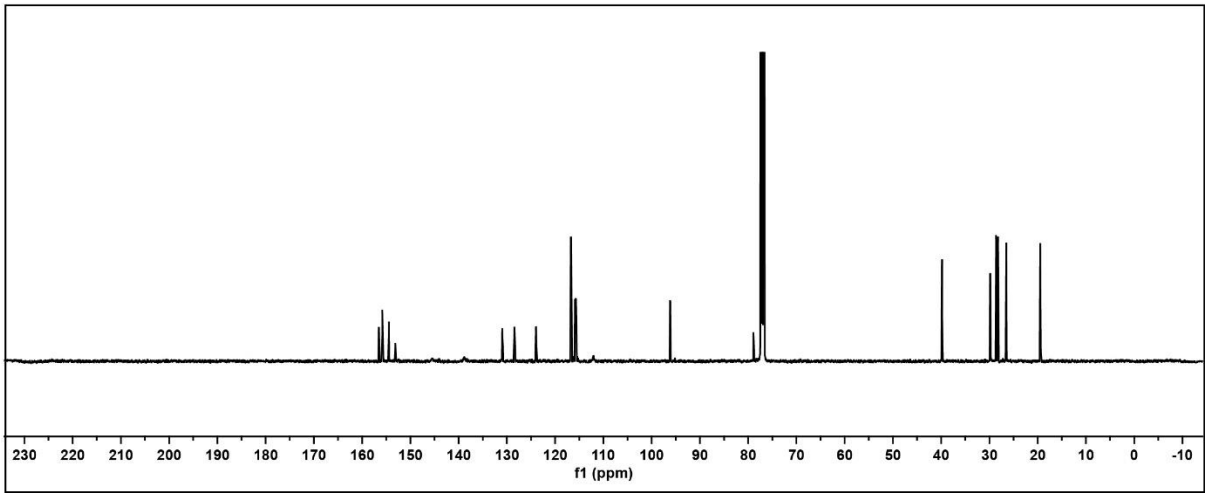

N-(6-methyl-4-oxo-1,4-dihydropyrimidin-2-yl)non-8-ynamide **63**

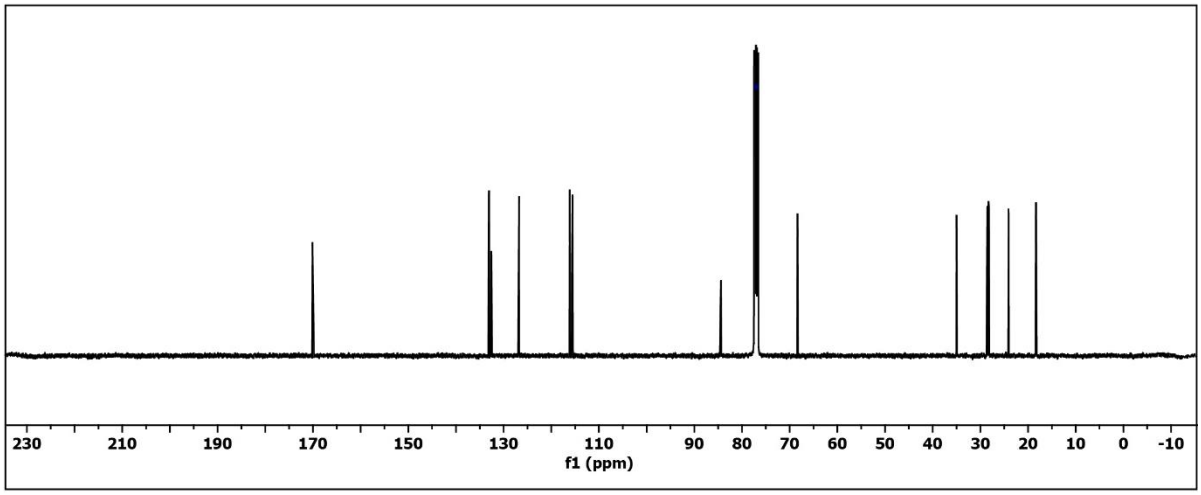

1-(8-(4-((4-Bromo-2,6-difluorophenyl)diazenyl)-3,5-difluorophenyl)-N-(6-methyl-4-oxo-1,4-dihydropyrimidin-2-yl))non-8-ynamide **67**

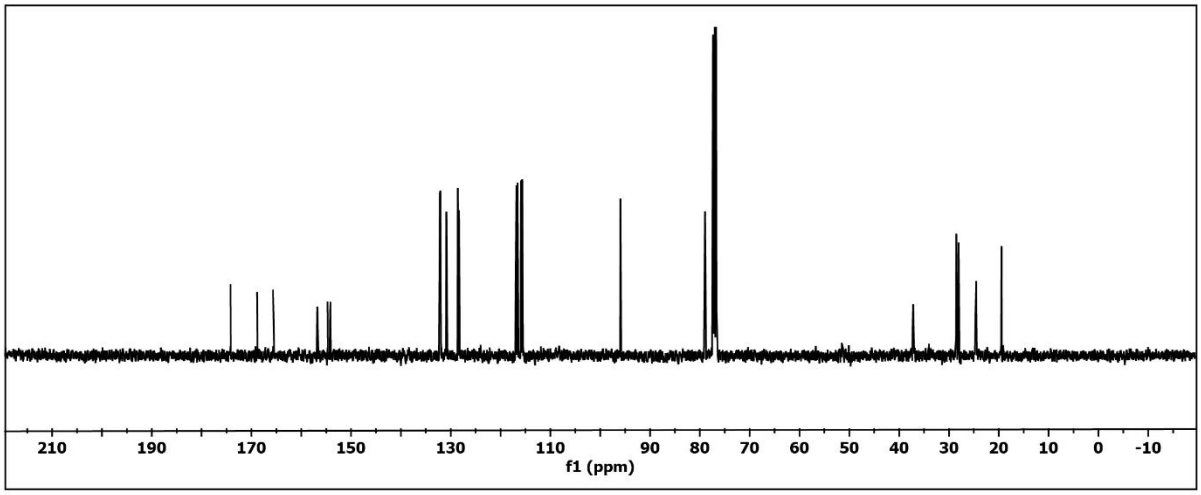

1-(Oct-7-yn-1-yl)-N-(4-(1-ethylpentyl)-1,6-dihydro-6-oxo-2-pyrimidinyl))urea **69**

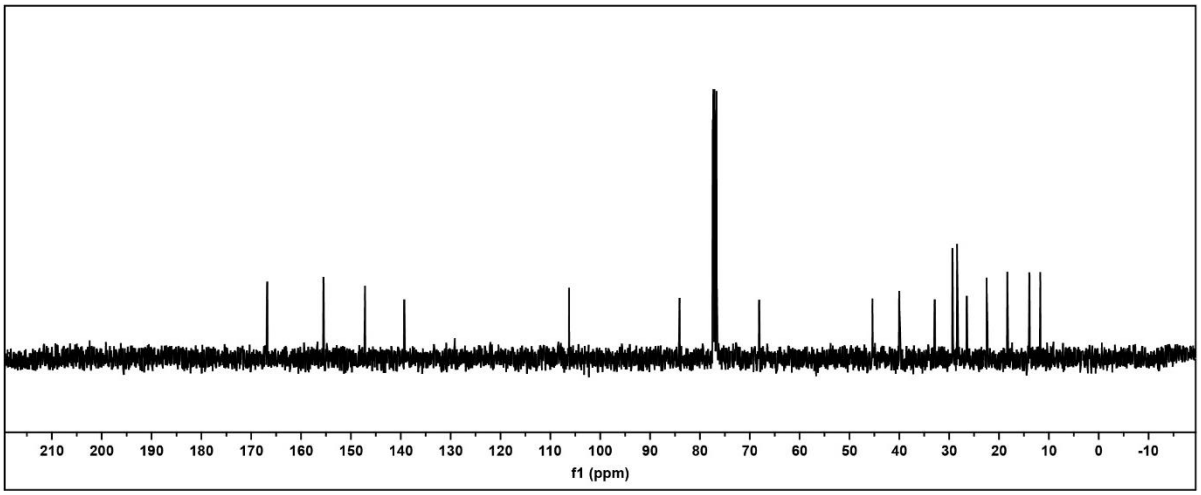

1,2-Bis(2,6-difluoro-4-iodophenyl)diazene **70**

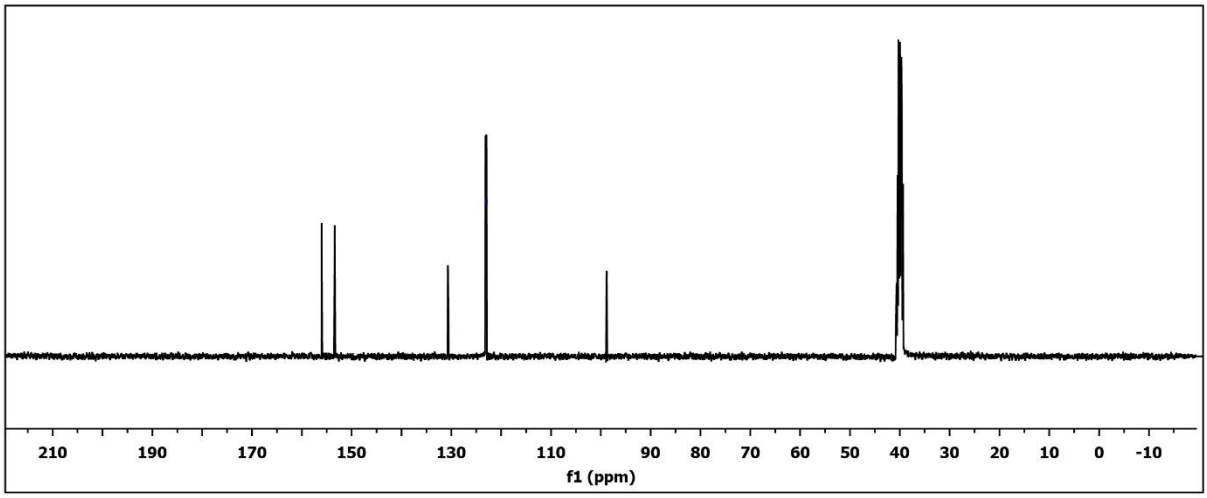

1-(8-(4-((4-Bromo -2,6- difluorophenyl) diazenyl)- 3,5-difluorophenyl) oct-7-yn-1-yl)-N-(4-(1-ethylpentyl)-1,6-dihydro-6-oxo-2-pyrimidinyl))urea) **71**

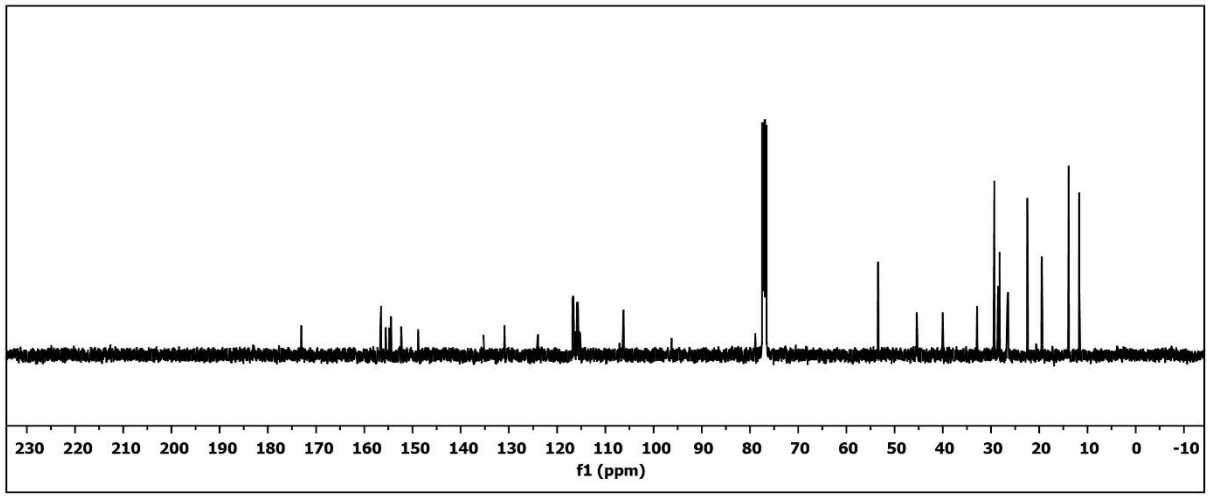

(*E*)-1,2-Bis(2,6-difluoro-4-1-(oct-7-yn-1-yl)-acid)diazene **72**

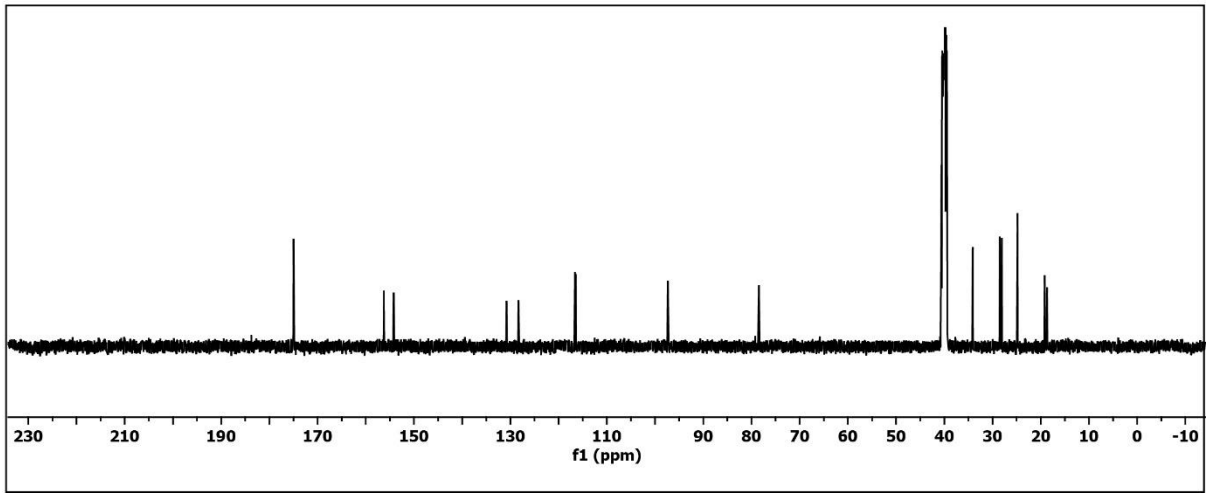

4-((2,6-Difluoroanaline)oct-7-yn-1-yl)-*N*-(4-(1-ethylpentyl)-1,6-dihydro-6-oxo-2-pyrimidinyl))urea **73**

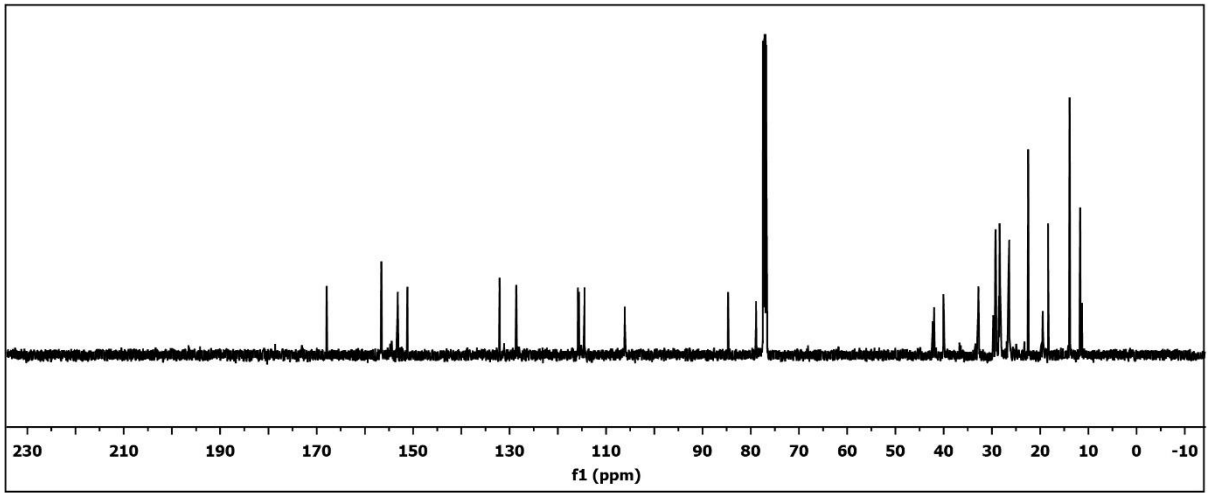

7-Hydroxy-1,8-naphthyridin-2-amine **75**

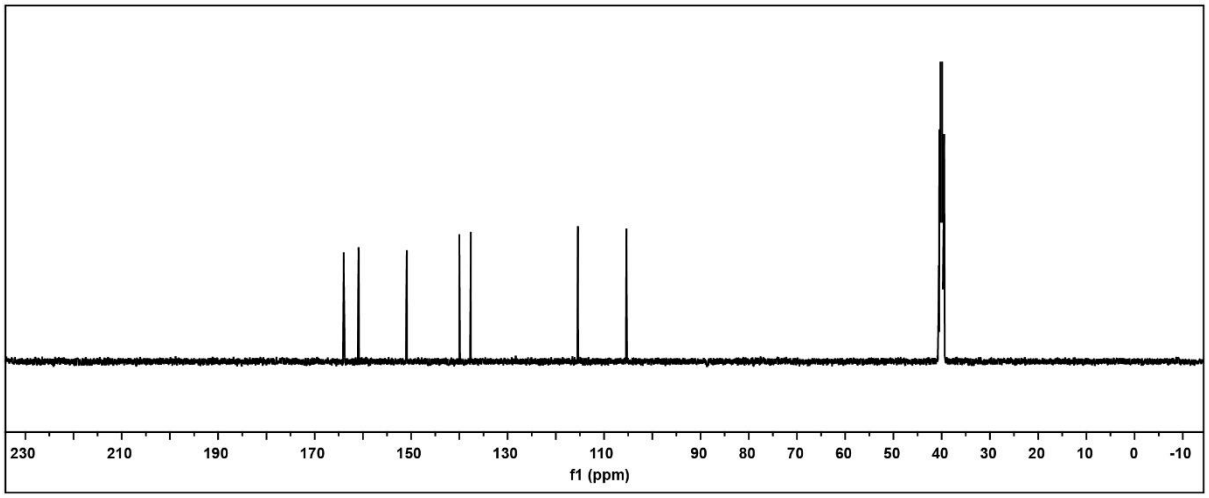

7-(2-Ethyl-hexanoyl)-amino-8H-(7-oxo-[1,8]-naphthyridine-2-yl) **76**

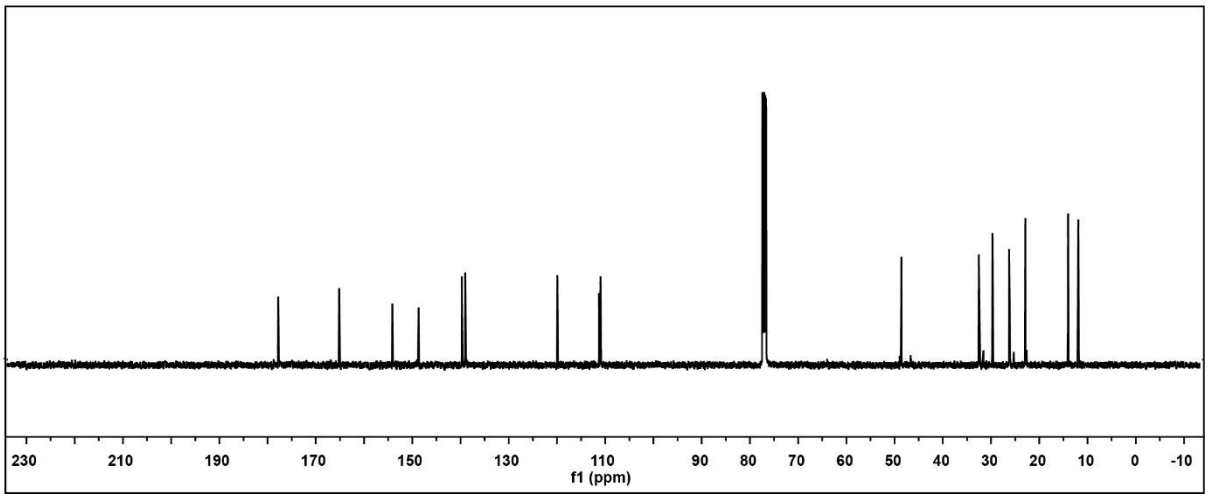

N-(7-Bromo-1,8-naphthyridin-2-yl)-2-ethylhexanamide **77**

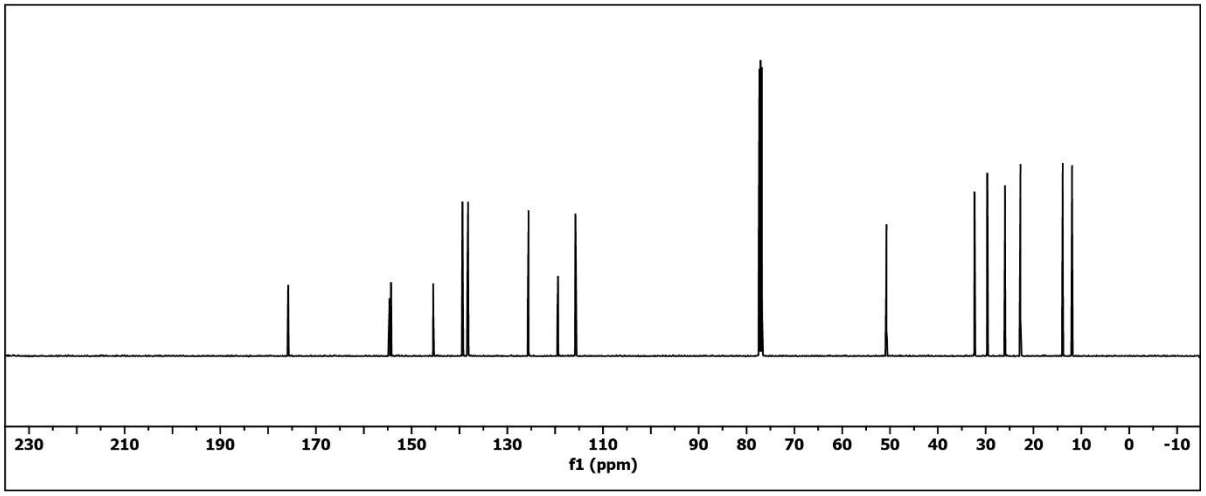

N-(7-Amino-1,8-naphthyridin-2-yl)-2-ethylhexanamide **78**

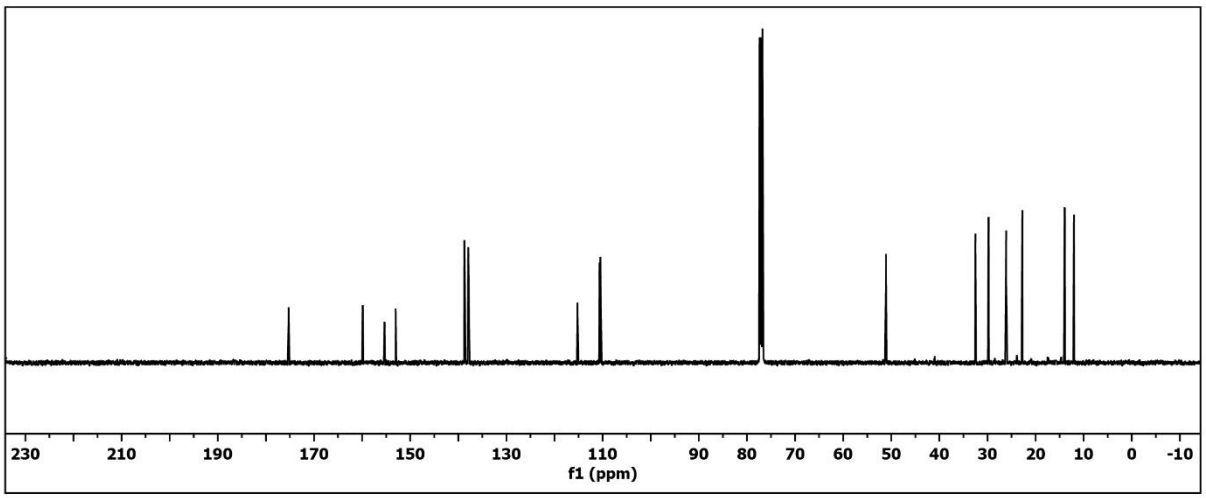

N-((1,8-Naphthyridin-2-yl)-2-ethylhexanamide)non-8-ynamide **79**

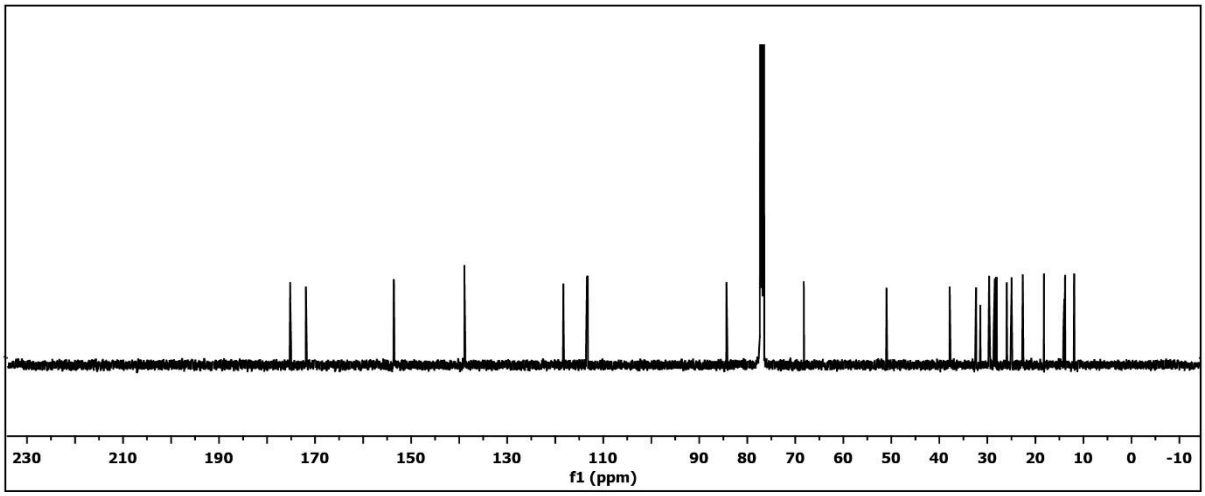

7-(2-Ethyl-hexanoyl)-amino-7-chloro-[1,8]-naphthyridine-2-yl **80**

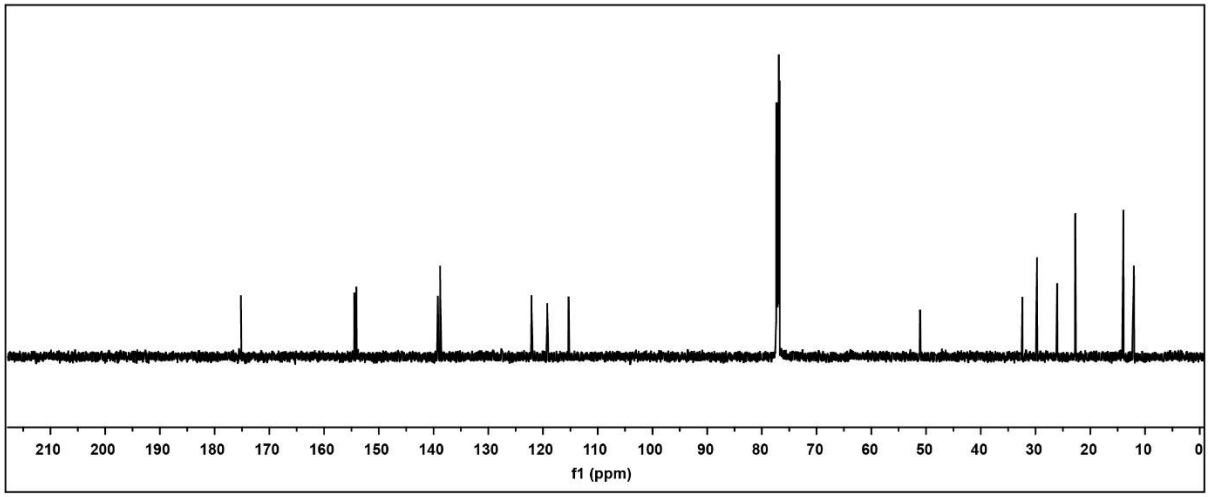

2-(3-(5,6-Dimethyl-1H-benzo[d]imidazol-2-yl)ureido)ethyl methacrylate **82**

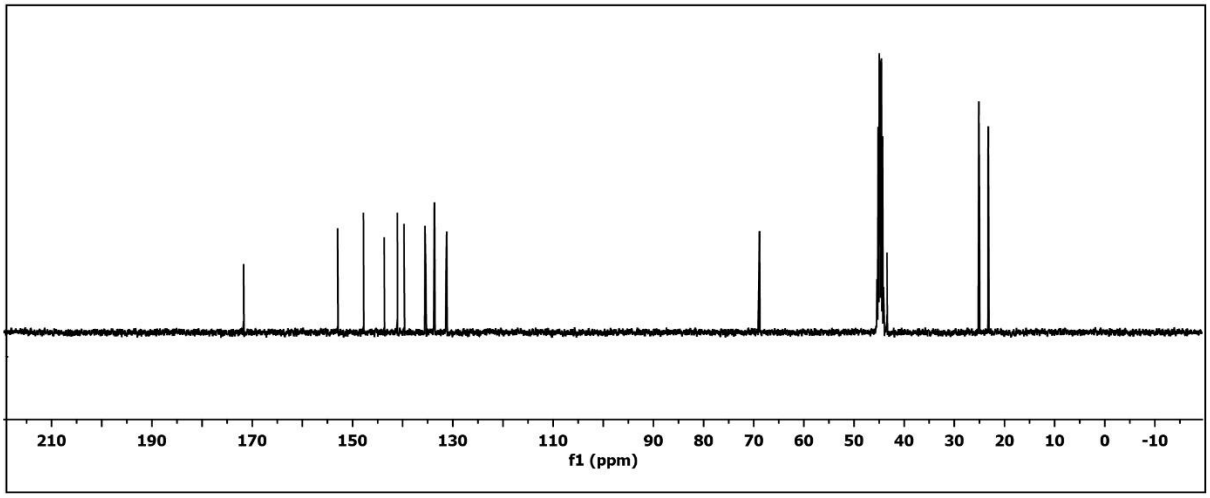

1-(Oct-7-yn-1-yl)-3-(pyridin-2-yl)ureido)ethyl methacrylate **83**

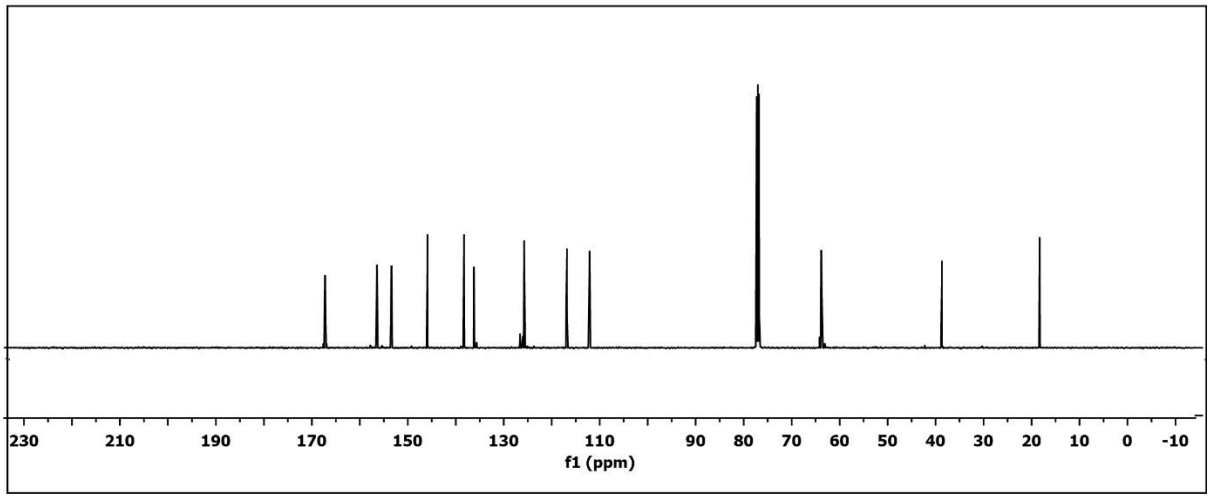

4-(1-Ethylpentyl)-1,6-dihydro-6-oxo-2-pyrimidinyl)ureido)ethyl methacrylate **84**

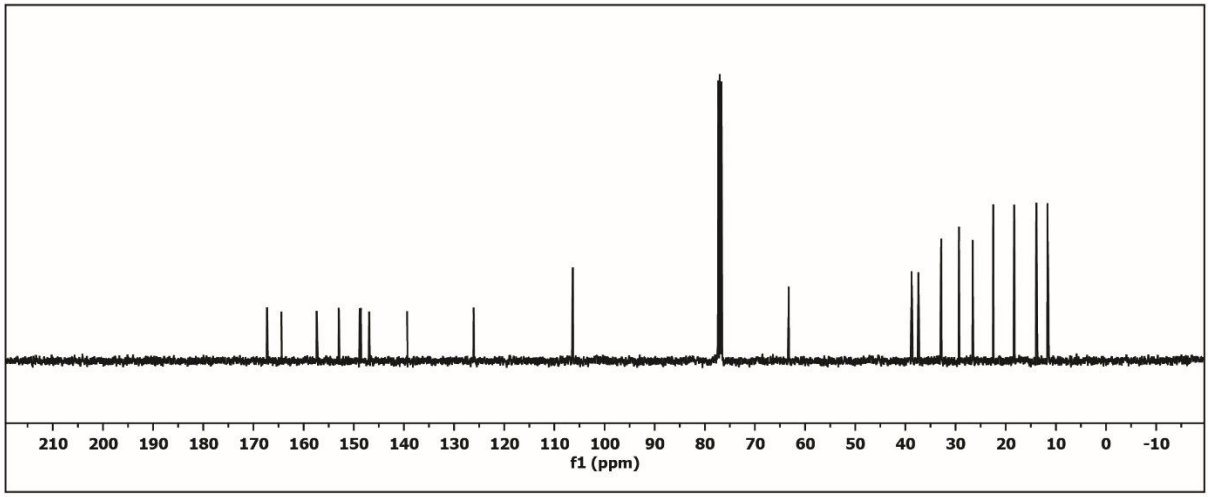

[1-[3-[2-[[(Dodecylthio)thioxomethyl]thio]-2-methyl-1-oxopropoxy]propyl]-1H-1,2,3-triazol-4-yl]-2- N-(1,8-naphthyridin-2-yl)oct-7-amide **92**

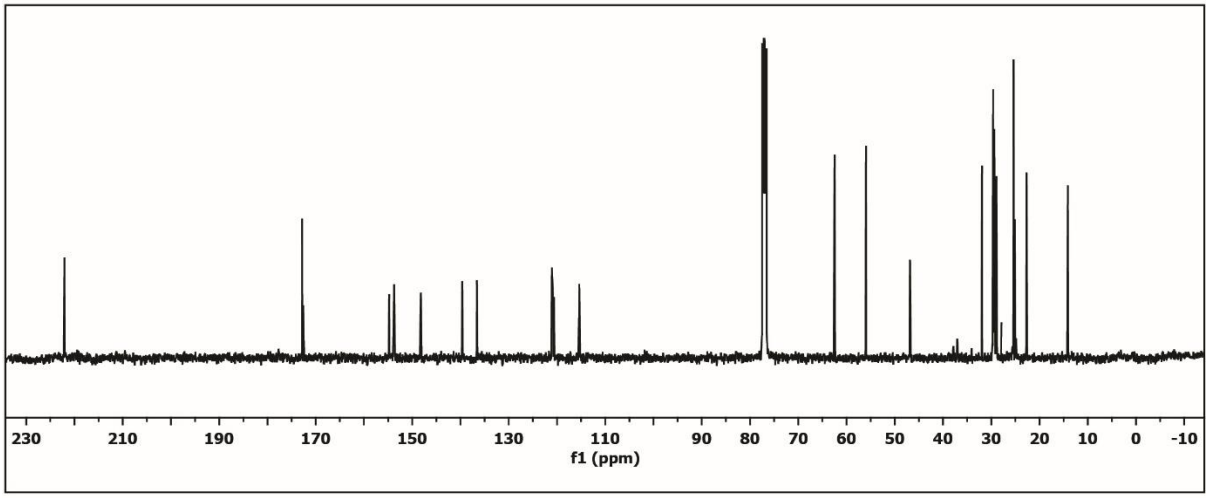

[1-[3-[2-[[(Dodecylthio)thioxomethyl]thio]-2-methyl-1-oxopropoxy]propyl]-1H-1,2,3-triazol-4-yl]-
2-(oct-1-yl)-*N*-(4-(1-ethylpentyl)-1,6-dihydro-6-oxo-2-pyrimidinyl))urea **93**

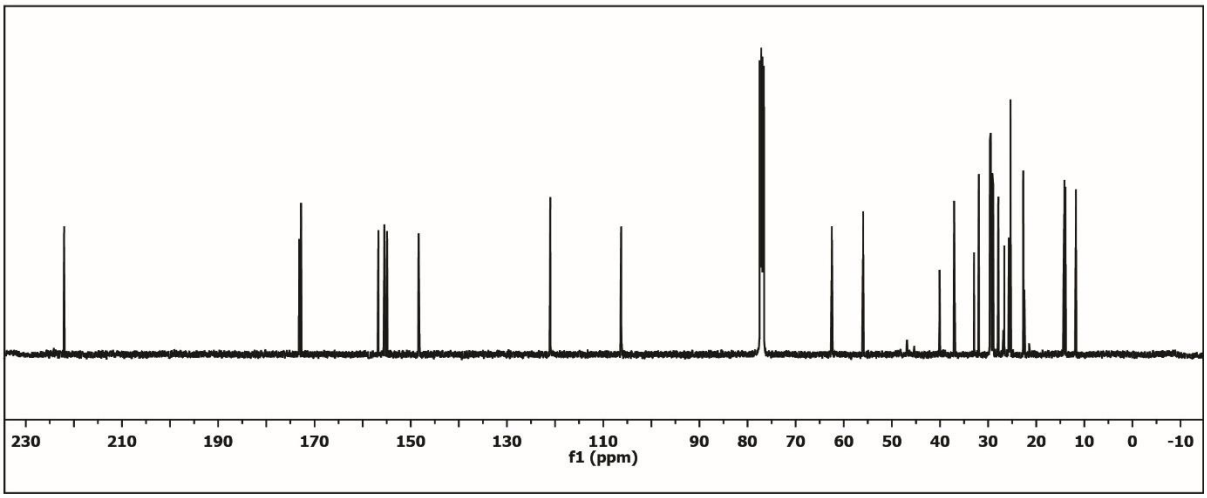

[1-[3-[2-[[(Dodecylthio)thioxomethyl]thio]-2-methyl-1-oxopropoxy]propyl]-1H-1,2,3-triazol-4-yl]-
2-((*N*-((1,8-naphthyridin-2-yl)-2-ethylhexanamide)oct-8-amide **94**

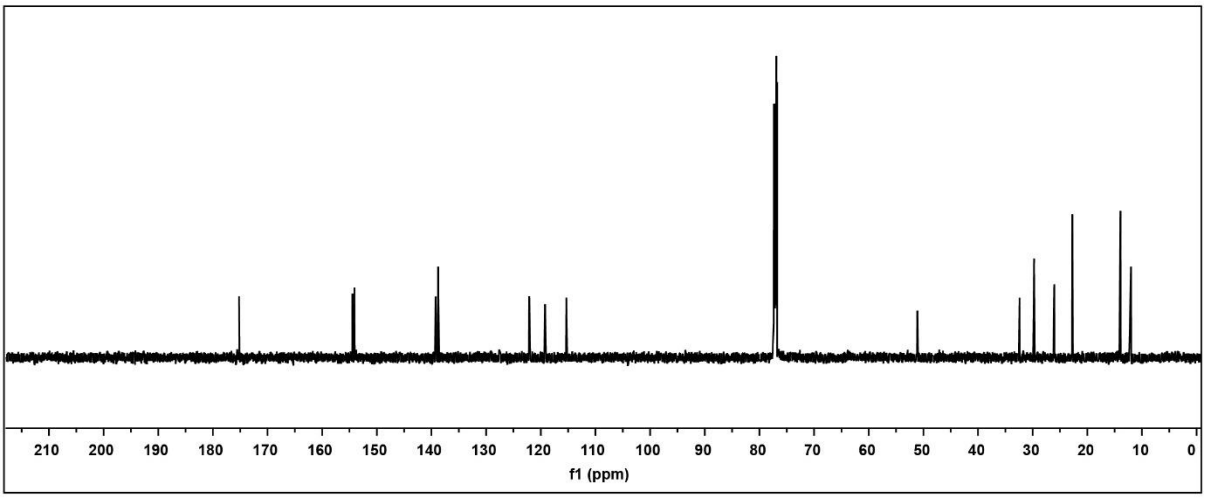

9-(4-((2,6-Difluoro-4-(8-(3-(pyridin-2-yl)ureido)oct-1-yn-1-yl)phenyl)diazenyl)-3,5-difluorophenyl)-N-
(1,8- naphthyridin-2-yl)non-8-ynamide **Foldamer I**

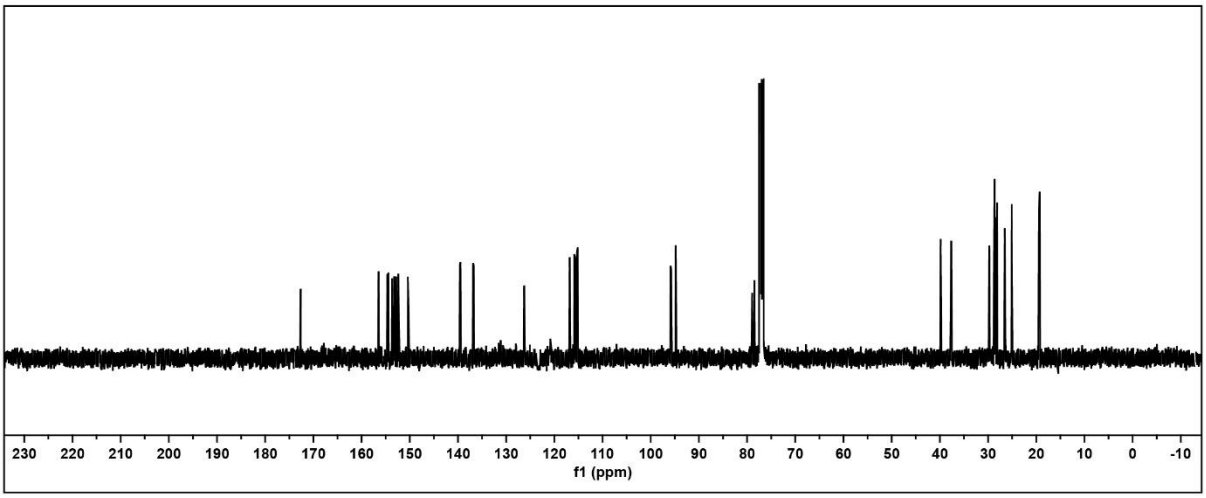

1,2-Bis(2,6-difluoro-4-1-(Oct-7-yn-1-yl)-N-(4-(1-ethylpentyl)-1,6-dihydro-6-oxo-2-pyrimidinyl))urea)diazene **Foldamer III**

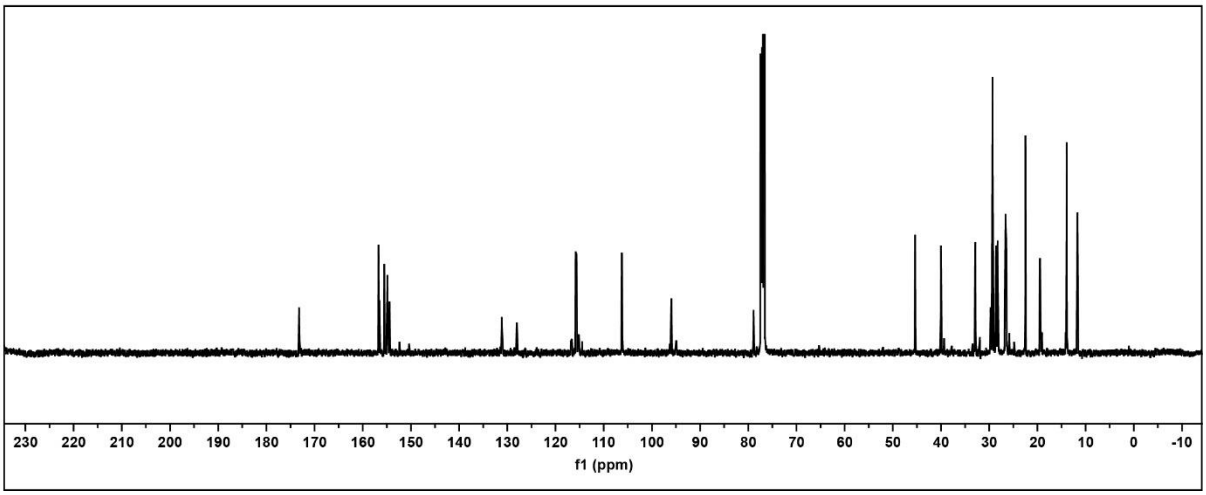

9- (4- ((2,6-Difluoro - 4 - (oct-7-yn-1-yl) -N- (4-(1-ethylpentyl) - 1,6 - dihydro-6-oxo -2-pyrimidinyl)) urea) phenyl) diazenyl) - 3,5 - difluorophenyl) -N- ((1,8-naphthyridin-2-yl)-2-ethylhexanamide)non-8-ynamide **Foldamer IV**

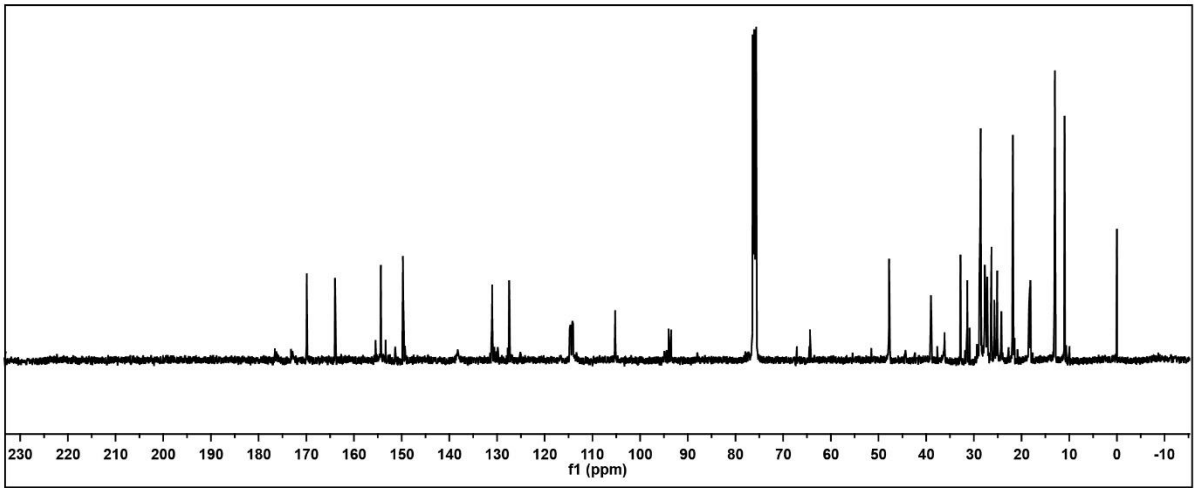

^{19}F NMR Spectra

1-(4-Bromo-2,6-difluorophenyl)-2-(2,6-difluoro-4-iodophenyl)diazene **52**

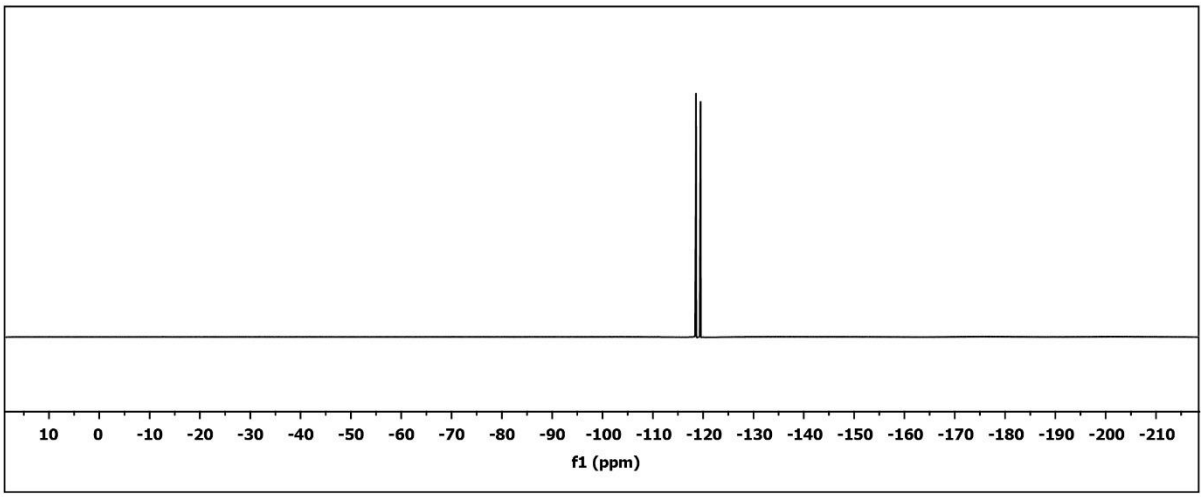

(*E*)-1- (8- (4-((4-Bromo -2,6- difluorophenyl)diazenyl)-3,5-difluorophenyl)oct-7-yn-1-yl)-3-(pyridin-2-yl)urea **61**

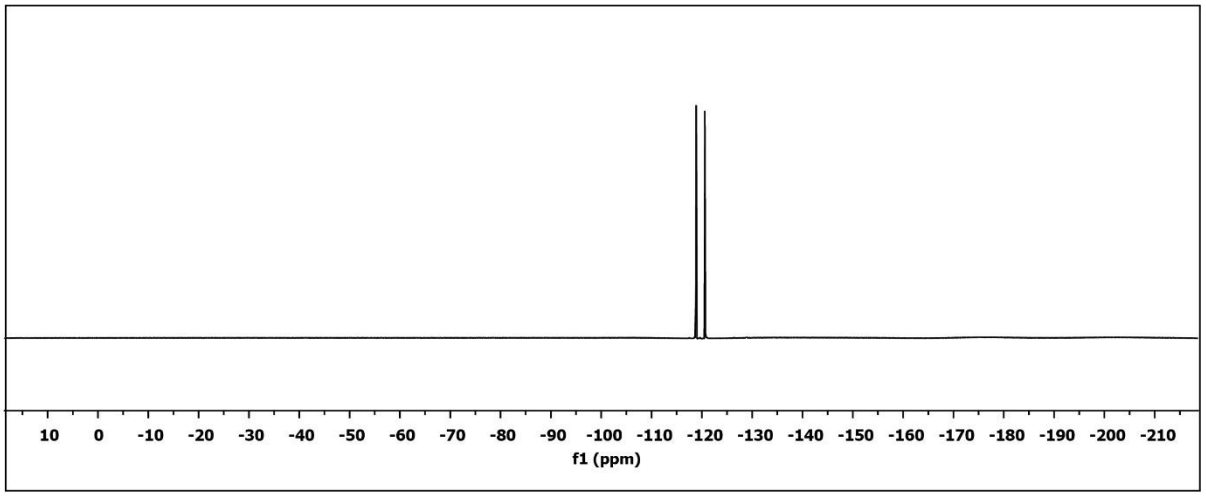

1-(8-(4-((4-Bromo-2,6-difluorophenyl)diazenyl)-3,5-difluorophenyl)-*N*-(6-methyl-4-oxo-1,4-dihydropyrimidin-2-yl))non-8-ynamide **67**

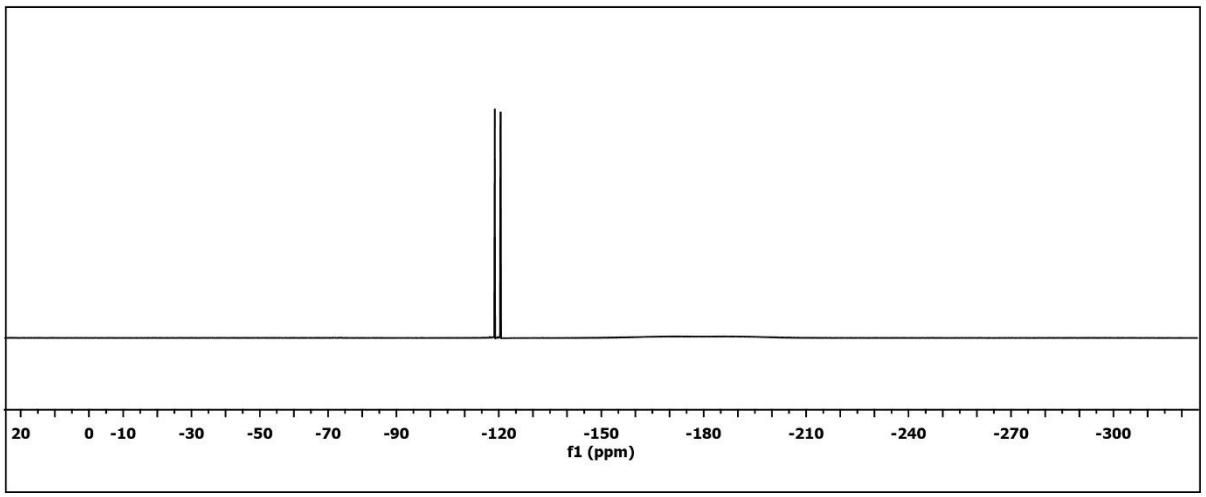

1,2-Bis(2,6-difluoro-4-iodophenyl)diazene **70**

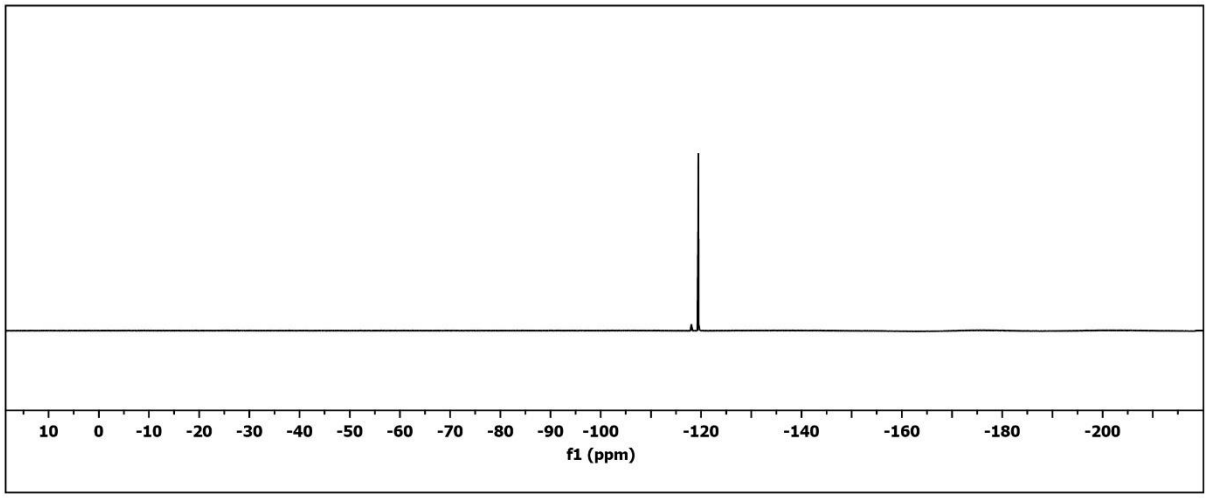

1-(8-(4-((4-Bromo -2,6- difluorophenyl) diazenyl)- 3,5-difluorophenyl) oct-7-yn-1-yl)-N-(4-(1-ethylpentyl)-1,6-dihydro-6-oxo-2-pyrimidinyl))urea) **71**

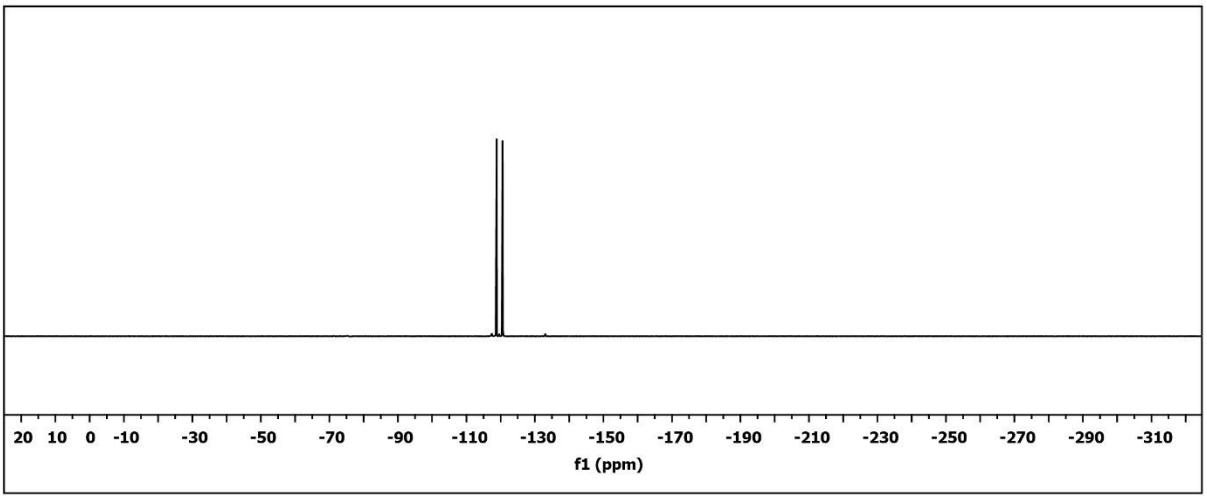

(*E*)-1,2-Bis(2,6-difluoro-4-1-(oct-7-yn-1-yl)-acid)diazene **72**

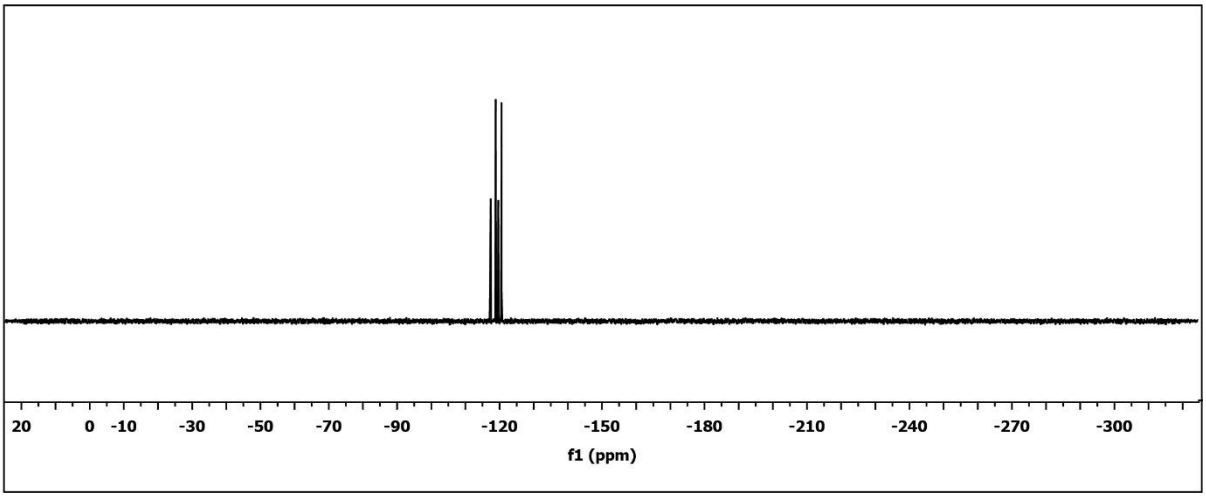

4-((2,6-Difluoroanaline)oct-7-yn-1-yl)-*N*-(4-(1-ethylpentyl)-1,6-dihydro-6-oxo-2-pyrimidinyl))urea) **73**

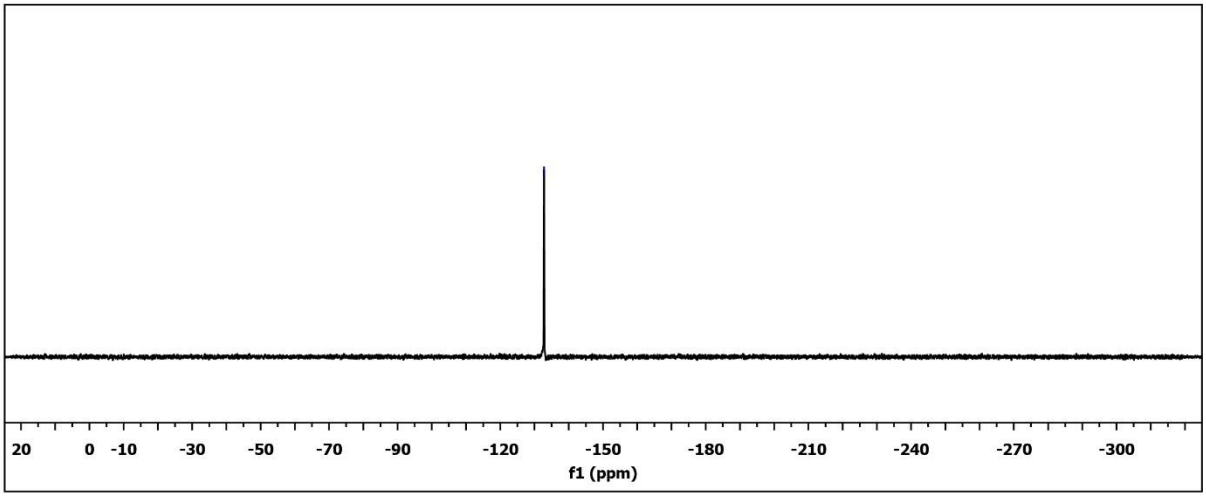

9-(4-((2,6-Difluoro-4-(8-(3-(pyridin-2-yl)ureido)oct-1-yn-1-yl)phenyl)diazenyl)-3,5-difluorophenyl)-N-(1,8- naphthyridin-2-yl)non-8-ynamide **Foldamer I**

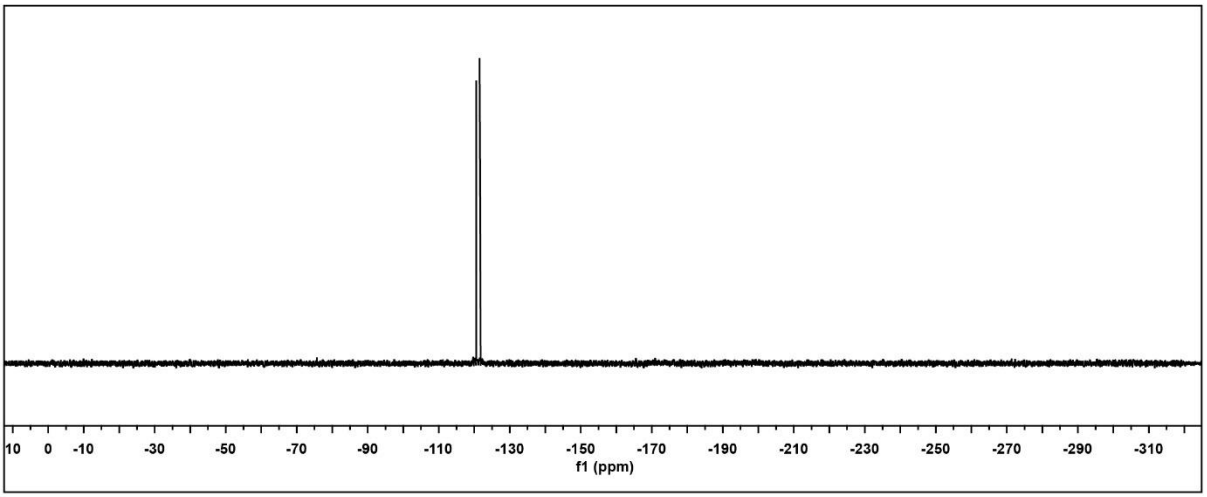

1,2-Bis(2,6-difluoro-4-1-(Oct-7-yn-1-yl)-N-(4-(1-ethylpentyl)-1,6-dihydro-6-oxo-2-pyrimidinyl))urea)diazene **Foldamer III**

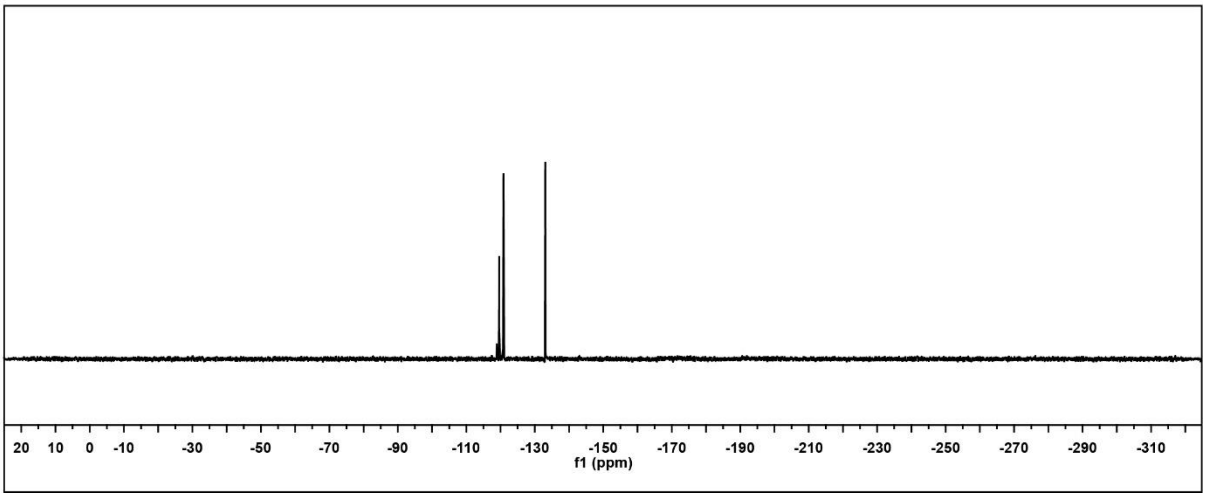

9- (4- ((2,6-Difluoro - 4 - (oct-7-yn-1-yl) -N- (4-(1-ethylpentyl) - 1,6 - dihydro-6-oxo -2-pyrimidinyl)) urea) phenyl) diazenyl) - 3,5 - difluorophenyl) -N- ((1,8-naphthyridin-2-yl)-2-ethylhexanamide)non-8-ynamide **Foldamer IV**

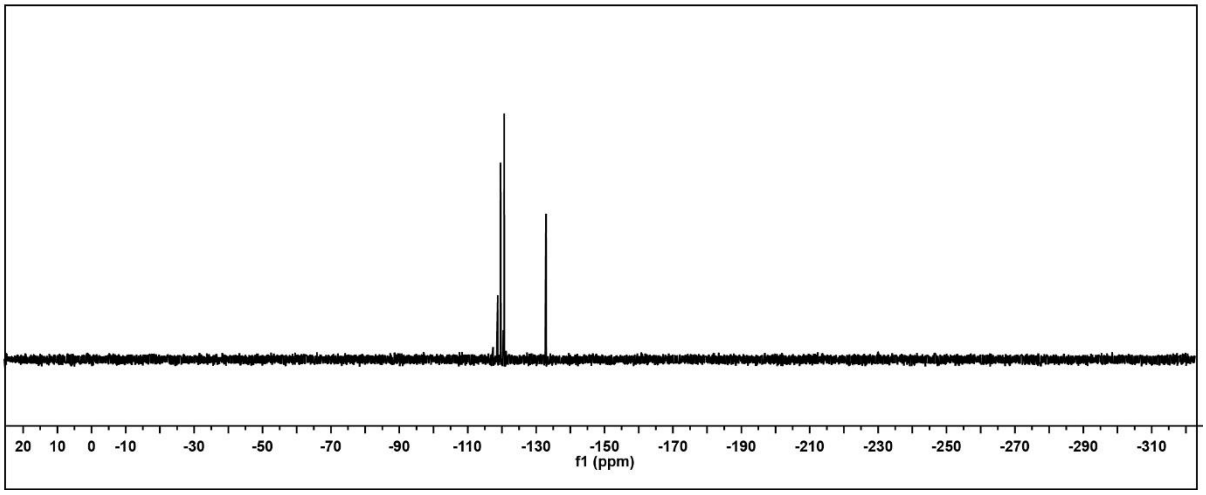

Appendix B

DOSY Spectra

Pyr·NAP Foldamer I 4 mM 405 nm

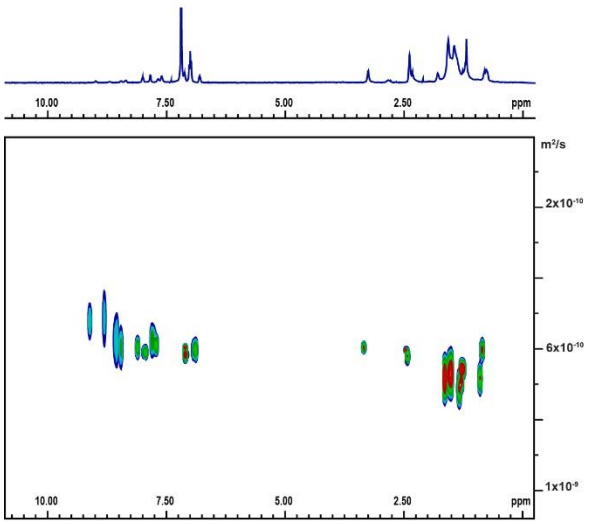

Pyr·NAP Foldamer I 4 mM 530 nm

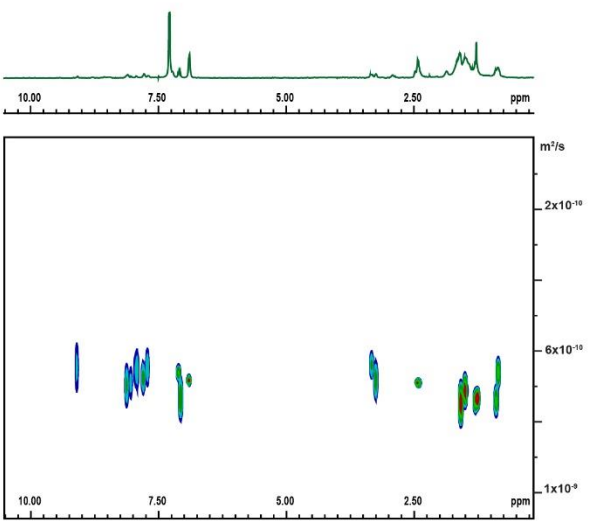

Pyr·NAP Foldamer I 8 mM 405 nm

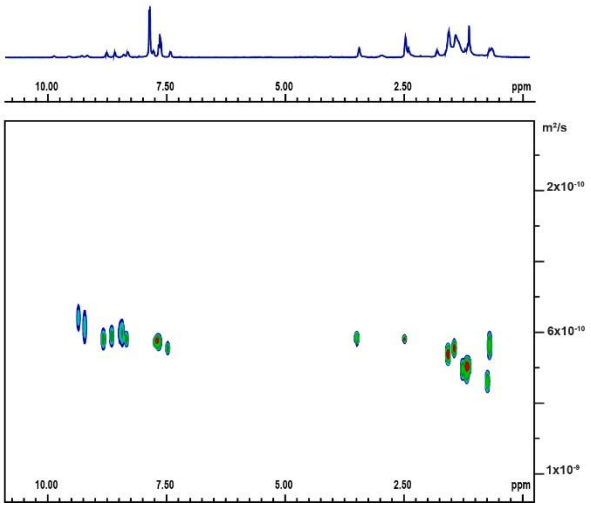

Pyr·NAP Foldamer I 8 mM 530 nm

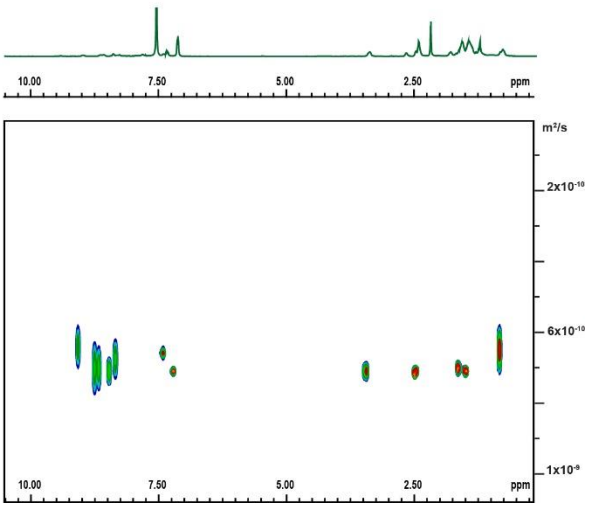

Pyr·NAP Foldamer I 12 mM 405 nm

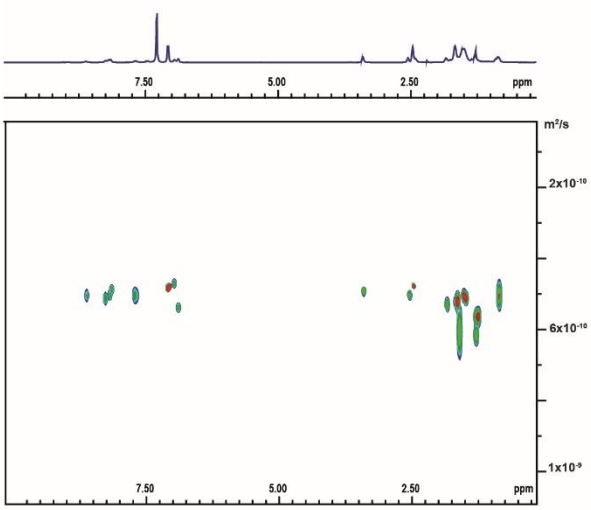

Pyr·NAP Foldamer I 12 mM 530 nm

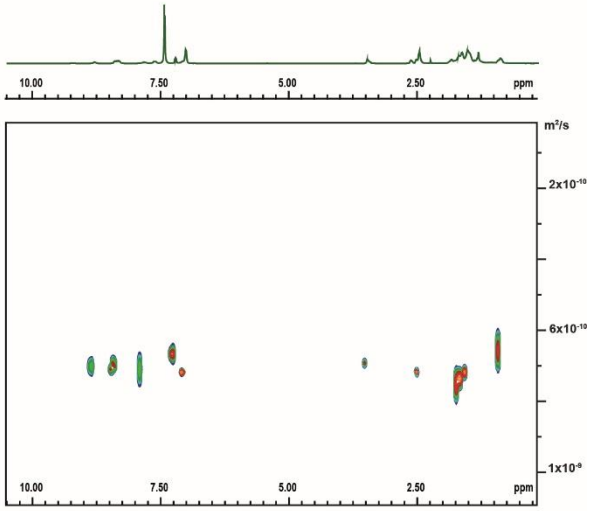

Pyr·NAP Foldamer I 16 mM 405 nm

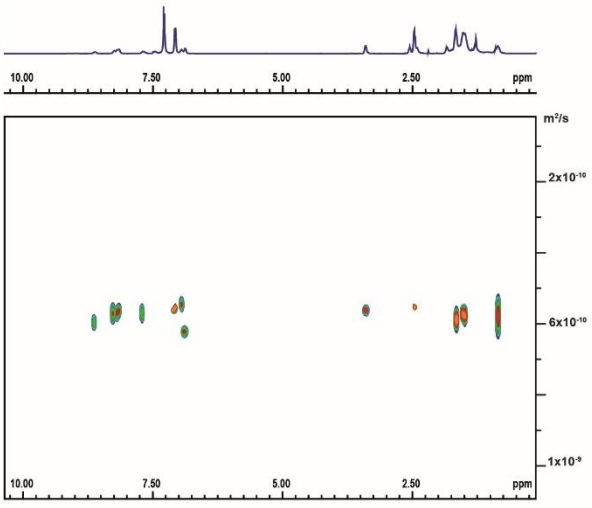

Pyr·NAP Foldamer I 16 mM 530 nm

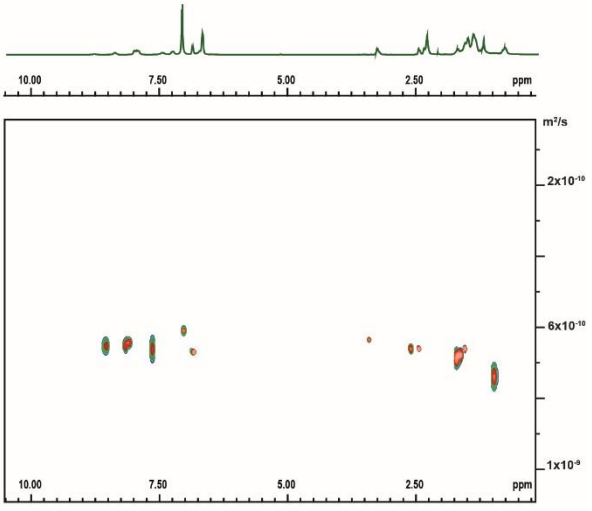

Pyr·NAP Foldamer I 20 mM 405 nm

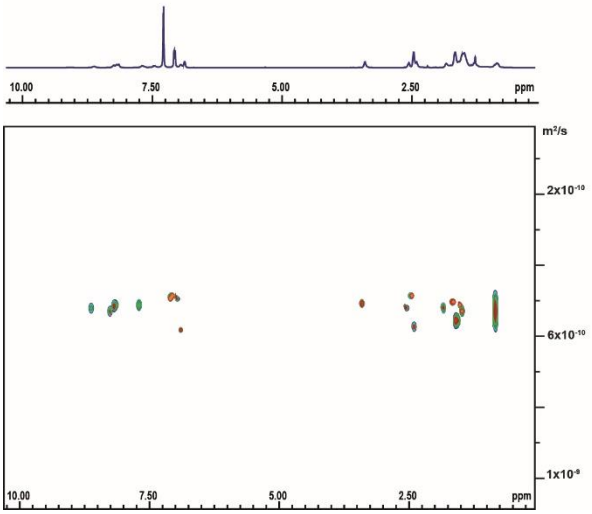

Pyr·NAP Foldamer I 20 mM 530 nm

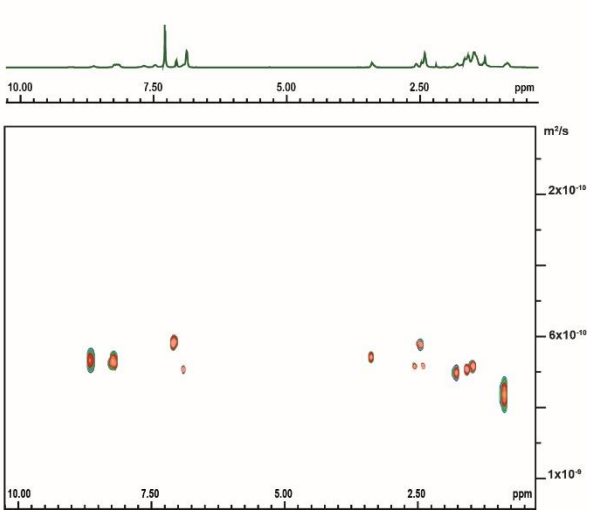

Pyr·NAP Foldamer I 24 mM 405 nm

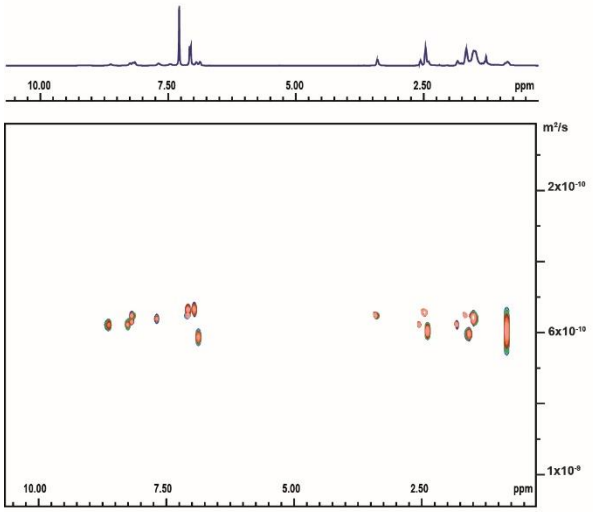

Pyr·NAP Foldamer I 24 mM 530 nm

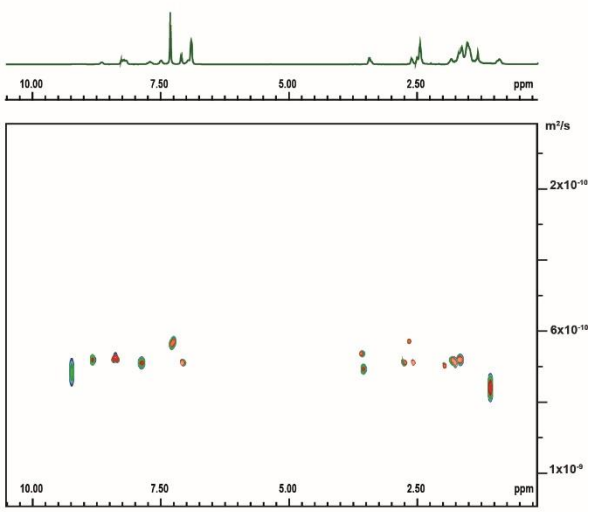

Pyr·NAP Foldamer I 28 mM 405 nm

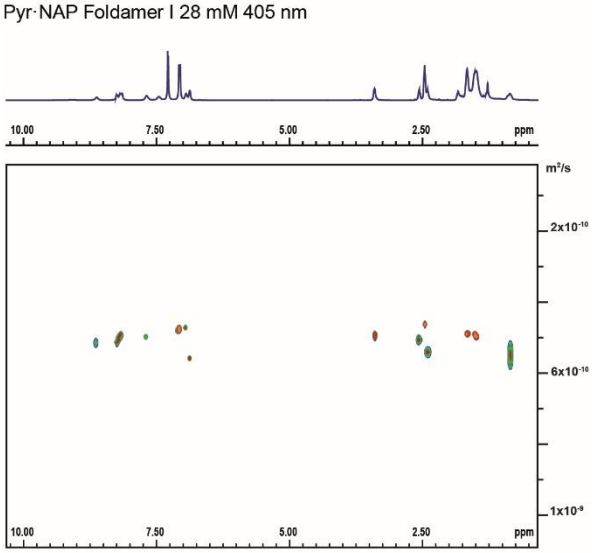

Pyr·NAP Foldamer I 28 mM 530 nm

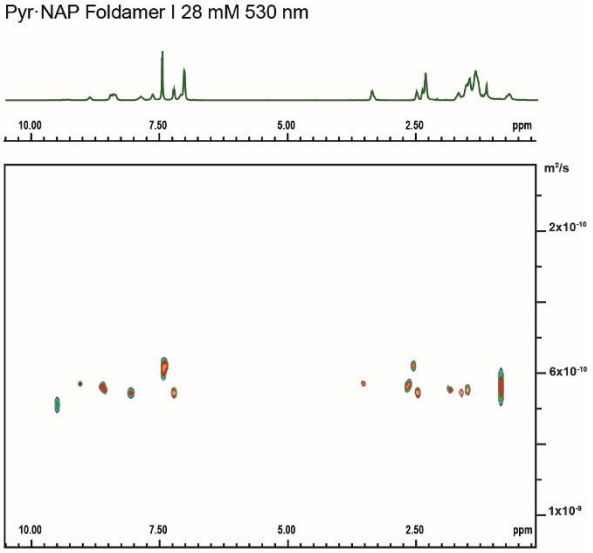

Pyr·NAP Foldamer I 32 mM 405 nm

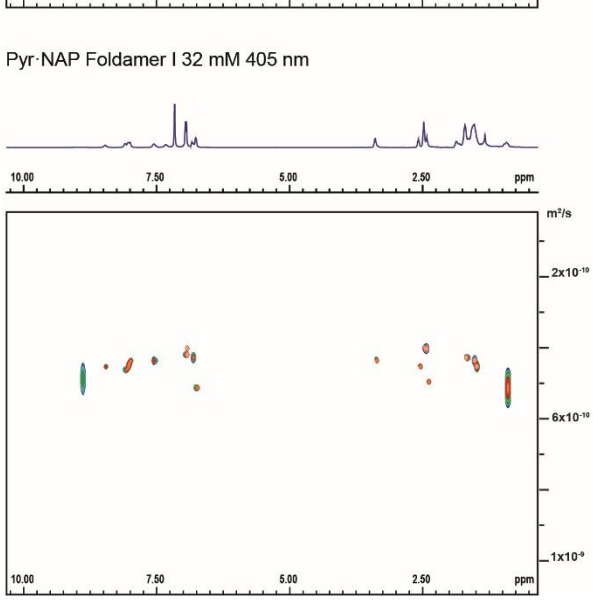

Pyr·NAP Foldamer I 32 mM 530 nm

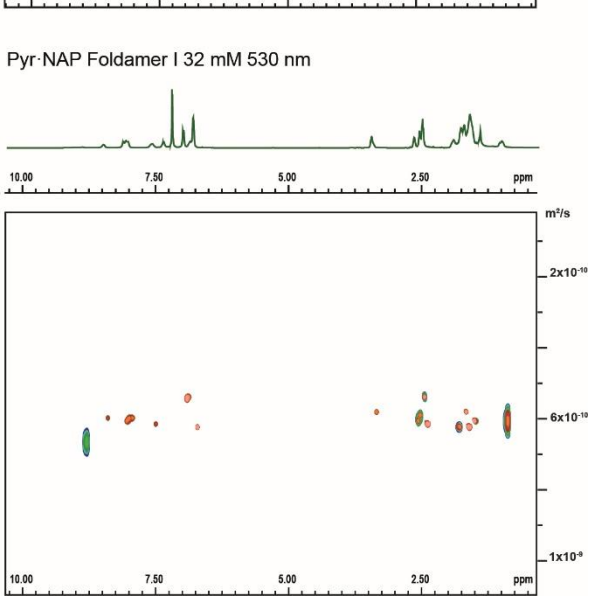

Pyr·NAP Foldamer I 36 mM 405 nm

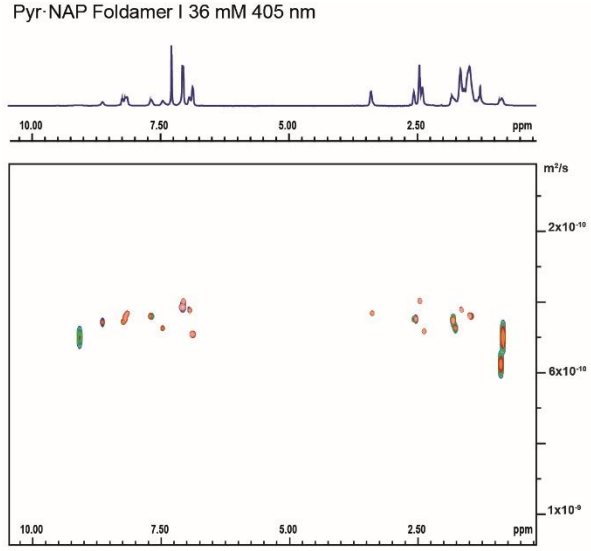

Pyr·NAP Foldamer I 36 mM 530 nm

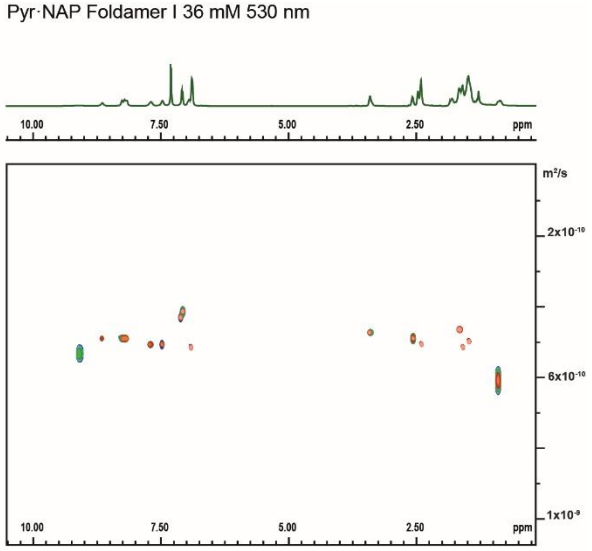

Pyr·NAP 40 mM 405 nm

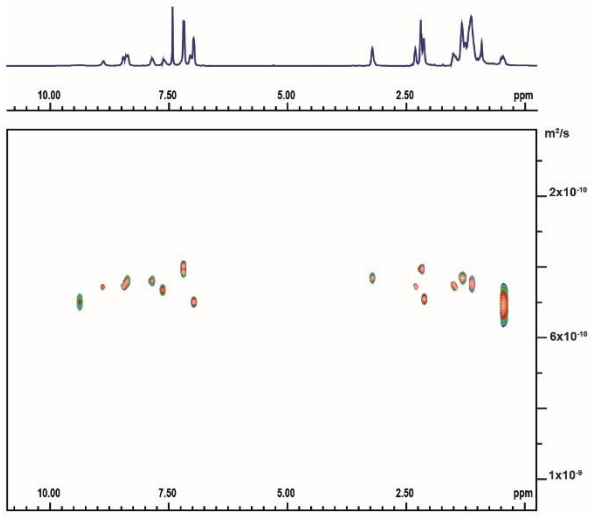

Pyr·NAP Foldamer I 40 mM 530 nm

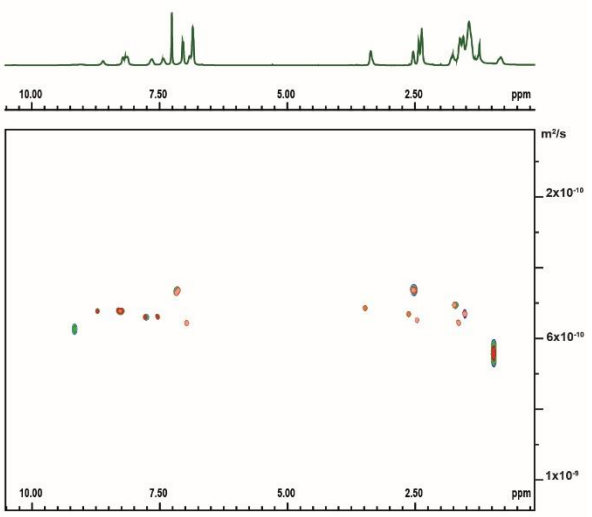

Pyr·NAP Foldamer I 44 mM 405 nm

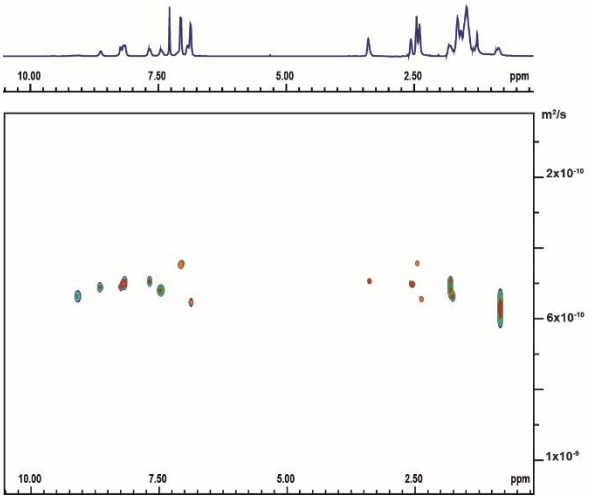

Pyr·NAP Foldamer I 44 mM 530 nm

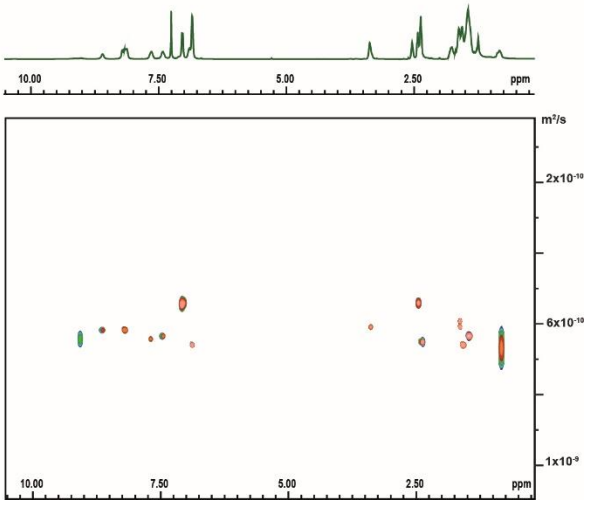

Pyr·NAP Foldamer I 48 mM 405 nm

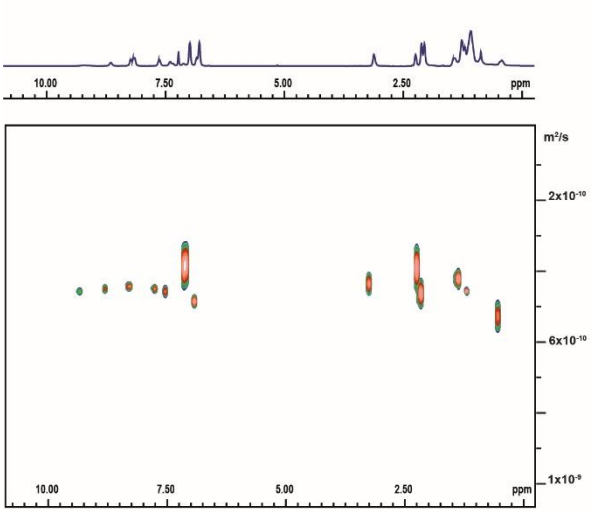

Pyr·NAP Foldamer I 48 mM 530 nm

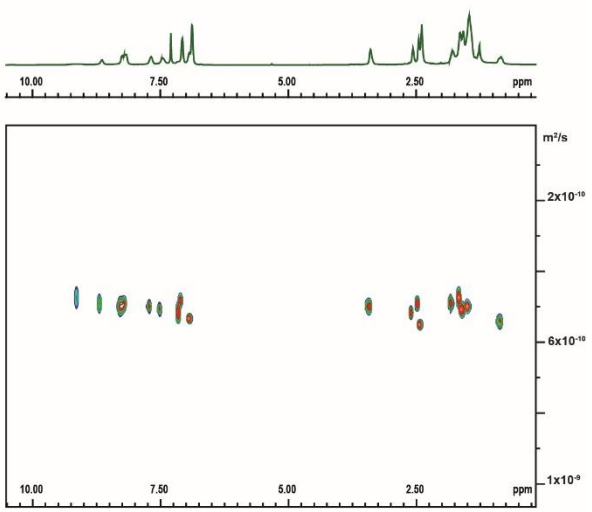

Pyr·NAP Foldamer I 52 mM 405 nm

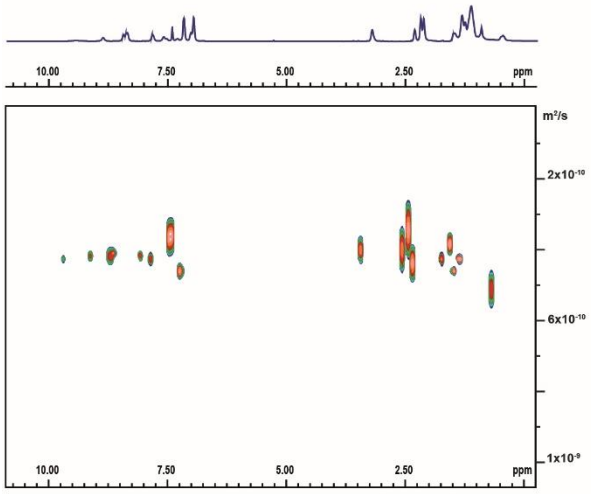

Pyr·NAP Foldamer I 52 mM 530 nm

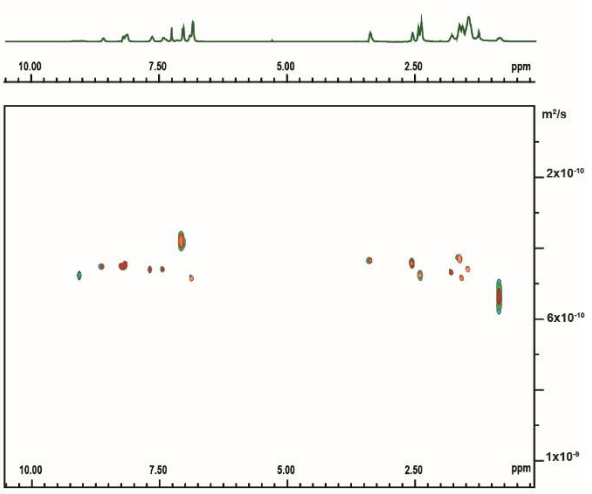

Pyr·NAP Foldamer I 56 mM 405 nm

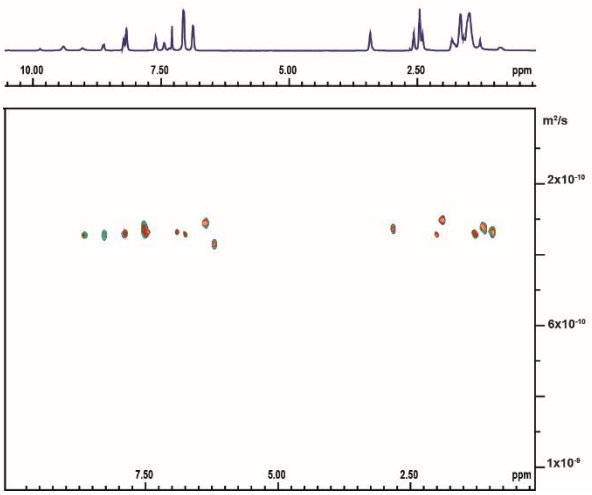

Pyr·NAP Foldamer I 56 mM 530 nm

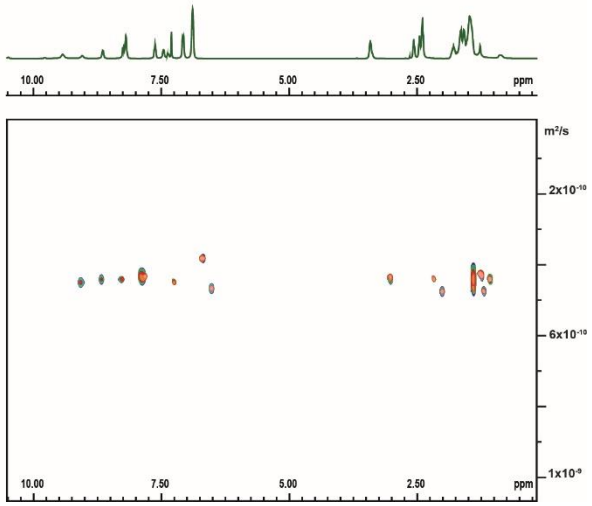

UPy·UPy Foldamer III 4 mM 405 nm

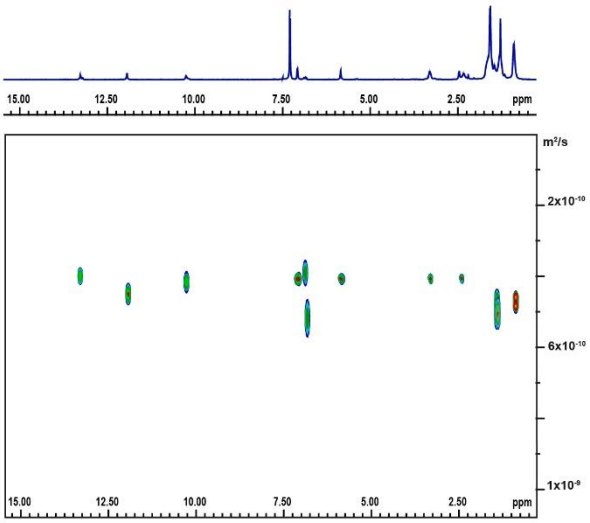

UPy·UPy Foldamer III 4 mM 530 nm

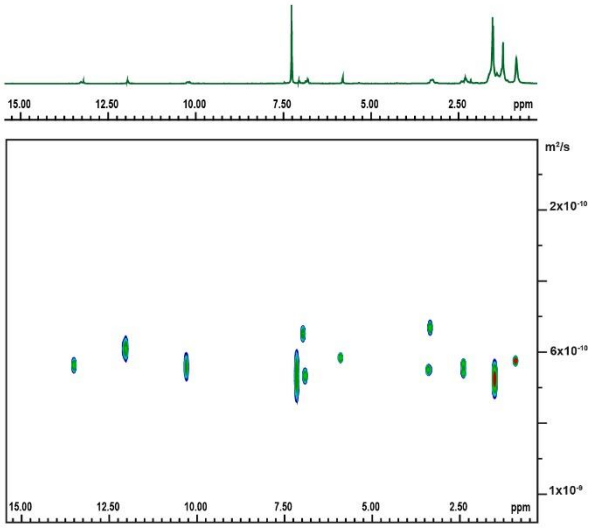

UPy·UPy Foldamer III 8 mM 405 nm

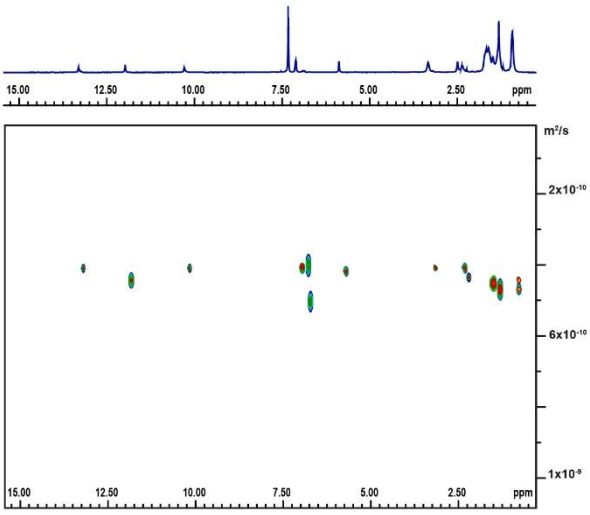

UPy·UPy Foldamer III 8 mM 530 nm

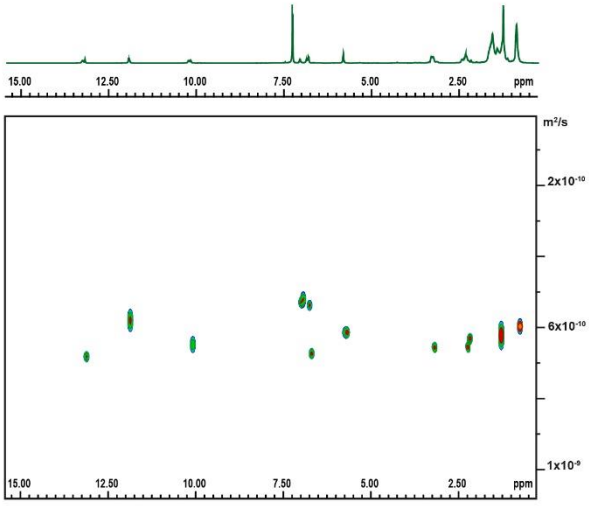

UPy·UPy Foldamer III 12 mM 405 nm

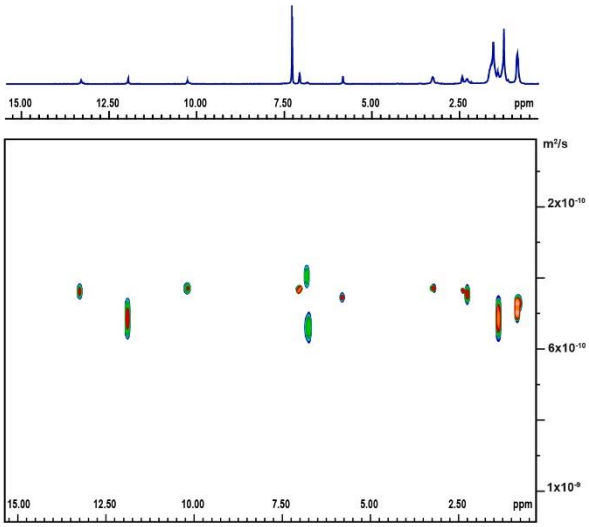

UPy·UPy Foldamer III 12 mM 530 nm

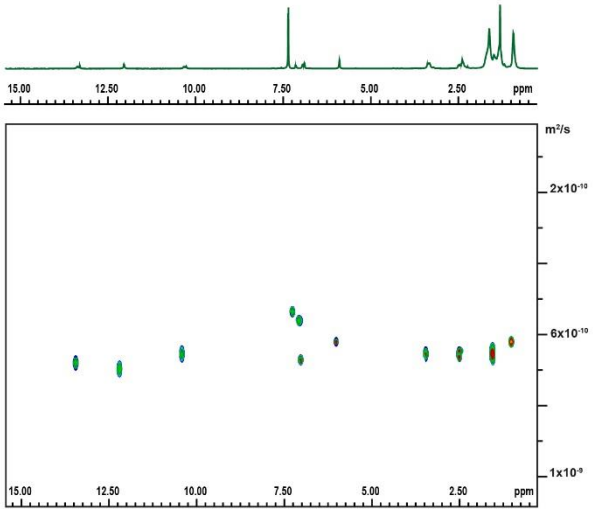

UPy·UPy Foldamer III 16 mM 405 nm

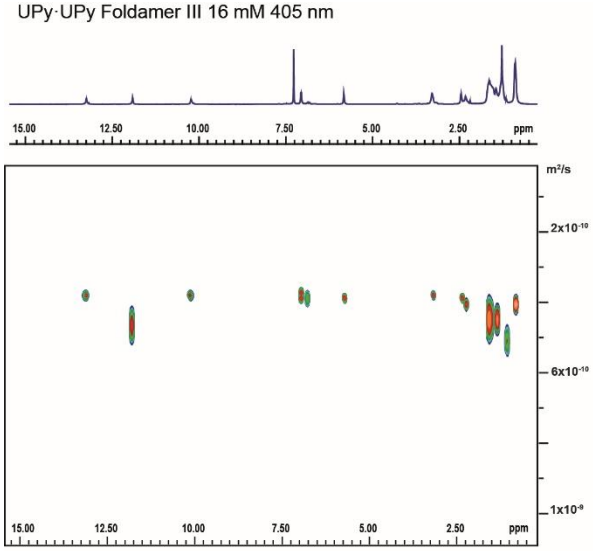

UPy·UPy Foldamer III 16 mM 530 nm

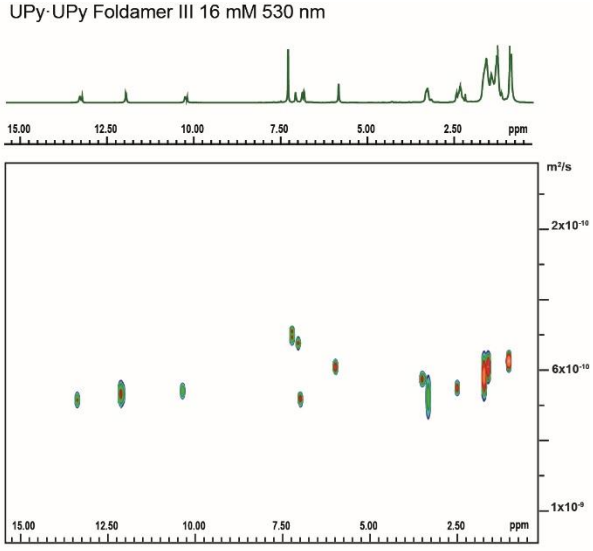

UPy·UPy Foldamer III 20 mM 405 nm

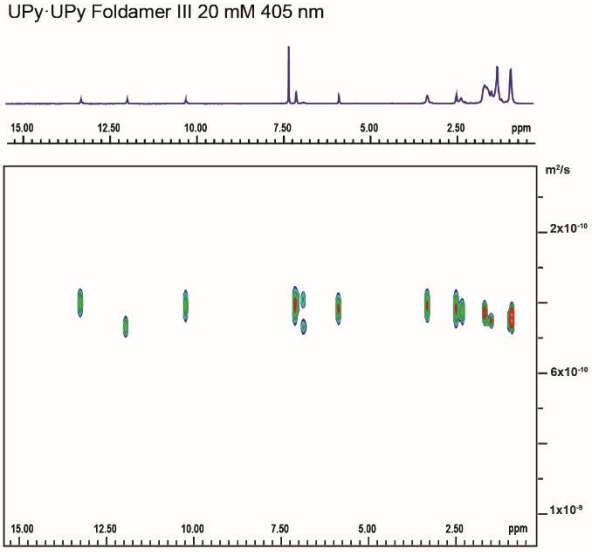

UPy·UPy Foldamer III 20 mM 530 nm

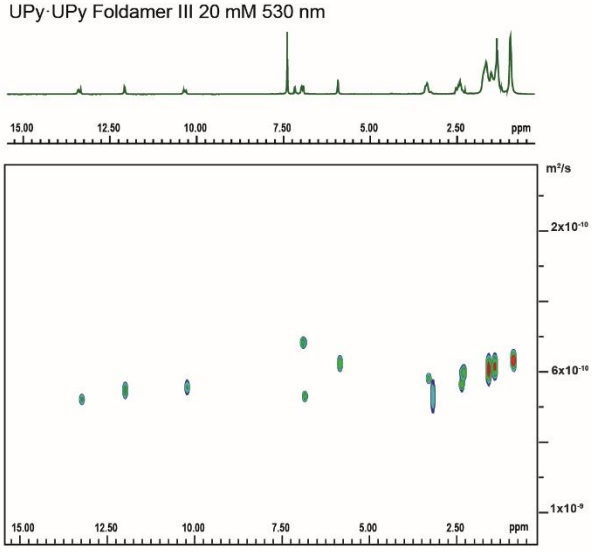

UPy·UPy Foldamer III 24 mM 405 nm

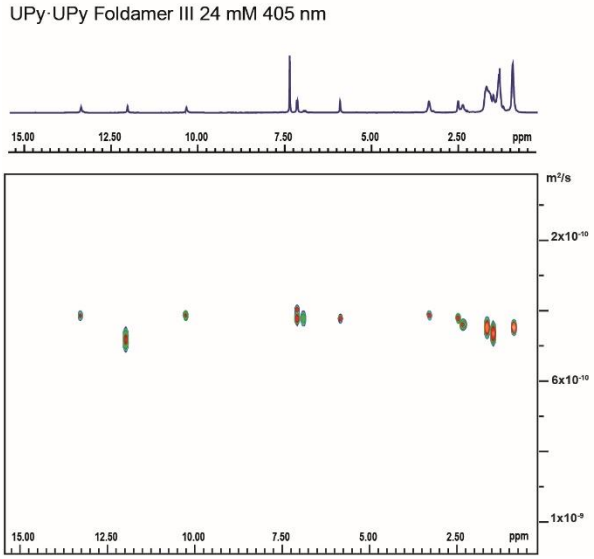

UPy·UPy Foldamer III 24 mM 530 nm

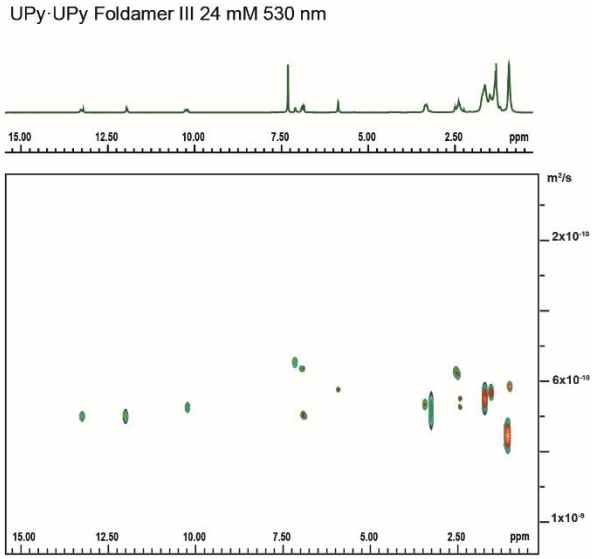

UPy·UPy Foldamer III 28 mM 405 nm

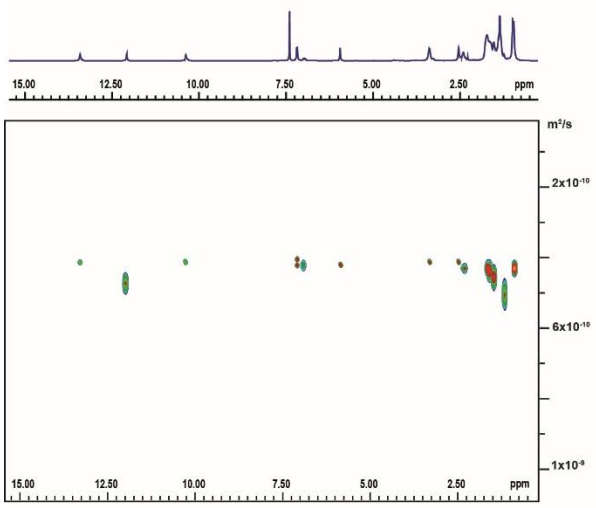

UPy·UPy Foldamer III 28 mM 530 nm

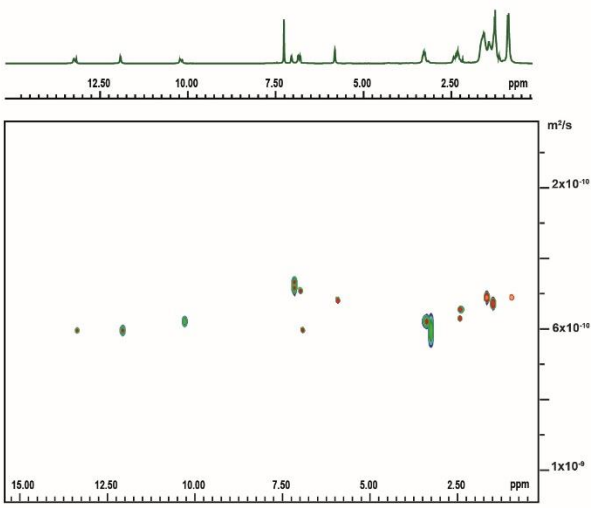

UPy·UPy Foldamer III 32 mM 405 nm

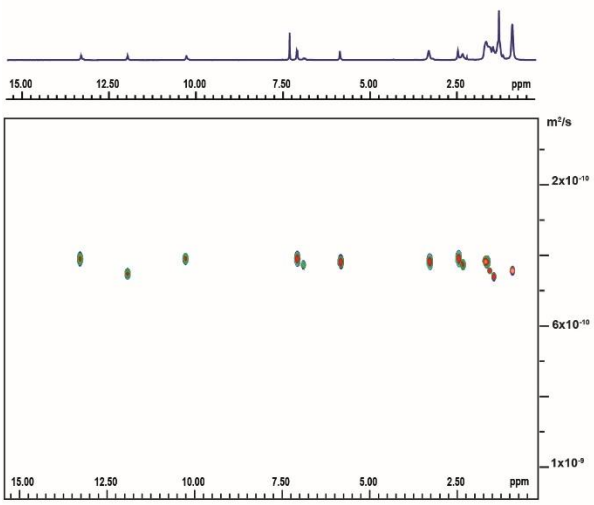

UPy·UPy Foldamer III 32 mM 530 nm

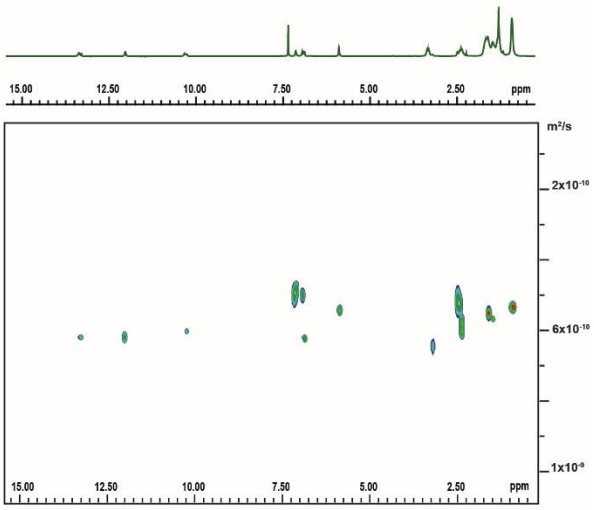

UPy·UPy Foldamer III 36 mM 405 nm

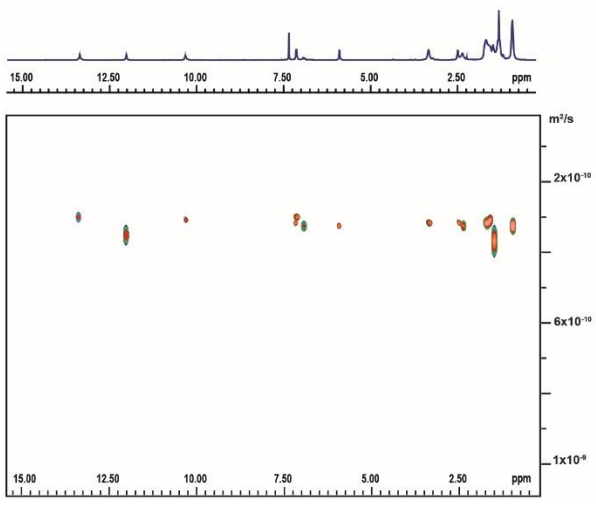

UPy·UPy Foldamer III 36 mM 530 nm

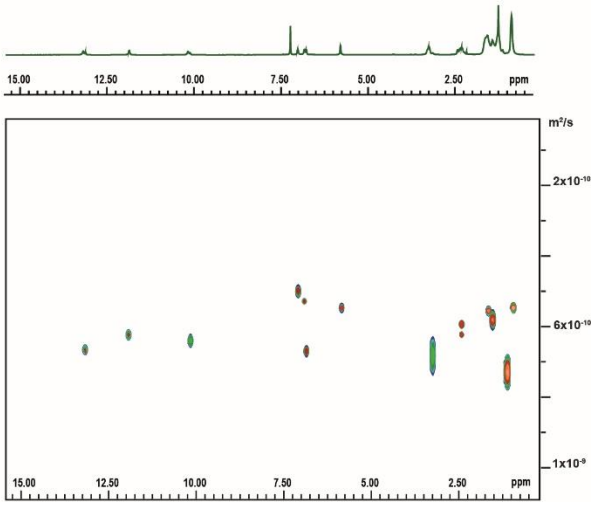

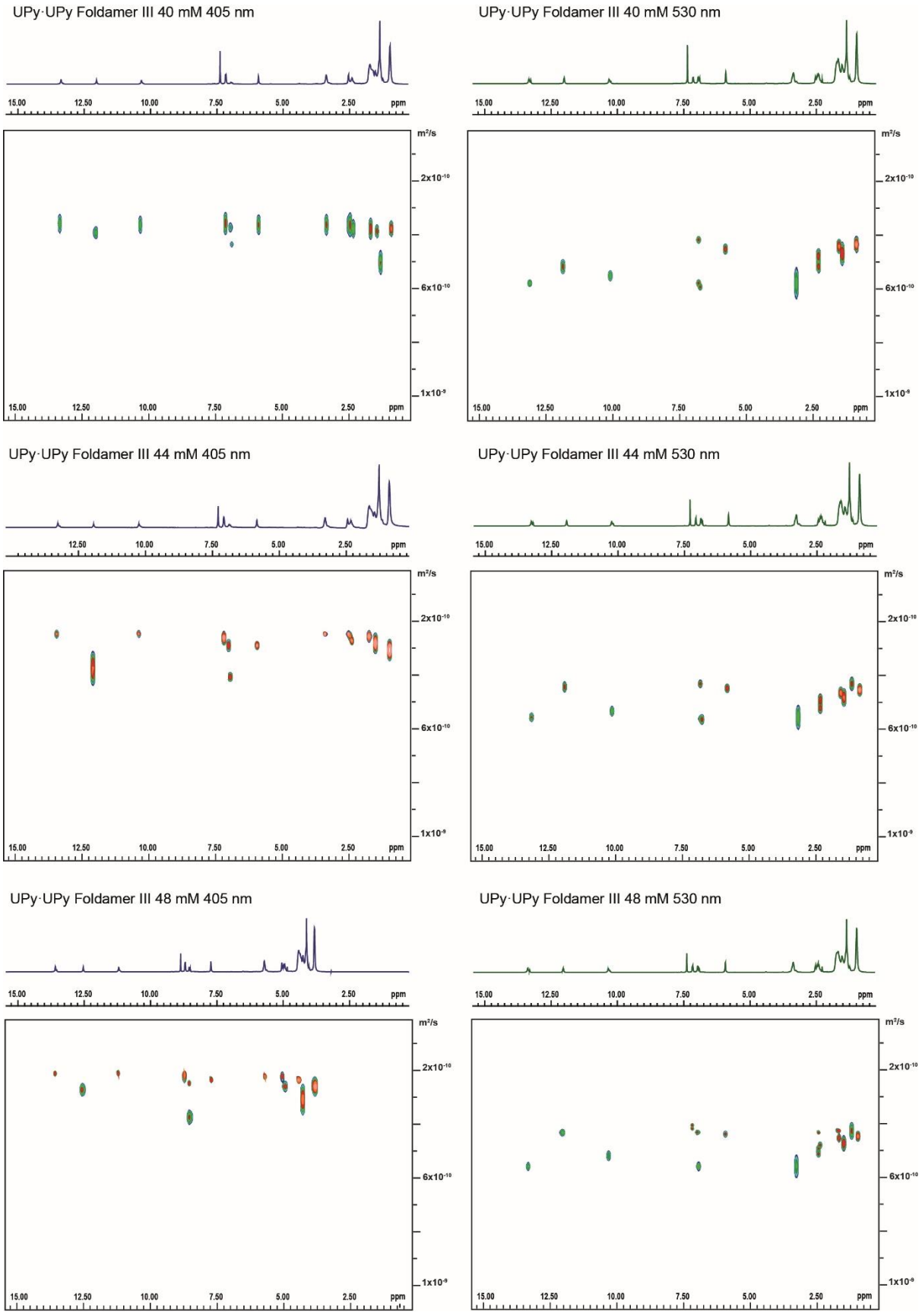
UPy·UPy Foldamer III 40 mM 405 nm
UPy·UPy Foldamer III 40 mM 530 nm
UPy·UPy Foldamer III 44 mM 405 nm
UPy·UPy Foldamer III 44 mM 530 nm
UPy·UPy Foldamer III 48 mM 405 nm
UPy·UPy Foldamer III 48 mM 530 nm
15.00
12.50
10.00
7.50
5.00
2.50
ppm
m²/s
2x10⁻¹⁰
6x10⁻¹⁰
1x10⁻⁹

UPy·UPy Foldamer III 52 mM 405 nm

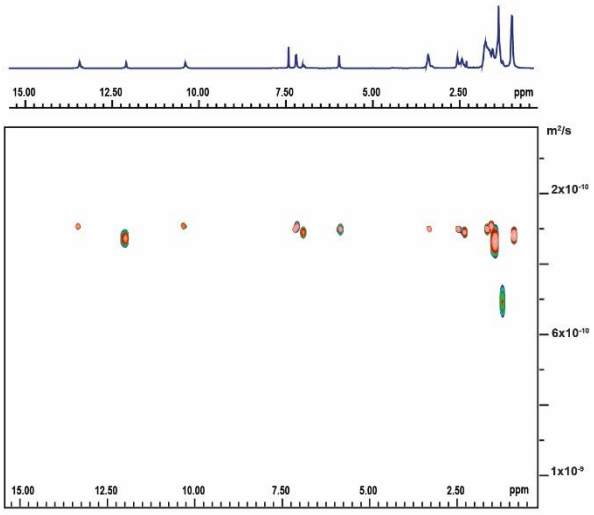

UPy·UPy Foldamer III 52 mM 530 nm

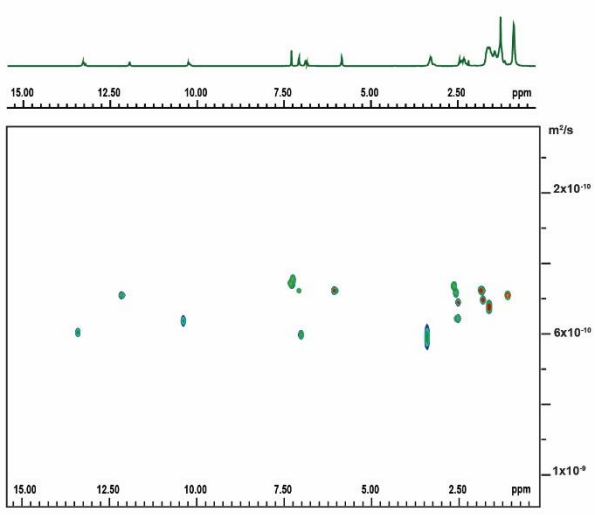

UPy·UPy Foldamer III 56 mM 405 nm

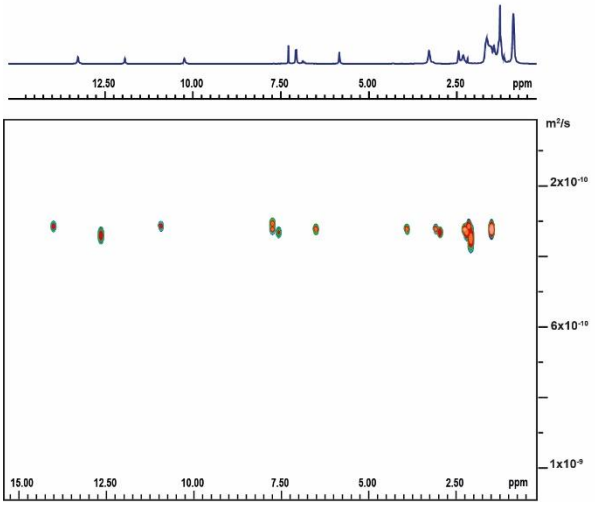

UPy·UPy Foldamer III 56 mM 530 nm

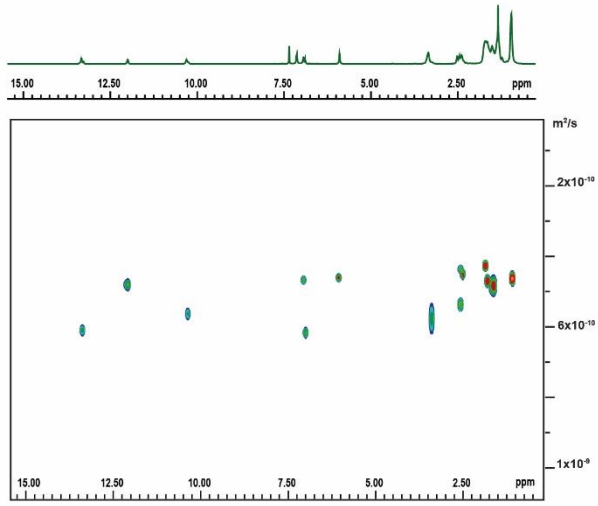

UPy·DAN Foldamer IV 4 mM 405 nm

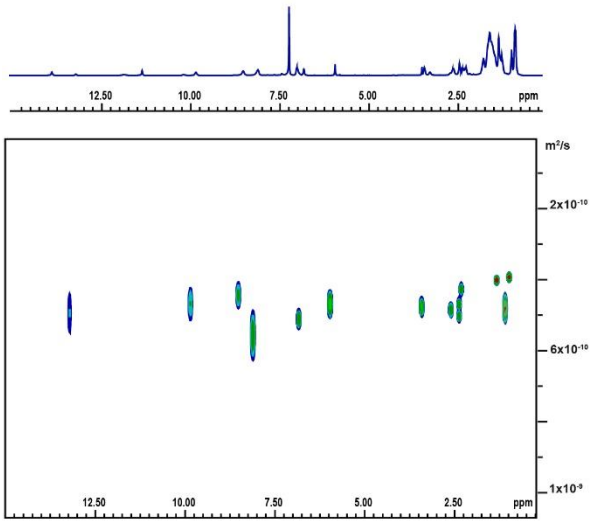

UPy·DAN Foldamer IV 4 mM 530 nm

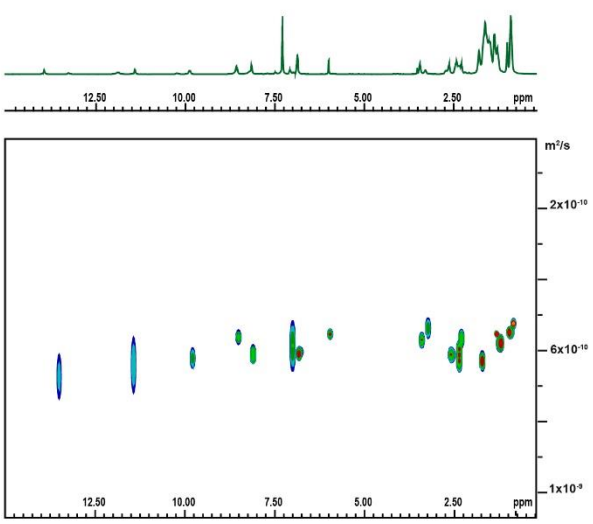

UPy·DAN Foldamer IV 8 mM 405 nm

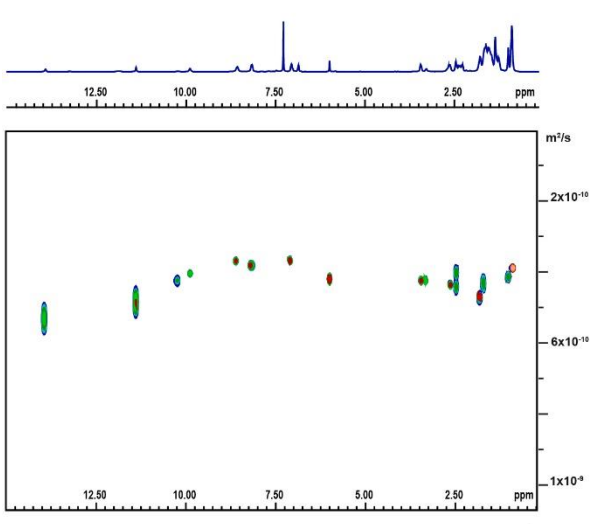

UPy·DAN Foldamer IV 8 mM 530 nm

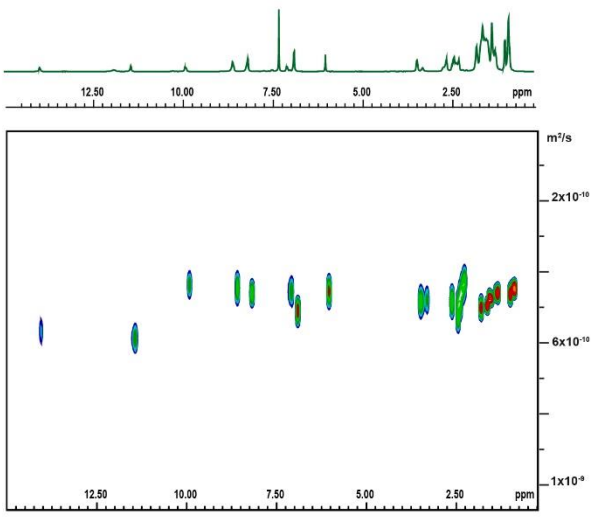

UPy·DAN Foldamer IV 12 mM 405 nm

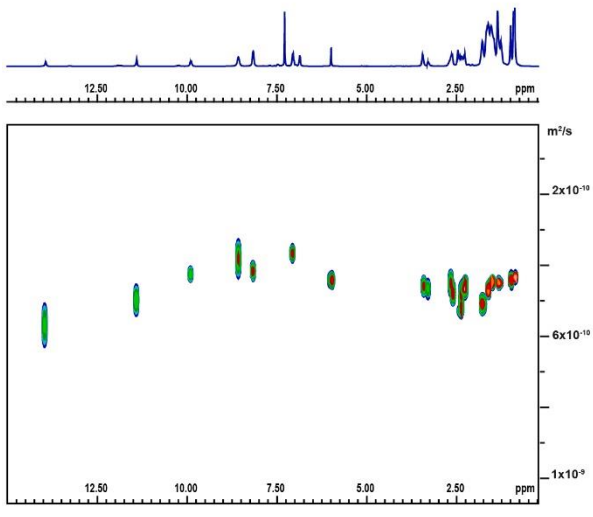

UPy·DAN Foldamer IV 12 mM 530 nm

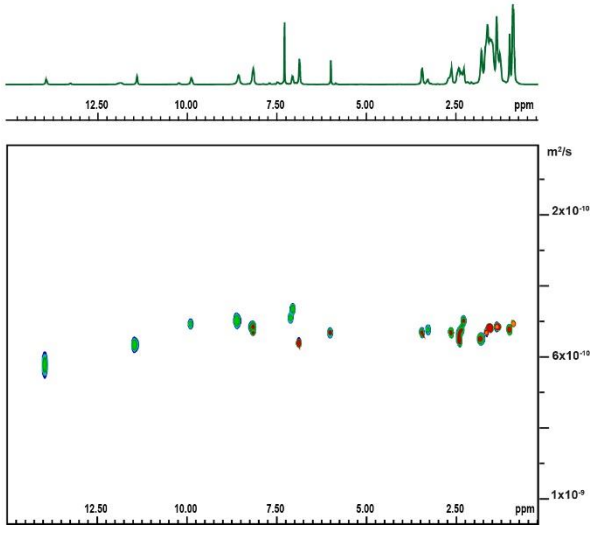

UPy·DAN Foldamer IV 16 mM 405 nm

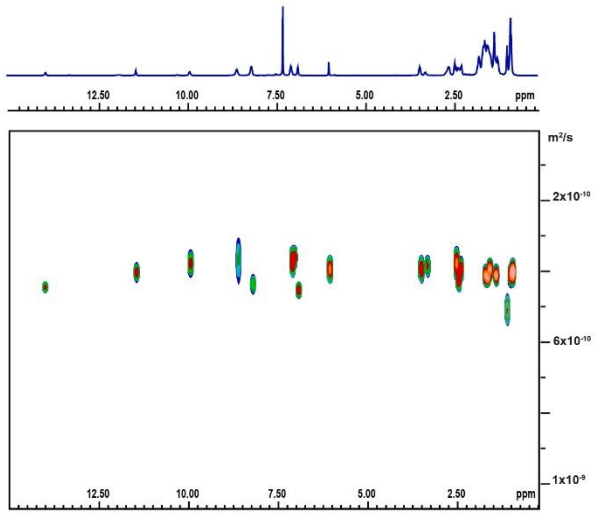

UPy·DAN Foldamer IV 16 mM 530 nm

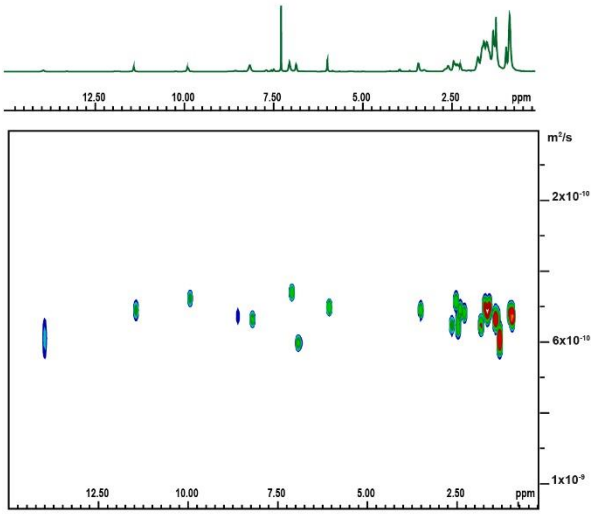

UPy·DAN Foldamer IV 20 mM 405 nm

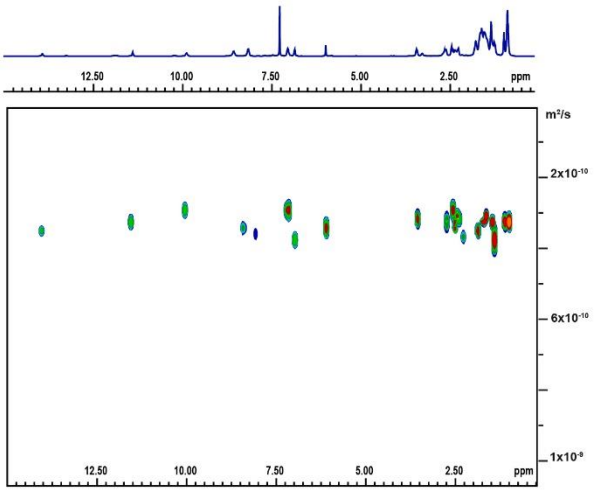

UPy·DAN Foldamer IV 20 mM 530 nm

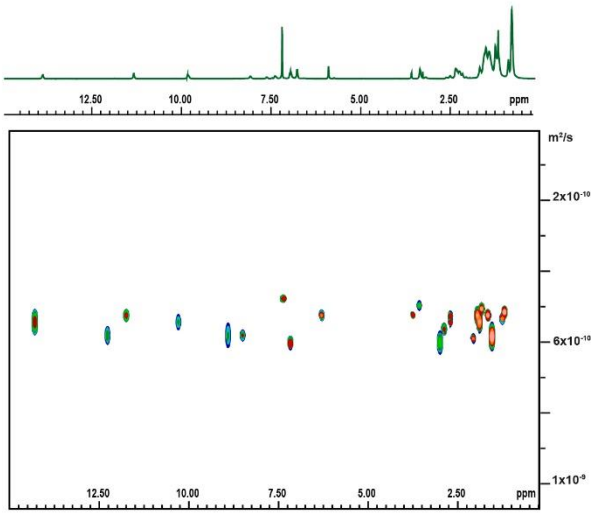

UPy·DAN Foldamer IV 24 mM 405 nm

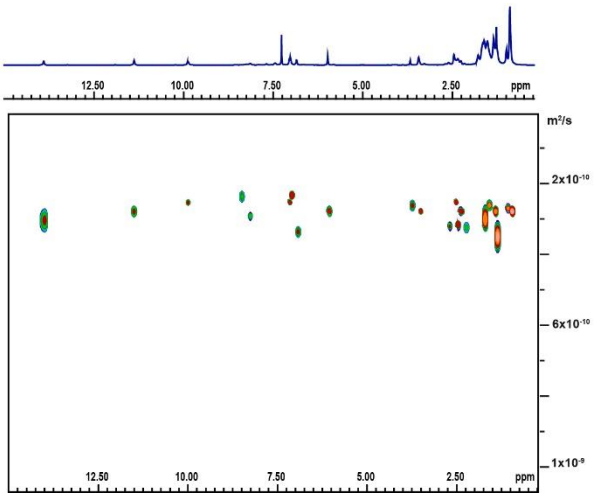

UPy·DAN Foldamer IV 24 mM 530 nm

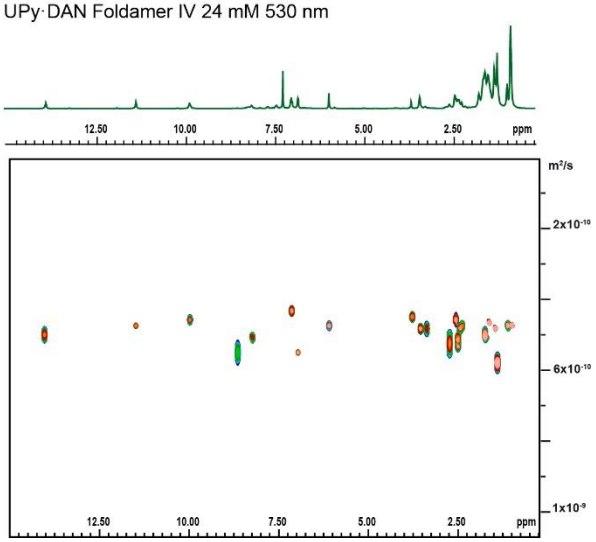

UPy·DAN Foldamer IV 28 mM 405 nm

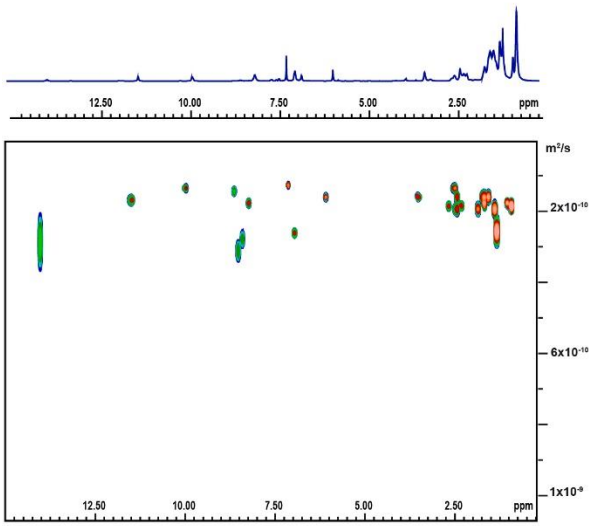

UPy·DAN Foldamer IV 28 mM 530 nm

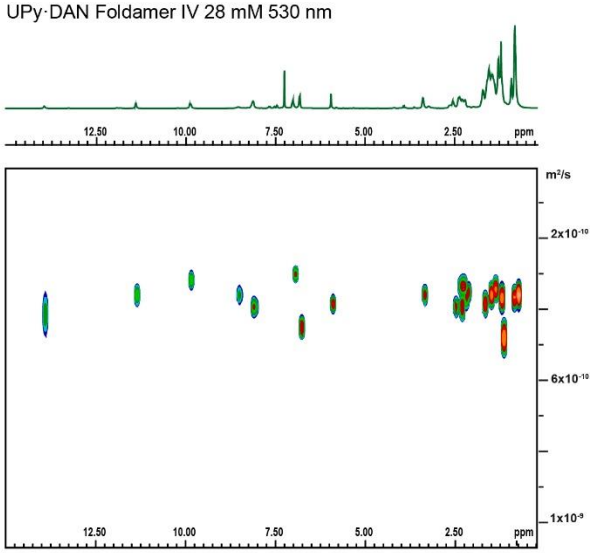

UPy·DAN Foldamer IV 32 mM 405 nm

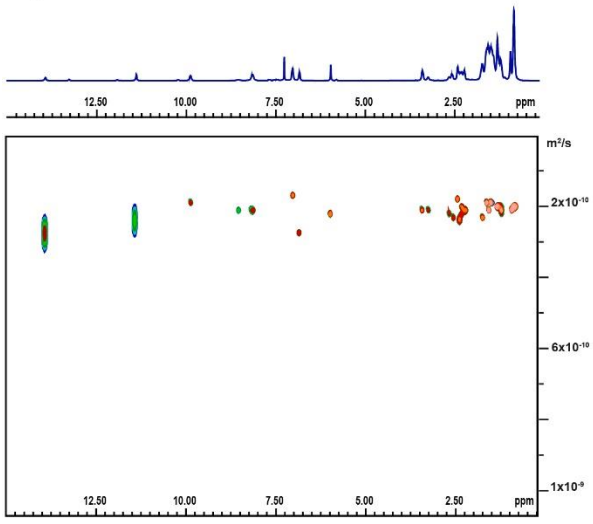

UPy·DAN Foldamer IV 32 mM 530 nm

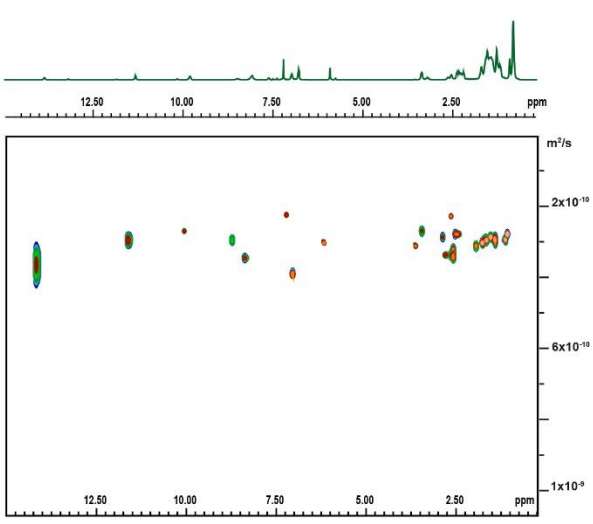

UPy·DAN Foldamer IV 36 mM 405 nm

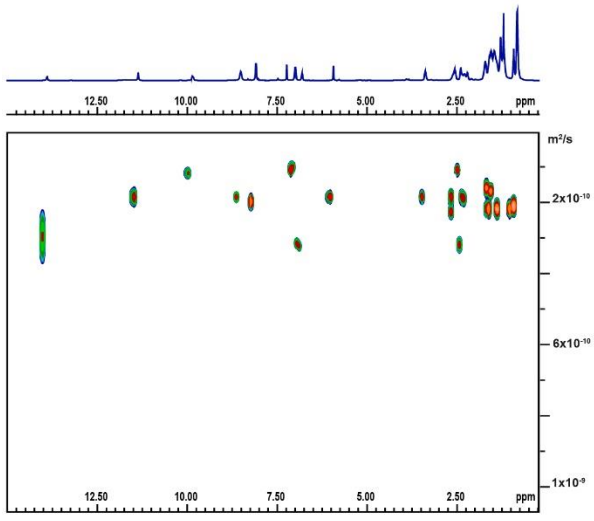

UPy·DAN Foldamer IV 36 mM 530 nm

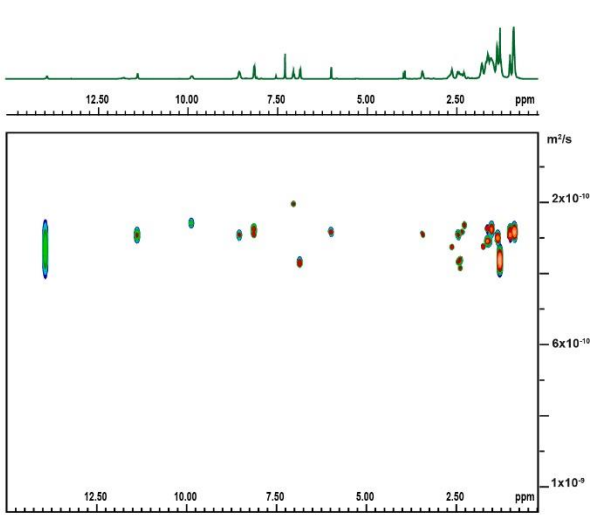

UPy·DAN Foldamer IV 40 mM 405 nm

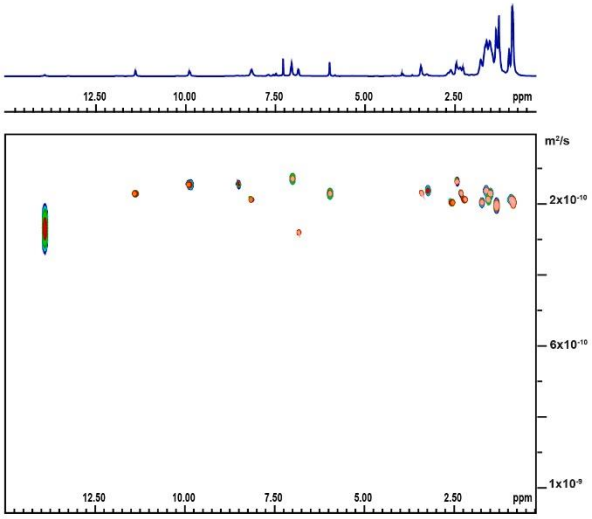

UPy·DAN Foldamer IV 40 mM 530 nm

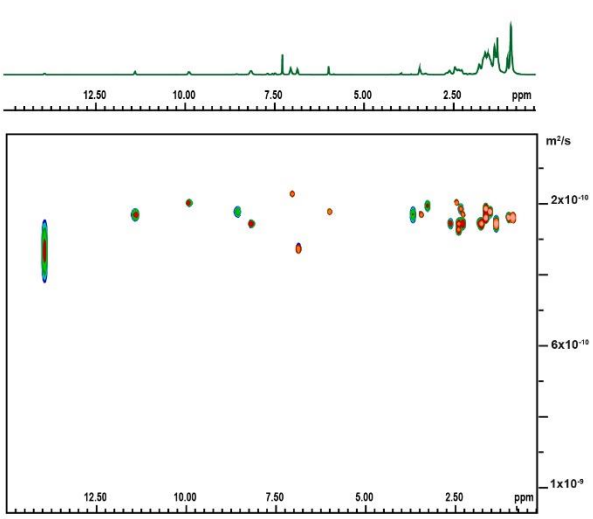

UPy·DAN Foldamer IV 44 mM 405 nm

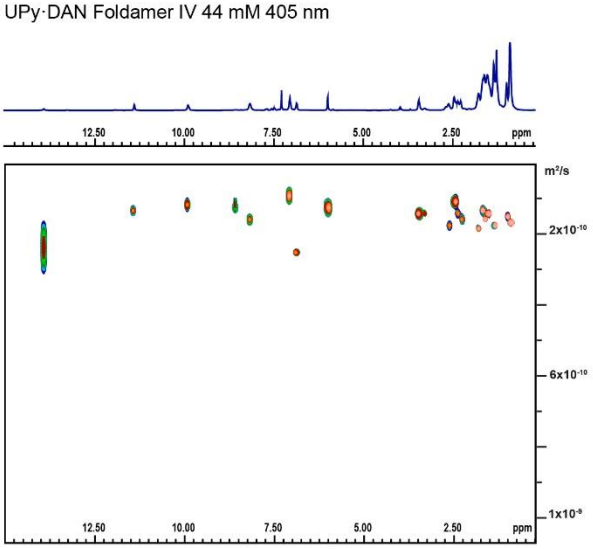

UPy·DAN Foldamer IV 44 mM 530 nm

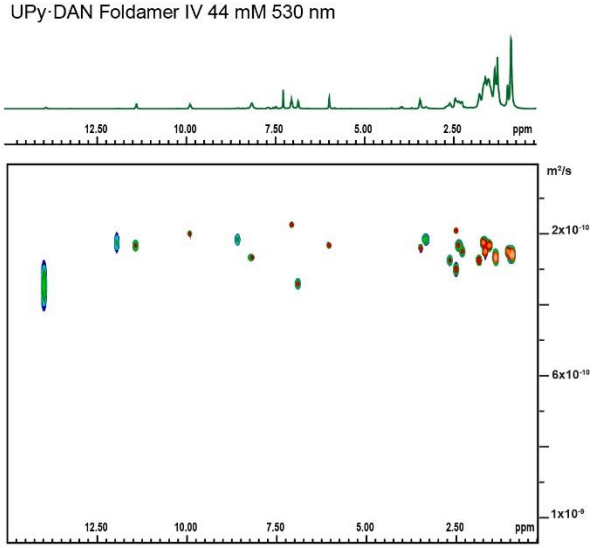

UPy·DAN Foldamer IV 48 mM 405 nm

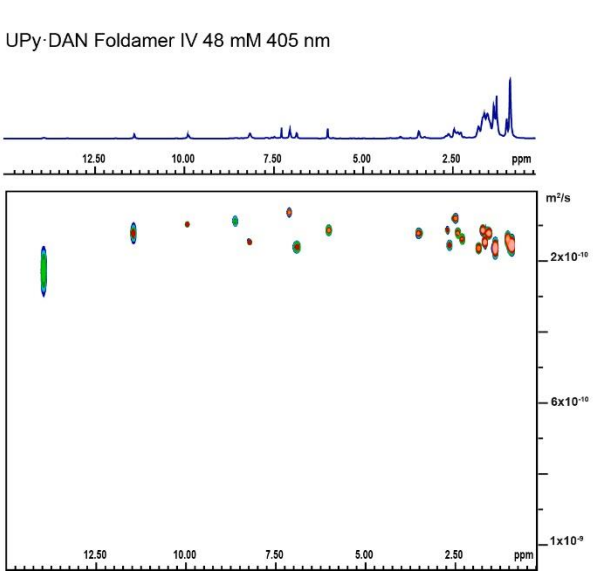

UPy·DAN Foldamer IV 48 mM 530 nm

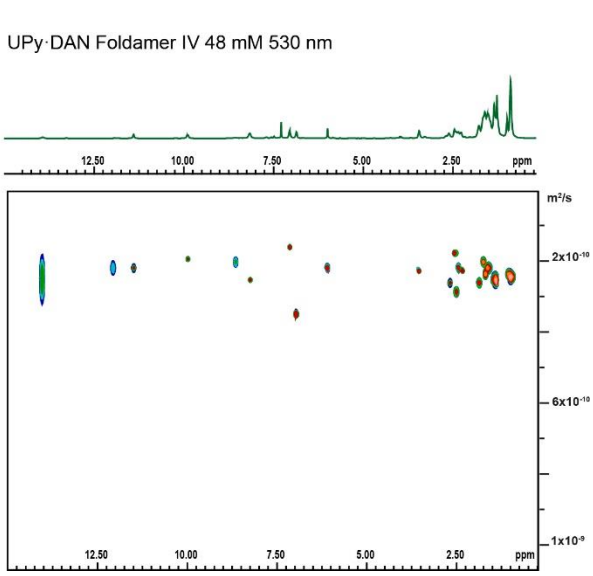

UPy·DAN Foldamer IV 52 mM 405 nm

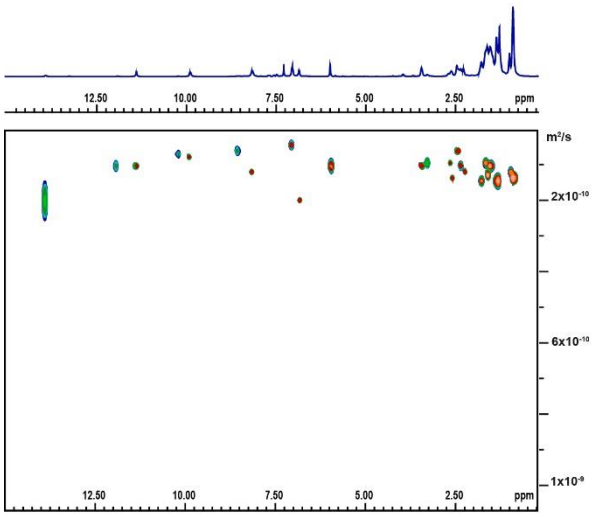

UPy·DAN Foldamer IV 52 mM 530 nm

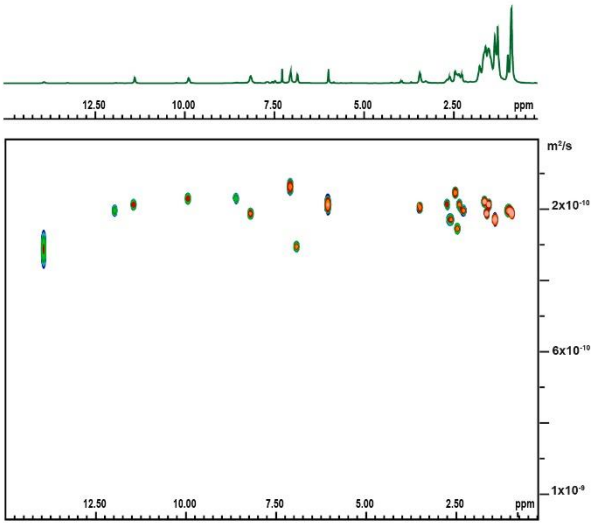

UPy·DAN Foldamer IV 56 mM 405 nm

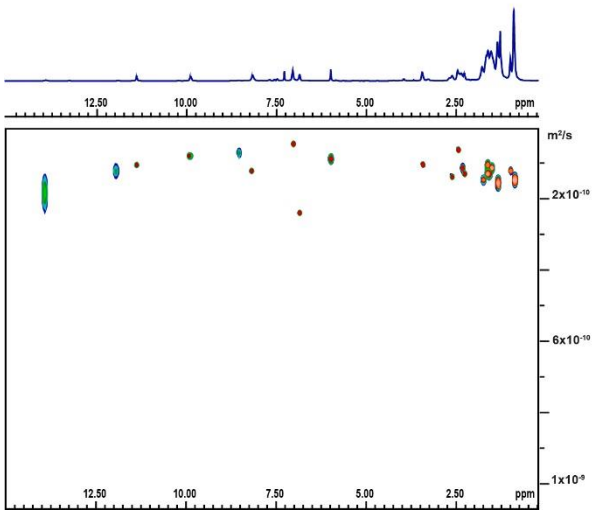

UPy·DAN Foldamer IV 56 mM 530 nm

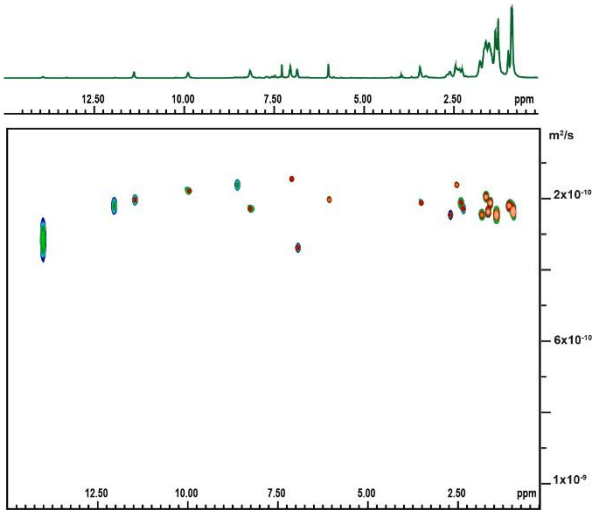

DAN-PMMA + UPy·UPy Foldamer 405 nm

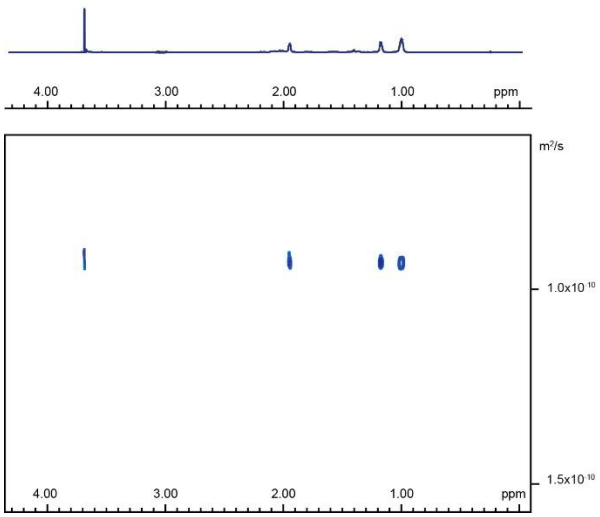

DAN-PMMA + UPy·UPy Foldamer 530 nm

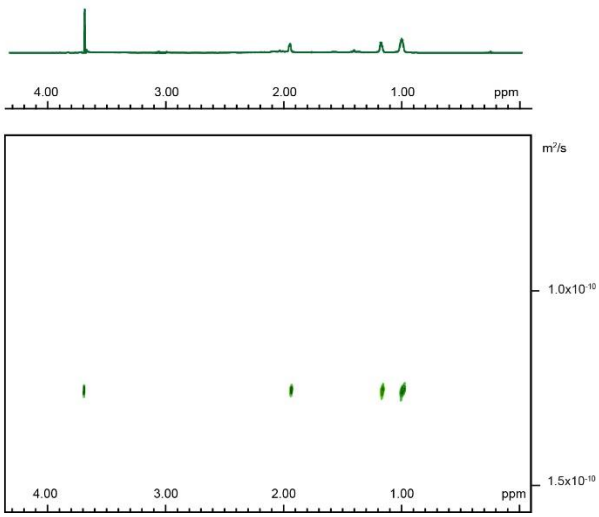

DOSY Data

Pyr·NAP Foldamer I

Concentration (mM)	*NAP·Pyr 405 nm*		*NAP·Pyr 530 nm*	
	D (m^2/s)	**Error (m^2/s)**	**D (m^2/s)**	**Error (m^2/s)**
4	6.00E-10	1.96E-11	6.99E-10	1.38E-11
8	6.30E-10	5.65E-12	6.61E-10	6.06E-12
12	5.86E-10	3.07E-12	6.99E-10	1.32E-11
16	6.04E-10	3.81E-12	7.01E-10	2.70E-12
20	5.30E-10	2.36E-12	7.13E-10	4.16E-12
24	5.99E-10	1.40E-12	7.15E-10	3.11E-12
28	5.21E-10	2.59E-12	6.54E-10	6.39E-12
32	4.94E-10	1.80E-12	6.35E-10	1.92E-12
36	4.97E-10	2.27E-12	5.55E-10	2.07E-12
40	5.31E-10	4.31E-12	5.81E-10	1.65E-12
44	4.39E-10	2.10E-12	5.01E-10	1.44E-12
48	4.32E-10	7.07E-12	4.83E-10	2.90E-12
52	3.72E-10	1.29E-12	4.66E-10	2.37E-12

Appendix B Table 1. Diffusion coefficients of foldamer **I** over concentration range 4 mM - 52 mM. Diffusion coefficients obtained from fitting data in Topspin Dynamics Center, errors estimated using the standard deviation from the fitting.

Concentration (mM)	*NAP·Pyr 405 nm*		*NAP·Pyr 530 nm*	
	DP	**Mw (g/mol^{-1})**	**DP**	**Mw (g/mol^{-1})**
4	1.58	1228.31	1.00	776.84
8	1.37	1061.06	1.18	918.67
12	1.70	1318.47	1.00	776.84
16	1.55	1204.07	0.99	770.21
20	2.29	1782.11	0.94	731.97
24	1.59	1234.48	0.93	725.85
28	2.42	1876.07	1.22	948.48
32	2.83	2200.81	1.33	1036.20
36	2.78	2161.19	2.00	1551.97
40	2.28	1772.06	1.74	1352.80
44	4.04	3135.95	2.72	2109.84
48	4.24	3290.88	3.03	2354.62
52	6.63	5153.88	3.38	2621.84

Appendix B Table 2. Degrees of polymerisation and molecular weight of each isomer of foldamer **I** over concentration range 52 – 4 mM.

UPy·UPy Foldamer III

Concentration (mM)	*UPy·UPy 405 nm*		*UPy·UPy 530 nm*	
	D (m^2/s)	**Error (m^2/s)**	**D (m^2/s)**	**Error (m^2/s)**
4	4.77E-10	7.34E-12	6.37E-10	1.40E-11
8	4.72E-10	6.31E-12	6.15E-10	8.71E-12
12	4.50E-10	1.50E-11	6.00E-10	9.79E-12
16	4.33E-10	5.06E-12	6.04E-10	1.19E-11
20	4.25E-10	3.49E-12	6.17E-10	1.18E-11
24	4.48E-10	6.62E-12	6.52E-10	4.19E-12
28	4.22E-10	1.52E-12	5.94E-10	8.27E-12
32	4.30E-10	6.98E-12	6.23E-10	4.96E-12
36	3.83E-10	4.70E-12	5.89E-10	5.40E-12
40	3.80E-10	3.46E-12	5.48E-10	1.35E-11
44	3.46E-10	4.81E-12	5.10E-10	1.06E-11
48	3.34E-10	1.37E-12	5.31E-10	1.15E-11
52	3.27E-10	2.21E-12	5.21E-10	9.39E-12

Appendix B Table 3. Diffusion coefficients of foldamer **III** over concentration range 4 mM - 52 mM. Diffusion coefficients obtained from fitting data in Topspin Dynamics Center, errors estimated using the standard deviation from the fitting.

Concentration (mM)	*UPy·UPy 405 nm*		*UPy·UPy 530 nm*	
	DP	**Mw (g/mol^{-1})**	**DP**	**Mw (g/mol^{-1})**
4	2.38	2312.88	1.00	971.16
8	2.46	2387.17	1.11	1079.15
12	2.84	2754.68	1.20	1162.13
16	3.18	3092.04	1.17	1139.20
20	3.37	3269.96	1.10	1068.69
24	2.87	2791.74	0.93	905.66
28	3.44	3340.19	1.23	1197.70
32	3.25	3157.21	1.07	1038.11
36	4.60	4468.00	1.26	1228.47
40	4.71	4574.65	1.57	1525.34
44	6.24	6060.11	1.95	1892.34
48	6.94	6737.05	1.73	1676.58
52	7.39	7179.03	1.83	1774.99

Appendix B Table 4. Degrees of polymerisation and molecular weight of each isomer of foldamer **III** over concentration range 52 – 4 mM.

UPy·DAN Foldamer IV

Concentration (mM)	*UPy.DAN 405 nm*		*UPy.DAN 530 nm*	
	D (m^2/s)	**Error (m^2/s)**	**D (m^2/s)**	**Error (m^2/s)**
4	5.33E-10	1.02E-11	6.60E-10	4.26E-12
8	4.98E-10	2.65E-12	5.46E-10	1.66E-11
12	5.02E-10	6.64E-12	5.84E-10	3.92E-12
16	3.92E-10	8.62E-12	5.45E-10	1.62E-11
20	3.66E-10	2.96E-12	5.63E-10	4.41E-12
24	2.98E-10	2.51E-12	5.32E-10	2.95E-12
28	2.62E-10	2.16E-12	4.39E-10	1.04E-11
32	2.57E-10	7.50E-13	3.26E-10	2.08E-12
36	2.35E-10	2.98E-12	3.13E-10	3.96E-12
40	2.03E-10	2.06E-12	3.16E-10	2.81E-12
44	1.87E-10	4.03E-12	2.71E-10	3.31E-12
48	1.42E-10	1.33E-12	2.67E-10	2.50E-12
52	1.40E-10	1.47E-12	2.52E-10	2.91E-12

Appendix B Table 5. Diffusion coefficients of foldamer **IV** over concentration range 4 mM - 52 mM. Diffusion coefficients obtained from fitting data in Topspin Dynamics Center, errors estimated using the standard deviation from the fitting.

Concentration (mM)	*UPy.DAN 405 nm*		*UPy.DAN 530 nm*	
	DP	**Mw (g/mol^{-1})**	**DP**	**Mw (g/mol^{-1})**
4	1.90	1961.77	1.00	1033.23
8	2.33	2405.14	1.77	1824.95
12	2.27	2348.11	1.44	1491.39
16	4.77	4931.40	1.78	1835.01
20	5.86	6058.79	1.61	1664.58
24	10.86	11224.84	1.91	1972.85
28	15.99	16516.76	3.40	3511.04
32	16.94	17499.65	8.30	8573.85
36	22.15	22888.92	9.38	9687.15
40	34.37	35509.18	9.11	9413.86
44	43.96	45425.95	14.45	14925.23
48	100.41	103744.19	15.10	15606.12
52	104.77	108254.19	17.97	18562.10

Appendix B Table 6. Degrees of polymerisation and molecular weight of each isomer of foldamer **IV** over concentration range 52 – 4 mM.

DAN-PMMA 100 + UPy·UPy Foldamer III DOSY data

Cycle	*Wavelength (nm)*	*DAN-PMMA + UPy·UPy*	
		D (m^2/s)	**Error (m^2/s)**
1	530	1.21E-10	1.23E-12
2	405	9.45E-11	1.23E-12
3	530	1.29E-10	2.53E-12
4	405	9.63E-11	1.85E-12

Appendix B Table 7. Diffusion coefficients of DAN-PMMA **100** + UPy·UPy Foldamer **III** over 4 cycles of irradiation. Diffusion coefficients obtained from fitting data in Topspin Dynamics Center, errors estimated using the standard deviation from the fitting.

Cycle	*Wavelength (nm)*	*DAN-PMMA + UPy·UPy*	
		DP	**Mw (g/mol^{-1})**
1	530	1.00	31200.00
2	405	2.10	65496.08
3	530	0.83	25747.89
4	405	1.98	61891.62

Appendix B Table 8. Degrees of polymerisation and molecular weight of DAN-PMMA **100** + UPy·UPy Foldamer **III** over 4 cycles of irradiation.

Appendix C

Viscometry Data

Pyr·NAP Foldamer I

Conc. (mM)	*λ (nm)*	*Isomer*	*T1 (s)*	*T2 (s)*	*T3 (s)*	*T4 (s)*	*Avg T(s)*	*$^{T1}\eta_{sp}$ (N/m²)*	*$^{T2}\eta_{sp}$ (N/m²)*	*$^{T3}\eta_{sp}$ (N/m²)*	*$^{T4}\eta_{sp}$ (N/m²)*	*$^{Avg}\eta_{sp}$ (N/m²)*
56	405	*E*	0.70	0.72	0.72	0.71	0.71	0.09	0.12	0.12	0.10	0.10
	530	*Z*	0.71	0.71	0.69	0.71	0.71	0.10	0.10	0.07	0.10	0.09
52	405	*E*	0.70	0.71	0.70	0.72	0.71	0.09	0.10	0.09	0.12	0.10
	530	*Z*	0.70	0.69	0.71	0.69	0.70	0.09	0.07	0.10	0.07	0.08
48	405	*E*	0.71	0.68	0.70	0.69	0.70	0.10	0.05	0.09	0.07	0.08
	530	*Z*	0.69	0.68	0.69	0.70	0.69	0.07	0.05	0.07	0.09	0.07
44	405	*E*	0.70	0.69	0.68	0.70	0.69	0.09	0.07	0.05	0.09	0.07
	530	*Z*	0.68	0.70	0.68	0.69	0.69	0.05	0.09	0.05	0.07	0.07
40	405	*E*	0.69	0.67	0.68	0.70	0.69	0.07	0.04	0.05	0.09	0.06
	530	*Z*	0.67	0.69	0.68	0.69	0.68	0.04	0.07	0.05	0.07	0.06
36	405	*E*	0.70	0.67	0.68	0.68	0.68	0.09	0.04	0.05	0.05	0.06
	530	*Z*	0.67	0.67	0.69	0.68	0.68	0.04	0.04	0.07	0.05	0.05
32	405	*E*	0.68	0.69	0.67	0.67	0.68	0.05	0.07	0.04	0.04	0.05
	530	*Z*	0.67	0.66	0.69	0.68	0.68	0.04	0.02	0.07	0.05	0.05
28	405	*E*	0.66	0.68	0.67	0.67	0.67	0.02	0.05	0.04	0.04	0.04
	530	*Z*	0.68	0.66	0.67	0.66	0.67	0.05	0.02	0.04	0.02	0.03
24	405	*E*	0.65	0.67	0.68	0.68	0.67	0.01	0.04	0.05	0.05	0.04
	530	*Z*	0.66	0.67	0.65	0.66	0.66	0.02	0.04	0.01	0.02	0.02
20	405	*E*	0.66	0.65	0.68	0.66	0.66	0.02	0.01	0.05	0.02	0.03
	530	*Z*	0.65	0.67	0.66	0.65	0.66	0.01	0.04	0.02	0.01	0.02
16	405	*E*	0.66	0.67	0.65	0.66	0.66	0.02	0.04	0.01	0.02	0.02
	530	*Z*	0.66	0.65	0.67	0.64	0.66	0.02	0.01	0.04	-0.01	0.02
12	405	*E*	0.67	0.65	0.65	0.66	0.66	0.04	0.01	0.01	0.02	0.02
	530	*Z*	0.65	0.67	0.65	0.64	0.65	0.01	0.04	0.01	-0.01	0.01
8	405	*E*	0.66	0.65	0.64	0.66	0.65	0.02	0.01	-0.01	0.02	0.01
	530	*Z*	0.64	0.65	0.66	0.65	0.65	-0.01	0.01	0.02	0.01	0.01
4	405	*E*	0.65	0.66	0.63	0.65	0.65	0.01	0.02	-0.02	0.01	0.00
	530	*Z*	0.64	0.65	0.65	0.65	0.65	-0.01	0.01	0.01	0.01	0.00
$CDCl_3$	N/A	N/A	0.64	0.64	0.65	0.65	0.65	N/A	N/A	N/A	N/A	N/A

Appendix C Table 1. Viscosity measurements for foldamer **I** over concentration range 56 – 4 mM.

UPy·UPy Foldamer III

Conc. (mM)	*λ (nm)*	*Isomer*	*T1 (s)*	*T2 (s)*	*T3 (s)*	*T4 (s)*	*Avg T (s)*	*$^{T1}\eta_{sp}$ (N/m²)*	*$^{T2}\eta_{sp}$ (N/m²)*	*$^{T3}\eta_{sp}$ (N/m²)*	*$^{T4}\eta_{sp}$ (N/m²)*	*$^{Avg}\eta_{sp}$ (N/m²)*
56	405	*E*	5.32	5.31	5.35	5.34	5.33	7.18	3.17	3.15	3.14	7.20
	530	*Z*	4.42	4.41	4.43	4.44	4.43	5.80	2.32	2.29	2.34	5.81
52	405	*E*	4.30	4.33	4.30	4.31	4.31	5.62	2.35	2.38	2.34	5.63
	530	*Z*	3.39	3.37	3.38	3.39	3.38	4.22	1.54	1.52	1.58	4.20
48	405	*E*	3.47	3.48	3.48	3.49	3.48	4.34	1.72	1.74	1.62	4.35
	530	*Z*	2.62	2.65	2.62	2.61	2.63	3.03	0.86	0.89	0.92	3.04
44	405	*E*	2.68	2.71	2.70	2.69	2.70	3.12	1.34	1.32	1.31	3.15
	530	*Z*	2.15	2.16	2.14	2.17	2.16	2.31	0.57	0.63	0.62	2.32
40	405	*E*	2.19	2.18	2.20	2.17	2.19	2.37	0.91	0.89	0.91	2.36
	530	*Z*	1.67	1.65	1.64	1.68	1.66	1.57	0.34	0.35	0.32	1.55
36	405	*E*	1.74	1.77	1.78	1.70	1.75	1.68	0.55	0.62	0.60	1.69
	530	*Z*	1.24	1.21	1.23	1.25	1.23	0.91	0.22	0.17	0.18	0.90
32	405	*E*	1.53	1.52	1.51	1.50	1.52	1.35	0.43	0.35	0.38	1.33
	530	*Z*	1.04	1.02	1.06	1.05	1.04	0.60	0.14	0.14	0.12	0.60
28	405	*E*	1.22	1.24	1.23	1.24	1.23	0.88	0.18	0.17	0.22	0.90
	530	*Z*	0.89	0.87	0.88	0.86	0.88	0.37	0.12	0.11	0.08	0.35
24	405	*E*	1.02	1.01	1.05	1.04	1.03	0.57	0.08	0.11	0.11	0.58
	530	*Z*	0.78	0.79	0.76	0.77	0.78	0.20	0.06	0.05	0.08	0.19
20	405	*E*	0.89	0.93	0.88	0.90	0.90	0.37	0.02	0.03	0.05	0.38
	530	*Z*	0.75	0.74	0.74	0.73	0.74	0.15	0.03	0.03	0.05	0.14
16	405	*E*	0.78	0.77	0.76	0.79	0.78	0.20	0.18	0.00	-0.02	0.19
	530	*Z*	0.73	0.73	0.72	0.70	0.72	0.12	0.12	0.02	0.02	0.11
12	405	*E*	0.71	0.70	0.72	0.72	0.71	0.09	0.08	0.11	0.11	0.10
	530	*Z*	0.69	0.69	0.68	0.70	0.69	0.06	0.06	0.05	0.08	0.06
8	405	*E*	0.69	0.66	0.67	0.68	0.68	0.06	0.02	0.03	0.05	0.04
	530	*Z*	0.67	0.67	0.67	0.68	0.67	0.03	0.03	0.03	0.05	0.03
4	405	*E*	0.66	0.67	0.65	0.64	0.66	0.02	0.03	0.00	-0.02	0.01
	530	*Z*	0.65	0.65	0.66	0.66	0.66	0.00	0.00	0.02	0.02	0.01
$CDCl_3$	N/A	N/A	0.65	0.63	0.66	0.66	0.65	N/A	N/A	N/A	N/A	N/A

Appendix C Table 2. Viscosity measurements for foldamer **III** over concentration range 56 – 4 mM.

Cycle 56 mM	λ (nm)	Isomer	T1 (s)	T2 (s)	T3 (s)	T4 (s)	Avg T (s)	$^{T1}\eta_{sp}$ (N/m²)	$^{T2}\eta_{sp}$ (N/m²)	$^{T3}\eta_{sp}$ (N/m²)	$^{T4}\eta_{sp}$ (N/m²)	$^{Avg}\eta_{sp}$ (N/m²)
0.5	405	*E*	5.32	5.31	5.35	5.34	5.33	7.18	7.17	7.23	7.22	7.20
1.0	530	*Z*	4.42	4.41	4.43	4.44	4.43	5.80	5.78	5.82	5.83	5.81
1.5	405	*E*	5.29	5.34	5.29	5.36	5.32	7.14	7.22	7.14	7.25	7.18
2.0	530	*Z*	4.43	4.45	4.41	4.37	4.42	5.82	5.85	5.78	5.72	5.79
2.5	405	*E*	5.31	5.27	5.29	5.36	5.31	7.17	7.11	7.14	7.25	7.17
3.0	530	*Z*	4.45	4.40	4.39	4.41	4.41	5.85	5.77	5.75	5.78	5.79
3.5	405	*E*	5.34	5.27	5.32	5.37	5.33	7.22	7.11	7.18	7.26	7.19
4.0	530	*Z*	4.39	4.48	4.40	4.41	4.42	5.75	5.89	5.77	5.78	5.80
4.5	405	*E*	5.36	5.29	5.34	5.34	5.33	7.25	7.14	7.22	7.22	7.20
5.0	530	*Z*	4.47	4.40	4.48	4.40	4.44	5.88	5.77	5.89	5.77	5.83
5.5	405	*E*	5.36	5.39	5.38	5.37	5.38	7.25	7.29	7.28	7.26	7.27
6.0	530	*Z*	4.46	4.42	4.45	4.50	4.46	5.86	5.80	5.85	5.92	5.86
6.5	405	*E*	5.42	5.39	5.37	5.35	5.38	7.34	7.29	7.26	7.23	7.28
7.0	530	*Z*	4.44	4.42	4.38	4.43	4.42	5.83	5.80	5.74	5.82	5.80
7.5	405	*E*	5.38	5.40	5.44	5.37	5.40	7.28	7.31	7.37	7.26	7.30
8.0	530	*Z*	4.50	4.51	4.49	4.43	4.48	5.92	5.94	5.91	5.82	5.90
8.5	405	*E*	5.36	5.48	5.39	5.44	5.42	7.25	7.43	7.29	7.37	7.33
9.0	530	*Z*	4.51	4.47	4.53	4.52	4.51	5.94	5.88	5.97	5.95	5.93
9.5	405	*E*	5.40	5.37	5.43	5.39	5.40	7.31	7.26	7.35	7.29	7.30
10.0	530	*Z*	4.47	4.47	4.50	4.53	4.49	5.88	5.88	5.92	5.97	5.91

Appendix C Table 3. Viscosity measurements for foldamer **III** (56 mM) after 10 cycles of irradiation at 405 nm and 530 nm.

Cycle 32 mM	λ (nm)	Isomer	T1 (s)	T2 (s)	T3 (s)	T4 (s)	Avg T (s)	$^{T1}\eta_{sp}$ (N/m²)	$^{T2}\eta_{sp}$ (N/m²)	$^{T3}\eta_{sp}$ (N/m²)	$^{T4}\eta_{sp}$ (N/m²)	$^{Avg}\eta_{sp}$ (N/m²)
0.5	405	*E*	1.53	1.52	1.51	1.50	1.52	1.35	1.34	1.35	1.35	1.33
1.0	530	*Z*	1.04	1.02	1.06	1.05	1.04	0.60	0.65	0.60	0.68	0.60
1.5	405	*E*	1.53	1.54	1.50	1.59	1.54	1.35	1.42	1.32	1.31	1.37
2.0	530	*Z*	1.06	1.07	1.09	1.06	1.07	0.63	0.68	0.66	0.66	0.65
2.5	405	*E*	1.50	1.51	1.49	1.52	1.51	1.31	1.32	1.29	1.34	1.32
3.0	530	*Z*	1.09	1.08	1.05	1.04	1.07	0.68	0.66	0.62	0.60	0.64
3.5	405	*E*	1.56	1.52	1.53	1.53	1.54	1.40	1.34	1.35	1.35	1.36
4.0	530	*Z*	1.10	1.07	1.04	1.09	1.08	0.69	0.65	0.60	0.68	0.65
4.5	405	*E*	1.58	1.57	1.51	1.50	1.54	1.43	1.42	1.32	1.31	1.37
5.0	530	*Z*	1.07	1.09	1.08	1.08	1.08	0.65	0.68	0.66	0.66	0.66
5.5	405	*E*	1.54	1.56	1.55	1.56	1.55	1.37	1.40	1.38	1.40	1.39
6.0	530	*Z*	1.12	1.09	1.10	1.11	1.11	0.72	0.68	0.69	0.71	0.70
6.5	405	*E*	1.53	1.50	1.52	1.59	1.54	1.35	1.31	1.34	1.45	1.36
7.0	530	*Z*	1.10	1.07	1.12	1.09	1.10	0.69	0.65	0.72	0.68	0.68
7.5	405	*E*	1.56	1.55	1.53	1.56	1.55	1.40	1.38	1.35	1.40	1.38
8.0	530	*Z*	1.12	1.11	1.09	1.08	1.10	0.72	0.71	0.68	0.66	0.69
8.5	405	*E*	1.54	1.55	1.55	1.57	1.55	1.37	1.38	1.38	1.42	1.39
9.0	530	*Z*	1.11	1.14	1.10	1.12	1.12	0.71	0.75	0.69	0.72	0.72
9.5	405	*E*	1.57	1.58	1.57	1.60	1.58	1.42	1.43	1.42	1.46	1.43
10.0	530	*Z*	1.13	1.11	1.15	1.09	1.12	0.74	0.71	0.77	0.68	0.72

Appendix C Table 4. Viscosity measurements for foldamer **III** (32 mM) after 10 cycles of irradiation at 405 nm and 530 nm.

Cycle 4 mM	λ (nm)	Isomer	T1 (s)	T2 (s)	T3 (s)	T4 (s)	Avg T (s)	$^{T1}\eta_{sp}$ (N/m²)	$^{T2}\eta_{sp}$ (N/m²)	$^{T3}\eta_{sp}$ (N/m²)	$^{T4}\eta_{sp}$ (N/m²)	$^{Avg}\eta_{sp}$ (N/m²)
0.5	405	E	0.66	0.67	0.65	0.64	0.66	0.02	0.03	0.00	-0.02	0.01
1.0	530	Z	0.65	0.65	0.66	0.66	0.66	0.00	0.00	0.02	0.02	0.01
1.5	405	E	0.65	0.65	0.67	0.66	0.66	0.00	0.00	0.03	0.02	0.01
2.0	530	Z	0.63	0.62	0.69	0.69	0.66	-0.03	-0.05	0.06	0.06	0.01
2.5	405	E	0.65	0.66	0.67	0.69	0.67	0.00	0.02	0.03	0.06	0.03
3.0	530	Z	0.68	0.61	0.67	0.68	0.66	0.05	-0.06	0.03	0.05	0.02
3.5	405	E	0.67	0.65	0.70	0.65	0.67	0.03	0.00	0.08	0.00	0.03
4.0	530	Z	0.66	0.66	0.68	0.67	0.67	0.02	0.02	0.05	0.03	0.03
4.5	405	E	0.64	0.67	0.65	0.69	0.66	-0.02	0.03	0.00	0.06	0.02
5.0	530	Z	0.69	0.65	0.66	0.66	0.67	0.06	0.00	0.02	0.02	0.02
5.5	405	E	0.65	0.70	0.65	0.63	0.66	0.00	0.08	0.00	-0.03	0.01
6.0	530	Z	0.68	0.65	0.63	0.67	0.66	0.05	0.00	-0.03	0.03	0.01
6.5	405	E	0.69	0.67	0.61	0.68	0.66	0.06	0.03	-0.06	0.05	0.02
7.0	530	Z	0.65	0.65	0.68	0.66	0.66	0.00	0.00	0.05	0.02	0.02
7.5	405	E	0.68	0.67	0.66	0.69	0.68	0.05	0.03	0.02	0.06	0.04
8.0	530	Z	0.65	0.68	0.70	0.66	0.67	0.00	0.05	0.08	0.02	0.03
8.5	405	E	0.69	0.67	0.63	0.66	0.66	0.06	0.03	-0.03	0.02	0.02
9.0	530	Z	0.67	0.66	0.69	0.67	0.67	0.03	0.02	0.06	0.03	0.03
9.5	405	E	0.66	0.65	0.66	0.69	0.67	0.02	0.00	0.02	0.06	0.02
10.0	530	Z	0.68	0.66	0.70	0.65	0.67	0.05	0.02	0.08	0.00	0.03

Appendix C Table 5. Viscosity measurements for foldamer **III** (4 mM) after 10 cycles of irradiation at 405 nm and 530 nm.

UPy·DAN Foldamer IV

Conc. (mM)	*λ (nm)*	*Isomer*	*T1 (s)*	*T2 (s)*	*T3 (s)*	*T4 (s)*	*Avg T (s)*	$^{T1}\eta_{sp}$ (N/m²)	$^{T2}\eta_{sp}$ (N/m²)	$^{T3}\eta_{sp}$ (N/m²)	$^{T4}\eta_{sp}$ (N/m²)	$^{Avg}\eta_{sp}$ (N/m²)
56	405	*E*	16.61	16.59	16.60	16.57	16.59	22.73	8.47	8.44	8.44	22.70
	530	*Z*	7.91	7.92	7.89	7.87	7.90	10.30	4.16	4.11	4.10	10.28
52	405	*E*	12.75	12.70	12.75	12.73	12.73	17.21	6.51	6.53	6.56	17.19
	530	*Z*	6.27	6.26	6.23	6.28	6.26	7.96	3.00	2.99	2.97	7.94
48	405	*E*	9.84	9.86	9.89	9.92	9.88	13.06	4.97	5.04	4.96	13.11
	530	*Z*	5.00	5.03	5.01	5.04	5.02	6.14	1.87	1.86	1.87	6.17
44	405	*E*	6.59	6.63	6.61	6.61	6.61	8.41	3.39	3.40	3.34	8.44
	530	*Z*	3.62	3.61	3.58	3.57	3.60	4.17	1.14	1.19	1.16	4.14
40	405	*E*	5.28	5.26	5.27	5.29	5.28	6.54	2.26	2.29	2.24	6.54
	530	*Z*	2.77	2.80	2.79	2.78	2.79	2.96	0.64	0.57	0.56	2.98
36	405	*E*	4.16	4.18	4.23	4.17	4.19	4.94	1.36	1.33	1.29	4.98
	530	*Z*	2.03	2.01	2.00	2.01	2.01	1.90	0.31	0.30	0.27	1.88
32	405	*E*	3.01	3.07	3.08	3.04	3.05	3.30	0.76	0.71	0.73	3.36
	530	*Z*	1.52	1.50	1.53	1.51	1.52	1.17	0.20	0.20	0.19	1.16
28	405	*E*	2.23	2.28	2.30	2.27	2.27	2.19	0.36	0.33	0.31	2.24
	530	*Z*	1.11	1.15	1.10	1.09	1.11	0.59	0.10	0.13	0.13	0.59
24	405	*E*	1.59	1.65	1.63	1.60	1.62	1.27	0.17	0.13	0.19	1.31
	530	*Z*	0.90	0.92	0.91	0.89	0.91	0.29	0.09	0.07	-0.03	0.29
20	405	*E*	1.19	1.23	1.20	1.21	1.21	0.70	0.00	0.11	0.03	0.73
	530	*Z*	0.85	0.84	0.84	0.83	0.84	0.21	0.01	0.03	0.03	0.20
16	405	*E*	0.94	0.95	0.93	0.92	0.94	0.34	0.36	0.00	0.01	0.34
	530	*Z*	0.78	0.77	0.79	0.79	0.78	0.11	0.10	0.00	-0.01	0.12
12	405	*E*	0.81	0.82	0.79	0.83	0.81	0.16	0.17	0.13	0.19	0.16
	530	*Z*	0.77	0.76	0.75	0.68	0.74	0.10	0.09	0.07	-0.03	0.06
8	405	*E*	0.70	0.70	0.78	0.72	0.73	0.00	0.00	0.11	0.03	0.04
	530	*Z*	0.72	0.71	0.72	0.72	0.72	0.03	0.01	0.03	0.03	0.03
4	405	*E*	0.73	0.69	0.70	0.71	0.71	0.04	-0.01	0.00	0.01	0.01
	530	*Z*	0.71	0.70	0.70	0.69	0.70	0.01	0.00	0.00	-0.01	0.00
$CDCl_3$	N/A	N/A	0.70	0.69	0.71	0.70	0.70	N/A	N/A	N/A	N/A	N/A

Appendix C Table 6. Viscosity measurements for foldamer **IV** over concentration range 56 – 4 mM.

Cycle 56 mM	λ (nm)	Isomer	T1 (s)	T2 (s)	T3 (s)	T4 (s)	Avg T (s)	$^{T1}\eta_{sp}$ (N/m²)	$^{T2}\eta_{sp}$ (N/m²)	$^{T3}\eta_{sp}$ (N/m²)	$^{T4}\eta_{sp}$ (N/m²)	$^{Avg}\eta_{sp}$ (N/m²)
0.5	405	E	16.61	16.59	16.60	16.57	16.59	22.73	22.70	22.71	22.67	22.70
1.0	530	Z	7.91	7.92	7.89	7.87	7.90	10.30	10.31	10.27	10.24	10.28
1.5	405	E	16.53	16.49	16.48	16.51	16.50	22.61	22.56	22.54	22.59	22.58
2.0	530	Z	7.98	7.88	7.97	7.85	7.92	10.40	10.26	10.39	10.21	10.31
2.5	405	E	16.59	16.61	16.63	16.58	16.60	22.70	22.73	22.76	22.69	22.72
3.0	530	Z	8.03	8.00	8.01	7.99	8.01	10.47	10.43	10.44	10.41	10.44
3.5	405	E	16.45	16.49	16.44	16.47	16.46	22.50	22.56	22.49	22.53	22.52
4.0	530	Z	8.15	8.14	8.12	8.16	8.14	10.64	10.63	10.60	10.66	10.63
4.5	405	E	16.50	16.51	16.49	16.47	16.49	22.57	22.59	22.56	22.53	22.56
5.0	530	Z	8.07	8.08	8.05	8.05	8.06	10.53	10.54	10.50	10.50	10.52
5.5	405	E	16.41	16.42	16.40	16.41	16.41	22.44	22.46	22.43	22.44	22.44
6.0	530	Z	8.05	8.09	8.10	8.08	8.08	10.50	10.56	10.57	10.54	10.54
6.5	405	E	16.41	16.38	16.37	16.40	16.39	22.44	22.40	22.39	22.43	22.41
7.0	530	Z	8.36	8.38	8.40	8.39	8.38	10.94	10.97	11.00	10.99	10.98
7.5	405	E	16.15	16.18	16.19	16.20	16.18	22.07	22.11	22.13	22.14	22.11
8.0	530	Z	7.69	7.73	7.70	7.65	7.69	9.99	10.04	10.00	9.93	9.99
8.5	405	E	16.10	16.16	16.13	16.15	16.14	22.00	22.09	22.04	22.07	22.05
9.0	530	Z	8.24	8.23	8.25	8.31	8.26	10.77	10.76	10.79	10.87	10.80
9.5	405	E	16.15	16.11	16.04	16.10	16.10	22.07	22.01	21.91	22.00	22.00
10.0	530	Z	8.47	8.51	8.62	8.49	8.52	11.10	11.16	11.31	11.13	11.18

Appendix C Table 7. Viscosity measurements for foldamer **IV** (56 mM) after 10 cycles of irradiation at 405 nm and 530 nm.

Cycle 32 mM	λ (nm)	Isomer	T1 (s)	T2 (s)	T3 (s)	T4 (s)	Avg T (s)	$^{T1}\eta_{sp}$ (N/m²)	$^{T2}\eta_{sp}$ (N/m²)	$^{T3}\eta_{sp}$ (N/m²)	$^{T4}\eta_{sp}$ (N/m²)	$^{Avg}\eta_{sp}$ (N/m²)
0.5	405	E	3.01	3.07	3.08	3.04	3.05	3.30	3.39	3.40	3.34	3.36
1.0	530	Z	1.52	1.50	1.53	1.51	1.52	1.17	1.14	1.19	1.16	1.16
1.5	405	E	3.10	3.12	3.08	3.07	3.09	3.43	3.46	3.40	3.39	3.42
2.0	530	Z	1.47	1.44	1.49	1.48	1.47	1.10	1.06	1.13	1.11	1.10
2.5	405	E	3.02	3.01	3.00	3.02	3.01	3.31	3.30	3.29	3.31	3.30
3.0	530	Z	1.56	1.54	1.58	1.55	1.56	1.23	1.20	1.26	1.21	1.23
3.5	405	E	2.99	3.02	2.98	3.00	3.00	3.27	3.31	3.26	3.29	3.28
4.0	530	Z	1.47	1.47	1.42	1.45	1.45	1.10	1.10	1.03	1.07	1.08
4.5	405	E	3.01	3.02	3.03	3.04	3.03	3.30	3.31	3.33	3.34	3.32
5.0	530	Z	1.52	1.58	1.53	1.52	1.54	1.17	1.26	1.19	1.17	1.20
5.5	405	E	2.95	2.95	2.90	2.99	2.95	3.21	3.21	3.14	3.27	3.21
6.0	530	Z	1.47	1.49	1.50	1.44	1.48	1.10	1.13	1.14	1.06	1.11
6.5	405	E	3.01	3.00	3.02	3.03	3.02	3.30	3.29	3.31	3.33	3.31
7.0	530	Z	1.47	1.49	1.44	1.45	1.46	1.10	1.13	1.06	1.07	1.09
7.5	405	E	2.97	2.93	2.89	3.00	2.95	3.24	3.19	3.13	3.29	3.21
8.0	530	Z	1.55	1.53	1.49	1.51	1.52	1.21	1.19	1.13	1.16	1.17
8.5	405	E	2.92	2.90	2.93	2.91	2.92	3.17	3.14	3.19	3.16	3.16
9.0	530	Z	1.56	1.55	1.53	1.51	1.54	1.23	1.21	1.19	1.16	1.20
9.5	405	E	2.96	2.97	2.93	2.94	2.95	3.23	3.24	3.19	3.20	3.21
10.0	530	Z	1.58	1.60	1.61	1.62	1.60	1.26	1.29	1.30	1.31	1.29

Appendix C Table 8. Viscosity measurements for foldamer **IV** (32 mM) after 10 cycles of irradiation at 405 nm and 530 nm.

Cycle 4 mM	*λ (nm)*	*Isomer*	*T1 (s)*	*T2 (s)*	*T3 (s)*	*T4 (s)*	*Avg T (s)*	*$^{T1}\eta_{sp}$ (N/m²)*	*$^{T2}\eta_{sp}$ (N/m²)*	*$^{T3}\eta_{sp}$ (N/m²)*	*$^{T4}\eta_{sp}$ (N/m²)*	*$^{Avg}\eta_{sp}$ (N/m²)*
0.5	405	*E*	0.73	0.69	0.70	0.71	0.71	0.04	-0.01	0.00	0.01	0.01
1.0	530	*Z*	0.71	0.70	0.70	0.69	0.70	0.01	0.00	0.00	-0.01	0.00
1.5	405	*E*	0.69	0.75	0.69	0.68	0.70	-0.87	0.07	-0.01	-0.03	0.00
2.0	530	*Z*	0.76	0.73	0.76	0.73	0.75	-0.86	0.04	0.09	0.04	0.06
2.5	405	*E*	0.72	0.76	0.74	0.71	0.73	-0.86	0.09	0.06	0.01	0.05
3.0	530	*Z*	0.74	0.69	0.68	0.73	0.71	-0.86	-0.01	-0.03	0.04	0.01
3.5	405	*E*	0.72	0.68	0.69	0.70	0.70	-0.86	-0.03	-0.01	0.00	0.00
4.0	530	*Z*	0.78	0.72	0.79	0.79	0.77	-0.85	0.03	0.13	0.13	0.10
4.5	405	*E*	0.76	0.73	0.76	0.74	0.75	-0.86	0.04	0.09	0.06	0.07
5.0	530	*Z*	0.77	0.79	0.78	0.77	0.78	-0.85	0.13	0.11	0.10	0.11
5.5	405	*E*	0.81	0.82	0.77	0.75	0.79	-0.85	0.17	0.10	0.07	0.13
6.0	530	*Z*	0.78	0.80	0.79	0.71	0.77	-0.85	0.14	0.13	0.01	0.10
6.5	405	*E*	0.79	0.82	0.77	0.85	0.81	-0.85	0.17	0.10	0.21	0.15
7.0	530	*Z*	0.75	0.83	0.75	0.77	0.78	-0.86	0.19	0.07	0.10	0.11
7.5	405	*E*	0.73	0.79	0.76	0.81	0.77	-0.86	0.13	0.09	0.16	0.10
8.0	530	*Z*	0.80	0.79	0.82	0.83	0.81	-0.85	0.13	0.17	0.19	0.16
8.5	405	*E*	0.76	0.78	0.73	0.68	0.74	-0.86	0.11	0.04	-0.03	0.05
9.0	530	*Z*	0.77	0.81	0.80	0.83	0.80	-0.85	0.16	0.14	0.19	0.15
9.5	405	*E*	0.78	0.86	0.82	0.80	0.82	-0.85	0.23	0.17	0.14	0.16
10.0	530	*Z*	0.81	0.80	0.77	0.83	0.80	-0.85	0.14	0.10	0.19	0.15

Appendix C Table 9. Viscosity measurements for foldamer **IV** (4 mM) after 10 cycles of irradiation at 405 nm and 530 nm.